Republic of Iraq
Ministry of Higher Education and Scientific Research
University of Babylon
College of Engineering
Civil Engineering Department

Experimental Behavior of Rubberized Reinforced Concrete Beams under Torsion

A Thesis

Submitted to the College of Engineering at the University of Babylon in Partial Fulfillment of the Requirements for the Degree of Doctor of Philosophy in Engineering / Civil Engineering / Structures

By

Ammar Abd Alameer Hussein abood

Supervised by

Prof. Dr. Hayder M.K. Al-Mutairee

2022

بِسْمِ اللهِ الرَّحْمَنِ الرَّحِيمِ

نَرْفَعُ دَرَجَاتٍ مِّن نَّشَاء وَفَوْقَ

كُلِّ ذِي عِلْمٍ عَلِيمٌ

صَدَقَ اللهُ العَلِيُّ العَظِيمُ

سورة يوسف / 76

Supervisor Certification

I certify that the preparation of this thesis titled **"Experimental Behavior of Rubberized Reinforced Concrete Beams under Torsion"**, is prepared by **" Ammar Abd Alameer Hussein abod "**, under my supervision at the Department of Civil Engineering / College of Engineering / University of Babylon in partial fulfillment of the requirements for the degree of Doctor of Philosophy in Civil Engineering (Structural Engineering).

Signature:

Name: Prof. Dr. Hayder M. K. Al-Mutairee

Date: / /

DEDICATION

To my parents

To my beloved wife

To my brother and sisters

To my supervisors Dr. Hayder M. K. Al-Mutairee

To my friends Mustafa Hamid Al Hussan, Wissam Nadir,

and Mohammed Al Ammar

With respec**t**

Acknowledgements

In the name of ALLAH, the most compassionate, the most merciful.

All thanks and praise to Allah who enabled me to achieve this research work.

Firstly, I would like to express my sincerest gratitude to my supervisor Prof. Dr. Hayder M.K. Al-Mutairee, for his invaluable insight, wisdom, and guidance. I am really indebted to him. I would like to thank the staff of the Department of Civil Engineering of Babylon University for their assistance with daily matters throughout my graduate academic life. Also, thanks to the technical staff of the structural laboratories for their assistance during the undertaking of my experimental program.

I would like to acknowledge the friendly support and assistance of my fellow graduate students who made my overall experience more gratifying.

Finally, a special thanks and gratitude to my family for their care, and patience, in particular: my parents, and my brothers, who have been by my side throughout this entire endeavor. Without their love, encouragement, and support I would not have been able to complete this academic achievement.

Ammar Abd Alameer Hussein Beiram

2022

Abstract

This work devoted to study the behavior of rubberized concrete beams under twisted load. The factors in this research include the percentage of coarse aggregate replaced by waste rubber chips (10%, 20%, and 30%), the depth-to-width ratio, and the kind of loads. A total of thirty specimens were used in the experiment, with sixteen beams being tested in pure torsion in group one, twelve beams being tested in combined torsion and bending loads in group two, and two beams being tested in pure bending in group three. Twenty-six specimens were subjected to identical longitudinal and transverse steel reinforcement, and four specimens were without steel reinforcement.

Compared to traditional concrete, rubberized concrete mixes are less dense and less workable about 9.08% and 37.04% respectively. In terms of compressive strength, splitting tensile strength, modulus of rupture, and modulus of elasticity, when replacing 30% of coarse aggregate by chip rubber, rubberized concrete showed a larger loss of mechanical properties of about 47.64%, 35.34%, 44.75%, and 50.49%, respectively. By replacing 30% of the gravel with rubber chips, impact resistance and thermal conductivity in rubberized concrete increased by 356% and 20.6%, respectively, meaning that rubberized concrete can absorb more energy, be more flexible, and be better at heat insulating.

It was found that the ultimate torque decreased by 14.75%, while the twist angle increased by 44.07% at the ultimate, the ultimate cracking stiffness decreased by 44.05% and the ductility index increased by 30.34%, when rubber was substituted by 30% under pure torsion. According to experimental results for specimens under combined (torsion and bending) conditions, when the ratio of moment/torsion (λ) is increased from 1 to 4, the ultimate torque decreases by 47.28% but the

bending moment increases by 107.78%. The maximum capacity of torque for beams decreases by 14.56% to 17.67% when 30% of coarse aggregate is replaced by chip rubber, for values of λ (0.5 to 4) while the angle of twist at ultimate torque increases by 33.04% to 44.37%.

The American code recommends using an analogy of a thin-walled tube space truss to compare experimental findings of ultimate torque with analytical results. American code results give an underestimated torsion capacity of reinforced normal concrete beams but an overestimated torsion capacity for rubberized reinforced concrete beams by about 15%. This method was shown to be ineffective in assessing the impact of rubber content in the concrete mix. It is thus advised to multiply the theoretical findings from the American Code by a factor from the suggested formula to fulfill experimental needs. Using the values of the mean (m) and the coefficient of variation (COV) of 1.009% and 0.874%, respectively, the predicted and experimental findings are in good agreement. According to the interaction diagram, the experimental findings follow a similar pattern to the theoretical results for beams subjected to combined (torsion and bending) loads. There is a highly tight relationship between the theoretical and practical curves when λ is less than 1, whereas the theoretical and practical curves progressively approach each other as λ increased.

List of Contents

List of Tables

List of Figures

List of Plates

List of Latin Notation

Symbol	Notation
A_o	The gross area contained by the shear flow channel, (mm^2).
A_{oh}	The area around the centerline of the outermost closed transverse torsional reinforcement, (mm^2).
A_k	The area enclosed by the centerlines of the connecting thin-walls, (mm^2).
A_ℓ	Torsional-reinforced longitudinal area, (mm^2).
A_t	A closed stirrup with torsion resistance equal to the area of one leg, (mm^2).
a/d	Shear span-to- depth ratio
D_i	Diagonal compression component
EI	The impact resistance at initial crack, (J).
Eu	The impact resistance at end crack, (J).
f'c	Concrete compressive strength for cylinder, (N/mm^2).
fc	Concrete compressive strength for cube, (N/mm^2).
f_r	The concrete rupture modulus, (N/mm2).
f_t	Concrete tensile strength, (N/mm2).
Fu	Ultimate stress of steel reinforcement, (N/mm2).
Fy	Yield strength of steel reinforcement, (N/mm2).
g	Gravity acceleration value, (9.81 m/s^2).
K	Cracking stiffness, (KN.m).
m	Mass, (Kg).
N	Number of blows.
P	Applied load, (KN).
P_h	The outermost closed stirrup's centerline perimeter, (mm).
q	shear flow, (N/mm).
T	torsional moment, (KN.m).
T/V_d	ratio of torsion/shear-depth.

t_d	wall thickness, (mm)
t_{ef}	Effective wall thickness of the equivalent thin-walled section (mm).
Tu	Ultimate torsional strength, (KN.m).
w/c	Water-cement ratio.

List of Greek Notation

Symbol	Notation
τ	torsional shear stress, (N/mm^2)
ρ_l	longitudinal reinforcement volumetric ratio
ρ_t	transverse reinforcement volumetric ratio
ϕ	Diameter of steel reinforcement, (mm)
λ	bending/torsion ratio
θmax	The rotational at ultimate torque, (rad/m)
θY	The rotational in this area at yield, (rad/m)
Δu	The ultimate deflection, (mm)
Δ_Y	The deflection at yield, (mm)
μ	Ductility index

List of Abbreviations

ACI	American Concrete Institute.
kN	kilo Newton.
MPa	Mega Pascal.
GPa	Giga Pascal.
et al.	And Others.
M25	Compressive Strength of Concrete = 25 MPa.
RC	Reinforced Concrete.
CC	Control Concrete.
CSC	Coconut Shell Concrete.
SCC	Self-Compacting Concrete.
VC	Vibrated Concrete.
RCA	Recycled Coarse Aggregate.
3D	Three-Dimensional.
GFRP	Glass Fiber Reinforced Polymer.
CFRP	Carbon Fiber Reinforced Polymer.
LWFC	Lightweight Foamed Concrete.
Vf	Volume Fraction of Steel Fiber.
PT	Pure Torsion.
CTB	Combined (Torsion + Bending).
PB	Pure Bending.
cm	Centimeter.
mm	Millimeter.
HRAWR	High-Range Admixture for Water Reduction.
ASTM	American Society for Testing and Material.
G54	Glenium 54.
BS	British Standard.
LVDT	Linear Displacement Measurement.

J	Joule.
R0, R10, R20, R30	Percent of Replacement Rubber.
EAI	The Energy Absorption Index.
EC	European Code.
COV	Coefficient of Variation.
SD	Standard of Deviation Value.

CHAPTER ONE
INTRODUCTION

1.1 General

Torsion can be a significant problem in concrete structural members, such as out-off-plane, horizontally curved beams, spandrel beam, helical stairways, etc. Figure (1-1) shows that the floor beam tends to rotate the spandrel beam laterally. Twisting the structural member about its longitudinal axis causes shear stresses, which are generated by the torsional moment. Pure torsion moments are seldom used as structural elements, though. Torsion moments, bending moments, and shear pressures often work together in cooperation.

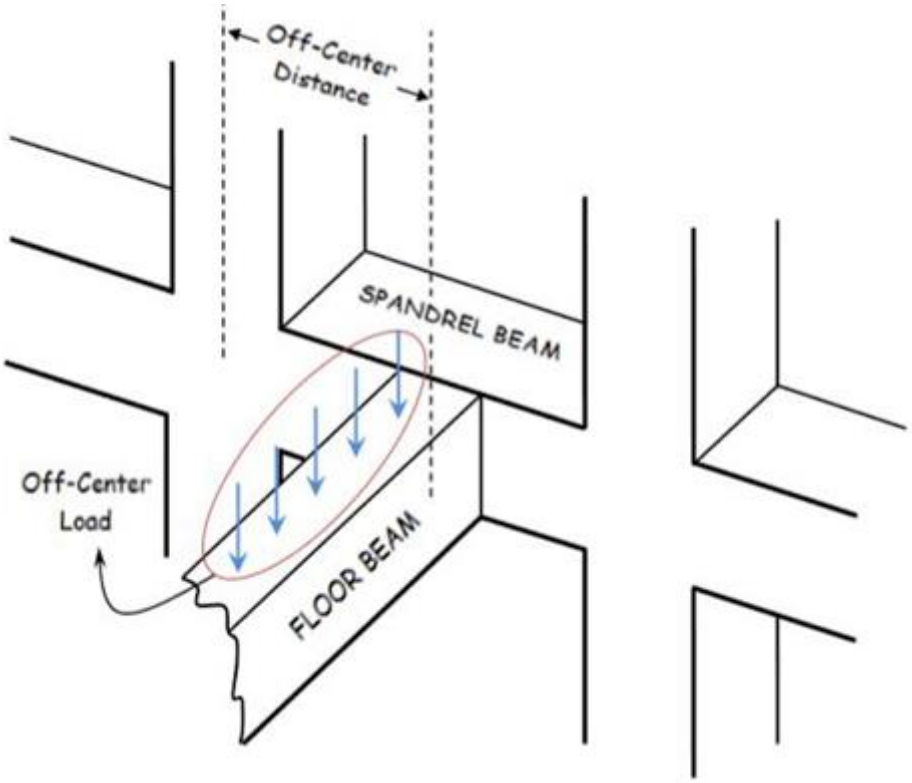

Figure (1-1): Torsion in spandrel beams, (**Mohaisen et al., 2016**).

Designers must distinguish between two sorts of torsions: balance and compatibility. Equilibrium torsion occurs when the torsional moment is required to be in equilibrium and the maximum torsional moment

cannot be reduced by redistribution of moments. In this case, torsion reinforcement must be provided to resist all of the torsional moment. This type of torsion is also known as primary torsion, such as an edge beam supporting cantilever slab as shown in Figure (1-2a) (**Kamara & Rabbat, 2007**).

Compatibility torsion occurs when the torsional moment can be reduced by the redistribution of internal forces while compatibility of deformation is maintained in the member. This type of torsion is also known as secondary torsion, such as an edge beam supporting two transverse beams producing a twisting moment as shown in Figure (1-2b). (**Fanella & Rabbat, 1997**).

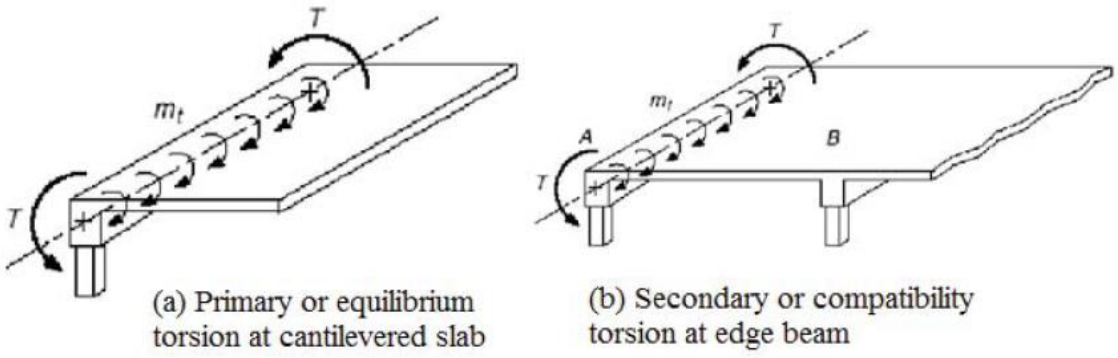

Figure (1-2): Types of torsion according to redistributed moment.

One of the most important elements that affect concrete beams' ability to resist torsion is their cross-sectional form, which includes their cross-sectional area and the ratio of their transverse to longitudinal reinforcement. The failure characteristics of concrete may be altered by varying its strength and reinforcing. Depending on the ratio of longitudinal and transverse reinforcement volumetric ratios, the failure mode might range from ductile to sudden and brittle **(ACI 445.1R-12, 2013**).

Cement and aggregates are the primary building blocks of concrete, making it one of the most commonly used construction materials in the world. Because of the high demand for concrete as a building material in society, it is necessary to use recycled or waste materials to replace natural aggregates in concrete.

Due to a rise in the vehicle sector, the waste tire is very difficult to shake off. It's simple to decompose rubber by burning, but the smoke and pollution products are enormous. Land filling is also a viable option, but landfills are becoming scarcer as the quantity of rubber they can hold is steadily decreasing. It has lately been possible to include rubber particles in a new form of concrete made from discarded tires.

Using waste tyres in a way that minimizes their environmental impact and maximizes the conservation of natural resources is the best way to handle scrap tyres effectively. With the use of discarded tyres as a partial replacement of coarse aggregates, concrete may be improved in several ways, including low unit weight, excellent resistance to abrasion, a high degree of ductility, and the ability to absorb shock and vibration.

1.2 Torsional Strength of Plain Concrete Members Under Pure Torsion

Saint-Venant's elastic theory describes the torsional member's behavior at low torque before cracking. The theory states that the cross-sectional shape remains unchanged after twisting, the angle of rotation per unit length is constant along a member's entire length and failure occurs when maximum principal stress reaches tensile strength of concrete directly applied perpendicular to a cross-sectional surface. Torsional strength may be underestimated by the elastic theory because of

concrete's complex structural reactivity and the material's plasticity (T. T. C. Hsu, 1984).

A rough approximation may be made for the observed increases in strength using the plastic hypothesis, but this is not a satisfying explanation since it assumes concrete can become flexible. It tends to overestimate the torsional strength. According to Hsu (1984), the elastic and plastic hypothesis say that torsion failure in plain concrete is brittle.

Skew-bending theory holds that torsion-damaged plain concrete members bend at a 45-degree angle to the longitudinal axis, parallel to the bigger cross-sectional face. Tensile stress on an inclined face owing to flexure causes failure when the modulus of concrete rupture drops below the tensile stress level (T. T. C. Hsu, 1968).

The torsional strength of the skew-bending theory may be stated as:

$$T_u = \frac{1}{3}\, x^2\, y\, (0.85 f_r) \qquad (1\text{-}1)$$

Where:

x, y = width and depth of beams.

f_r= The concrete rupture modulus.

The torsion stress factor is constant, which lies between the elastic and plastic theories, as shown in Figure (1-3).

Bredt's equation (1-2) may be used to determine the connection between torsional shear stress ($\tau = \frac{q}{t_d}$) and the torsional moment (T) in thin-walled tubes (**Leonard, 1967**).

$$\tau = \frac{T}{2A_\circ\, t_d} = \frac{T}{A_{cp}^2 / P_{cp}} \qquad (1\text{-}2)$$

Where: It is suggested that the torsional stress (τ) may be linked to (T) by the parameter (A_{cp}^2/p_{cp}) if a solid section is substituted by a tube with the

same outer dimensions but with a wall thickness of t_d= 0.75A_{cp}/p_{cp} and that A_o= (2/3)A_{cp}. The ACI code utilizes it to address compatibility torsion of spandrel beams. When the nominal torsional stress T_n required forming a torsional plastic hinge was found to be 0.33$\sqrt{f_c'}$ MPa, the design torsional moment T_n for the spandrel beam was 0.33 $\sqrt{f_c'}(A_{cp}^2/p_{cp})$ MPa **(ACI 318-19, 2019)**.

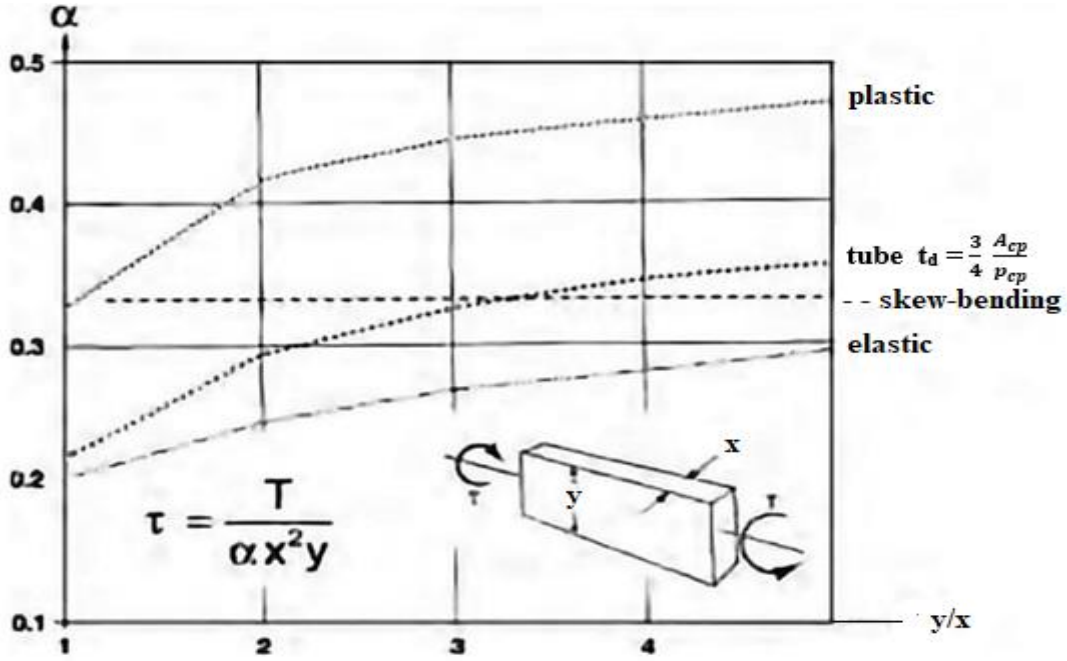

Figure (1-3): Torsion stress factors for solid rectangular section, **(Collins, 1973)**.

1.3 Torsional Strength of Reinforced Concrete Members Under Pure Torsion.

ACI 318-19 traditionally required that members strengthened for torsion have closed stirrups, and every corner of the stirrups must have at least one longitudinal bar. Under pure torsion, an uncracked beam only experiences shear forces in a plane orthogonal to its longitudinal axis. Spiral cracks appear around the beam's surface with an inclination in the

major compressive stress direction due to the tensile stress. Tensile fractures form in concrete when strain occurs in the direction of the primary tensile tension. Compression in the perpendicular direction is weakened by the tensile forces, which have the opposite effect and are known as "softening" of the concrete's compressive strength. Cracking causes the concrete struts between the diagonal cracks to compress and the longitudinal and transverse reinforcement to elongate, as seen in Figure (1-4). Bending stresses and compressive stresses are both induced by the twisting motion of the beam, which warps its faces **(Mitchell & Collins, 1974)**. Because it can work in tension, the concrete between the cracks improves the torsional rigidity of the beam as a whole. This is called "tension stiffening," and it happens right after the first cracks appear then the effect fades with increased torsion.

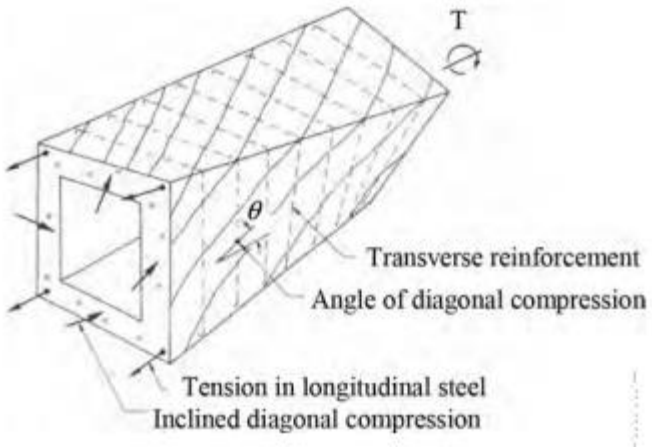

Figure (1-4): Diagonal cracks in members under pure torsion, **(Mitchell & Collins, 1974)**.

Under pure torsion, the longitudinal and transverse reinforcement volumetric ratios (ρ_l and ρ_t) have a big impact on how RC beams behave. The ratios affect crack angle, breadth, stiffness, and failure mode. The principal tensile strain has a direct correlation to fracture width. When ρ_l and ρ_t, two volumetric ratios, are equivalent, the cracks have the

shortest breadth since the longitudinal and transverse stresses are likewise equal. For beams with ρ_t greater than ρ_l, the angle relative to the horizontal is more than 45 degrees, and the longitudinal strain is greater, but for beams with ρ_t smaller than ρ_l, the angle relative to the horizontal is lower than 45 degrees, and the transverse strain is greater. When the volumetric ratios ρ_l and ρ_t are not equal, the crack width is wider **(Mitchell & Collins, 1974)**.

From Figure (1-5), when the concrete achieves its ultimate strain, both transverse and longitudinal reinforcing begin to yield simultaneously; the balanced failure point has been reached. Under-reinforced beams are those whose ρ_l and ρ_t ratios are less than the reinforcement ratios in a balanced state (Region I). It is possible for under-reinforced beams to continue twisting even after the reinforcement yields. The failure mode for over-reinforced beams is brittle in Region IV. In the presence of lower longitudinal or transverse reinforcing strength ratios, longitudinal or transverse reinforcing yields before the concrete has been crushed. Partially under-reinforced beams are those that fit this description (Regions II and III) (**Leu & Lee, 2000**).

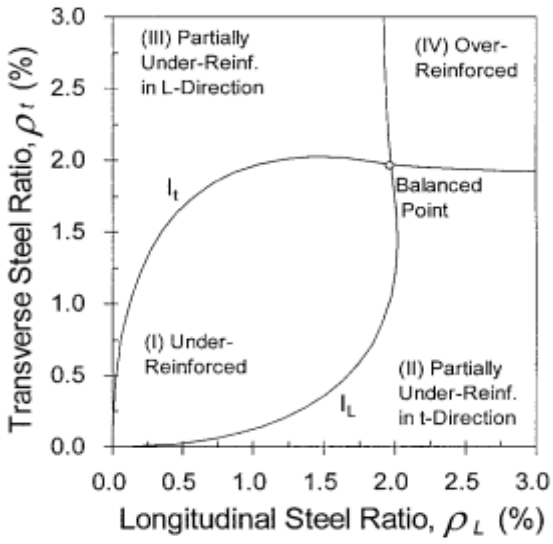

Figure (1-5): Failure Mode Diagram, (**Leu & Lee, 2000**).

As illustrated in Figure (1-6), the post-cracking torsional stiffness and strength of a beam are greatly influenced by the volumetric ratios of longitudinal and transverse reinforcement. After cracking, torsional stiffness (torque-twist curve slope after cracking) is increased by increasing the total reinforcement for under-reinforced beams with identical volumetric ratios (ρ_l and ρ_t). Additionally, it raises the beam's torsional yield strength, a measure of how much torque it can withstand before yielding. However, the post-yield twist reduces as the overall quantity of reinforcement rises. As a consequence, adding more reinforcement makes a beam stiffer and stronger, but it also reduces the beam's ductility. The least quantity of reinforcing steel that the amount causes the yield of reinforcement under the same torque that produces cracking. therefore, once cracked, a beam with less than the bare minimum of reinforcing will fail in a brittle manner (T. T. C. Hsu, 1984).

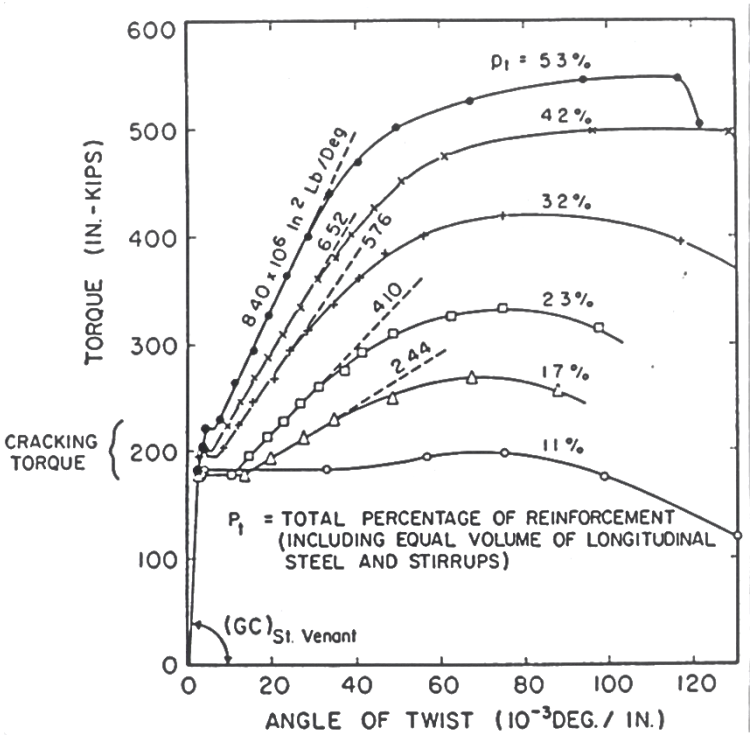

Figure (1-6): Torque-twist curves of beams with various percentages of reinforcement, (**T. T. C. Hsu, 1984**).

When compared to hollow members, the behavior of solid members demonstrates that after cracking, the inner core of solid members is ineffective. Hollow members have a lower cracking strength than solid members because shearing pressures operate on the whole section before cracking. This is true even after cracking, though, both solid and hollow sections can handle the same amount of torque after they break, as long as the wall thickness can handle the shear flow zone (**Thomas T. C. Hsu, 1968**).

Severe torques may cause concrete spalling due to high shearing forces outside the stirrups. Compressive stress resisting torsion after cracking changes directions at the outer corners of the beam in order to maintain balance. After a certain tensile stress in the concrete is reached, the concrete cover begins to spall. The stirrups are often the site of a spall. As a consequence, the cross-sectional area is lower and its torsional strength is lower **(Mitchell & Collins, 1974)**. In specimens with tiny coverings, spalling did not occur until after the torsional strength had been attained in tests conducted by **(Rahal & Collins, 1995)**. The torsional strength was not reached by beams with bigger coverings. There is a direct correlation between concrete cover thickness and spalling prevention. Spalling occurs when the thickness exceeds 30% of the cross-section area to perimeter ratio. This has been shown in experiments **(Rahal & Collins, 1996)**.

1.4 Torsional Strength of Reinforced Concrete Members Under Combined Torsion and Flexural.

In concrete constructions, torsion seldom happens on its own without the presence of other types of stresses. There can be no more than six stress resultants in the orthogonal system of coordinates for a beam cross-section under general loading. A torsional moment, two shearing

forces along the primary and secondary axes, two bending moments along the primary and secondary axes, and an axial force (tension or compression) are all possible results (**ACI 445.1R-12, 2013**).

Loading that causes both bending and torsion in members indicates that the two effects will interact to some degree. As in a member subject to both bending and compression, axial loads acting via lateral deflections induced by the bending loads produce extra moments, which in turn magnify deflections. Bending and torsion may create extra warping moments and torsional shears because of the torsion's angle of twist being increased by the bending moment. Torsional deformations also add extra minor-axis moments, which must be taken into account. This includes the amplification shown above, which must be taken into account **(Nethercot et al., 1989)**.

Beam fracture patterns are influenced by the bending/torsion ratio (M/T). Due to the existence of flexural moments, the bottom and top sides of the section are subjected to tensile and compressive stresses, respectively. Cracking may be delayed in certain circumstances by compressing the top face. A diagonal crack angle is formed on the bottom face of a beam in the event of pure torsion, while a normal angle is formed in the case of flexure. The tensile stresses at the bottom of the section cause the angle on the sides to be steeper, while the compressive forces at the top of the section cause the angle to be flatter **(Johnston & Zia, 1975)**.

1.5 Rubberized Concrete

Rubberized concrete can be obtained by partially or fully replaced the aggregate with scrap tyre rubber. Using scrap tyre rubber in concrete has been emphasized by scientists for more than two decades. They've

found that using recycled scrap rubber tyres in concrete as a partial substitute for mineral aggregates is the most effective solution. There is a double benefit to this replacement: it reduces the depletion of limited supplies of valuable natural resources and protecting the environment from the harmful effects of diversely utilized materials.

Reducing the weight of concrete by using waste tyres as a part of the aggregates may increase its properties, such as low unit weight and high resilience to wear and tear, durability, shocks and vibrations, and high ductility. Reduces mechanical properties or other characteristics, including tensile and compressive strength, as well as workability.

Table (1-1) and Figure (1-7) demonstrate how waste tire rubber may be categorized based on the size of the rubber particles.

Table (1-1): Waste tires rubber classification.

Types	Size	Application in concrete
Shredded/chipped	Shredded Length: 300mm - 430mm 100mm - 150mm Width: 100mm - 230mm Chip: 13mm - 76mm	Gravel replacement
Crumb rubber	0.425mm - 4.75mm	Sand replacement
Ground rubber	0.0075mm - 0.475mm	Cement replacement
Fiber rubber	Length: 8.5mm - 21.5mm Strips: ≤ 8mm long	Reinforced fiber

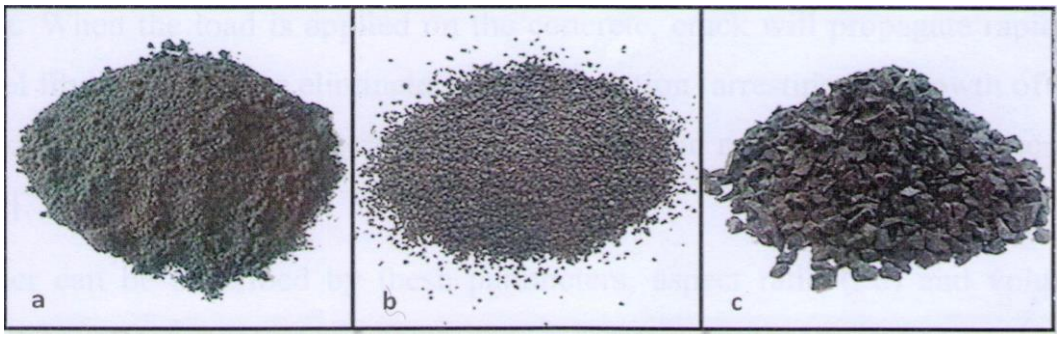

Figure (1-7): Type of tyre rubber: (a) ground rubber; (b) crumb rubber; (c) chip rubber **(Hasan, 2018)**.

1.6 Aims of the Current Research

The following are the study's primary objectives:

1- Experimental test to better understand the effects of partly replacing aggregate with recycled rubber on the behavior of concrete beams under torsion. In addition, additional parameters such as the aspect ratio of the cross-section, the ratio of replacement rubber, and the kind of loading all have an impact on the torsional strength and the angle of twist.
2- Suggesting a formula for determining the torsional strength of rubberized concrete, taking into account the ratio of replacement rubber.

1.7 Thesis Layout

The present study consists of six chapters as follows:

Chapter one: includes a general introduction about torsion, rubberized concrete.

Chapter two: A literature review of past research that is relevant to this topic is reviewed.

Chapter three: The details of the experimental works, material properties and the test procedure are presented.

Chapter four: presents the results of experimental works and discussion.

Chapter five: introduces a comparison between the experimental and numerical results, as well as the parametric studies.

Chapter six: consists a summary of the conclusions for present study and recommendations for further work.

CHAPTER TWO

LITERATURE REVIEW

2.1 General

Solid tire wastes are non-biodegradable compounds that are hazardous to the environment and human health. Rubber tire waste is depicted in Figure (2-1). About one billions tires reach the end of their service life each year (end-of-life tires), with more than half of them being disposed of without being treated **(Thomas et al., 2016**). The overall number of end-of-life tires is expected to reach 1.2 billion by 2030. Furthermore, burning tire waste has a negative environmental impact by increasing pollution in the air, water, and soil. To limit environmental damage and the depletion of available disposal sites, alternate storage and disposal options for this massive volume of tire debris are urgently required. Several research have also been conducted on the feasibility of replacing natural aggregates in concrete with rubber recovered from scrap tyres (**Aniruddh et al., 2016**).

Figure (2-1): Rubber tire waste, (**Alfayez et al., 2020**).

Fattuhi & Clark, 1996, suggested that waste tyre rubberized concrete might be utilized as a foundation pad for rotating equipment and railway stations as a vibration damper, or where impact or blast resistance is needed.

Bignozzi & Sandrolini, 2006, researched the use of scrap tyre rubber in self-compacting concrete. Self-compacting rubberized concrete, according to the authors, has a diverse and unique mechanical behavior and features that make it appealing to the development of noise-reducing pavements.

Benazzouk et al., 2007, investigated developing lightweight construction materials. Researchers looked into the possibility of using waste rubber from the automobile sector as fine aggregates in a cementitious matrix.

The prior researches were organized into four sections, reinforced concrete beams under pure torsional stress have been studied in the first study. The second focuses on reinforced concrete beams that are subjected to combined bending and torsion. The third comprises studies related to the behavior of rubberized concrete members. The last section describes the properties of rubber-modified concrete.

2.2 Experimental Work on Reinforcement Concrete Beams under Pure Torsion

Chalioris, 2003, presented the results of an experimental research on the behavior of 12 reinforced concrete beams subjected to pure torsion, sorted into two groups A and B. For all specimens, the overall length and cross-section dimensions of the beams were 1.60 m and 10/30cm, respectively. The transverse reinforcement of each group was 8 mm in diameter, with closed plain stirrups spaced uniformly at 300 mm, 200

mm, 150 mm, 100 mm, 50 mm, and 30 mm. Group A specimens had a longitudinal reinforcement of 4ϕ8mm, whereas group B beams had a longitudinal reinforcement of 8ϕ8mm. The torque capacity increases by around 100% as the volume of transversal reinforcement increases. When a large amount of transversal reinforcement (ϕ8@30 mm) is used, the amount of increase is smaller. Furthermore, the insertion of longitudinal steel bars increased the ultimate torque moment of the tested beams by 18%. This increase, however, is not proportionate to the amount of longitudinal reinforcement used.

Gunasekaran et al., 2014, investigated the tests of torsion on coconut shell concrete (CSC) beams and conventional concrete (CC) beams and compared them. There were four coconut shell concrete beams and four conventional concrete beams made and evaluated for their strength. Beam cross-sectional dimensions were 200 x 275 mm, and the length of the beam was 1200 mm center-to-center for both beams in this experiment. Similarly, M25 concrete has been utilized in both circumstances. It is shown in Table (2-1) how much total volumetric torsional reinforcement has been calculated for longitudinal and transverse reinforcements, as well as the diameter and number of bars employed for each. The cantilevered section of the specimen is shown in Figure (2-2) as a top view.

In terms of ultimate torque resistance, CSC beams outperformed the CC beams. This could be because the coconut shell's natural structure has long and distinct fibers, which increases its ductility in comparison to normal crushed stone aggregate and increases its angle of twist in turn resistance to ultimate torque. For the same reinforcing ratios, when comparing CSC beams to CC beams, the fracture width is wider in the former. This is because the CS material used in CSC is less stiff than the

traditional aggregate material used in CC. The CSC and CC specimens have approximately comparable experimental stiffness.

Table (2-1): Details of reinforcement for beams, **(Gunasekaran et al., 2014**).

Beams	Longitudinal reinforcements	Transverse reinforcement	Total volumetric torsional reinforcement %
CC1 & CSC1	2ϕ8mm@ top 2ϕ10mm@ bottom	Φ8mm @ 150 mm c/c	0.924
CC2 & CSC2	2ϕ10mm@ top 2ϕ10mm@ bottom	Φ8mm @ 120 mm c/c	1.142
CC3 & CSC3	2ϕ10mm@ top 2ϕ12mm@ bottom	Φ8mm @ 100 mm c/c	1.381
CC4 & CSC4	2ϕ12mm@ top 2ϕ12mm@ bottom	Φ8mm @ 90 mm c/c	1.584

CC: control concrete. CSC: Coconut shell concrete.

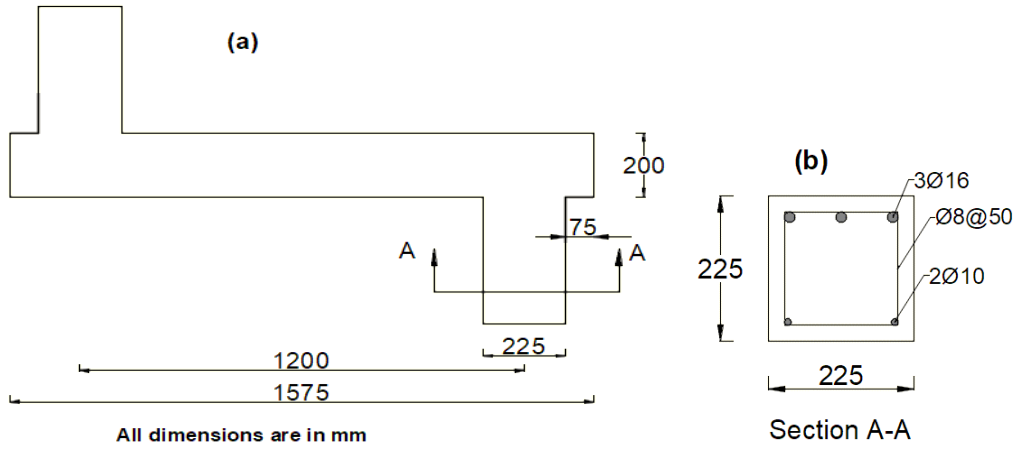

Figure (2-2): (a) Schematic diagram of the top view of the specimen with loading points, (b) The cross sectional and the reinforcement details of the cantilever portion, **(Gunasekaran et al., 2014)**.

Mohaisen et al., 2016, investigated the effects of pure torsion on continuous reinforced concrete beams. Figure (2-3) shows four reinforced concrete beams with the same reinforcing.

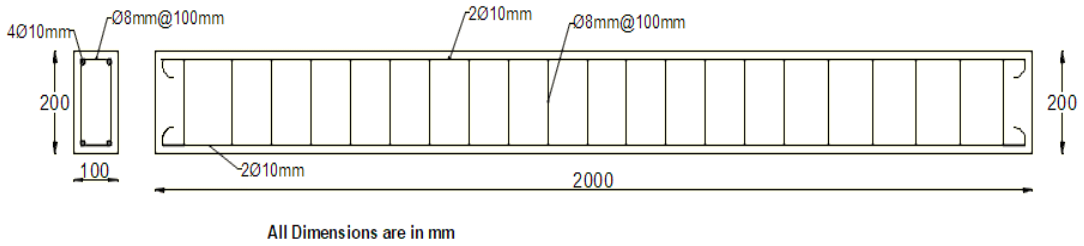

Figure (2-3): Details for dimension & reinforcement of beams, **(Mohaisen et al., 2016)**.

According to achieve the condition of pure torsion, the load must be transferred from the universal testing machine's core to exterior places that represent the load eccentricity, such as the moment arm. There were loading eccentricities ranging from 30 cm to 60 cm. The angle of twist increased by 45.76% when the load eccentricity was increased from 30 cm to 60 cm, while the final failure loads decreased by about 49.65%. The first fracture was also identified, and it was revealed that it happened at higher levels of stress with low eccentricity. The first crack recordings occurred at 75.86%, 70.80%, 63.16%, and 54.79% of ultimate loading for the eccentricities of 30, 40, 50, and 60 cm, respectively.

Kandekar & Talikoti, 2018, investigated the use of aramid fiber strips to strengthen reinforced concrete (RC) beams for torsional behavior. In order to test for torsional failure, the RC beam is reinforced with aramid fiber strips and torqued lever arms are used. A total of 21 reinforced concrete rectangular beams, with and without torsional reinforcement, were cast for the experimental research as illustrated in Figure (2-4). Three controlled beams were cast for each one, with normal reinforcement and with torsional reinforcement, respectively, and the remaining 15 beams with normal reinforcement have been grouped into five sets. Strengthening of these five sets is accomplished by the use of 150 mm-wide Aramid fiber strips spaced at intervals of 100-125-150-

175-200 mm. Figure (2-5) depicts a pure torsion test setup attached to a universal testing equipment.

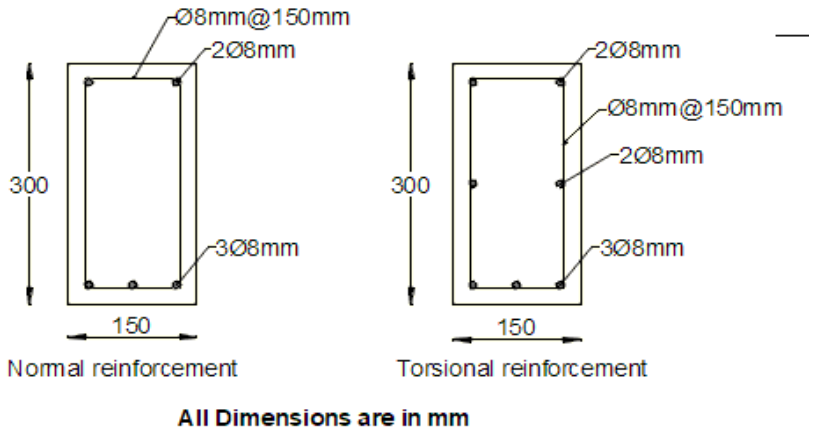

Figure (2-4): Cross section of controlled beam (normal reinforcement) and beam designed for torsion, **(Kandekar & Talikoti, 2018**).

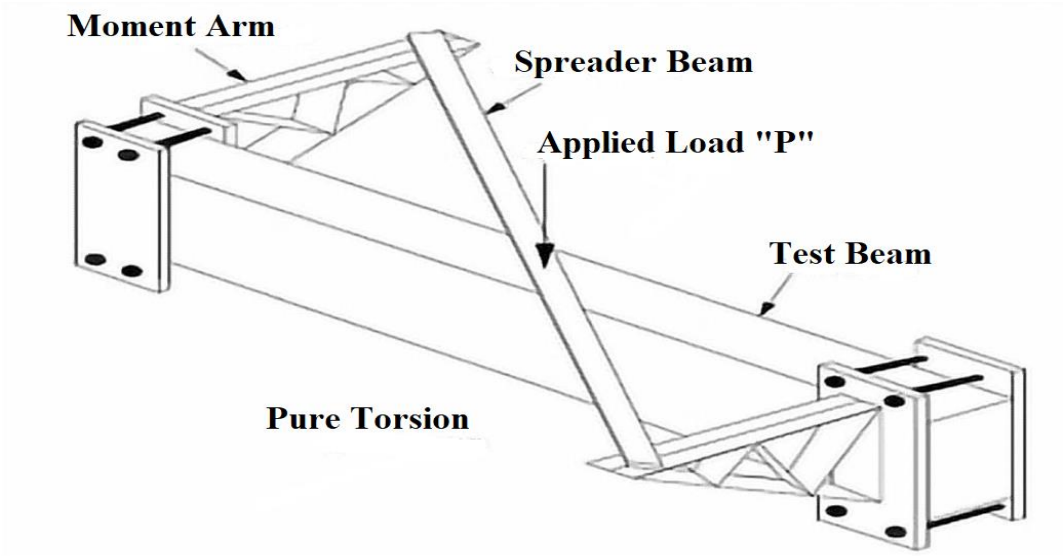

Figure (2-5): Torsion test setup diagram, **(Kandekar & Talikoti, 2018)**.

When compared to the controlled beam, the torsional moment bearing capacity of strengthened beams is improved. In the case of strengthened beams, initial cracks emerge for higher moments. The moment-bearing capability of the reinforced beam coated in aramid fiber

strip at 100 mm spacing with 150 mm aramid fiber strip was greatest. As beams are strengthened with 100 mm and 200 mm spacing, their ultimate moment carrying capacity increases by 140% and 100%, respectively, when compared to controlled beams and is 11% and 25% less when compared to torsional designed beams. With slight differences in the angle of twist, the torsional moment carrying capacity decreases as strip spacing increases.

Nitesh et al., 2019, studied the impact of steel fiber with varrying aspect ratios on the fresh, hardened, and torsional characteristics of self-compacting concrete (SCC), as well as compared it to vibrated concrete (VC). Using crushed concrete examples, the impact of recycled coarse aggregate (RCA) with a quarter replacement of natural aggregates is studied. A parametric variation in plain and fiber reinforced concrete, an aspect ratio of hook end steel fiber, a concrete form with a 20 MPa and an 80 MPa capacity, and 0.5 percent fiber dosage by volume of concrete were used to cast 32 beams with dimensions of 100x200x2300mm.An improvement in torsional strength and twist angle compared to plain beams was achieved with the addition of steel fibers with an aspect ratio of 70 to the conventional concrete mixture. As opposed to this, adding steel fibers with an aspect ratio of 70 to high-strength concrete (VC and SCC) increased ultimate torsional strength and twist angle by 14.28%, 57.75%, and 18.38%, 83.02%, respectively. Plain SCC to mix with aspect ratio 70 RCA, twist at maximum torque, angle of twist, and toughness improved by 21.33%, 31.5%, and 75.36%, respectively, compared to plain VC. When plain VC was compared to mixes with an aspect ratio of 70 RCA, the twist at maximum torque, angle of twist, and torsional toughness increased by 21.98%, 24.77%, and 57.41%, respectively.

Ibrahim et al., 2020, investigated nine RC beams were tested for pure torsion, with thicknesses of clear concrete cover varying from 16–46 mm. The impact of the spacing of transverse reinforcement on beam strength was thoroughly evaluated in conjunction with concrete cover depth. The specimens had a rectangular shape with a width of 300 mm and a depth of 200 mm when they were cast. The specimen measured 1.5 meters in length as shown in Figure (2-6).

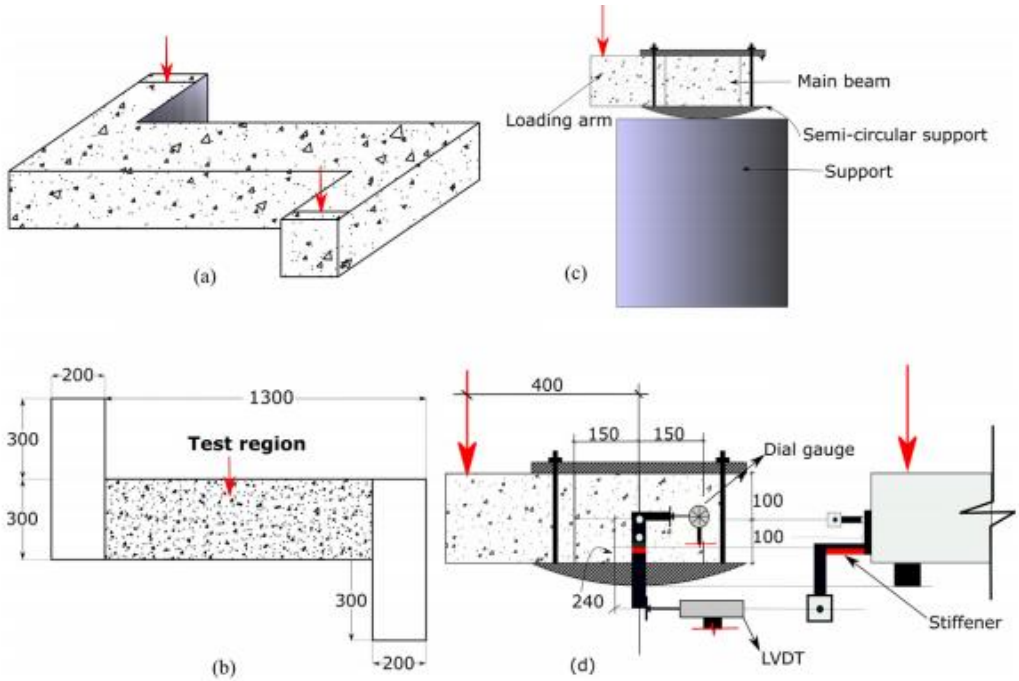

Figure (2-6): Test set up (a) 3D view of the specimen (b) Top view and test region (c) Support detail (d) instrumentation (front and side view) (all dimensions are in mm), **(Ibrahim et al., 2020)**.

Three groups of specimens there, each one contains three specimens. The first and second sets had a 40 MPa design compressive strength. In third Set, the cubic compressive strength of the concrete was 60 MPa. As a consequence, four 12-mm-diameter longitudinal rebars were inserted into each specimen. The first and third sets of transverse rebar are 8 mm in diameter and placed 80 mm apart, as indicated in

Figure (2-7). Set 2 specimens are reinforced with a 10 mm diameter rebar separated by 130 mm center to center, as shown in Figure (2-8).

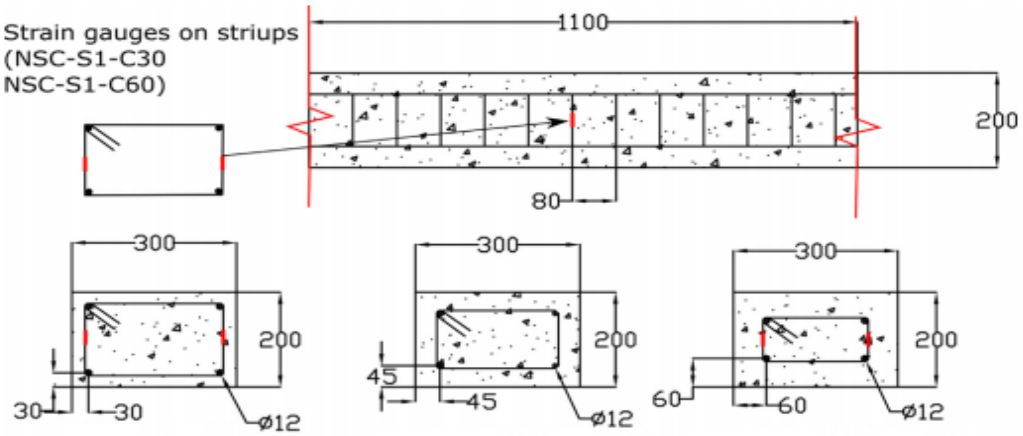

Figure (2-7): Detailing of the specimens for first and third sets (all dimensions are in mm), **(Ibrahim et al., 2020)**.

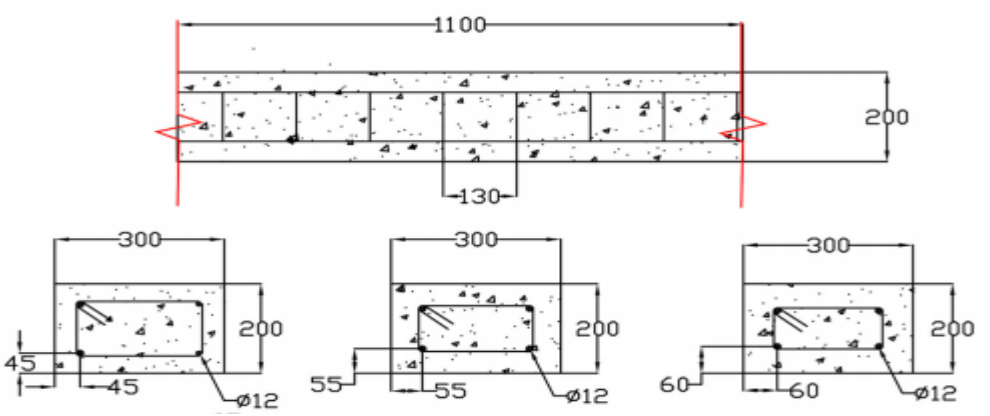

Figure (2-8): Detailing of the specimens for second set (all dimensions are in mm), (**Ibrahim et al., 2020**).

According to the experiment, the thickness of the cover concrete has a significant influence on the torsional and failure behavior of the member. Crushing diagonally softened concrete and spalling concrete cover together controlled the collapse of beams with limited protection. Concrete cover spalling reduced the torsional capacity of specimens with a large cover.

2.3 Experimental Work on Reinforcement Concrete Beams under Combined Bending and Torsion.

Tudu, 2012, investigated the experimental behavior of rectangular reinforced concrete simple supported beams reinforced with externally bonded Glass Fiber Reinforced Polymer (GFRP) textiles and subjected to combined flexure and torsion. For the experimental study, a total of nine reinforced concrete rectangular beams were cast with the same reinforcement for all beams as shown in Figure (2-9).

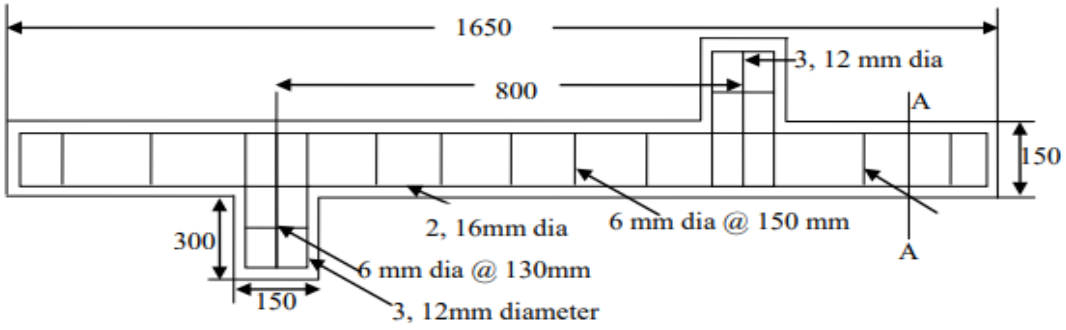

Top view of Torsional Beam

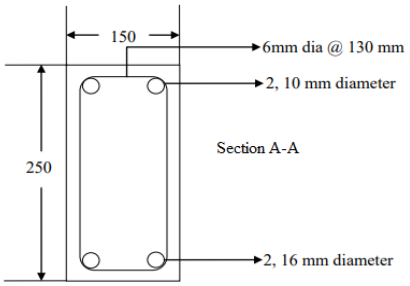

Figure (2-9): Detailing of beam reinforcement, **(Tudu, 2012)**.

All nine torsional weak beams are cast, with one being used as a control beam and the other eight being strengthened with (GFRP). In four separate series, the eight beams were strengthened with GFRP. Each series includes two beams, one unidirectional and the other bidirectional GFRP. SERIES-1 were continually totally wrapped GFRP, SERIES-2 with 100mm GFRP strips, SERIES-3 with 50mm GFRP strips, and

SERIES-4 with 50mm GFRP strips forming 45° with the axis of the beam. The use of bidirectional GFRP sheets did not raise the ultimate strength of the beam, but it did raise its ductility, according to the test results. When compared to the control beam, the load carrying capability of the reinforced beam entirely wrapped with unidirectional fiber was determined to be the highest of all the beams, increasing by 88.46 %. In terms of load carrying capacity and angle of twist, the beams in Series 4 provided the best results.

Abduljalil et al., 2012, investigated carbon fiber reinforced polymer (CFRP) reinforcement of reinforced concrete rectangular beams subjected to coupled torsion and bending. Eight medium-sized reinforced concrete rectangular beams with a length of 1500 mm and a cross section of 120 x 200 mm were cast. All beams were reinforced as shown in Figure (2-10).

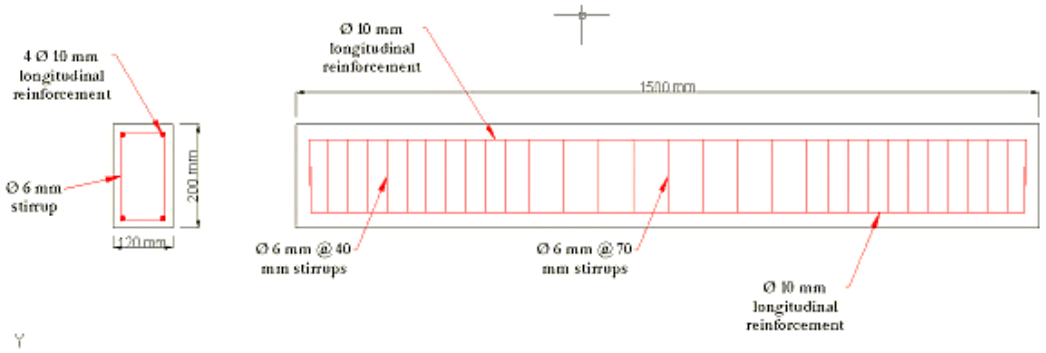

Figure (2-10): Details of beam reinforcement, **(Abduljalil et al., 2012)**.

The beams that were put to the test were classified into four categories as shown in Figure (2-11). In the first category, two beams were subjected to combined torsion and bending testing (with T/M > 1). In the second category, two beams were tested for pure torsion. Third category beams are subjected to combined torsion and bending testing when T/M is less than 1. Two beams were tested under pure bending in the fourth category. The ultimate torque of R.C. rectangular beams strengthened with CFRP strips rose by 108.5 percent under combined

torsion and bending (T/M > 1), whereas pure torsion increased the ultimate torque by 150 percent. Strengthening R.C. rectangular beams with CFRP strips increased the ultimate bending moment by 68.8 percent under combined torsion and bending (T/M < 1), whereas pure bending increases the ultimate bending moment by 65.9 percent. The cracking strength, post-cracking twist, and cracking stiffness increased in pure torsion more than in coupled torsion and bending. When torsion and bending are coupled (T/M < 1), the maximum bending deflection is smaller than in the case of pure bending.

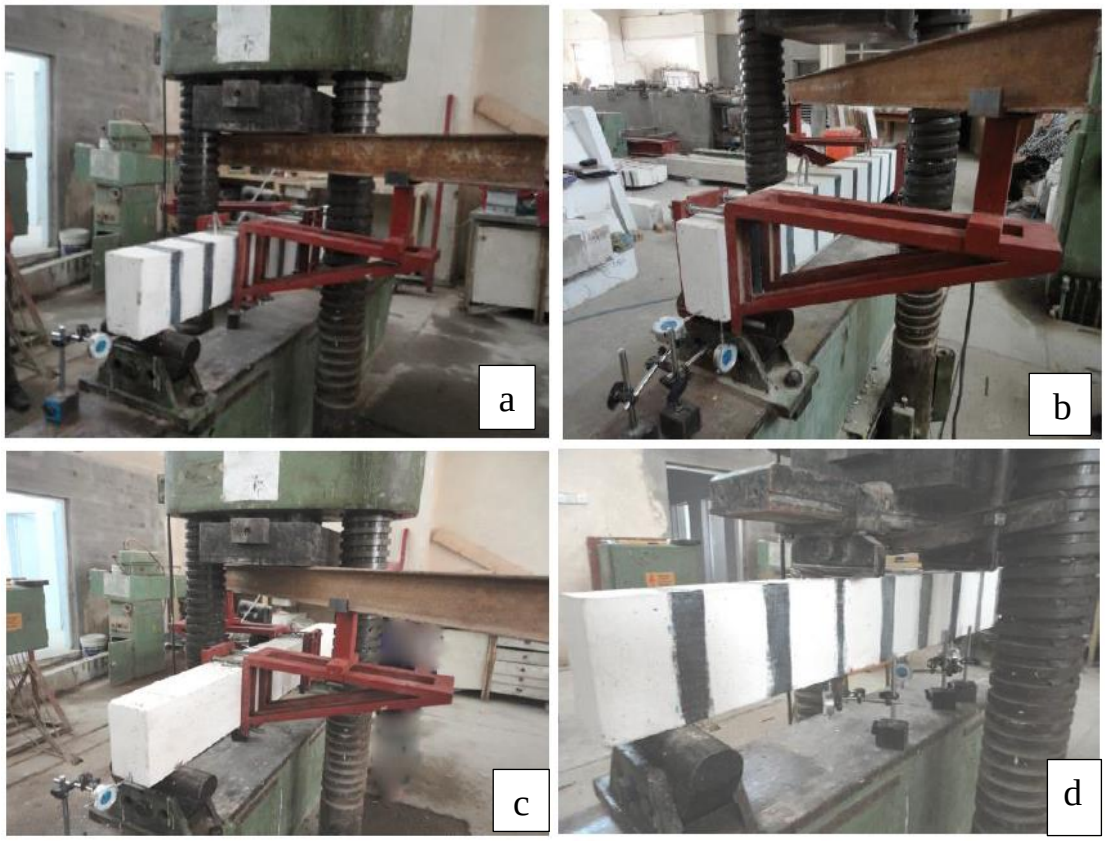

Figure (2-11): The setup of beams in the universal measuring machine. a: Clamping torsional arm (T / M =1.38), b: under pure torsion, c: Clamping torsional arm (T / M = 0.75), and d: Pure bending moment setup.

Ajeel, 2016, studied six similar beams with the same dimensions and reinforcement as shown in Figure (2-12), but the external loading configuration was different. Under torsion, bending, and shear, four beam

specimens with gradually descended values of bending/torsion ratio (λ) from 2 to 1.7 were tested. Another two beam specimens were examined as reference specimens for the other four, one under pure bending moment and the other under pure torsion moment.

Diverting concentric points load in the middle zone to reduce λ (from 2 to 1.7) resulted 200% increase in beam resistance to combined torsion, bending, and shear. For combined loaded reinforced concrete beams exposed to combined torsional moments, bending moments, and shear forces, the loading setup may also restore stiffness, preserve the flexure mode of failure, and raise the design safety factor.

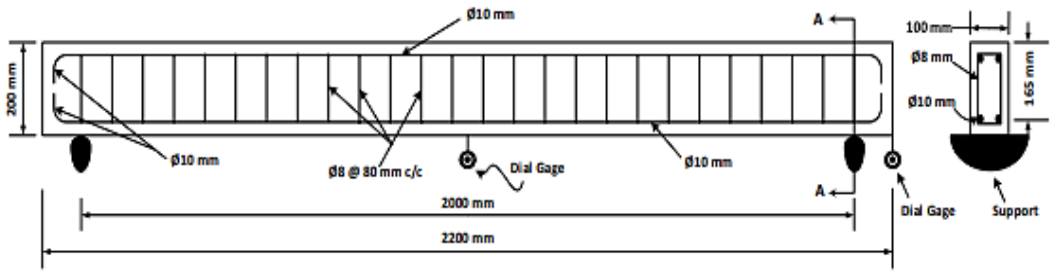

Figure (2-12): Details of beams (reinforcement & dimension),**(Ajeel, 2016)**.

Xu et al., 2018, studied three large specimens of U-shaped thin-walled RC beams under variable torque–bending moment ratios (T–M ratios) of 1:5, 1:1, and 1:0 to study mechanical characteristics such as crack patterns, reinforcing stresses, failure modes, and ductility. All three beam specimens had the same steel reinforcement, including longitudinal bars and stirrups as shown in Figure (2-13). It is seen in Figure (2-14) that the specimens are referred to as the T-M ratios of 1:5, 1:1, and 1:0, respectively.

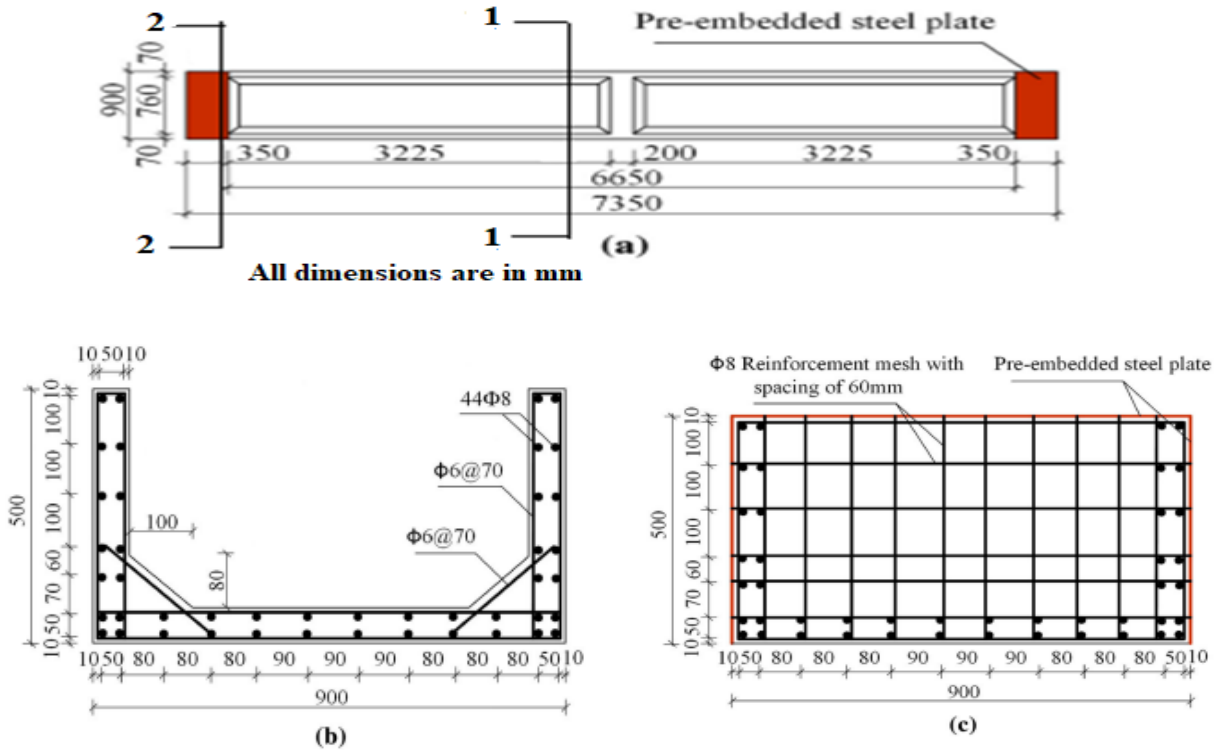

Figure (2-13): Information of U-shaped thin-walled RC beam specimens. a: Top view of U-shaped thin-walled RC beams, b: Cross-section 1-1, and c: cross-section 2-2, **(Xu et al., 2018)**.

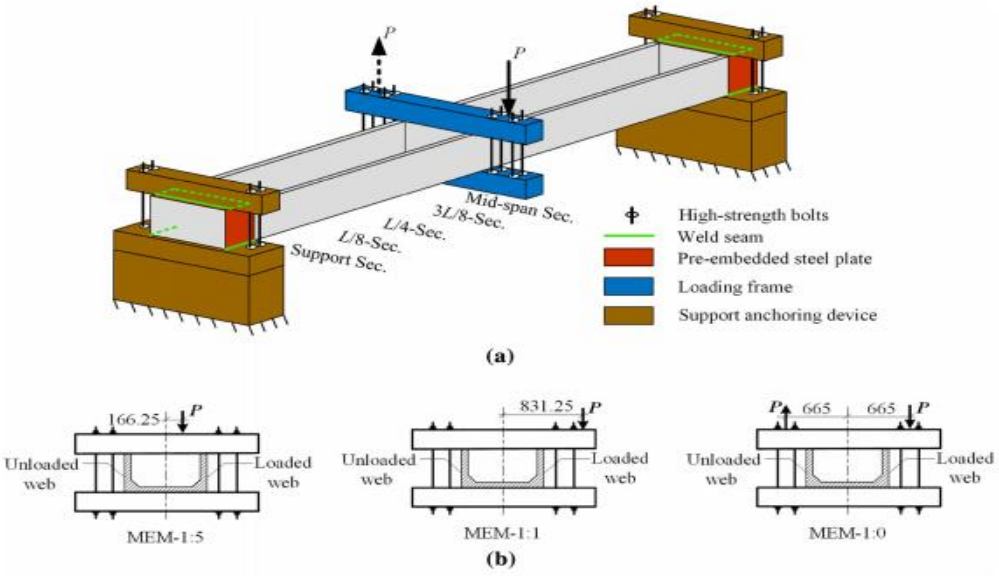

Figure (2-14): Testing setup of U-shaped thin-walled beams (all dimensions are in mm). a: Schematic diagram of testing setup, b: loading information of test specimens, **(Xu et al., 2018)**.

Using a T–M ratio of 1:5, the first diagonal crack began at the 3L/8 part, using a T–M ratio of 1:1, at the 5L/16 section, and using a T–M ratio of 1:1, at the L/4 section. As the T–M ratio climbed from 1:5 to 1:1, the diagonal cracking torque was reduced from 49% of the ultimate torque to 24%. While mid-span deflections decrease with increasing T–M ratio, rotations increase with increasing T–M ratio. There were more diagonal fractures and more strains in the stirrups as the T–M ratio rose. This meant that the overall shear stress caused by circulatory torque, warping torque, and shear force went up.

Deifalla et al., 2020, investigated the behavior of lightweight foamed concrete (LWFC) T-beams under combined shear, torsion, and moment. The researchers looked at shear-span-to-depth ratio (a/d), torsion-to-shear depth ratio (T/V_d), flange-to-web-width ratio, and transversal reinforcement ratio in five distinct beams. A combination of bending moment, shear stress, and torsion moment might be provided in the crucial area of a continuous T-beam on the interior support. A half-scale model of the beam from the inflection point to maximum moment at support has been selected for the test specimen, as shown in Figure (2-15).

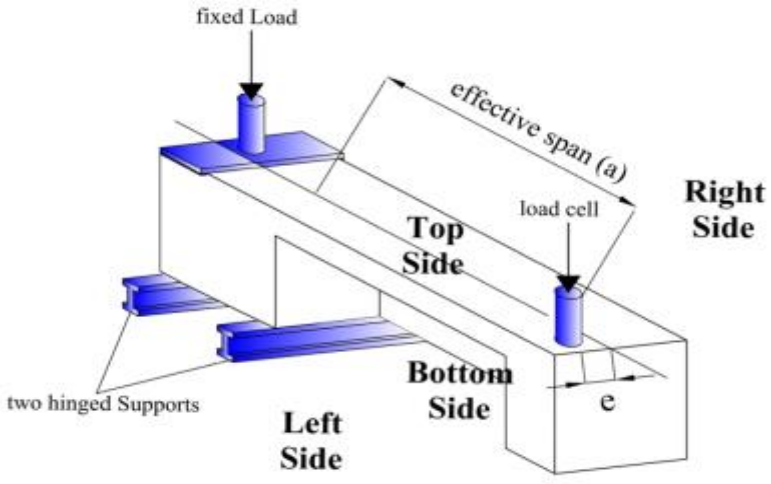

Figure (2-15): diagram of the test setup, **(Deifalla et al., 2020)**.

Figure (2-16), illustrates the cross-section reinforcements details of all specimens. The T-beam designation that has been tested is a three-portion term. The first portion reflects the type of concrete, L for light weight concrete or N for normal weight concrete, the second portion appears to be the ratio of (a/d), and the third portion symbolizes the ratio of torsion/shear-depth (T/V_d). Normal concrete was used to cast the first beam, N-3.5–0.13, and LWFC was used to cast the other four beams, L-3.5–0.13, L-3.5–0.38, L-1.2–0.13, and L-1.2–0.38.

The maximum strength of reinforced LWFC T-beams decreased by 9 to 12 percent, but the maximum deflection rose by a factor of 25 to 35 percent compared to ordinary weight concrete.

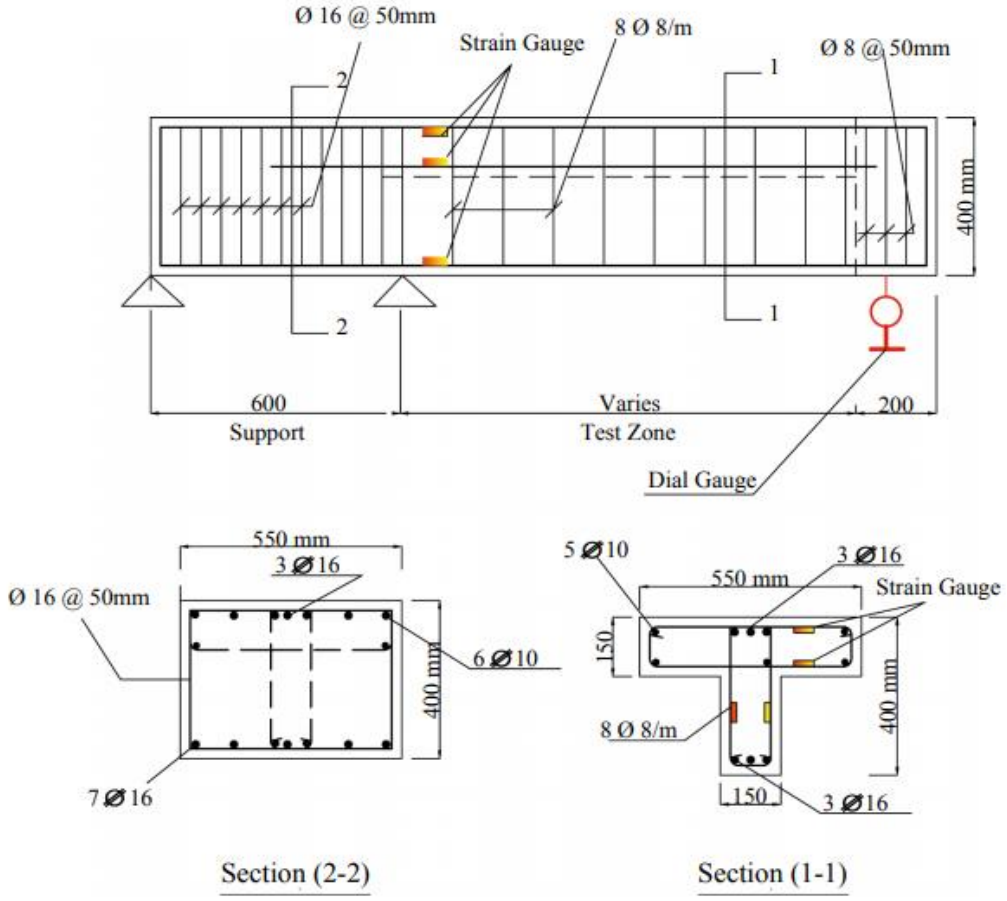

Figure (2-16): Typical dimensions, reinforcing details, and strain gauge distribution for tested T-beams, **(Deifalla et al., 2020)**.

The strength of reinforced LWFC T-beams enhanced by 40% with a 65% reduction in the (a/d). When raising the ratio of torsion/shear-depth by 67%, the failure load was reduced by 28% for T-beams with a ratio of shear-span/depth of 1.2.

2.4 The Behavior of Rubberized Concrete Members subjected to loads

Hassanli et al., 2017, investigated the behavior of rubberized concrete in structural applications. Four reinforced concrete (RC) beam specimens composed of rubberized concrete with crumb rubber replacing 0%, 6%, 12%, and 18% of the sand volume, tested. The specimens were subjected to cyclic loading and their results were compared, including damage pattern, failure mode, force-displacement response, and energy dissipation behavior. As seen in Figure (2-17), all beam specimens were 130 mm wide, 220 mm high, and 2800 mm in length. Similar flexural and shear reinforcements were put in place for each of them.

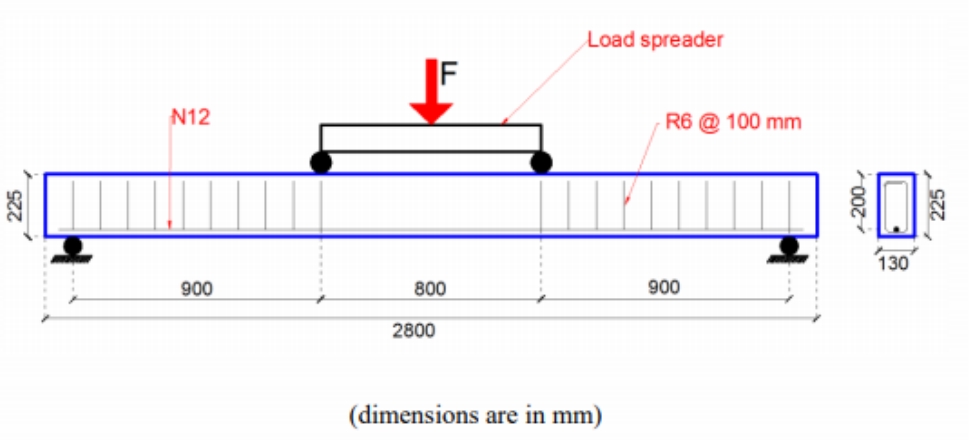

Figure (2-17): Beam specimen dimensions and details of reinforcement, **(Hassanli et al., 2017)**.

The deflection capability of the rubberized concrete beam increase from 7.7 percent to 27.9 percent when compared to a concrete beam with

no rubber ingredient. As a result, although the compressive strength of concrete decreased by 31%, the strength of the equivalent tested beam decreased by only 6%. This is because the capacity of the member is mostly determined by reinforcement, and concrete's compressive strength has less of an impact. The use of rubberized concrete for flexural members with ductile reactivity is being promoted.

Hasan, 2018, studied the behavior of fiber reinforced self-compacting rubberized concrete beams. The geometry of specimens, twelve beams as indicated in Figure (2-18). Two reference beams were included in the first of five groups created for the beams (self-compacting concrete and steel fiber reinforced self-compacting concrete with a volume fraction of Vf=1.5%). Other group's beams had various sizes and percentages of discarded tire rubber with steel fiber (Vf=1.5%). Rubbers were utilized in these beams in varying quantities (10% and 20%) instead of coarse aggregate with size (9.5-1.18) mm and fine aggregate with size (4.75-0.15) mm. Also, instead of limestone dust (125µm size) and silica fume (2.5µm size), waste tire rubbers were employed as filler materials in various ratios (12%, 25% and 50%).

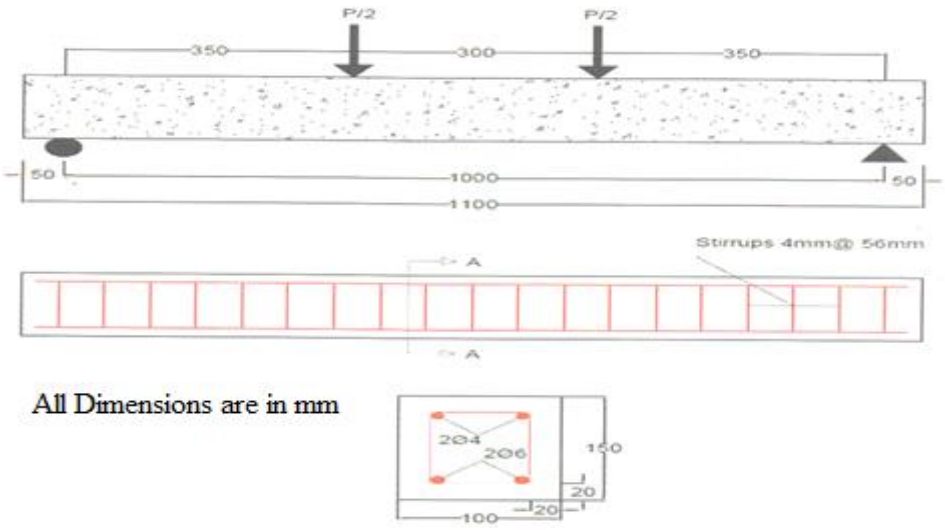

Figure (2-18): Beam dimension and reinforcement details, **(Hasan, 2018)**.

When 20% of coarse aggregate was substituted with chip rubber and 20% of fine aggregate was replaced by crumb rubber, the ultimate load fells about 3.9% and 21.6%, while the deflection rose by about 77.3% and 46.1%, respectively. It is preferable to replace the coarse aggregate with rubber rather than fine particles. When 12%, 25%, and 50% of the limestone was replaced with ground rubber, the load carrying capacity varies by 1.9%, -2.0%, and 0%, respectively, while the deflection increased as the rubber content increased. When 12%, 25%, and 50% of the silica fume was replaced by extremely fine rubber, the load carrying capacity was reduced by 3.9%, 9.9%, and 32.5%, respectively. As the rubber content increase, the deflection at ultimate load decreased. By introducing rubber particles and tiny steel fibers, the failure mode of the tested beams changes from brittle to ductile.

Karthikeyan et al., 2019, conducted their research about the rubberized concrete beams with micro-reinforcement for strength and ductility. Seven full-scale beams with dimensions of 150mm × 250mm and a length of 3m were manufactured and tested. One of the beams was used as a control. The remaining six beams were made with micro-reinforcement and pretreated additional aggregates. The key variables were the amount of rubber shreds and the amount of micro-reinforcement. Rubber shreds of 20 mm diameter with a specific gravity of 1.24 were made from conveyer belt. There were three distinct pretreatment rubber shred levels used in the creation of the specimens (2.5, 5, and 7.5 percent), as well as two different degrees of micro-reinforcement in the final product (0.5 and 1.0 percent). Figure (2-19) shows where the reinforcement will be placed. Until failure, the constructed specimens were subjected to monotonic loading.

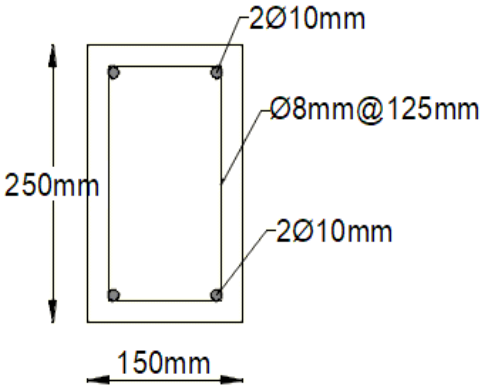

Figure (2-19): Geometry and reinforcement details of specimens, **(Karthikeyan et al., 2019)**.

Flexural strength is increased by 20.8 percent, deformation capacity is increased by 107.5 percent, ductility is increased by 40%, and energy capacity is increased by 83% for rubberized concrete beams with replacement 7.5% rubber and added micro-reinforcement of 1%. This suggests that they are suitable for structural applications. In all of the specimens, the major mode of failure was flexure.

Kadhim, 2020, investigated the experimental behavior of continuous deep beams with rubber as the replacement aggregate in concrete. In this study, the influence of shear span-to-overall-height ratios, size effect, and the quantity of rubber used to replace natural aggregate on continuous deep beam shear load capacity is examined. The test specimens are fourteen two-span large-scale models, two of which are composed of regular reinforced concrete and the others from rubberized reinforced concrete. The test specimens were identical in terms of geometrical dimensions and reinforcing details, as illustrated in Figure (2-20).

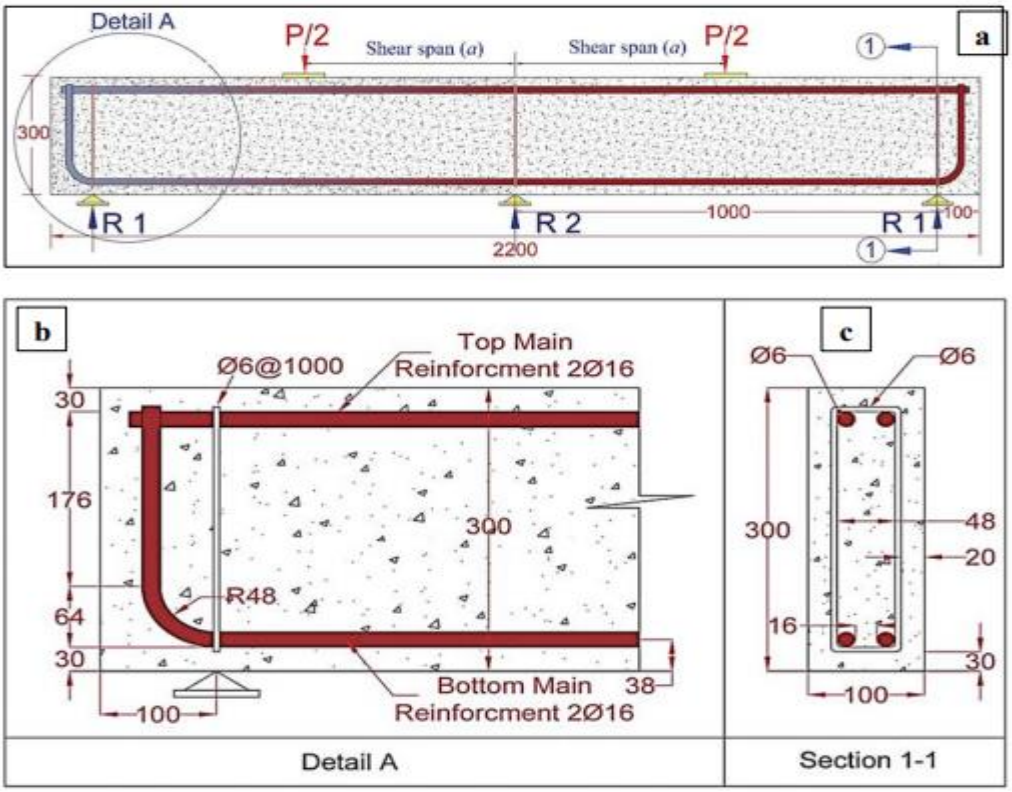

Figure (2-20): Details of the test specimens: a- Overall dimensions and reinforcement details; b- Detail A; c- Section (1-1), **(Kadhim, 2020)**.

Increasing the ratio of chip and crumb rubber from 0%–20% reduced the shear load of tested beams at ultimate by 32.06 % and 32.65 %, respectively, but significantly increased the deflection at ultimate by 106.28 % and 83.07 %, confirming that crumb rubber replacement has a slightly greater negative impact on beam shear strength than chip rubber replacement. Increasing the a to h ratio from 1.33 to 1.67 raises the load of beams at failure by 2.16–3.41%, and rubberized beams behave similarly to conventional beams. As the rubber content in the continuous deep beam rises, so does its ductility. Chip and crumb rubber replacements of 20% of the reference mixture of gravel and sand resulted in toughness indices of 36.95% and 20.42 %, respectively, confirming that chip rubber replacement had a slightly greater beneficial influence on toughness than crumb rubber replacement.

Sahib, 2020, studied the punching shear strength of rubberized reinforced concrete flat plates. The experimental program is made up of fifteen flat plates that represent inner connections between the slab and the column. The dimensions of the slab are 900 x 900 x 80 mm. The model type column was investigated, as well as the chip rubber ratio, which was employed instead of coarse aggregate. According to the shape of the column, there are three types of cases: square, rectangular, and circle. Each case contains five specimens, the first of which was cast with normal strength concrete and the others with chipped rubberized concrete, in percentages of 5%, 10%, 15%, and 20%.

When the replacement ratio is equal to 5%, 10%, 15%, and 20%, increasing the percentage of chip rubber instead of the coarse aggregate reduces the punching strength by 3.25%, 7.12%, 9.97%, and 13.54% for square column specimens, 3.31%, 7.27%, 12.51%, and 18.52% for rectangle column specimens and 2.79%, 8.84%, 12.77%, and 20.89% for circle column specimens. Chips of rubber enhanced the specimen's final deflection. The following were the increments in ultimate center deflection of all slabs: 7.11%, 12.30%, 15.56%, and 24% for square column specimens, while for rectangle column specimens were 3.49%, 8.64%, 14.29%, and 24.58%, and 6.27%, 13.41%, 17.25%, and 24.22% for circle column specimens, for the replacement ratio is equal to 5%, 10%, 15%, and 20%, respectively. Increases in the energy-absorbing of 41.41%, 28.75%, and 20.88% for the square column, rectangle column, and circle column models, respectively, when the percentage of rubber has increased from 0-20%. The ductility index of samples increased by 20.38%, 15.60%, and 12.87% for square, rectangle, and circle column models, respectively, when chips of rubber were employed instead of coarse aggregate.

2.5 Rubberized Concrete

Ganjian et al., 2009, studied the concrete mixes that used 5%, 7.5%, and 10% recycled rubber as aggregate and cement substitutes. Two sets of concrete specimens were constructed to study the features of tire crumb-containing concrete. For aggregate replacement at 28 days, concrete had a 10%–23% drop in compressive strength, while cement replacement had a 20%–40% reduction. Concrete's modulus of elasticity decreased by 17%–25% when 5%–10% of the aggregate was replaced by chipped rubber, but the loss was 18–36% when cement was substituted by powdered rubber. Concrete's tensile strength decreased by 30%–60% when 5%–10% of the aggregate was replaced with chipped tire rubber, whereas tensile strength decreased by 15%–30% when cement was substituted with powdered rubber. The replacement of 10% of coarse aggregates by rubber resulted in a 37% loss in the flexural strength of concrete and a 29% reduction when replacing the cement with powdered rubber. In the case of replacing coarse aggregate with rubber, it increased the depth of water permeability in the concrete mix and raised absorption of water, when cement was replaced with powder rubber, it decreased water absorption.

Dumne, 2013, studied recycled rubber tire aggregates were used as a partial substitute for coarse aggregates in a concrete mix. Rubberized concrete is made by preparing three distinct concrete mixes of the same concrete grade, with coarse particles partly replaced by 5%, 10%, and 15% of rubber aggregates of equal volume. Furthermore, normal concrete of the same grade is made without the use of coarse aggregates. Test findings for rubberized concrete reveal that adding rubber particles reduces compressive strength significantly when compared to normal concrete, which has compressive strengths ranging from 28.95% to 55.21%. Substitution of 15% of coarse aggregates with rubber in the

sample results in a 14.33% reduction in unit weight.

Siddiqui, 2016, examined the possibility of using rubber fragments as coarse aggregate in concrete. On a volume basis, natural aggregates are substituted by rubber aggregates and the rubber percentages of 0%, 5%, 10%, and 15% were evaluated. By manually cutting the tire, the chipped rubber samples were acquired and passed through a 20 mm sieve, as shown in Figure (2-21). The compressive strength of concrete specimens is one of the investigation's parameters. Concrete cubes of 150 × 150 × 150 mm are cast for compressive strength testing.

The slump has been reduced as a result of increasing the ratio of rubber particles in all concrete mix samples. Due to the increase in the amount of rubber tyre aggregates to 15%, the unit weight of rubberized concrete lowers by 14.33%. The test findings demonstrate that adding rubber aggregates in proportions of 5%, 10%, and 15% results in a large reduction in compression strength of 28.96%, 42.90%, and 55.22%, respectively when compared to conventional concrete.

(a) Before Cutting (b) after cutting

Figure (2-21): Rubber samples, **(Dumne, 2013)**.

Marie, 2017, investigated the feasibility of integrating different percentages of recycled concrete aggregate and crumb rubber to make a hybrid recycled aggregate-rubberized concrete with appropriate physical and mechanical qualities and thermal conductivity lowered. In varying amounts ranging from 5% to 20% by weight, recycled concrete aggregate partially substitutes aggregate. Fine aggregates were substituted for 10% and 20% of the volume in concrete mixes by crumb rubber. Hybrid recycled aggregate-rubberized concrete mixes were made using a fixed percentage of 10% crumb rubber and recycled concrete aggregate that partially replaced aggregate in varying percentages ranging from 5% to 20% by weight. The thermal conductance of hybrid recycled aggregate-rubberized concrete, which contains 10% rubber and 10% recycled concrete aggregate, is reduced by 32% when compared to the reference mix of conventional aggregate concrete. This decrease in thermal conductivity of hybrid recycled aggregate-rubberized concrete might be advantageous as an insulator and help conserve the environment.

Miller & Tehrani, 2017, looked at the mechanical characteristics of an innovative new lightweight aggregate concrete made from recycled tires. A thorough assessment of rubberized lightweight aggregate concrete, as illustrated in Figure (2-22), made use of 38 specimens of cylinders and 36 specimens of the beam. The target strength of the control mix was 21 MPa. Afterward, the lightweight coarse aggregate was replaced by volume with the tire-derived material. Replacement ratios ranging from 0% to 100% in 20% increments were employed for both cylinder and beam specimens. Cylinders were used to measure compressive strength, static modulus of elasticity, and splitting-tensile strength. A flexural strength and toughness test were investigated using beam specimens.

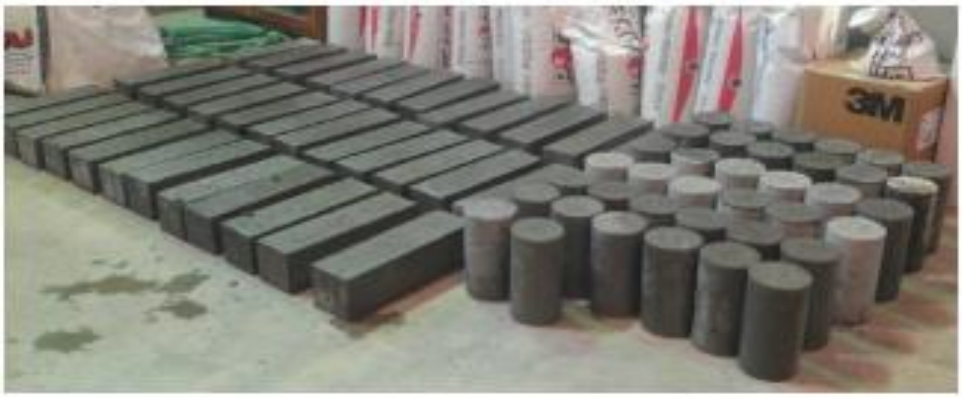

Figure (2-22): Cylinder and beam specimens, **(Miller & Tehrani, 2017)**.

The static mechanical properties of a product decrease as the quantity of rubber used in it increases. Flexural toughness is improved when rubber replacement values of 80 percent and 100 percent are employed. Energy absorption at high rubber replacement values looks to be a good use for this material.

2.6 Concluding Remarks

The following findings may be taken from the prior literature review:

1- The transversal reinforcement volume has a greater effect on the torque capacity of the beam because the associated principal tensile stress causes inclined cracks on the beam surface in the principal compressive stress direction.
2- The ultimate failure loads decreases and the angle of twist increases when the load eccentricity was increased because the torsional moment increased.
3- The failure of the specimens for beams with little cover was regulated by the dual-action of crushing the diagonally concrete and spalling the cover of concrete. Concrete cover spalling reduced the strength of the specimens with a large concrete cover because it decreased the cross-section area.

4- The inclusion of torsional moment increases the beam's resistance to combined loads as compared to pure bending or torsional moment alone.
5- Rubberized concrete should be used more for flexural members with ductile response since the loss in capacity of flexural strength caused by the content of rubber is less than that produced by compression strength.
6- Reinforced concrete beams' ultimate load decreased while their deflection increased when coarse aggregate was substituted with chip rubber.
7- The ductility and the Energy Absorption Index of the reinforced concrete beam increases as the rubber content increases.
8- As it is known, when chipped rubber was used instead of coarse aggregate, the compression strength, splitting tensile strength, rupture strength, and elasticity all decreased.
9- As a result of the lack of good bonding between rubber particles and cement paste, water permeability depth and absorption rise, but the concrete's unit weight is reduced.
10- As a result of the low specific gravity of rubber particles relative to the specific gravity of coarse aggregate, the slump has been decreased when increasing the amount of rubber particles in all concrete mix samples.
11- When compared to a reference mix of traditional aggregate concrete, The thermal conductivity of a mixture of recycled aggregate and rubberized concrete is lower.

As a result, the goal of this study is to present the experimental and analytical analysis into the ultimate torque, angle of rotation, stiffness, ductility, energy absorption, and failure modes of rubberized

reinforced concrete beams under torsion. The experimental investigation looked at how cross section area, loading type (pure torsion or combined loading), and torsional strength was affected by the quantity of rubber substituted for natural aggregate.

CHAPTER THREE

EXPERIMENTAL WORK

3.1 Introduction

The fundamental objective of this research is to determine whether chip rubber may be used to replace coarse aggregate in reinforced concrete beams exposed to pure torsion and to compound (torsion and bending). Only the study methodology is described in this chapter. All materials and the testing techniques were covered thoroughly, as well as the characteristics of the reinforcements. Also, the amounts of fresh and hardened concrete that mixed are detailed. In addition, a description and an identification of the examined beam specimens will be provided. A detailed description of all the transducers utilized in the testing frame as well as the technique for installing and arranging them is also presented. An experimental flowchart is shown in Figure (3-1).

3.2 Description of the Test Specimens

Experiments were conducted on a variety of building materials and control specimens, including cubes, cylinders, prisms, and thirty concrete beams.

The experiment was carried out at the labs of the University of Babylon department of civil engineering. Normal-strength or rubberized concrete were used to make the tested beams. Table (3-1) lists the specifics of all beams. The specimens are divided into three groups with identical longitudinal and transverse steel reinforcement. An investigation into the effects of partial replacement rubber percentage, depth to width ratio, and loading type was carried out on the specimens in this study.

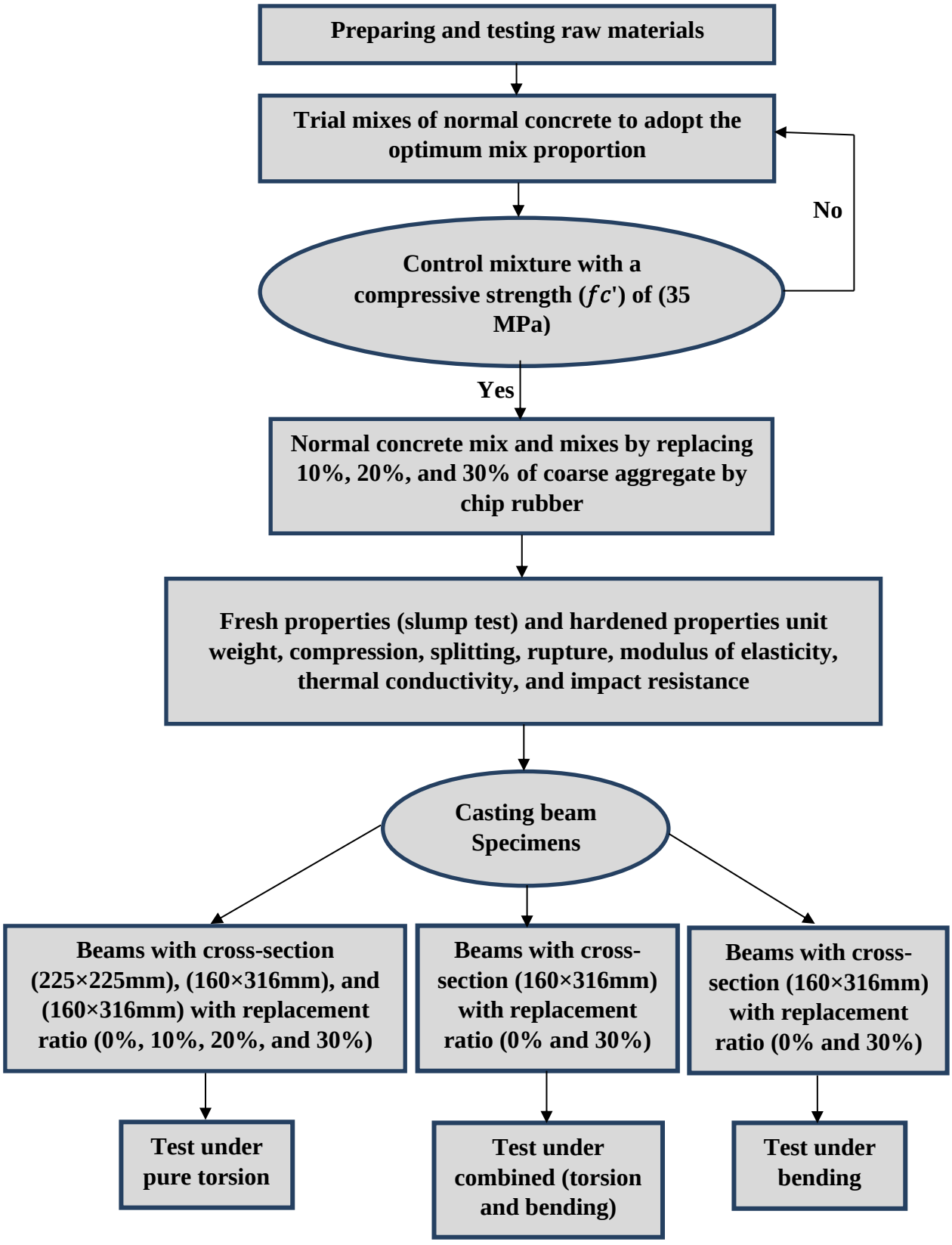

Figure (3-1): Flowchart of experimental work for the research plan.

In the first group of sixteen beams, three sections were evaluated under pure torsion. The first section has six beams are cast of normal strength concrete or rubberized concrete with varied volumetric percentages of rubber as 10%, 20%, and 30% of coarse aggregate in the form of 225×225mm cross-sections. The second section consists of four beams, each one has a cross-section of 160×316mm and a cast of conventional strength concrete as a control beam or rubberized concrete with varied volumetric percentages of rubber as 10%, 20%, and 30%. In the third section, six beams have a cross-section of 130×390mm and are cast of normal strength concrete as a control beam or rubberized concrete with varied volumetric percentages of rubber as 10%, 20%, and 30%. All sections have the same cross-sectional area about (50625mm^2).

The second group has twelve beams with cross-sections of 160×316mm tested under combined bending and torsion, divided into six parts depending upon the ratio of bending to torsion (λ). Each part has two beams; one is cast of normal strength concrete and the other is cast of rubberized concrete with a volumetric percentage of rubber equal to 30% of coarse aggregate. For six parts, the bending to torsion (λ) ratio is 0.5, 0.75, 1, 2, 3, and 4.

Concrete of normal strength and rubberized concrete containing a volumetric proportion of rubber equivalent to 30% of coarse aggregate are used in the third group's tests, which include two beams with 160×316mm cross sections undergo to pure bending.

Longitudinal reinforcement is provided by 4 ϕ12 mm deformed steel bars with concrete cover of 20 mm for all beams. Additionally, the beam is equipped with 86 mm center-to-center steel stirrups, each measuring 8 mm in diameter. In accordance with (**ACI 318-19, 2019**) requirements, all beams have been designed as indicated in Appendix A. The reinforcement

details for the beams are shown in Figure (3-2). The length of the loading arm for the beams in the second group is calculated as indicated in Appendix B.

Table (3-1): Details of the tested beams. (continue)

Group No.	Chip rubber (%)	Type of loading	Specimen Symbol	Case details	depth/ width ratio
1	0	PT	PT-S1R0	Cross-section (225×225mm) Torsion moment arm = 500mm S1	1
	10		PT-S1R10		
	20		PT-S1R20		
	30		PT-S1R30		
	0	PT	PT-S1R0P		
	30		PT-S1R30P		
	0	PT	PT-S2R0	Cross-section (160×316mm) Torsion moment arm = 500mm S2	2
	10		PT-S2R10		
	20		PT-S2R20		
	30		PT-S2R30		
	0	PT	PT-S3R0	Cross-section (130×390mm) Torsion moment arm = 500mm S3	3
	10		PT-S3R10		
	20		PT-S3R20		
	30		PT-S3R30		
	0	PT	PT-S3R0P		
	30		PT-S3R30P		
2	0	CTB	C0.5-S2R0	Cross-section (160×316mm) Torsion moment arm =500mm bending to torsion (λ)=0.5	2
	30		C0.5-S2R30		
	0		C0.75-S2R0	Cross-section (160×316mm) Torsion moment arm =333.3mm bending to torsion (λ)=0.75	
	30		C0.75-S2R30		
	0		C1-S2R0	Cross-section (160×316mm) Torsion moment arm =675mm bending to torsion (λ)=1	
	30		C1-S2R30		
	0		C2-S2R0	Cross-section (160×316mm) Torsion moment arm =337.5mm bending to torsion (λ)=2	
	30		C2-S2R30		

Table (3-1): Details of the tested beams. (Continued)

2	**0**	**CTB**	**C3-S2R0**	**Cross-section (160×316mm) Torsion moment arm =225mm bending to torsion (λ)=3**	**2**
	30		**C3-S2R30**		
	0		**C4-S2R0**	**Cross-section (160×316mm) Torsion moment arm =170mm bending to torsion (λ)=4**	
	30		**C4-S2R30**		
3	**0**	**PB**	**PB-S2R0**	**Cross-section (160×316mm)**	**2**
	30		**PB-S2R30**		

PT: Pure Torsion	**S1, S2, S3: Cross-section one, two, and three**	**P: Plain concrete without reinforcement**
R0, R10, R20, R30: Rubber percentage	**CTB: Combined (Torsion + Bending)**	**PB: Pure Bending**
C1, C2, C3, C4, C0.5, C0.75: Combined bending and torsion with various ratio of bending/torsion (λ)		

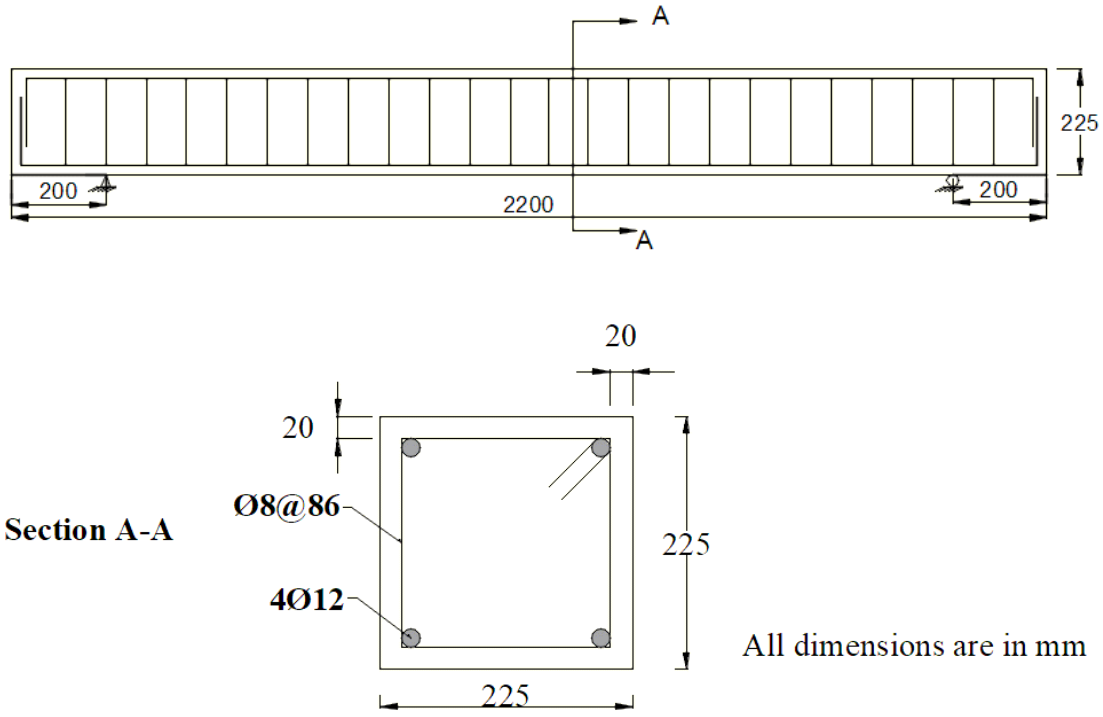

(a) : Details of reinforcement for section one.

Figure (3-2): Reinforcement details of tested beams for three sections.

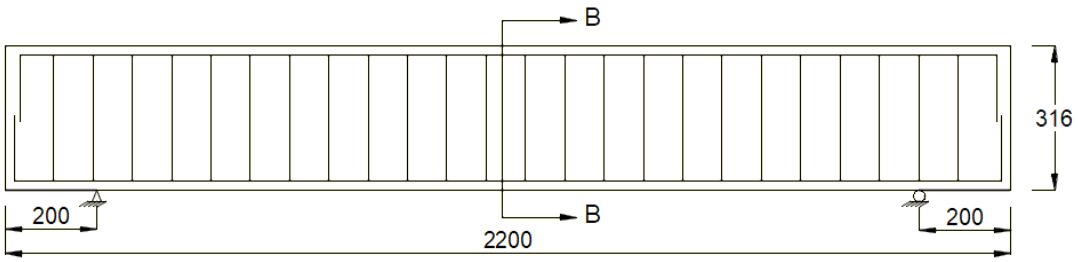

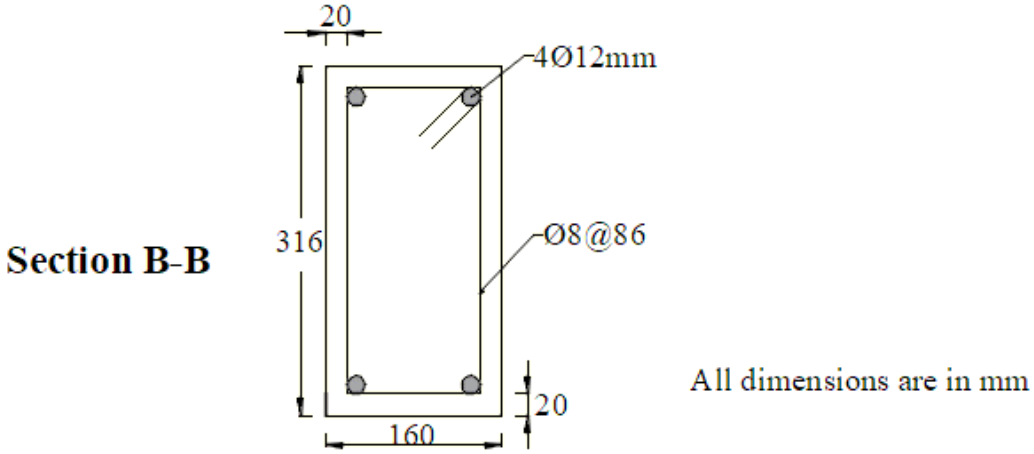

(b) : Details of reinforcement for section two.

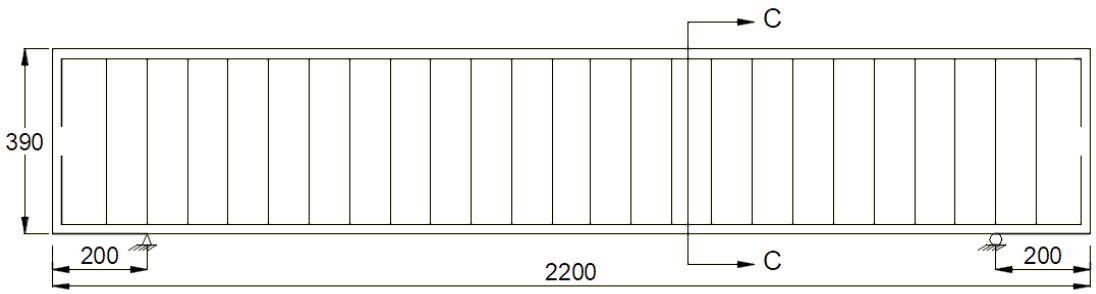

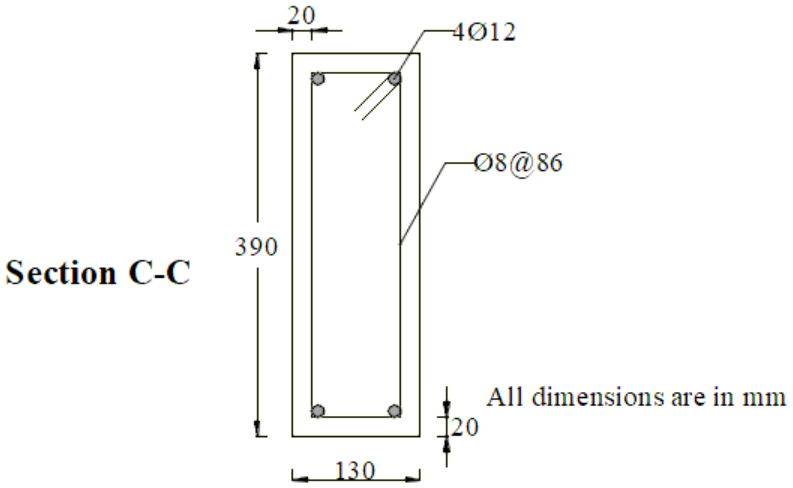

(c) : Details of reinforcement for section three.

Figure (3-2): Continued

3.3 Properties of Materials

In order to prepare concrete, a number of different ingredients must be placed together. These ingredients include aggregate, water, cement, and admixtures. Therefore, understanding the qualities and features of the ingredients is important. Concrete manufacturing requires tight processes in the selection, management, and proportion of all the ingredients in order to assure appropriate output. The materials employed in this experiment are explained in the following paragraphs, which show their origins, chemical compositions, and physical qualities.

3.3.1 Cement

This study made use of ordinary Portland cement. produced in Iraq under the trade name "Karasta" and available in the country's marketplaces. To meet the requirements of the standard, cement is necessary **(Iraqi Specification No.5 -1984, 2010**). Cement's chemical and physical properties are shown in Tables (3-2) and (3-3).

Table (3-2): Chemical characteristics of cement.

Oxides	Content, %	Iraqi criteria (No.5/2010), %
CaO	62.5	-
SiO_2	21.3	-
Al_2O_3	4.2	-
Fe_2O_3	4.4	-
MgO	3.6	<5
SO_3	2.05	<2.5
Free lime	0.82	-
L.O.I.	3.35	<4
L.S.F.	0.91	0.66- 1.02
Insoluble residue	1.18	<1.5

Table (3-3): Cement's physical properties.

Properties	Result	Iraqi criteria (No.5)
Setting time (Vicat apparatus)		
Initial setting, min	105	≥45
Final setting, hrs	3.5	≤10
Compressive strength, MPa		
3 days	18.1	≥15
7 days	27.8	≥23

3.3.2 Fine Aggregate

Natural sand was employed in the production of this study's mixtures. 4.75mm nominal maximum size fine aggregate, having rounded particle form and smooth texture, with fineness modulus of 2.92. Table (3-4) shows the fine aggregate grading according to **(Iraq Specification No.45/1984, 2010**), whereas Table (3-5) lists the fine aggregate's physical and chemical qualities. It was done at Al-mussaib technical institute's testing facilities.

Table(3-4): Sieve analysis of sand

Mesh opening (mm)	Percentage of passing, %	Iraqi criteria (No.45), %
10	100	100
4.75	94.6	90-100
2.36	83.9	75-100
1.18	70.6	55-90
0.60	40.2	35-59
0.30	13.4	8-30
0.15	4.9	0-10

Table (3-5): Physical and chemical properties of fine aggregate

Property	Result	Iraqi specifications (No.45)
Fineness modulus	2.92	----
Materials finer than sieve 75 μm %	2.7	≤ 5
SO3, %	0.32	≤ 0.5

3.3.3 Coarse Aggregate

In the mixes, Badra quarry gravel with a maximum particle size of 14 mm was used as coarse aggregate. To remove the oversize, the pebbles were sieved to a size of 14 mm and then washed several times with water before being allowed to dry. The aggregate's chemical qualities and sieving analysis met (**Iraq Specification No.45/1984, 2010**), as shown in the table below (3-6). This test was conducted in the laboratories of Al-mussaib technical institute.

Table (3-6): Gravel sulfate content and sieve analysis.

Mesh opening (mm)	Percentage of passing, %	Iraqi criteria (No.45), %
20	100	100
14	95.4	90-100
10	63.1	50-85
5	4.9	0-10
0.075	0.09	≤ 3
Sulfate content		
Property	Result	Iraqi criteria (No.45), %
SO3, %	0.072	≤ 0.1

3.3.4 Chip Rubber

In this investigation, we used scrap tire rubber from the General Company for Rubber Industries and Tires (Al-Najaf) that had a maximum diameter of 14 mm. Cutting up leftover tire rubber and running it through a 14-millimeter sieve were the methods used to collect rubber samples for the experiment. The required size was chosen to be equivalent to coarse aggregates in terms of grading. Tables (3-7) and (3-8) show the sieve analysis and chemical and physical parameters of waste tire rubber, respectively. Particles of chip rubber are seen in Plate (3-1).

Table (3-7): Sieve analysis of chip rubber

Mesh opening (mm)	Percentage of passing, %	Iraqi criteria (No.45), %
20	100	100
14	98.1	90-100
10	70.4	50-85
5	3.2	0-10

Table (3-8): Chemical and physical qualities of rubber (from Company)

Chemical structure		**Physical characteristics**	
Essential rubber elements	Values (%)	Properties	Values
Extract of acetone	10	Finesse modulus	3.15
Rubber hydrocarbon	25	Specific gravity	1.78
Carbon black content	30	Water absorption	2.0%
Natural rubber amount	31		
Ash amount	4		

Plate (3-1): Chip rubber.

3.3.5 High-Range Admixture for Water Reduction (HRWR)

Additive with a high water-reduction potential, Glenium 54 (G54), is used to modify the workability of concrete mixes. According to **(ASTM C494/C494M, 2017**), it's made by BASF and conforms to their requirements. **Table (3-9)** shows the main properties of Glenium 54 from manufacturer data sheet.

Table (3-9): Technical description of Glenium 54**.**

Form	Viscous Liquid
Commercial name	Glenium 54
Chemical composition	Sulphonated melamine and naphthaline formaldehyde condensates
Appearance	Whitish to straw colored liquid
Relative density	1.07 gm/cm^3 at 20 ℃
Chloride content	Nil.
pH	5-8
Storage	Should be stored in original containers and at above 5 ℃
Transport	Not classified as dangerous
Labeling	Not hazard label required
Alkali content (as NaO_2) equivalent	0.26%
* According to manufacturer	

3.3.6 Water

The water used in the concrete mix and curing was tap water.

3.3.7 Steel Reinforcement

In this investigation, the steel reinforcing deformed bars of a Ukrainian producer were employed. Steel reinforcements of 12 mm and 8 mm were used for longitudinal reinforcement and transverse reinforcement, respectively. According to the American standard (**ASTM A615 / A615M-16, 2016**), the yield and ultimate strengths are shown in Tables (3-10). Material testing were done at Al-Mussaib Technical Institute, and the tested samples were subjected to a computerized tensile testing equipment until break down of steel samples fracture, as shown in Plate (3-2).

Plate (3-2): Tensile strength testing machine

Table (3-10): Steel reinforcement test results

ϕ (mm)	*Fy (MPa)	*Fu (MPa)
8	432.0	635.1
12	570.8	718.1

* Each value represents the average of three samples of reinforcement.

3.4 Mix Proportion of Concrete

The American technique of mix proportion selection was used to develop the normal strength concrete (**ACI Committee 211.1-91, 2002**). The concrete strength (f'c) goal for normal concrete beams was set at 35 MPa at 28 days to ensure that rubberized concrete mixtures achieve a cylinder concrete strength (f'c) greater than 17 MPa when gravel is partially replaced with rubber because it is typically used as a minimum requirement in structural requests. Table (3-11) shows the ideal mixtures for 1 m^3.

Table (3-11): Mix proportion of normal concrete and rubberized concrete.

Mix symbol	Cement, kg/m^3	Sand, kg/m^3	Gravel, kg/m^3	Chip rubber kg/m^3	w/c	Super-plasticizer, kg/m^3
N.C	440	710	1050	0	0.36	2.33
R10	440	710	945	31.82	0.36	2.33
R20	440	710	840	63.64	0.36	2.33
R30	440	710	735	95.45	0.36	2.33
N.C: Normal concrete, R10: Rubber concrete with replacing 10% R20: Rubber concrete with replacing 20%, R30: Rubber concrete with replacing 30%						

3.5 Mixing Procedure of Concrete

Weigh and pack all of the raw ingredients (gravel, sand, and cement) into a clean plastic container before commencing the mixing method for normal strength concrete. As indicated in Plate (3-3), an electrical mixer is used to mix all concrete mixtures mechanically. There have been just a few small changes made to the overall mixing procedure, which is based on ASTM C192(**ASTM C192/C192M-00, 2000**). The following are the stages involved in mixing:

- For easy operation, the water used for mixing is separated into two halves. The majority (roughly 75 percent) is mixed separately with the full volume of super plasticizer (G54) for about a minute.

- The coarse aggregate, chip rubber, and a small amount of mixing water (about 25 percent) are put into the mixer before it is switched on and operated for a few rotations (about 0.5 minutes).
- The sand, cement, and most of the mixing water plus G54 are then put into the mixer, which is then operated for three minutes.
- After that, the mixer is left to cool for one minute before it is used again.
- Afterwards, the concrete materials are mixed for another 2 minutes.

As a result, the entire mixing time is about 5.5 minutes, excluding rest time.

Plate (3-3): Mixers used in present work.

3.6 Casting, Compaction, and Curing Process of the Specimens

In order to begin, the materials had to be selected and weighed to meet the volume requirements of the mix. Plate (3-4) illustrates the plywood formwork and reinforcing preparations before casting in all

specimens used in this investigation, with a specified size for three sections (225×225mm), (160×316mm), and (130×390mm) with a length of 2200 mm. As part of the preparation for steel reinforcement, the inside faces of the plywood formworks were oiled, and 20 mm plastic spacers were used as a concrete cover on all faces. The cube, cylinder, and prism were cleaned and oiled well to prevent concrete from adhering to them when hardened. Mixing and pouring concrete onto formwork using a vibrator and an electric concrete mixer, as illustrated in Plate (3-5), To keep water from evaporation, the concrete was smoothed out with a trowel and then covered with nylon sheets. Curing the specimen with water every day and keeping it moist for 28 days after the plywood mold has been removed after 24 hours of curing the specimen and covering it with a burlap layer and nylon sheet as shown in the Plate (3-6). A thin coating of white paint was applied to all beams after the curing period had passed so that the first fracture during the test could be clearly seen.

Plate (3-4): Plywood formwork and reinforcing preparations.

Plate (3-5): Cast the concrete into formwork and using a vibrator.

Plate (3-6): Curing the specimen and covering it with a burlap layer.

3.7 Testing of Samples

3.7.1 Properties of Fresh Concrete-Slump Test:

In Plate (3-7) the workability of conventional and rubberized concrete was checked to make sure it met (**ASTM C143M, 2012**).

Plate (3-7): Slump test.

3.7.2 Concrete's Hardened Properties

3.7.2.1 Density:

The purpose of the experiment was to compare the densities of normal concrete versus rubberized concrete.

3.7.2.2 Testing for Compressive Strength:

This test is performed using 150×150×150 mm cubes in accordance with (**BS 1881-116, 1983**) and 150 x 300 mm cylindrical specimens in accordance with (**ASTM C39/C 39M-01, 2001**) and loaded axially by the compressive machine type MATEST as shown in Plate (3-8) to monitor the compression strength development of concrete mixes over time. At the predetermined age, each mix is shaped into three cubes and cylinders. Specimens are soaked in tap water for the duration of the testing procedure once been demolded.

Plate (3-8): Compressive strength testing machine**.**

3.7.2.3 Splitting Tensile Test

Testing for splitting tensile strength was performed in accordance with ASTM C496 (**ASTM C496/Ca96M-11, 2011**) on concrete specimens with a 100 mm diameter and a 200 mm height. The specimens were tested at ages 7 and 28 days using automatic compression testers with a 2000 kN capacity. Plate (3-9) depicts the split test setup. The splitting tensile strength was calculated using Equation (3-1).

$$f_t = \frac{2P}{\pi DL} \qquad (3\text{-}1)$$

where:

f_t = stress of splitting tensile (MPa),

P = Maximum applied load measured by the testing equipment (N),

D = diameter of cylinder (100mm),

L = length of cylinder (200mm).

Plate (3-9): Splitting tensile test.

3.7.2.4 Modulus of Rupture

According to (**ASTM C78/C78M-18, 2018**), rupture strength tests are carried out on concrete specimens. Prism specimen's 100×100×400 mm that have been cured in a water container in the laboratory for seven or 28 days are used to test for flexural strength. When we tested the beam with the third-point load, we used our 150 kN-capacity flexural machine, according to Plate (3-10). Using the following equation (3-2), the modulus of rupture was determined by taking the average of three samples for each case.

$$f_r = \frac{PL}{bd^2} \qquad (3\text{-}2)$$

f_r = flexural stress (MPa).

P = failure load (N).

L = distance between supports (mm).

b = width of Prism (mm).

d = depth of Prism (mm).

Plate (3-10): Flexural machine.

3.7.2.5 Modulus of Elasticity

According to the method (**ASTM C469/469M-14, 2014**), Cylindrical specimens having a dimension of 100 × 200 millimeters were used to measure the concrete modulus of elasticity. It was necessary to use electric grinding to properly smooth the cylinder's two sides in order to prevent any weakening of the structure. All of the samples were put through on a hydraulic machine with an approximately (1000 kN). Linear displacement measurement (LVDT) with a 100 mm sensor length was used. LVDT sensor testing and installation are shown in Plate (3-11).

Plate (3-11): Modulus of elasticity test system.

3.7.2.6 Impact Resistance by Drop-Weight Test

Using concrete cylinder samples with 152×65 mm diameters and depths, the drop-weight test measures the potential energy absorption, according to ACI Committee 544 (**ACI 544.2R-89, 1999**). Each mix was tested with a total of three samples. Fall steel hammer balls were repeatedly dropped on the sample from a specific height to get the necessary grade of failure (first and failure fracture) as well as the number of blows. An example of the test apparatus is shown in Figure (3-3), which include a 4.54-kilogram steel ball that falls to the ground from a height of 457 millimeters onto another 65-millimeter steel ball.

The impact resistance at the initial crack (EI) and the end crack (Eu) was calculated using the joule (J) values in equations (3-3) and (3-4).

$$EI = N1\ mgh \quad (3\text{-}3)$$

$$Eu = N2\ mgh \quad (3\text{-}4)$$

Using (m) as the fall hammer mass, (g) as the ground acceleration (9.81 m/s^2), (h) as the releasing elevation of the drop hammer, (N1) the number of impacts on the first apparent fracture, (N2) blows amount that caused cracks to be visible and significant. The method adopted in the present work is based on previous research **(Kadhim, 2020 & Sahib, 2020)**.

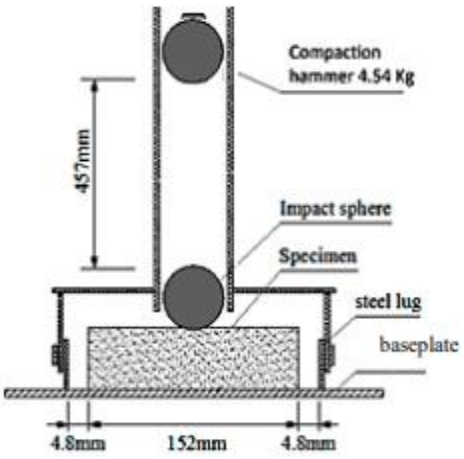

Figure (3-3): Section through test equipment for impact strength.

3.7.2.7 Thermal Conductivity

According to **(ASTM C1113/C1113M-09, 2013**), this test was done using a Quick Thermal Conductivity Meter (QTM-500) as stated in Plate (3-12). Thermal conductivity tests are performed on cube specimens that measure 150×150×150 mm in size. Four samples were prepared and dried for 24 hours at 110±5°C in an oven. A standard deviation of less than 3% was used to determine the average thermal conductivity of each specimen after the test was conducted three times for each specimen.

Plate (3-12): Test of thermal Conductivity.

3.8 Test Setup and Procedure

The beams were put to the test on a hydraulic machine with a load capability of 480 kN (see Plate 3-13- A, B and C). At the College of Engineering/University of Babylon's laboratory for Civil Engineering. The experiments were carried out. Each specimen was put through its paces with a basic span (L) between supports of 1800 mm. The load applied was calculated using an electric pressure transducer as shown in plate (3-14).

3.8.1 Pure Torsion Test Procedure

According to the experimental criteria, the load must be transferred from the center of the testing hydraulic machine to exterior places that reflect load eccentricity, such as the torsion arm of a steel girder. Figure (3-4) shows the clamping loading frame that was employed in this research on both ends of the beam. When transferring the load from the steel beam

to the torsion arm, an iron ball resting on a cup hollow from the inside in the shape of half of a hemisphere was employed between them to keep the length and position of the torsion arm's impact on the beam constant as shown in Plate (3-15). The supports used in this study in two ends of beam allowed to rotate around the constant axis of rotation as shown in Plate (3-16). If you want pure torsion, you need to align the center of support with the center of the torsion arm, which is the torsion moment arm (500mm from the center of the beam). The bottom fiber twist angle was calculated by utilizing a dial gage with 0.01 mm divisions and a 30 mm capacity at the end of the beam span to measure the twist angle. The beams were loaded at a constant rate of 0.1 kN/sec after they had been tested under conditions of pure torque. Every time a load was applied, the twist angle and cracking width measurements were taken, and data on the initial crack load was recorded, allowing us to keep track of the many kinds of cracking and load failure that occurred.

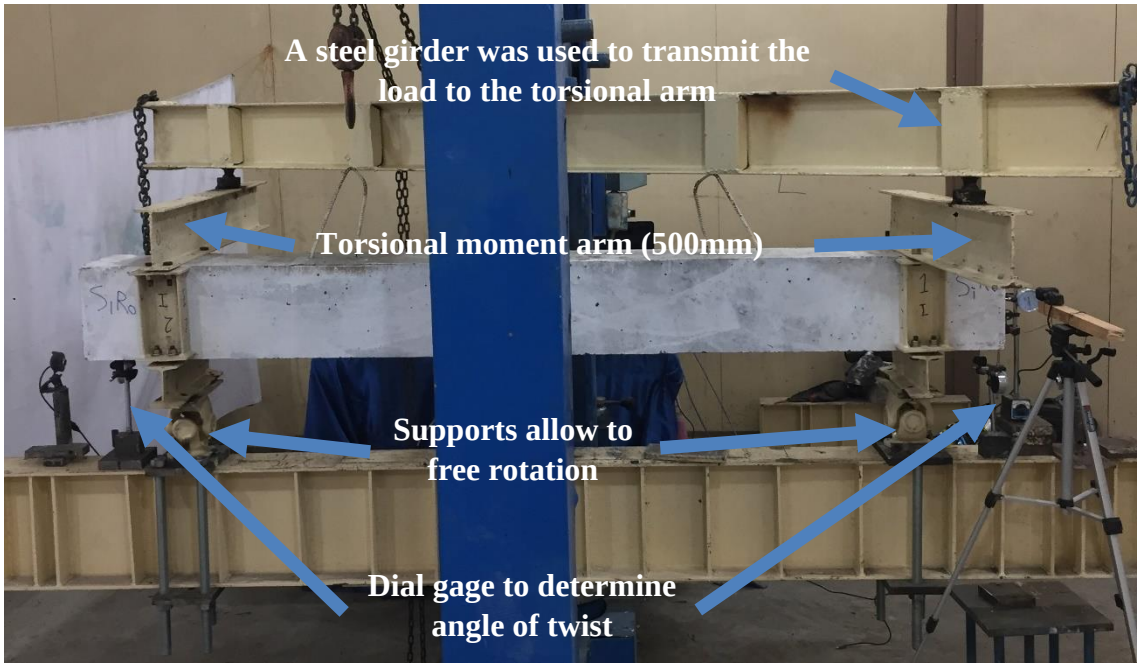

A. The beam tested under pure torsion.

Plate (3-13): The universal measuring machine is used to test specimens.

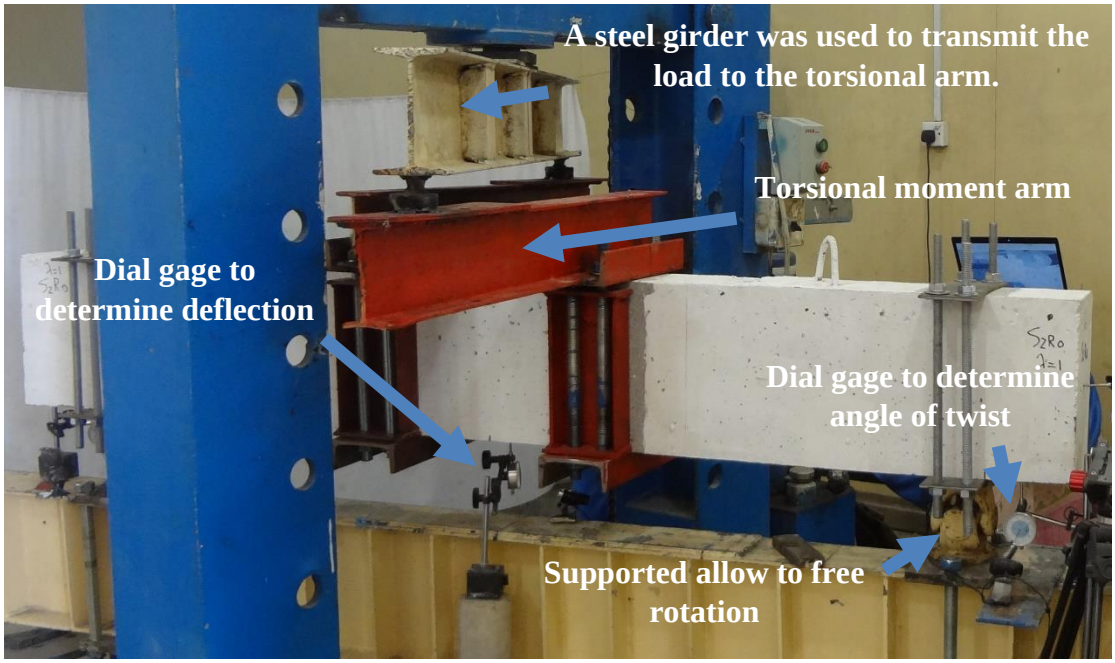

B. The beam tested under combined torsion and bending.

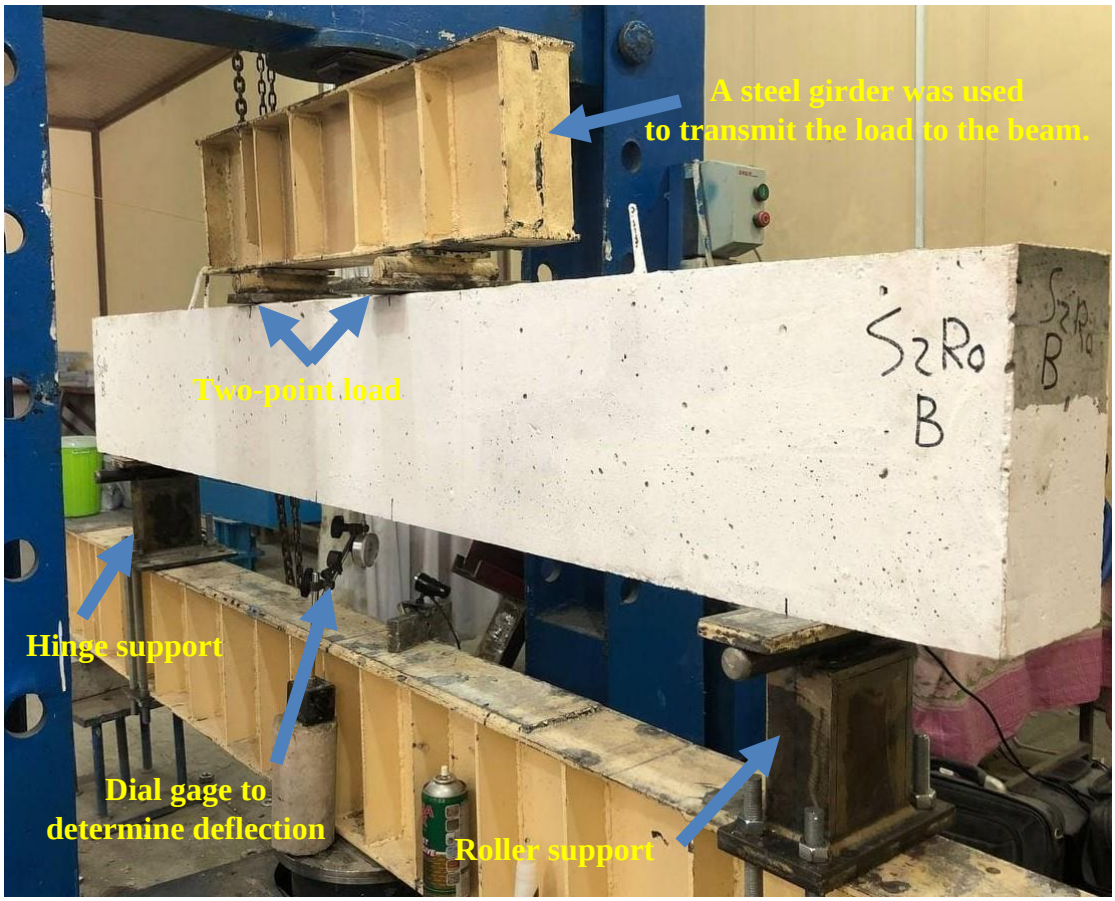

C. The beam tested under bending.

Plate (3-13): Continued

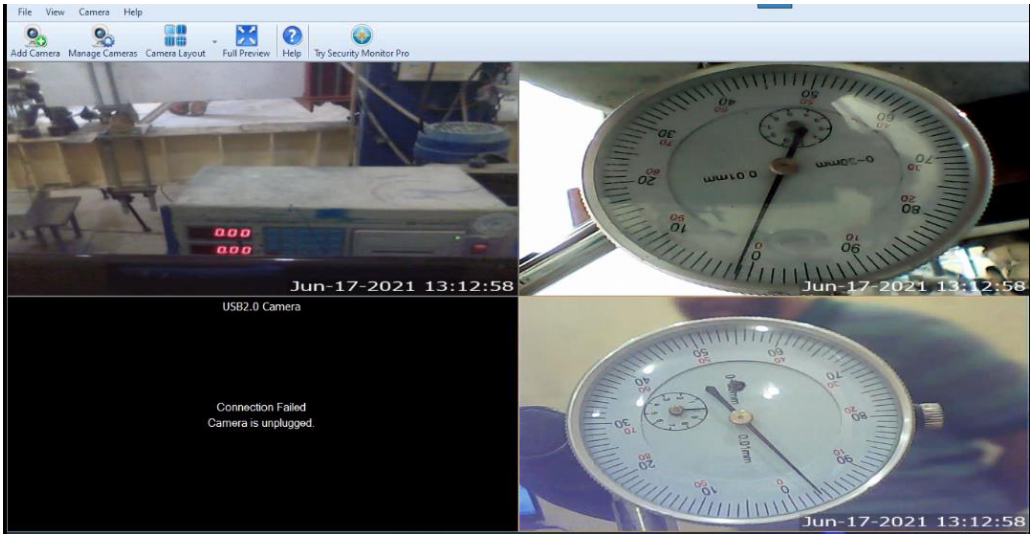

Plate (3-14): The computer recording for beams at each loading stage.

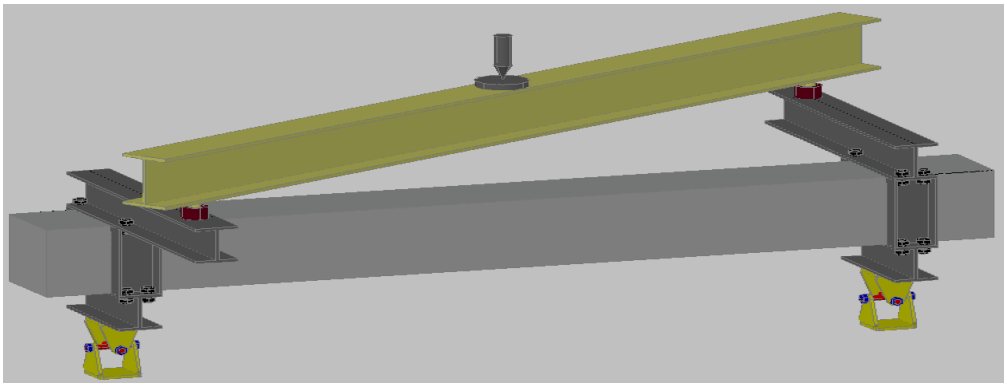

Figure (3-4): Set-up a mutual of pure torsion in a schematic test diagram.

Plate (3-15): Iron ball resting on a cup hollow.

Plate (3-16): The supports used in beam to allowed rotating**.**

3.8.2 Combined Torsion and Bending Test Procedure

Identical loads and supports in the pure torsion test technique for beams in the first group were employed, but the center of support did not match the center of the torsion arm, as illustrated in Figure (3-5). Torsion moment arm lengths vary depending on the bending/torsion ratio (λ) of the beam. A dial gage with 0.01 mm divisions and a 30 mm capacity was used at the end of the beam span to measure the twist angle in the bottom fiber, and another dial gage was used to record deflection in the center of the beam. They were then loaded at a rate of 0.1 kN/sec after being tested under bending and torsion in combination. Accordingly, twist angle measurements as well as deflections and cracking width were recorded at each loading interval, and the first crack's load was recorded, tracking forms the types of cracking and load failure.

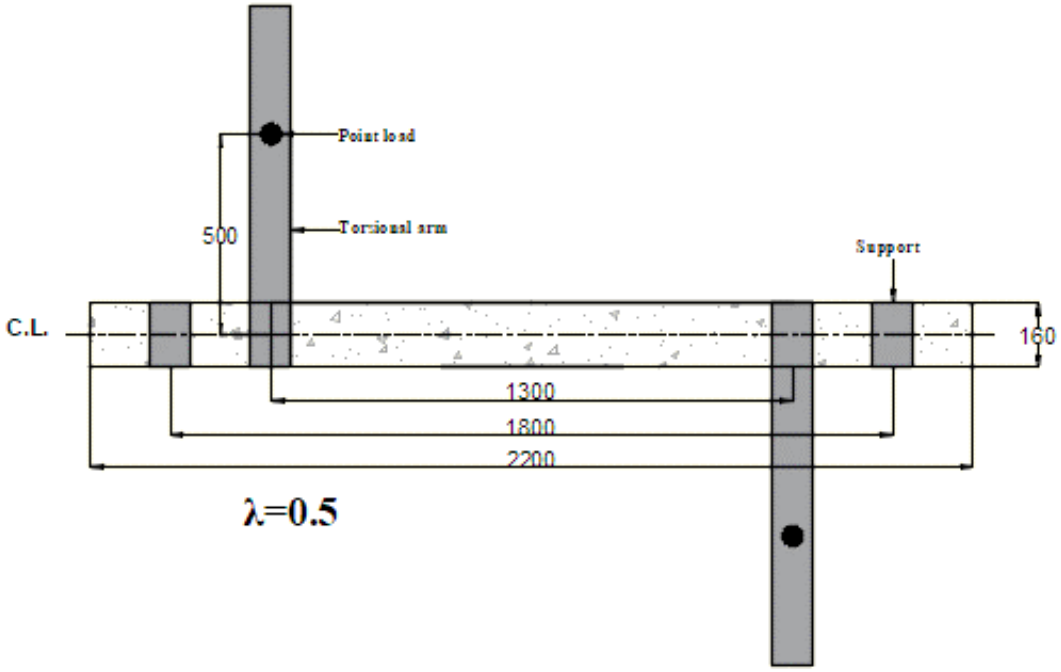

A: When bending / torsion = 0.5 (λ=0.5).

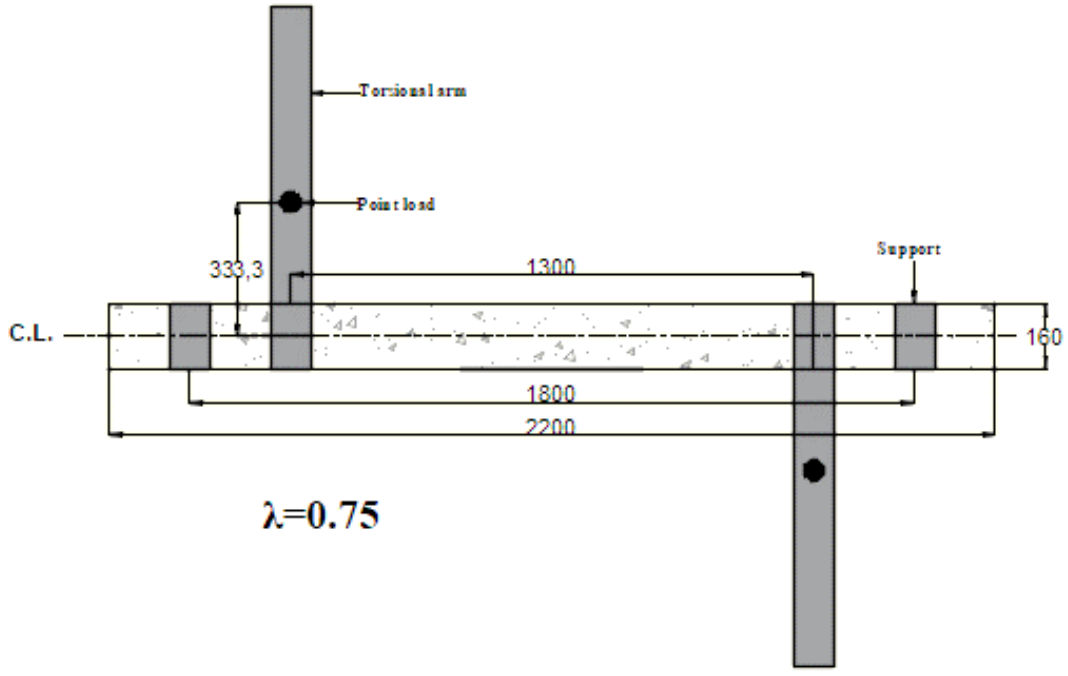

B: When bending / torsion = 0.75 (λ=0.75).

Figure (3-5): Details of supporting and loading position for beams under combined torsion and bending (all dimension in mm).

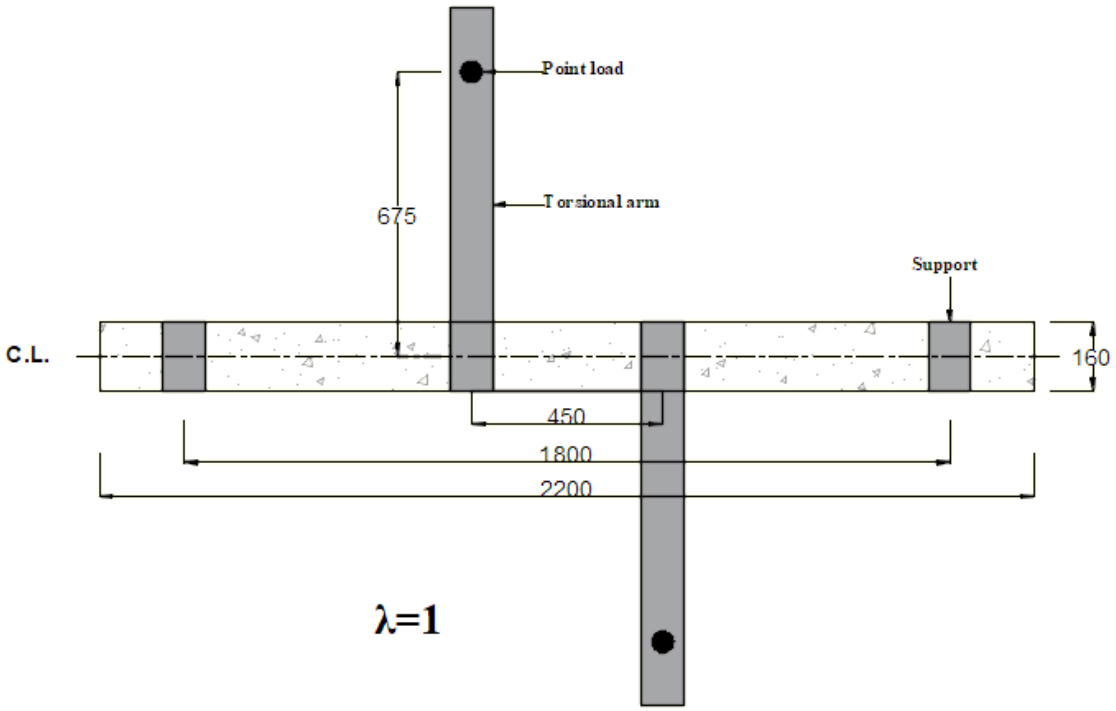

C: When bending / torsion = 1 (λ=1).

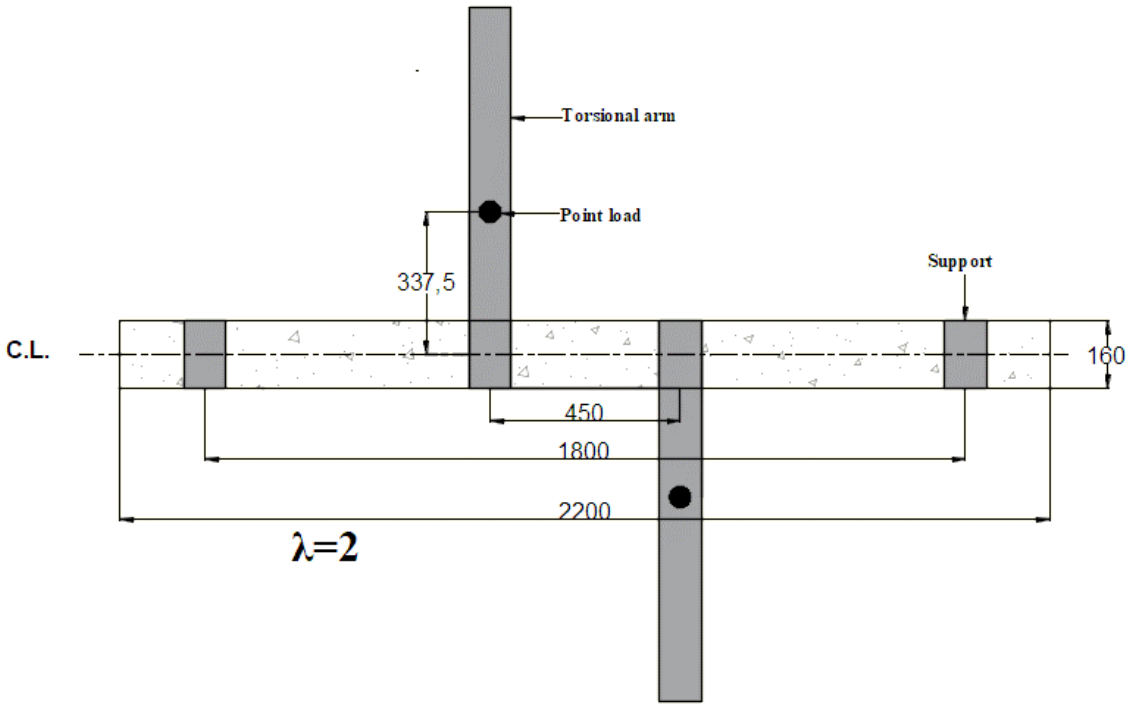

D: When bending / torsion = 2 (λ=2).

Figure (3-5): Continued

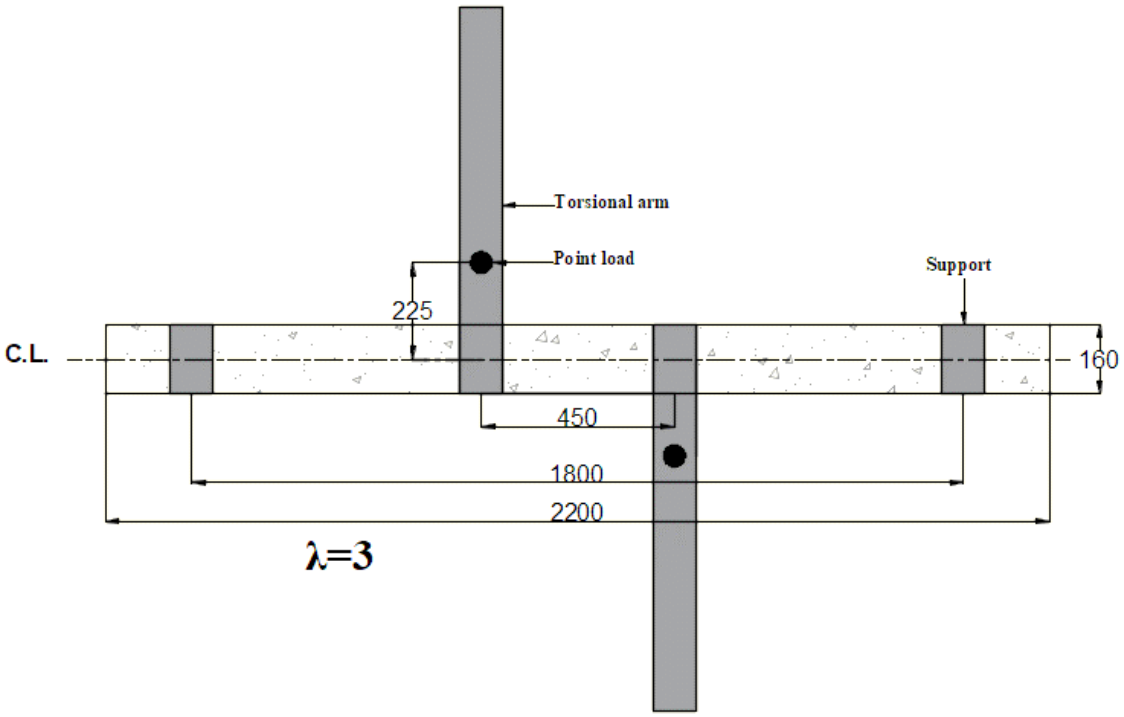

E: When bending / torsion = 3 (λ=3).

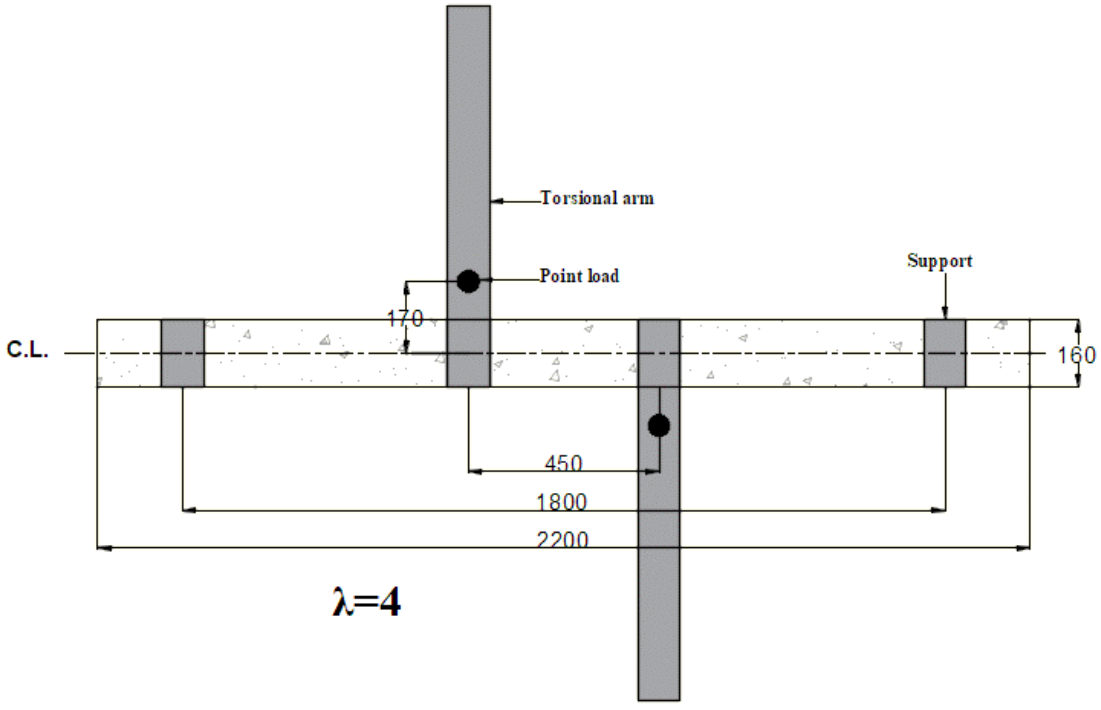

F: When bending / torsion = 4 (λ=4).

Figure (3-5): Continued

3.8.3 Bending Test Procedure

Beams in the third group were placed from one end on a roller and the other on hinge support, as shown Figure (3-6). The load is applied to the tested beam through a spreader beam. Bearing plates with a dimension of (200×100×12) mm was inserted at supports and loading points to avoid local concrete crushing. In order to measure deflection, a dial gauge with 0.01 mm divisions and a 30 mm capacity was placed in the center of the beam. They were then loaded at a rate of 0.1 kN/sec after being tested under bending. Accordingly, deflections and crack width were recorded at each loading interval, and the first crack's load was recorded, tracking forms the types of cracking and load failure.

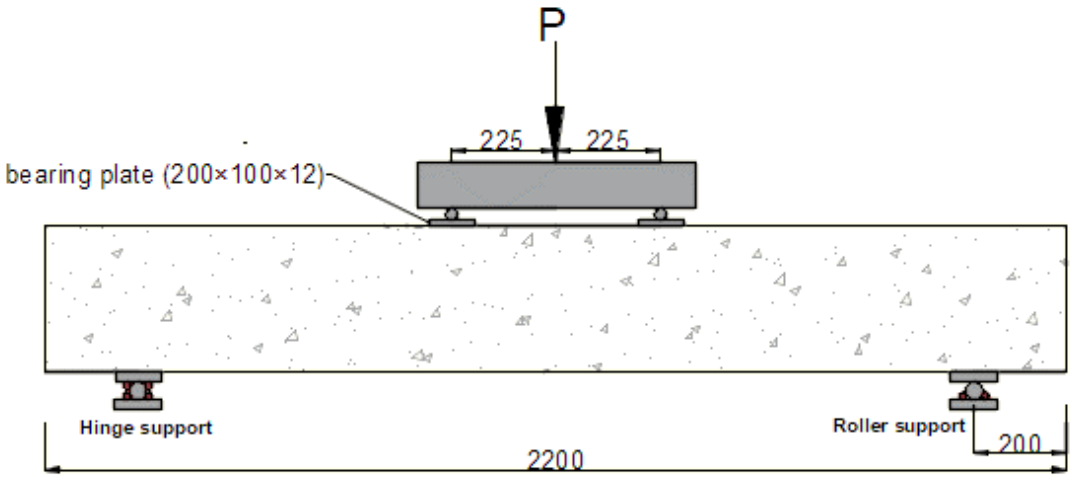

Figure (3-6): Details of supporting and loading condition of beams under bending (all dimensions are in mm).

CHAPTER FOUR

RESULTS AND DISCUSSION

4.1 Introduction

This chapter will present the results and discussions of the experimental tests performed on reinforced concrete beams, undergo pure torsion, combined torsion with bending, and pure bending behavior for samples (normal and rubberized), the study will be divided into two parts. The first part will focus on obtaining successful structural mixes with various percentages of waste tire rubber by checking and evaluating the fresh properties (workability) and hardening properties (hardness) (density, compression, splitting tensile, flexural, modulus of elasticity, impact, and thermal conductivity). In the second part, the thirty specimens distributed as follows, ten ordinary reinforced concrete beams specimens, sixteen rubberized reinforced concrete beams specimens, two ordinary concrete beams specimens without reinforced, and two rubberized concrete beams specimens without reinforced are presented. The discussion of the results is based around ultimate torque, ultimate load, deflection and rotation, energy absorption, ductility index, cracking stiffness, first cracking, and the crack pattern.

Finally, the effectiveness of the effect of partial replacement rubber percentage, depth to width ratio, and type of loading on ultimate strength and angle of twist are discussed.

4.2 Fresh Concrete Properties (test of slump)

In Table (4-1), four concrete mixes were tested for slump, and the results are shown. All of the combinations worked well, and there were just a few minor differences. Workability was lowered by increasing the

volumetric ratio of rubber replacement with a natural aggregate, as illustrated in Figure (4-1). This decreasing in workability is related to the properties of the coarse aggregates that had higher specific gravity values with smoother surfaces. This led to a decrease in the friction coefficient of natural aggregates compared to rubber particles, which led to an increase in the resistance of flow and a little decrease in the mix mobility. The thin layer of defilements, such as fine rubber fuzz or dust, on the rubber particles' surface reduces the fresh rubber concrete free water, which also reduces the flow capacity. Slump values of concrete mixes utilizing 30% chip rubber instead of coarse aggregate (R30) dropped by 37.04% as compared to conventional concrete mixtures (R0).

Table (4-1): The slump values for different mixes.

Mix. symbol	Slump Value (mm)	%Difference.
R0	135	0.00
R10	121	-10.37
R20	103	-23.07
R30	85	-37.04

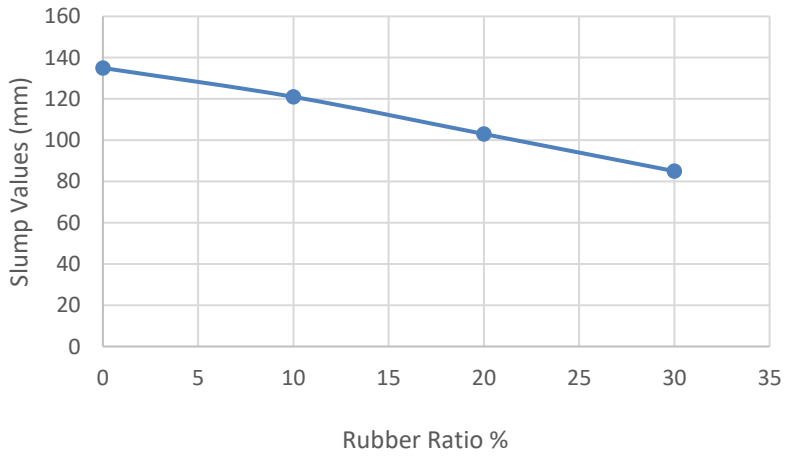

Figure (4-1): The slump values for different rubber ratio.

4.3 Hardened Concrete Properties

4.3.1 Concrete Density

Four distinct mixing samples' densities are summarized in Table (4-2). When coarse aggregate is partially replaced with rubber in concrete mixes as a volumetric substitute, rubber particles have a hydrophobic characteristic that repels water from rubber surfaces and retains air on their rough surfaces. Therefore, the density of rubberized concrete mixes is lower than that of a reference mixture because coarse aggregate has a larger specific gravity than chip rubber. The amount of air in a given volume of rubberized concrete increases as the volumetric rubber replacement ratio increases. Density of concrete mixes utilizing 30% chip rubber replace coarse aggregate (R30) reduces by 9.08% as compared to conventional concrete mixture (R0) as shown in Figure (4-2).

Table (4-2): The density values for different mixes.

Mix. symbol	density of mixes (kg/m^3)	%Difference.
R0	2411	0.00
R10	2325	-3.57
R20	2252	-6.59
R30	2192	-9.08

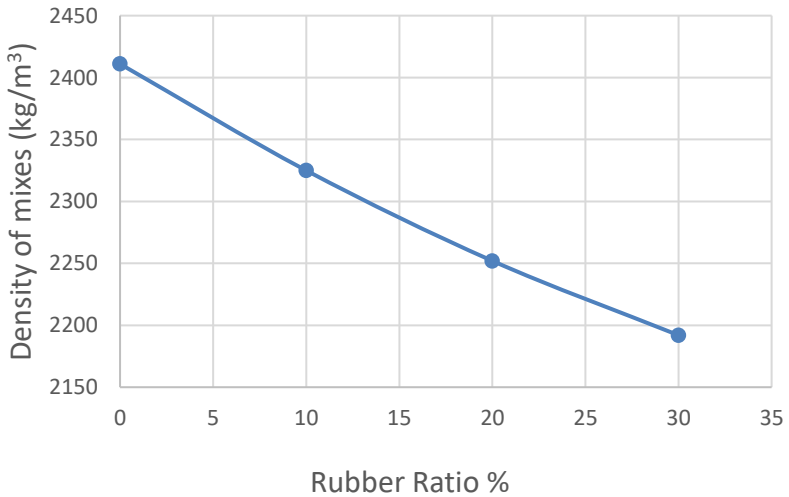

Figure (4-2): The density of concrete mixes.

4.3.2 Compressive Test

As can be observed in Table (4-3), as the percentage of rubber increase, the compressive strength decreased. Particle softness differences between scrap tire rubber and aggregates account for this decrease. The adhesion of rubber and cement paste is poor (weak strength of the interfacial transition region between both the rubber particles and the cement paste). The compressive strength of the cubes and cylinders samples decreased by 48.03 percent and 47.64 percent, respectively, when 30 percent of the coarse aggregate was substituted with chip rubber as shown in Figure (4-3). These results are consistent with previous studies **(Kadhim, 2020 & Sahib, 2020)**, which estimated the reduction to be 37.4% and 30%, when samples contained 20% chip rubber.

Table (4-3): Compressive strength values.

Mix. symbol	(fcu) for cube (MPa)				($f'c$) for cylinder (MPa)		$f'c$ / fc
	At 7 days	%Diff.	At 28 days	%Diff.	At 28 days	%Diff.	
R0	34.28	0.00	43.58	0.00	34.97	0.00	0.802
R10	28.90	-15.69	35.37	-18.84	28.67	-18.02	0.811
R20	23.40	-31.74	29.10	-33.23	23.46	-32.91	0.806
R30	19.63	-42.74	22.65	-48.03	18.31	-47.64	0.808

$f'c$: Compression strength (MPa) according to the American Standard.
fcu: Compression strength (MPa) according to the British Standard.

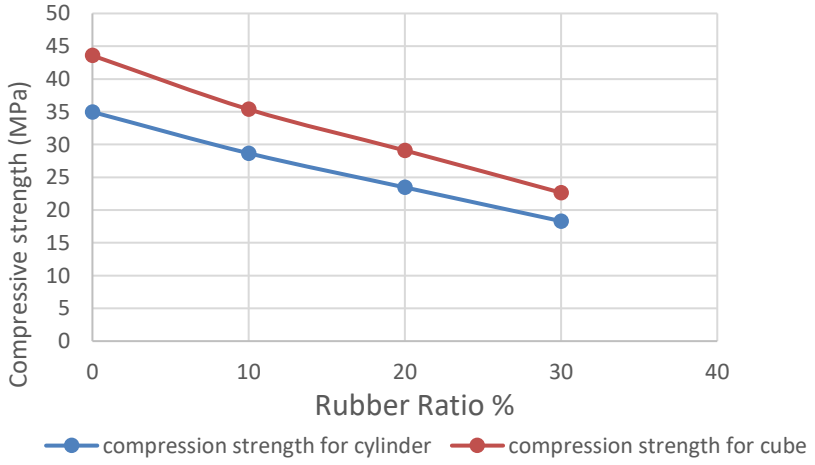

Figure (4-3): Compressive strength at 28 days for various ratios of rubber.

The results of the experiment reveal that the American Standard's compression strength to the British Standard's compression strength ratio is (0.8-0.81). From the experimental findings, the percentage of decreases in compressive strength at 7 days is lower than at 28 days.

4.3.3 Splitting Tensile Test

A tensile strength test was performed, and the results are shown in Table (4-4) However, splitting tensile strength losses were found to be below the compression strength losses. Brittle failure mode (R0) of the control mix resulted in a cylinder being divided into two individual pieces (brittle failure). There were no other chip rubber-based mixes that failed in this manner. It was a progressive breakdown rather than a sudden failure that caused these mixes to fail. When compared to normal concrete mixes (R0), the tensile resistance of samples containing 30% chip rubber instead of coarse aggregate (R30) was reduced by 35.34% as shown in Figure (4-4). From the experimental findings, the percentage of decreases in splitting tensile strength at 7 days is lower than at 28 days. Plate (4-1) shows the effect of rubber ratio on tensile strength.

Table (4-4): Splitting tensile strength values.

Mix. symbol	Splitting tensile strength (ft) (MPa)			
	At 7 days	% Diff.	At 28 days	% Diff.
R0	2.79	0.00	3.65	0.00
R10	2.54	-8.96	3.18	-12.88
R20	2.25	-19.35	2.83	-22.46
R30	1.93	-30.82	2.36	-35.34

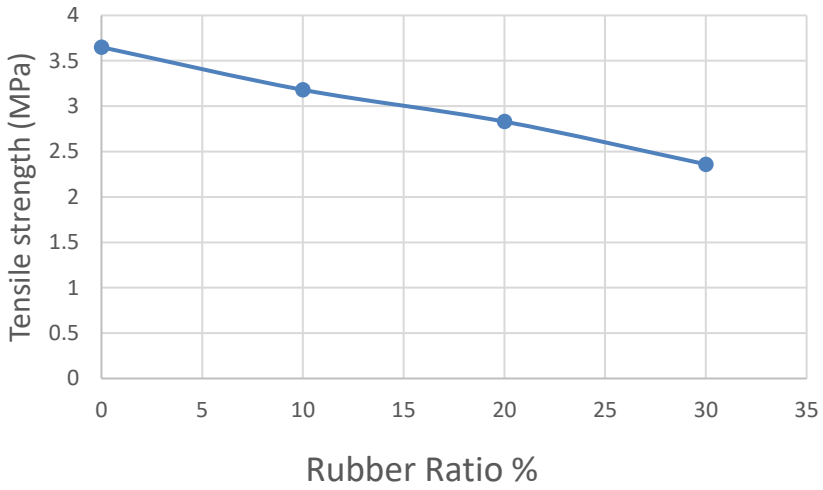

Figure (4-4): Splitting tensile strength values at 28 days.

Plate (4-1): Testing of splitting tensile strength

4.3.4 Modulus of Rupture

Table (4-5) and Figure (1-2) show the findings on rupture strength. Rubber particles lower the flexural strength. The control mix's failure mode (R0) shows that the prism failed in the specimen's middle positions. The uniformity of the mix is to blame for this. The non-uniform distribution of rubber in the mixes containing rubber particles led to a failure mode that was not precisely in the center of this sample, but still within one-third of the sample. In this case, replacing 30% of the coarse aggregate with rubber chips decreased the modulus of rupture by about 44.75%. From the experimental findings, the percentage of decreases in

modulus of rupture strength at 7 days is lower than at 28 days. Plate (4-2) show the final shape of the beams after failure.

Table (4-5): Modulus of rupture strength values.

Mix Symbol	Modulus of rupture (fr) (MPa)			
	At 7 days	% Diff.	At 28 days	% Diff.
R0	3.64	0.00	4.67	0.00
R10	3.09	-15.11	3.95	-15.42
R20	2.57	-29.40	3.2	-31.48
R30	2.16	-40.66	2.58	-44.75

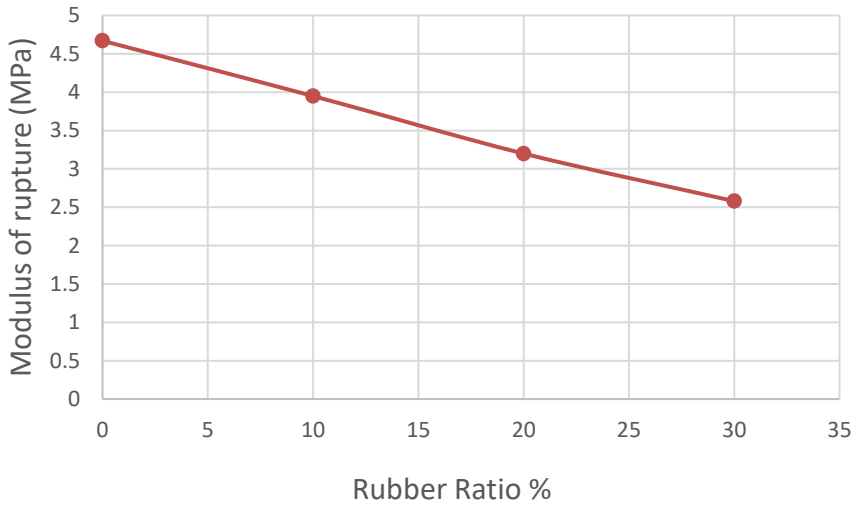

Figure (4-5): Modulus of rupture values at 28 days.

Plate (4-2): Final shape for the specimens after failure.

4.3.5 Elastic Modulus

The findings of the young modules for various mixes are shown in Tables (4-6). As can be seen, the modulus of elasticity is reduced by employing recycled tire rubber instead of coarse material. It is noticed that the impact on aggregates is due to modulus of elasticity and the volumetric ratio of these particles in concrete, by utilizing concrete as a foundational model, composite compounds made up of aggregate and cement may be modeled. As a consequence, concrete's elasticity modulus increases in direct proportion to the aggregate elasticity modulus. As illustrated in Figure (4-6), since rubber's elasticity has a lower modulus than that of concrete, increasing the amount of rubber substituted for coarse particles reduces the elastic modulus of concrete. Rubber chips, when used to replace 30% of the coarse aggregate, reduce the modulus of elasticity of ordinary concrete by 50.49 percent.

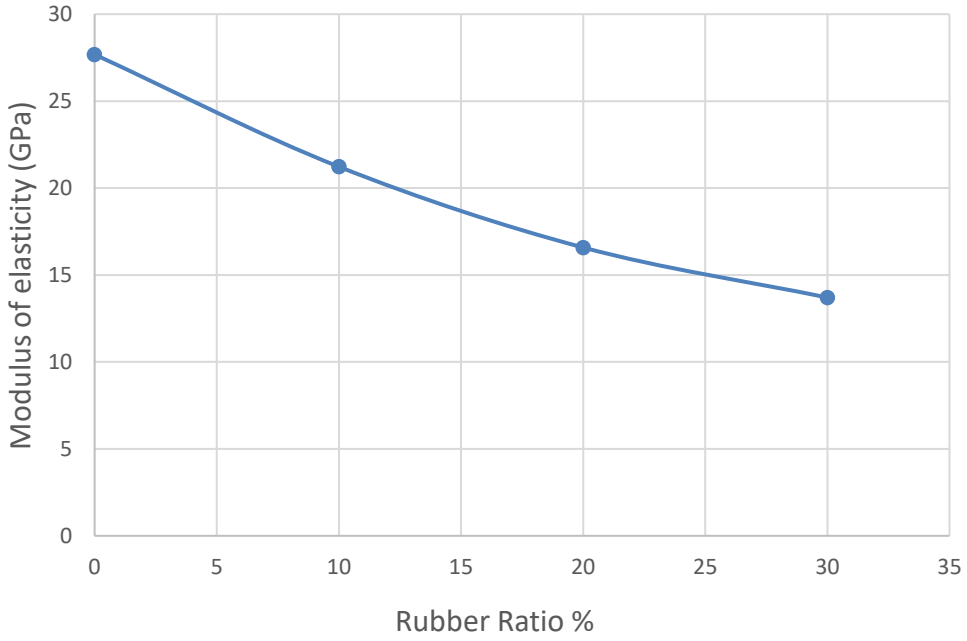

Figure (4-6): Modulus of rupture values at 28 days with different ratio of rubber.

Table (4-6): Modulus of elasticity values.

Mix symbol	Modulus of elasticity (GPa)	
	At 28 days	% Diff.
R0	27.680	0.00
R10	21.228	-23.31
R20	16.582	-40.09
R30	13.705	-50.49

4.3.6 Test of Impact Resistance

The numeral of the drop hammers for all specimens is shown in Table (4-7). The numeral of hits it takes to cause the first fracture and the ultimate failure is documented. The gap between the number of final failures blows and the number of early notch blows (N2-N1) increases as the amount of rubber replacement increases. When more tire rubber is substituted, the rubber cement mixture becomes more flexible, resulting in a greater level of energy absorption compared to the control mixture. The ultimate impact resistance increases by 356.66% compared to normal concrete (R0) when substituting 30% of rubber chips as shown in Figure (4-7). Plate (4-3) shows the final shape of the specimens after failure.

Table (4-7): Impact resistance by drop weight test results.

Mix. symbol	N1 ave. for 3 sample	N2 ave. for 3 sample	N2-N1	Impact Energy (J)	
				First crack	Ultimate failure
R0	52	60	8	1058.39	1221.22
R10	89	106	17	1811.47	2157.48
R20	168	197	29	3419.40	4009.66
R30	236	274	38	4803.45	5576.88

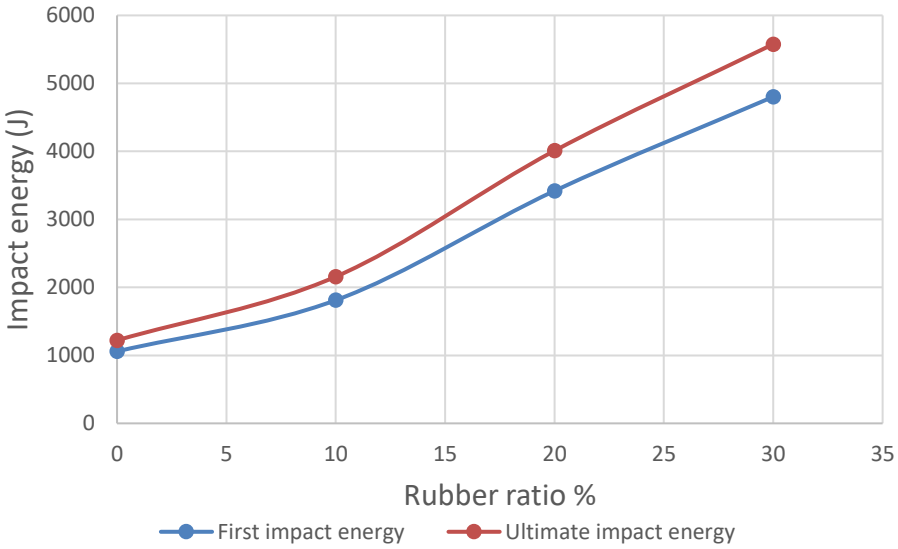

Figure (4-7): Impact energy with various ratios of rubber.

Plate (4-3): Final shape for the specimens after failure.

4.3.7 Thermal Conductivity

Table (4-8) shows the thermal conductivity of all the created concrete mixes. According to the data, the thermal conductivity decreases with increasing rubber content. The conductivity of thermal worth for conventional concrete ranges from 1.1614 W/(m.k) to 0.9221 W/(m.k), for rubberized concrete with 30% replacement, representing a 20.6% decrease as shown in Figure (4-8). As a result of the cement mortar's poor adherence to the rubber-to-cement mortar surface, some of the

trapped air lowered the thermal conductivity. Rubberized concrete's decreased thermal conductivity is due to the rubber particles' poorer thermal conductivity compared to the cement mortar matrix. Consequently, the heat conductivity of concrete is cut down, which makes it lighter in weight.

Table (4-8): The thermal conductivity results for each mix**.**

Mix. symbol	Thermal conductivity (W/m K)	Differences %
R0	1.1614	----
R10	1.1355	- 2.23
R20	1.0315	- 11.18
R30	0.9221	- 20.6

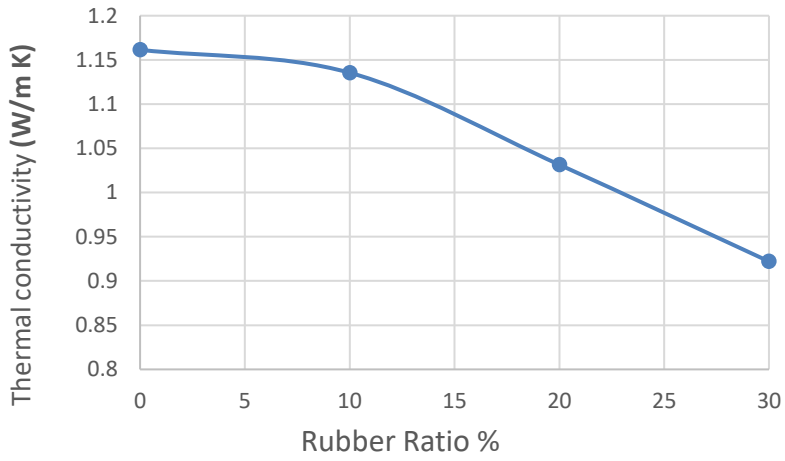

Figure (4-8): Thermal conductivity for mixes with different rubber ratios.

4.4 Experimental Results of Tested Beams.

4.4.1 Group One: (Result for Beams Under Pure Torsion).

The test result includes control specimens without replacement rubber and specimens with different percentages of replacement rubber for each cross-section of beams exposed to pure torsion. The main experimental results of cracking torque, ultimate torque, and angle of twist of the tested beam specimens are illustrated in Table (4-9).

Table (4-9): Experimental results for specimens in group one.

Sample	At Cracking Torque				At Ultimate Torque			
	Torque (KN.m)	* Diff. %	Twist $\times 10^{-3}$ (rad/m)	** Diff. %	Torque (KN.m)	* Diff. %	Twist $\times 10^{-3}$ (rad/m)	** Diff. %
PT-S1R0	9.33	-----	12.82	-----	13.59	-----	52.26	-----
PT-S1R10	8.88	-4.82	13.84	7.96	12.98	-4.49	58.09	11.16
PT-S1R20	8.60	-7.82	14.85	15.83	12.22	-10.08	66.26	26.79
PT-S1R30	8.38	-10.18	15.90	24.02	11.69	-13.98	73.00	39.69
PT-S1R0P	----	----	----	----	9.05	-----	13.84	-----
PT-S1R30P	----	----	----	----	8.25	-8.84	17.36	25.43
PT-S2R0	8.25	-----	10.85	-----	13.14	-----	43.5	-----
PT-S2R10	7.83	-5.40	11.83	9.03	12.42	-5.48	49.8	14.48
PT-S2R20	7.42	-10.06	13.20	17.60	11.68	-11.11	55.8	28.28
PT-S2R30	7.08	-14.18	14.55	34.1	10.96	-16.59	64.5	48.28
PT-S3R0	6.83	-----	8.60	-----	12.13	-----	38.78	-----
PT-S3R10	6.45	-5.56	9.78	13.72	11.58	-4.53	44.17	13.90
PT-S3R20	5.95	-13.32	10.53	22.44	11.15	-8.08	50.00	28.93
PT-S3R30	5.62	-17.72	11.48	33.49	10.47	-13.69	55.94	44.25
PT-S3R0P	----	----	----	----	6.62	-----	12.00	-----
PT-S3R30P	----	----	----	----	5.66	-14.5	19.40	61.67

* Difference in torque when compared with the control beam (for the same cross-section).

** Difference in twist angle when compared with the control beam (for the same cross-section).

The specimens are reinforced with 4ϕ12mm steel bars as longitudinal reinforcement and transverse reinforcement ϕ8mm at 86 mm spacing, a torsion moment arm of 500 mm is applied from the center of the beam. To produce pure torsion, the center of support must line up with the center of the torsion arm.

Reinforced concrete beams for the control beams are free of fractures in the early phases of loading. Cracks started on one of the

beam's two bigger faces. They quickly spread across the whole depth of the face, before the beam broke on the other face.

4.4.1.1 Section One: (225×225) mm Square Section.

- **Specimen PT-S1R0**

This specimen is made from reinforced normal concrete without replacement rubber. The first obvious crack occurred in the middle of the beam. As shown in Plate (4-4), A 45-degree spiral fracture formed and spread over the test area when torque was increased. The values of cracking twisting moments, ultimate twisting moments, and angles of twist are presented in Table (4-9). The curve of torque and the angle of the twist are illustrated in Figure **(**4-9**)**.

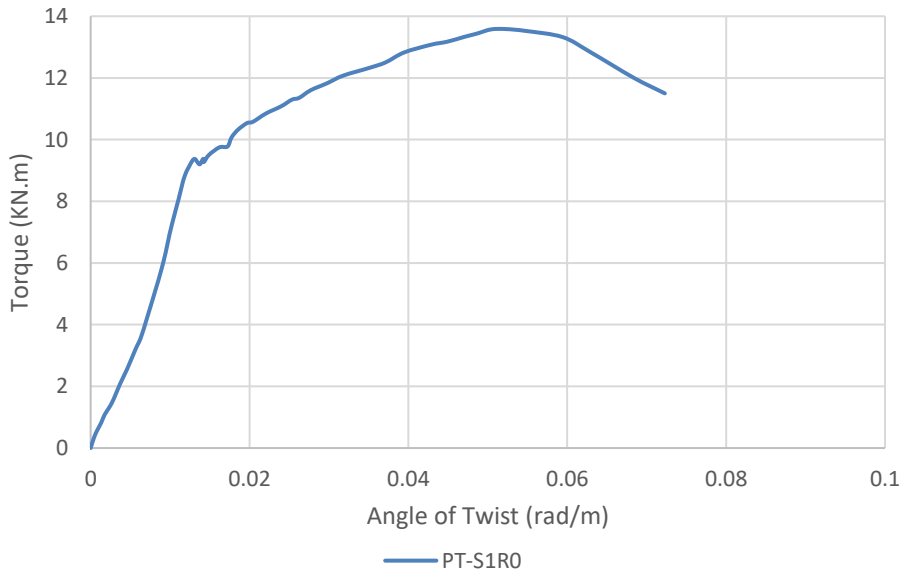

Figure (4-9): The curve of torque – angle of twist for specimen **PT-S1R0**.

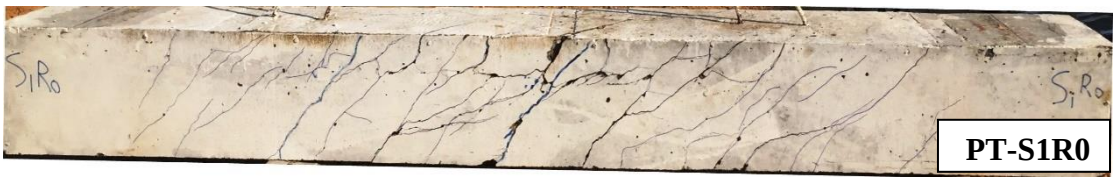

Plate (4-4): Failure mode and crack pattern of beam specimen **PT-S1R0**.

♦ **Specimen PT-S1R0P**

No substitute rubber or steel reinforcements were used in the construction of this specimen. It is just plain concrete. The ultimate torque for plain concrete is about similar to the cracking torque of **PT-S1R0** because the beam would fracture in a brittle manner when the greatest shear stress equals the concrete tensile cracking strength. The cracking failure occurred near the right support of the beam with an approximate 45-degree angle, as shown in Plate (4-5). The values of failure twisting moments and angles of twist are presented in Table (4-9). The curve of torque and the angle of the twist are illustrated in Figure (4-10).

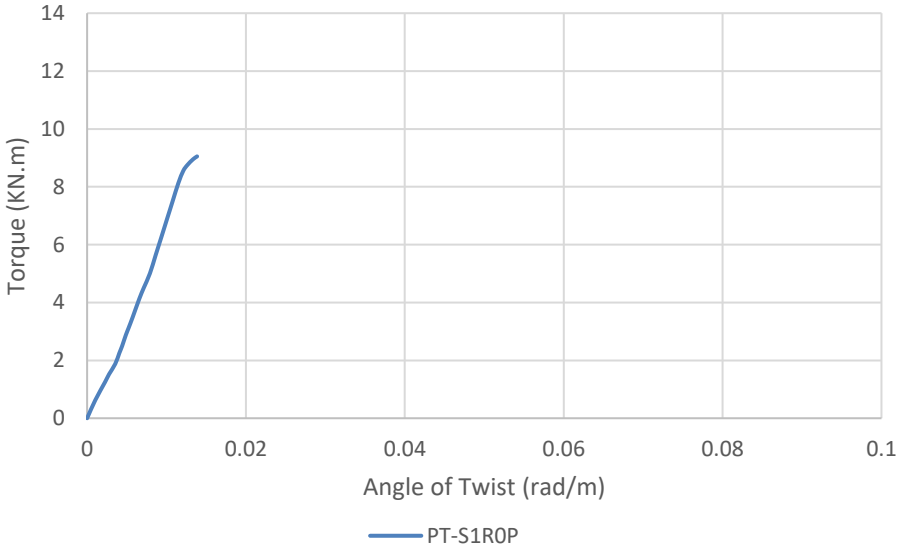

Figure (4-10): The curve of torque – angle of twist for specimen **PT-S1R0P.**

Plate (4-5): Failure mode and crack pattern of beam specimen **PT-S1R0P**.

♦ Specimen PT-S1R10

Reinforced normal concrete with 10% chip rubber replacement is used to make this specimen. The first noticeable fracture appeared on the beam's left side. When torque was increased, spiral fractures occurred at a 45-degree angle, as illustrated in Plates (4-6). Table (4-9) lists the values of cracking twisting moments, ultimate twisting moments, and twist angle. In the comparison beam (**PT-S1R0**), the angle of twist increase by 11.16%, despite a 4.82% decrese in the cracking torque and a 4.49 percent decrease in ultimate torque. Figure (4-11) illustrates the torque curve and twist angle.

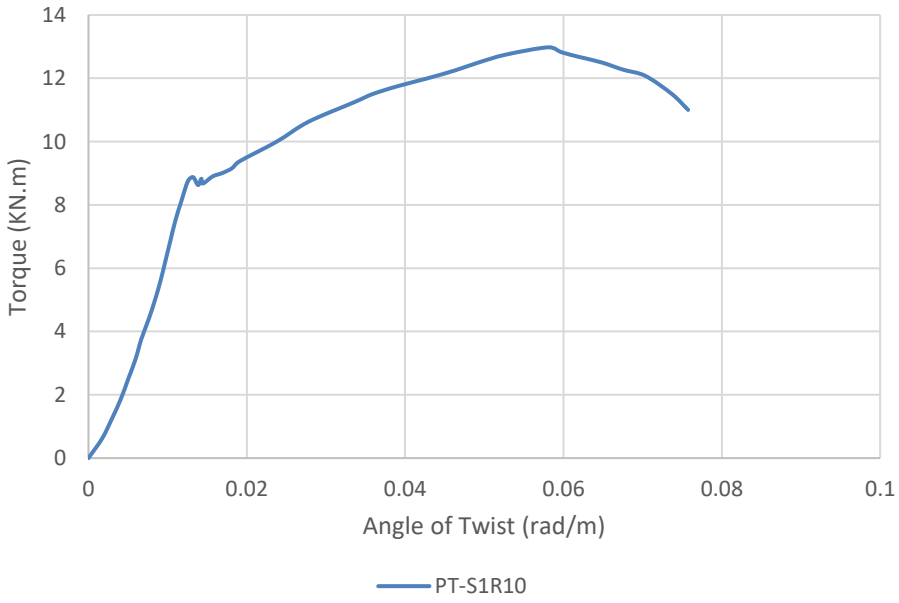

Figure (4-11): The curve of torque – angle of twist for specimen **PT-S1R10.**

Plate (4-6): Failure mode and crack pattern of beam specimen **PT-S1R10**.

- **Specimen PT-S1R20**

The coarse aggregate in this specimen has been replaced with chip rubber to the tune of 20% of the total weight of the specimen. In the center of the beam, the first noticeable break appeared. Spiral fractures occurred and propagated over the test region when torque was applied, as illustrated in Plate (4-7). Table (4-9) lists the values of cracking twisting moments, ultimate twisting moments, and twist angle. The cracking torque decreased by 7.8% and the ultimate torque decreased by 10%. It was a 26.79 percent increase in twist angle as a result of the control beam (**PT-S1R0**). Figure (4-12) illustrates the torque curve and twist angle.

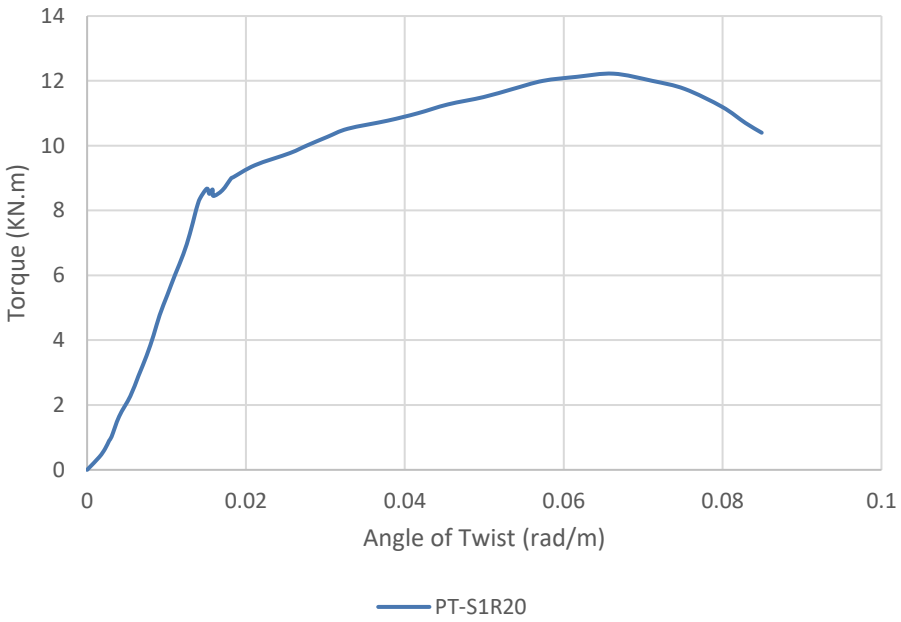

Figure (4-12): The curve of torque – angle of twist for specimen **PT-S1R20.**

Plate (4-7): Failure mode and crack pattern of beam specimen **PT-S1R20**.

♦ **Specimen PT-S1R30**

With a 30% substitution of coarse aggregate with chip rubber, reinforced normal concrete was used to make this specimen The left side of the beam was the first to show signs of a fracture. Spiral fractures developed at 45 degrees and propagated over the test area when torque was increased, as illustrated in Plate (4-8). Table (4-9) lists the values of cracking twisting moments, ultimate twisting moments, and twisting angle. While the angle of twist increased roughly 39.69%, the cracking torque fell nearly 10% and the ultimate torque decreased approximately 13.98% as compared to the control beam (**PT-S1R0**). A diagram depicting the torque curve and twist angle is shown in Figure (4-13).

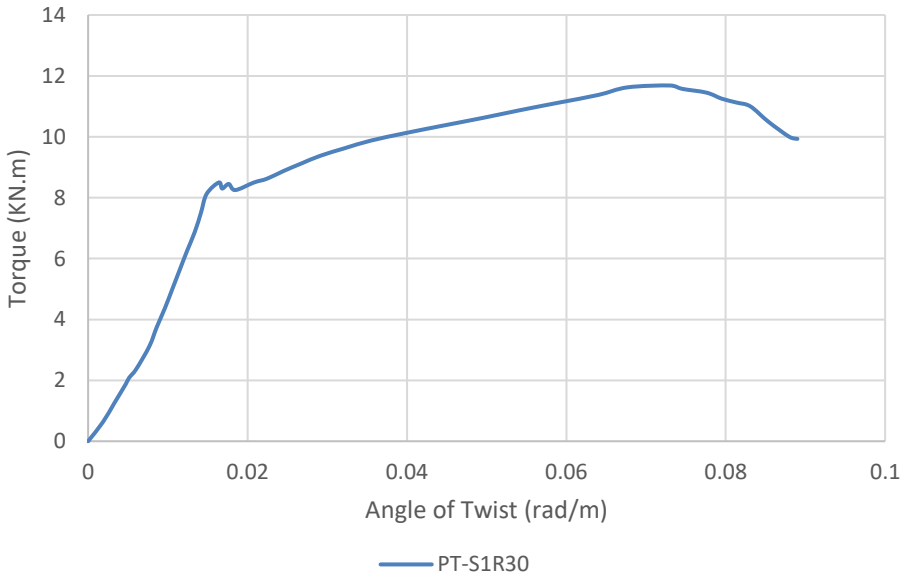

Figure (4-13): The curve of torque – angle of twist for specimen **PT-S1R30.**

Plate (4-8): Failure mode and crack pattern of beam specimen **PT-S1R30**.

♦ Specimen PT-S1R30P

The specimen may be made without the need of steel reinforcement by substituting 30% of the coarse aggregate with chip rubber (plain concrete). This is due to the fact that the beam would snap brittlely if the maximum shear stress surpassed the concrete's tensile cracking strength. In the center of the beam, at around a 45-degree angle, the cracking failure is depicted in Plate (4-9). Table (4-9) displays the failure twisting moment and twist angle values. When compared to the control beam (**PT-S1R0P**), the maximum torque was decreased by 8.84% while the twist angle was increased by 25.43%. The torque curve and twist angle are shown in Figure (4–14).

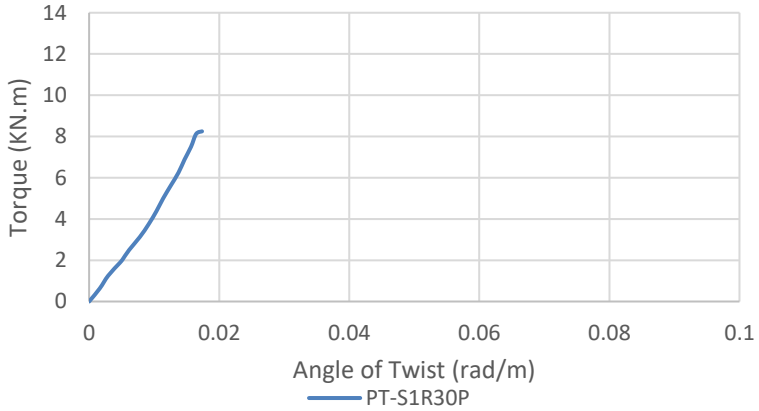

Figure (4-14): The curve of torque – angle of twist for specimen **PT-S1R30P**.

PT-S1R30P

Plate (4-9): Failure mode and crack pattern of beam specimen **PT-S1R30P**.

In the comparison of reinforced beams in section one, the relation between the torque and the angle of the twist is illustrated in Figure (4-15). At 30% replacement of rubber, the ultimate torsion decreased by about 13.98%, but the angle of twist increased by about 39.69%.

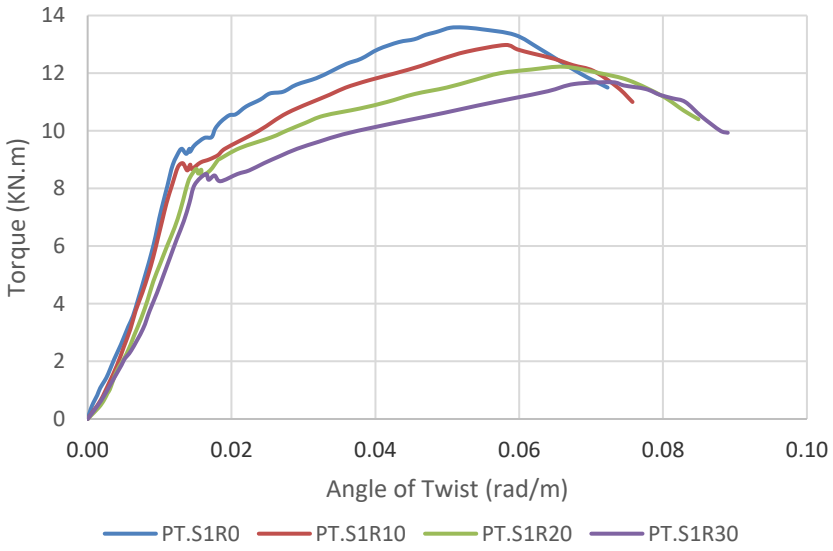

Figure (4-15): The curve of torque – angle of twist for reinforced beams in group one of section one.

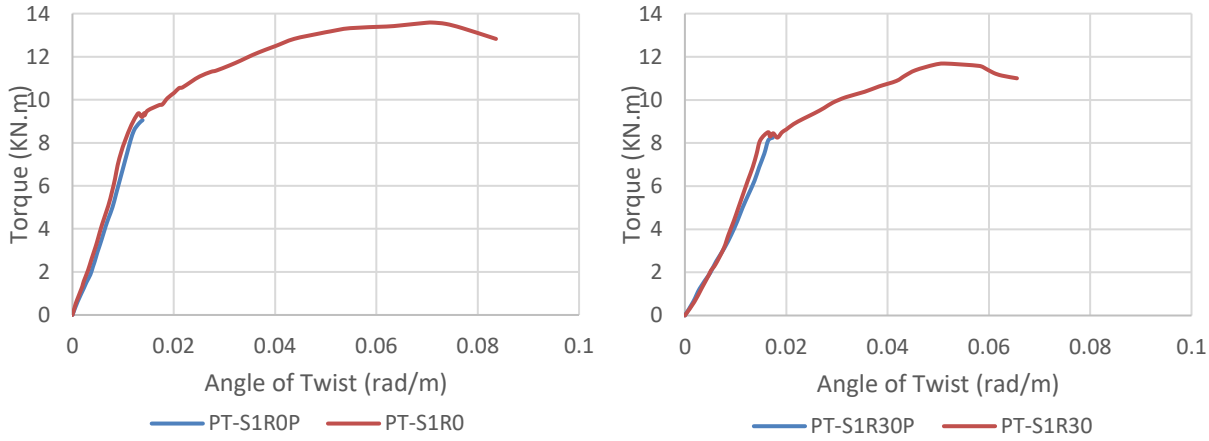

a- Normal concrete b- rubberized concrete

Figure (4-16): Variation of torsional moment with angle twist of plain concrete with reinforced concrete in group one of section one.

This may be shown by looking at data from specimen **PT-S1R0P** and **PT-S1R30P** for regular and rubberized concrete, respectively, to see how steel reinforcement affects the results. It is found that, in comparison to **PT-S1R0**, the failure torque and the angle of twist of **PT-S1R0P** were decreased 33.41% and 73.52%. It can be shown in Figure (4-16) that **PT-**

S1R30P torque was decreased by 29.43% and its twist angle was decreased by 76.22% when compared to **PT-S1R30**.

4.4.1.2 Section Two: (160×316) mm Rectangle Section.

- **Specimen PT-S2R0**

Reinforced normal concrete was used to construct this specimen, and there is no replacement rubber used in the construction process. There was a visible fracture in the middle of the beam. The spiral fractures started to develop and spread throughout the test area at 45 degrees, as seen in Plate (4-10). Table (4-9) lists the values of cracking twisting moments, ultimate twisting moments, and twisting angle. A diagram depicting the torque curve and twist angle is shown in Figure (4-17).

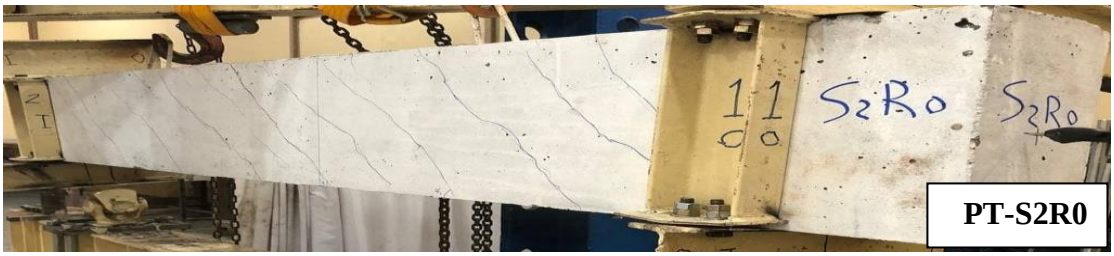

Plate (4-10): Failure mode and crack pattern of beam specimen **PT-S2R0**.

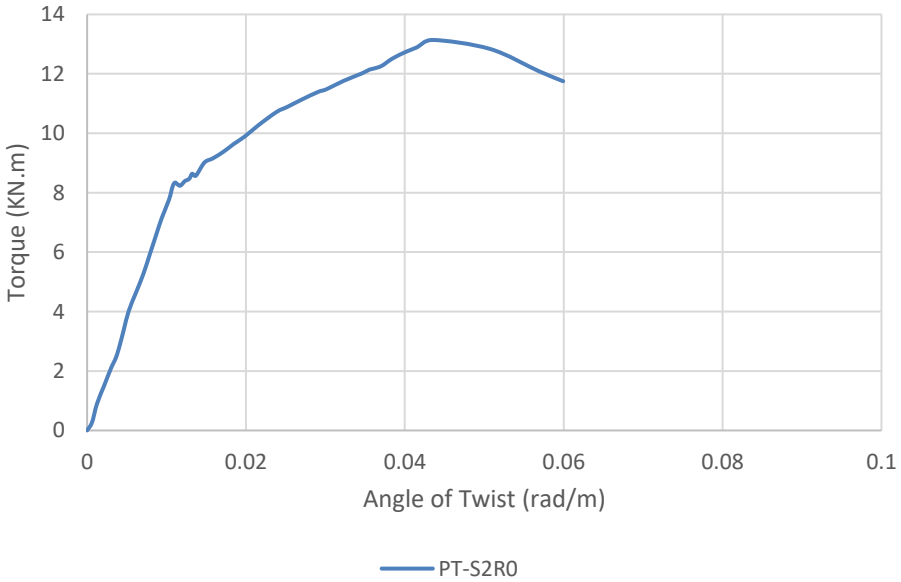

Figure (4-17): The curve of torque – angle of twist for specimen **PT-S2R0**.

♦ **Specimen PT-S2R10**

Normal reinforced concrete with 10% chip rubber coarse aggregate is used to make this example. In the middle position of the beam, there was a visible fracture. As shown in Plate (4-11), the test region was blasted with spiral cracks at 45 degrees. Table (4-9) lists the values of cracking twisting moments, ultimate twisting moments, and twisting angle. Twist angle increased by roughly 14.48 percent compared to the control beam (**PT-S2R0**) even while cracking torque and ultimate torque decreased by 5.40% and 5.48%, respectively. Figure (4-18) illustrates the torque curve and twist angle.

Plate (4-11): Failure mode and crack pattern of beam specimen **PT-S2R10**.

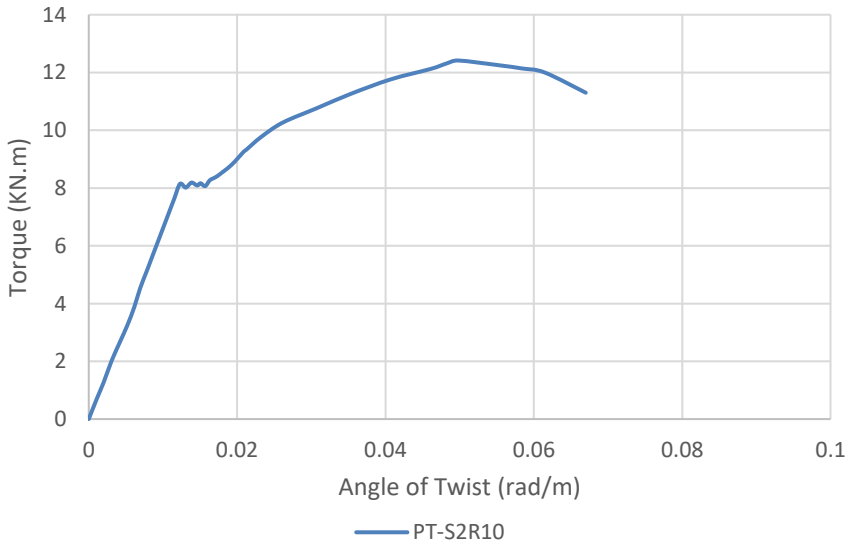

Figure (4-18): The curve of torque – angle of twist for specimen **PT-S2R10**.

♦ Specimen PT-S2R20

Reinforced normal concrete was used in the construction of this example, however chip rubber was used to substitute the coarse aggregate to the tune of 20%. The right-hand side of the beam showed the first signs of a fracture. As seen in Plate (4-12) by the increase in torque, spiral fractures started to occur and spread over the test area at 45 degrees. Table (4-9) lists the values of cracking twisting moments, ultimate twisting moments, and twisting angle. When compared to the control beam, the twist angle increased by 28.28%, yet the cracking torque reduced by 10.06% and the ultimate torque decreased by 11.11% (**PT-S2R0**). A diagram depicting the torque curve and twist angle is shown in Figure (4-19).

Plate (4-12): Failure mode and crack pattern of beam specimen **PT-S2R20**.

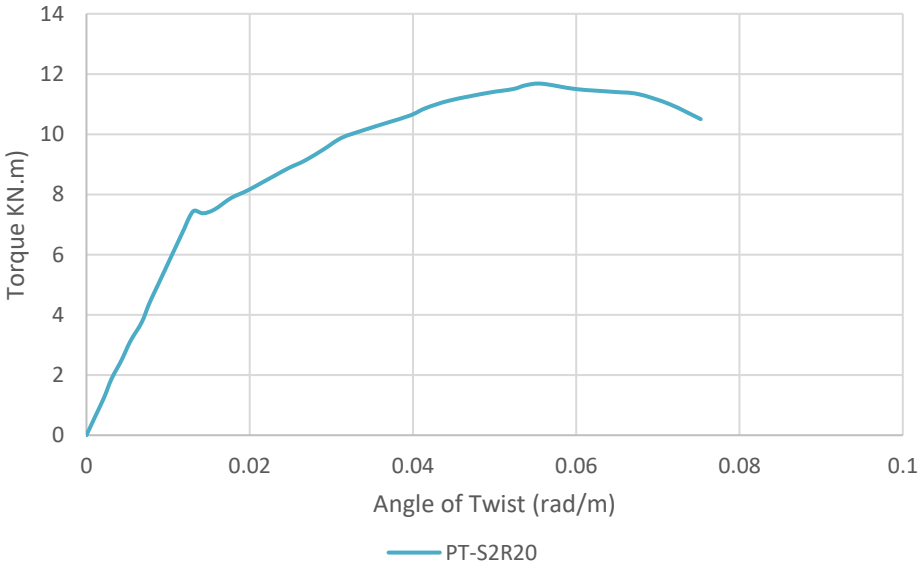

Figure (4-19): The curve of torque – angle of twist for specimen **PT-S2R20**.

- **Specimen PT-S2R30**

A 30% substitution of coarse aggregate with chip rubber was used to create this sample of reinforced concrete. Middle of the beam, there was a visible fracture. Twice as much force led to 45-degree spiral fractures in plate (4-13), which propagated across the test area. Table (4-9) lists the values of cracking twisting moments, ultimate twisting moments, and twisting angle. Twist angle increased by about 48.28 percent as compared to the control beam while cracking torque and ultimate torque reduced by roughly 14.18 and 16.59 percent, respectively (**PT-S2R0**). Figure (4-20) illustrates the torque curve and twist angle.

Plate (4-13): Failure mode and crack pattern of beam specimen **PT-S2R30**.

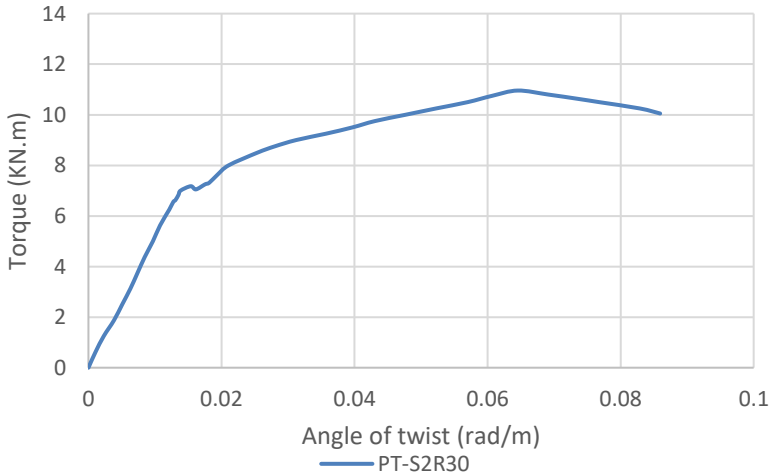

Figure (4-20): The curve of torque – angle of twist for specimen **PT-S2R30**.

For reinforced beam comparison in section 2, Figure illustrates the torque-twisting-angle relation (4-21). At a 30% substitute of rubber, the ultimate torsion decreased by 16.59% and the angle of twist increased by 48.28%.

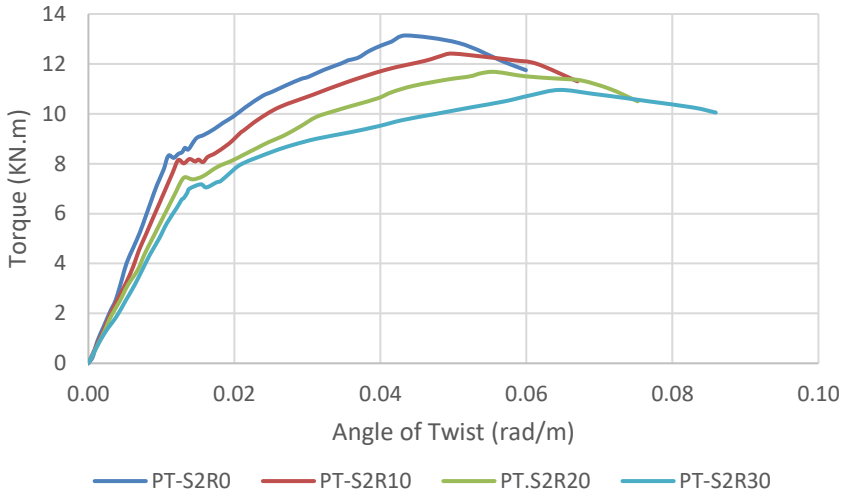

Figure (4-21): The curve of torque – angle of twist for reinforced beams in group one of section two.

4.4.1.3 Section Three: (130×390) mm Rectangle Section.

- **Specimen PT-S3R0**

Reinforced normal concrete was used to construct this beam, however replacement rubber was omitted. At a torque of 6.83 KN.m, a fracture initially appeared in the center of the beam. At a 45-degree angle, the spiral fractures first appeared as shown in Plate (4-14), then cracks expanded outward with increasing pressure. Table (4-9) lists the values of cracking twisting moments, ultimate twisting moments, and twist angle. Figure (4-22) illustrates the torque curve and twist angle.

Plate (4-14): Failure mode and crack pattern of beam specimen **PT-S3R0**.

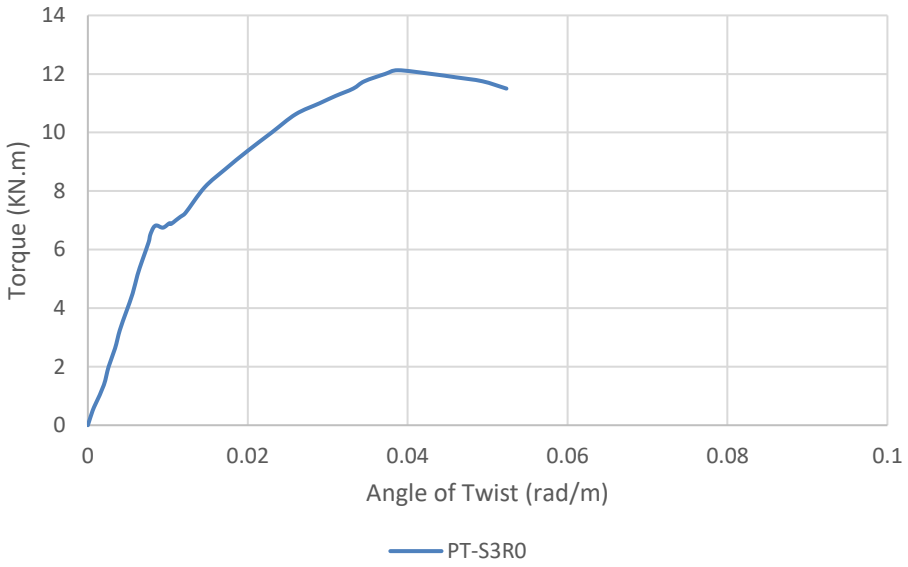

Figure (4-22): The curve of torque – angle of twist for specimen **PT-S3R0**.

♦ **Specimen PT-S3R0P**

Concrete without steel reinforcement and without rubber substitutes was used to build this specimen. To put it simply, if the maximum shear stress exceeds the concrete tensile cracking strength, the beam will fracture in a brittle manner if the maximum shear stress is exceeded. Plate (4-15) shows the location of the crack failure near the hinge support of the beam at a 45° angle. Table (4-9) displays the failure twisting moment and twist angle values. Figure (4-23) illustrates the torque curve and twist angle.

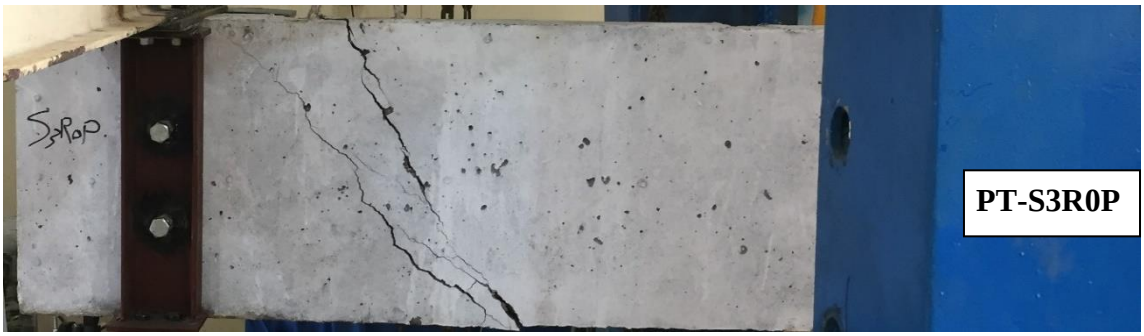

Plate (4-15): Failure mode and crack pattern of beam specimen **PT-S3R0P**.

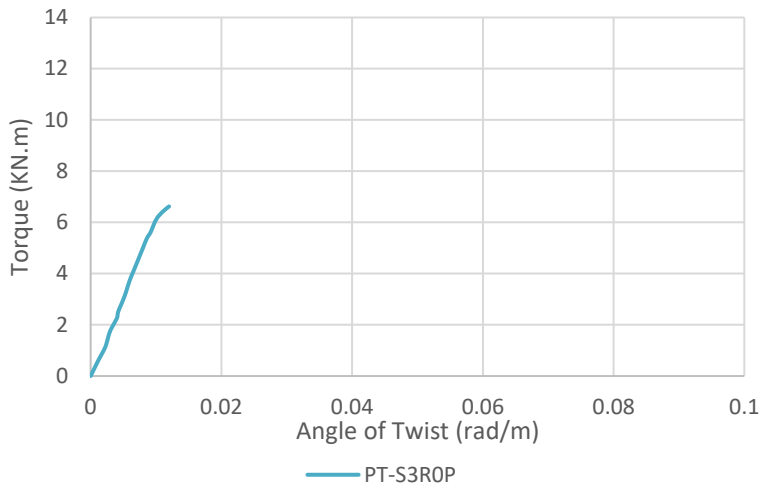

Figure (4-23): The curve of torque – angle of twist for specimen **PT-S3R0P.**

- **Specimen PT-S3R10**

When it comes to making this specimen, we employed reinforced normal concrete with a substitution of 10% chip rubber. The first apparent crack emerged in the middle of the beam. An increasing force caused spiral fractures to occur at a 45-degree angle in the test zone, as shown in Plate (4-16). Table (4-9) lists the values of cracking twisting moments, ultimate twisting moments, and twisting angle. As compared to the control beam (**PT-S3R0**), twist angle increased by 13.9 percent, while cracking torque decreased by 5.56% and ultimate torque decreased by 4.53%. According to the Figure (4-24), the torque versus twist angle relationship.

Plate (4-16): Failure mode and crack pattern of beam specimen **PT-S3R10**.

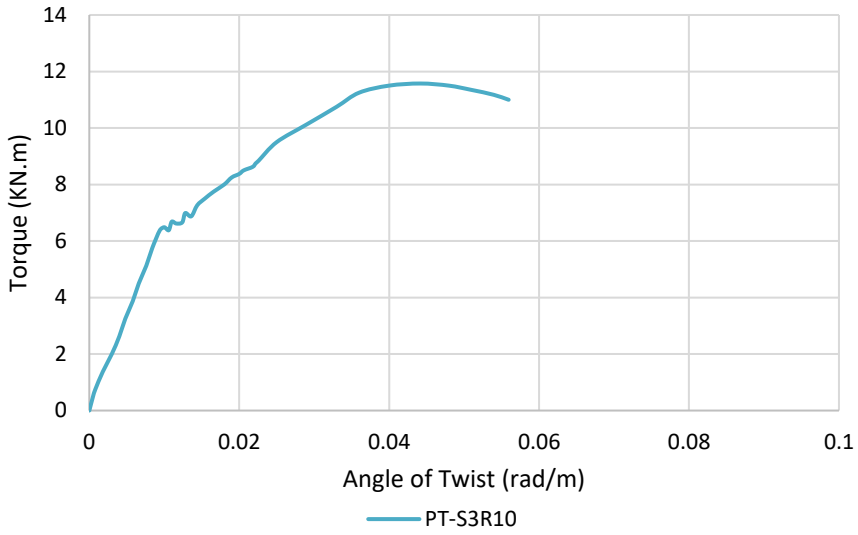

Figure (4-24): The curve of torque – angle of twist for specimen **PT-S3R10.**

- **Specimen PT-S3R20**

The coarse aggregate in this specimen has been replaced with chip rubber to the amount of 20% of the total weight of the specimen. A crack appeared on the beam's left edge, and this was the first. A spiral fracture that started at a 45-degree angle and propagated over the test area is shown in Plate (4-17). Table (4-9) lists the values for twist, breaking moment, and ultimate twisting moment. The twist angle increased by 28.93% as compared to a control beam (**PT-S3R0**), which had a 13.32% reduction in cracking torque and ultimate torque decreased by 8.08%. The curve of torque and the angle of the twist are illustrated in Figure (4-25).

Plate (4-17): Failure mode and crack pattern of beam specimen **PT-S3R20**.

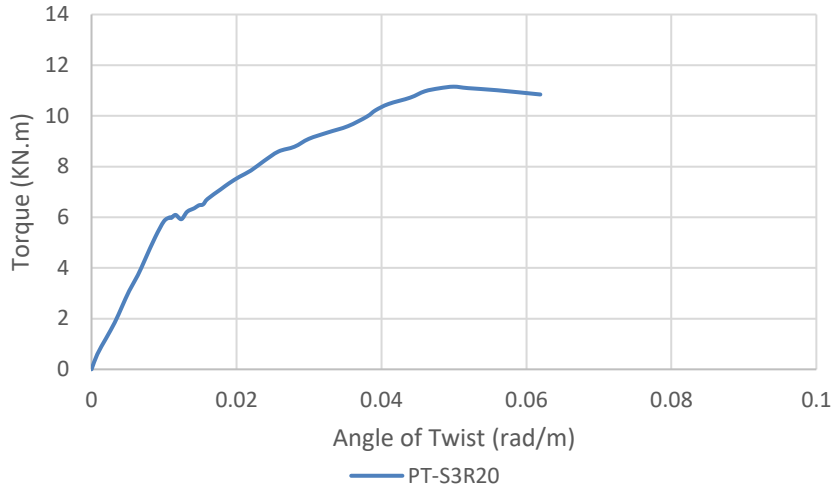

Figure (4-25): The curve of torque – angle of twist for specimen **PT-S3R20.**

- **Specimen PT-S3R30**

Reinforced concrete with a 30% replacement of coarse aggregate with chip rubber was created. Middle of the beam, there was first noticeable fracture. Plate (4-18) indicates that the spiral fractures began at around 45 degrees and expanded over the test area when the torque was increased. Table (4-9) shows the values of cracked twisting moments, ultimate twisting moments, and twist angles. In comparison with **PT-S3R0**, the cracking torque was 17.72% lower and the maximum torque 13.69% lower. In spite of this, the twist angle widened by 44,25%. Figure (4-26) depicts the torque curve and twist angle in their proper context.

Plate (4-18): Failure mode and crack pattern of beam specimen **PT-S3R30**.

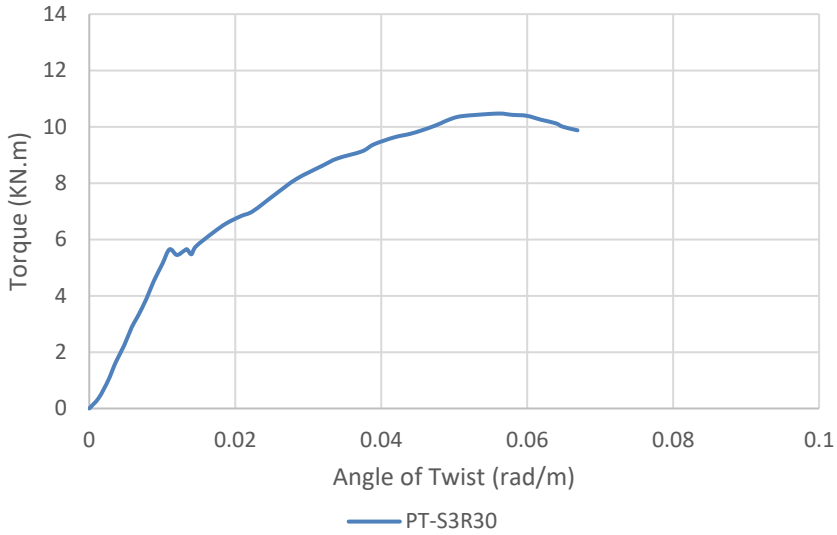

Figure (4-26): The curve of torque – angle of twist for specimen **PT-S3R30.**

- **Specimen PT-S3R30P**

This sample was created with normal concrete without steel reinforcement by substituting 30 percent of the coarse aggregate with chip rubber. Because the tensile cracking strength of plain concrete is equal to the maximum shear stress and it breaks in a brittle manner, the ultimate twisting torque of a beam is almost identical to its cracking torque. There was a 45-degree angle of failure, as illustrated in Plate (4-19), on the left side of the beam. The failure twisting moments and the twisted angles are shown in the table (4-9). Despite a 14.5% decrease in maximum torque, the twist angle increased by 61.67% when compared to the control beam (**PT-S3R0P**). Figure (4-27) illustrates the torque curve and twist angle.

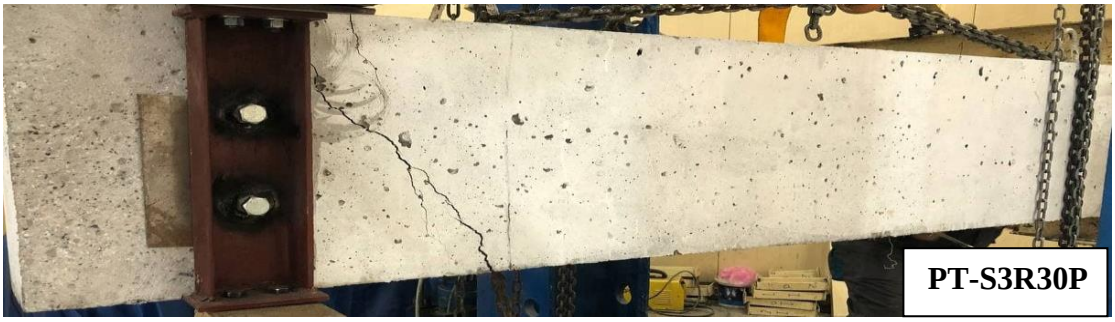

Plate (4-19): Failure mode and crack pattern of beam specimen **PT-S3R30P**.

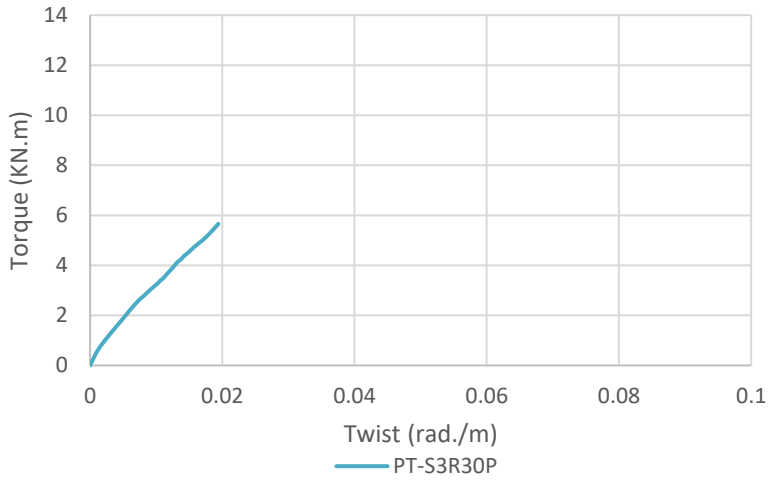

Figure (4-27): The curve of torque – angle of twist for specimen **PT-S3R30P.**

Figure (4-28) illustrates the relationship between torque and twist angle in the comparison of reinforced beams in Section 3. When the coarse aggregate was replaced by 30% with rubber. The torsion decreased by 13.69%, and the angle of twist increased by 44.22%.

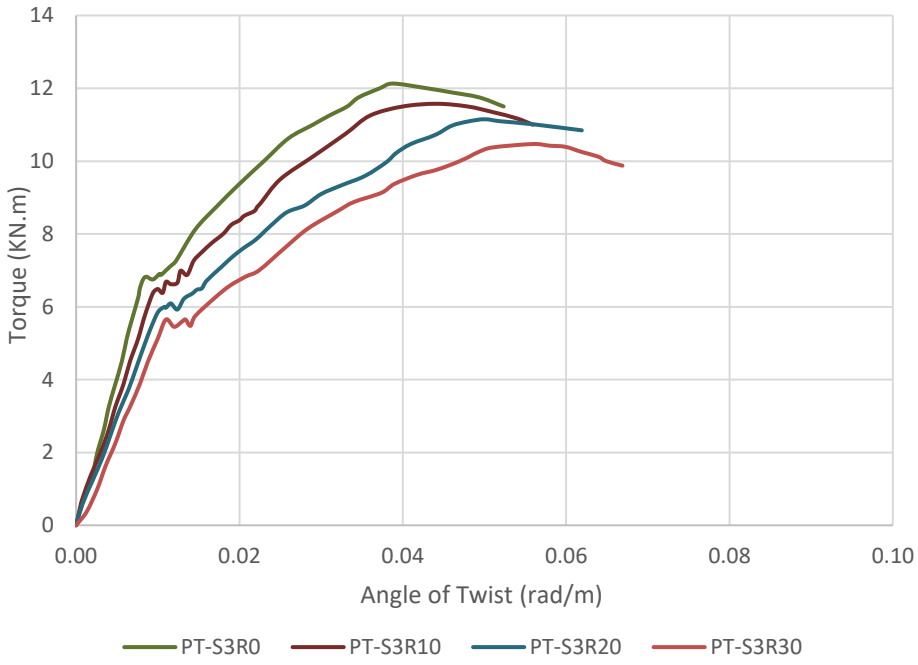

Figure (4-28): The curve of torque – angle of twist for reinforced beams in group one of third section.

The comparison of **PT-S3R0** with **PT-S3R0P** and **PT-S3R30** with **PT-S3R30P** for regular and rubberized concrete shows the influence of steel reinforcement. When compared to the failure torque of the beam **PT-S3R0**, the failure torque of the beam **PT-S3R0P** was reduced by 45.42 percent, and the twist angle was reduced by 69.06 percent. As shown in Figure (4-29), the failure torque of the beam **PT-S3R30P** was reduced by about 45.94% compared with the failure torque of the beam **PT-S3R30**, and the angle of twist decreased by about 65.32%.

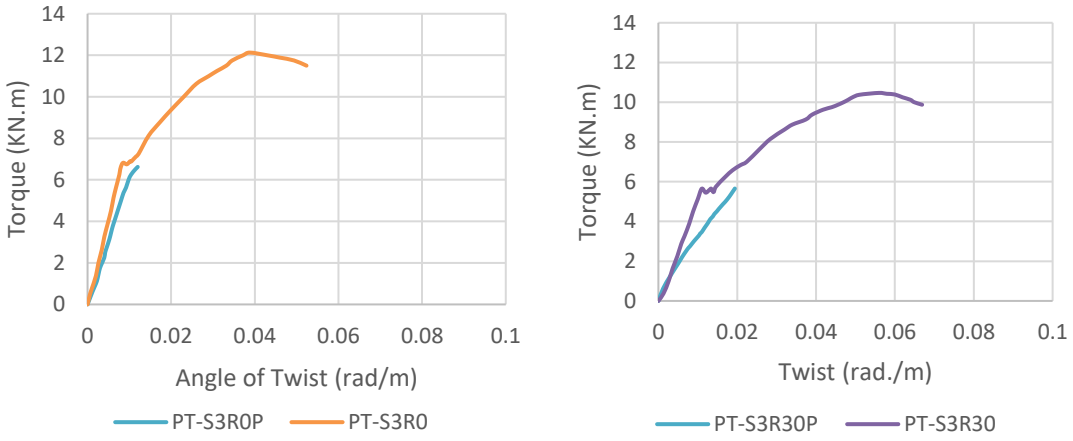

a- Normal concrete b- rubberized concrete

Figure (4-29): Variation of torque with angle twist of plain concrete with reinforced concrete in group one of third section.

For three sections, S1, S2, and S3, when h/b increases from 1 to 3, the ultimate torque decreases by about 10% for N.C and rubberized concrete (R30%) under pure torsion.

4.4.2 Group Two: (Results for Beams Under Combined Load).

The test results include control specimens without replacement rubber and specimens with 30% replacement rubber for section two of beams exposed to a combined load with a different ratio of bending to torsion. The main experimental results of cracking torque, ultimate

torque, angle of twist, ultimate bending, and deflection of the tested beam specimens are illustrated in Tables (4-10) to (4-12).

The specimens are reinforced longitudinally with 4 ϕ 12 mm steel bars and transversely with ϕ 8 mm steel bars at 86 mm spacing, with the load applied with varying torsion moment arms from the middle of the beam with respect to a different ratio of bending to torsion (λ).

Reinforced concrete beams are devoid of cracks in the early phases of loading. Between loads, the first noticeable cracks emerged on one of the beam's two broader faces, swiftly traversing the length of the face before spreading to the shorter face and collapsing.

Table (4-10): Cracking torque and bending moment for specimens in group two at the first crack.

Sample	λ	Cracking torque (KN.m)	* Diff. %	Flexural cracking (KN.m)	* Diff. %	Type of crack
C0.5-S2R0	0.5	7.25	----	----	----	torsion
C0.5-S2R30	0.5	5.48	-24.41	----	----	torsion
C0.75-S2R0	0.75	6.32	----	----	----	torsion
C0.75-S2R30	0.75	5.04	-20.25	----	----	torsion
C1-S2R0	1	9.88	----	----	----	torsion
C1-S2R30	1	7.54	-23.68	----	----	torsion
C2-S2R0	2	5.84	----	----	----	torsion
C2-S2R30	2	4.96	-15.07	----	----	torsion
C3-S2R0	3	----	----	11.72	----	bending
C3-S2R30	3	----	----	10.03	-14.42	bending
C4-S2R0	4	----	----	12.52	----	bending
C4-S2R30	4	----	----	9.51	-24.04	bending
* Compare with control beam (for same λ).						

Table (4-11): Ultimate torque and twist angle for specimens in group two.

Sample	λ	Ultimate torque (KN.m)	* Diff. %	Ultimate twist, θ (rad/m) ×10^{-3}	* Diff. %
C0.5-S2R0	0.5	13.64	----	33.9	----
C0.5-S2R30	0.5	11.23	-17.67	47.6	40.41
C0.75-S2R0	0.75	12.89	----	30.9	----
C0.75-S2R30	0.75	10.82	-16.06	43.1	39.48
C1-S2R0	1	18.90	----	17.8	----
C1-S2R30	1	15.80	-16.40	24.9	39.89
C2-S2R0	2	14.34	----	14.2	----
C2-S2R30	2	12.15	-15.27	20.5	44.37
C3-S2R0	3	11.89	----	12.6	----
C3-S2R30	3	10.02	-15.73	17.4	38.22
C4-S2R0	4	9.89	----	11.2	----
C4-S2R30	4	8.45	-14.56	14.9	33.04

Table (4-12): Ultimate bending moment and deflection for specimens in group two.

Sample	λ	Ultimate moment (KN.m)	* Diff. %	Ultimate deflection (mm)	* Diff. %
C0.5-S2R0	0.5	6.82	----	3.09	----
C0.5-S2R30	0.5	5.62	-17.60	4.16	34.63
C0.75-S2R0	0.75	9.67	----	4.09	----
C0.75-S2R30	0.75	8.12	-16.03	5.54	33.45
C1-S2R0	1	18.9	----	3.83	----
C1-S2R30	1	15.8	-16.40	5.18	35.25
C2-S2R0	2	28.68	----	6.0	----
C2-S2R30	2	24.30	-15.27	7.99	33.17
C3-S2R0	3	35.67	----	7.23	----
C3-S2R30	3	30.06	-15.73	9.85	36.24
C4-S2R0	4	39.27	----	7.75	----
C4-S2R30	4	33.56	-14.57	10.34	33.42

4.4.2.1 Beams with λ= 0.5

- **Specimen C0.5-S2R0**

This specimen is built of regular reinforced concrete with no rubber substitution. There were torsional fractures that formed between the loads as a spiral crack with a twisting torque of 7.25 KN.m, as indicated in Table (4-10). As the applied stresses increased, a bending fracture formed between the loads, as well as spiral cracks, as shown in Plate (4-20). There are also values for bending and twisting that are presented in Tables (4-11) and (4-12).

- **Specimen C0.5-S2R30**

With a 30% rubber substitute in this specimen, reinforced concrete is created. According to Table (4-10), the initial apparent fracture had a 5.48 KN.m torsional crack in its center. It was found that the test area between loads had both spiral and bending fractures. Plate (4-21) shows it. Tables (4-11) and (4-12) illustrate deflection, bending, torque, and twist angles. Compared to the control beam (**C0.5-S2R0**), the cracking torque was decreased by 24.41%, the ultimate torque by 17.67%, the bending moment was also lowered, but the twist angle was increased by 40.41%, and increased deflection by about 34.63%.

Plate (4-20): Failure mode and crack pattern of beam specimen **C0.5-S2R0**.

Plate (4-21): Failure mode and crack pattern of beam specimen **C0.5-S2R30**.

Figures (4-30) and (4-31) illustrate the torque-rotation and bending moment-deflection curves for comparing beams when λ=0.5, respectively.

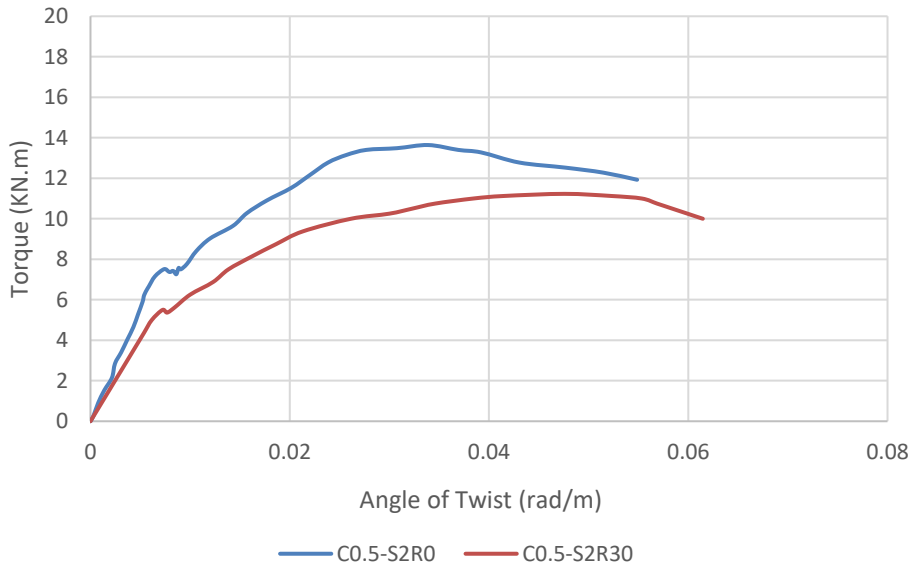

Figure (4-30): The curve of torque–angle of twist for specimens when **λ=0.5.**

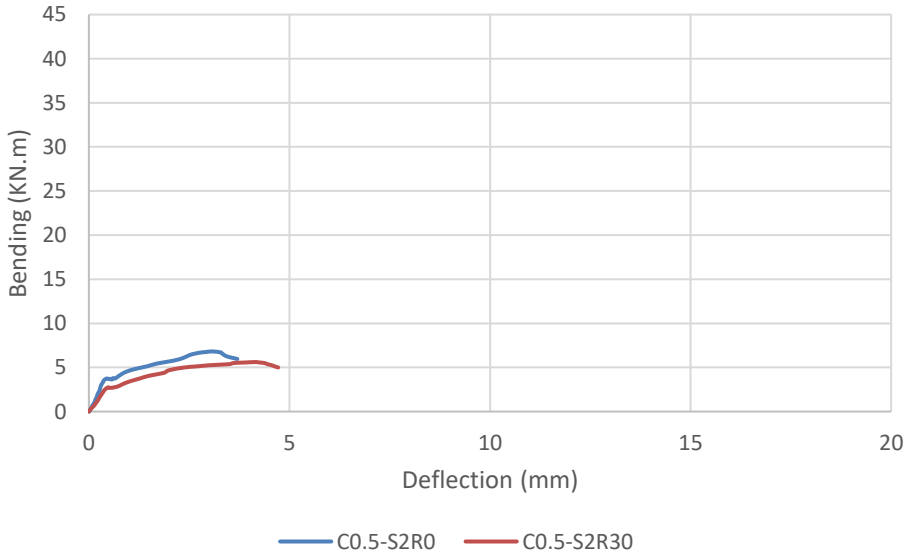

Figure (4-31): The curve of bending – deflection for specimens when **λ=0.5.**

4.4.2.2 Beams with λ= 0.75

- **Specimen C0.75-S2R0**

This specimen is composed entirely of reinforced concrete, and no rubber was utilized in its construction. A spiral crack with a twisting

torque of 6.32 kN.m occurred between the loads at the left load as a first crack, as shown in Table (4-10). There were some bending fractures between the loads as applied stresses rose, as seen in Plate (4-22). There are also values for twisting and bending, which you can find in Tables (4-11) and (4-12).

- **Specimen C0.75-S2R30**

Due to a 30% rubber replacement, reinforced concrete is available in this specimen. According to Table (4-10), the first apparent fracture exhibited a 5.04 kN.m torsional crack in the center of the beam. There were a few bending fractures and spiral cracks in the test zone between the loads, as seen in Plate (4-23). Using the Tables (4-11) and (4-12), the angles of twist, deflection, bending, and torque. There was a 16.06% decrease in ultimate torque, and a 20.25% drop in the torque needed to crack. When compared to the control beam (**C0.75-S2R0**), the bending moment was reduced as well, but the twist angle increased by 39.48%.

Plate (4-22): Failure mode and crack pattern of beam specimen **C0.75-S2R0**.

Plate (4-23): Failure mode and crack pattern of beam specimen **C0.75-S2R30**.

At λ=0.75, the torque-rotation and bending moment-deflection curves are shown in Figures (4-32) and (4-33) respectively.

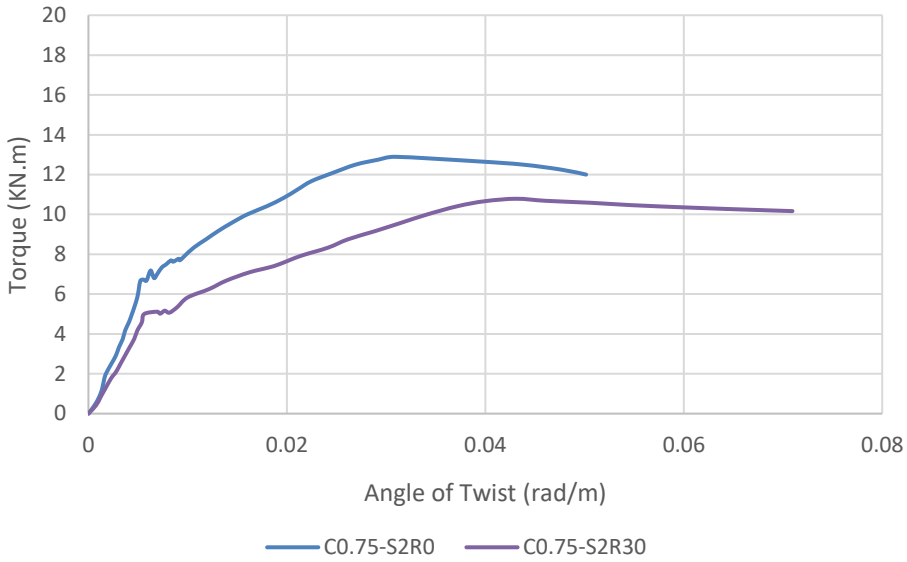

Figure (4-32): The curve of torque-angle of twist for specimens when **λ=0.75.**

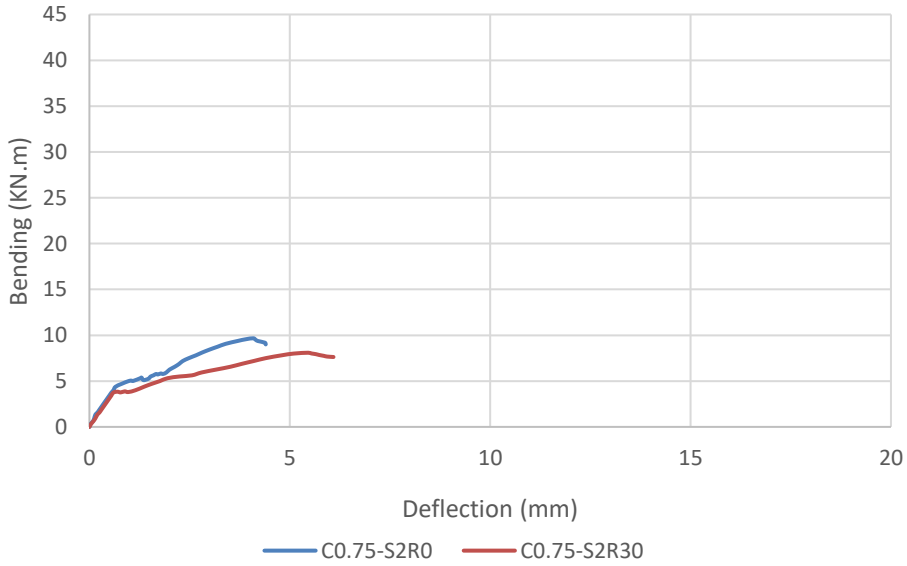

Figure (4-33): The curve of bending-deflection for specimens when **λ=0.75.**

4.4.2.3 Beams with λ= 1

- **Specimen C1-S2R0 (control beam)**

No rubber has been used in the construction of this specimen, which is composed of normal reinforced concrete. A torsional fracture, with a cracking torque of 9.88 kN.m, was first seen in the middle of the

beam, according to Table (4-10). At a 45-degree angle, spiral fractures developed and bending cracks propagated across the test area, as illustrated in Plate (4-24). Data on ultimate torque, ultimate moment, twist angle, and deflection may be found in Tables (4-11) or (4-12).

- **Specimen C1-S2R30**

Reinforced concrete with a 30% rubber substitution is used to make this specimen. There was a 7.54 kN.m cracking torque in the first apparent crack, which occurred between loads from left to right, as illustrated in Table (4-10). In addition to spiral cracks, some bending fractures were seen in the test zone between loads, as shown in Plate (4-25). There are two tables (4-11) and (4-12) that indicate the maximum bending and deflection as well as maximum torque and twist angles. It reduced cracking torque by 23.68%, ultimate torque and bending moment by 16.4% when compared to the control beam (**C1-S2R0**), but increased twist angle by 39.89% and increased deflection by 35.25%.

Plate (4-24): Failure mode and crack pattern of beam specimen **C1-S2R0**.

To compare a beam to another, the torque-rotation and bending moment-deflection curves in Figures (4-34) and (4-35) are shown.

Plate (4-25): Failure mode and crack pattern of beam specimen **C1-S2R30**.

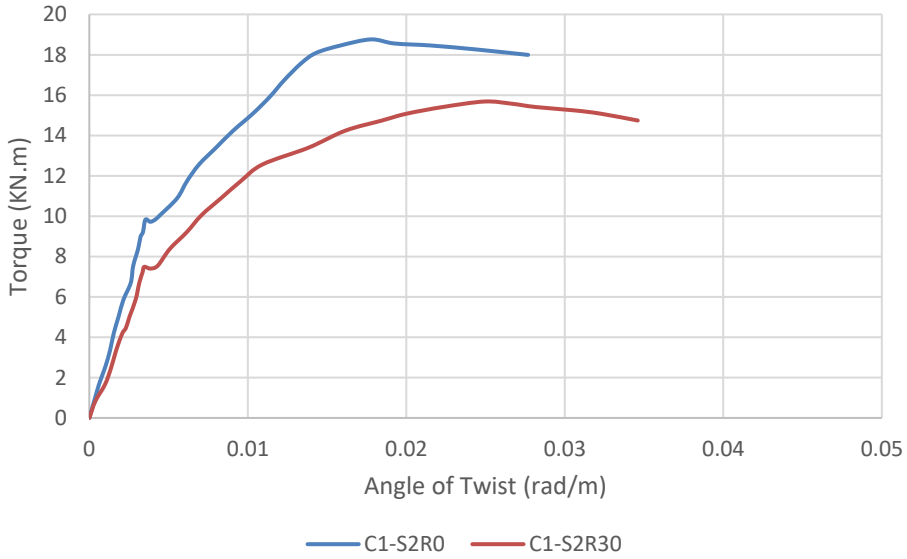

Figure (4-34): The curve of torque – angle of twist for specimens when **λ=1.**

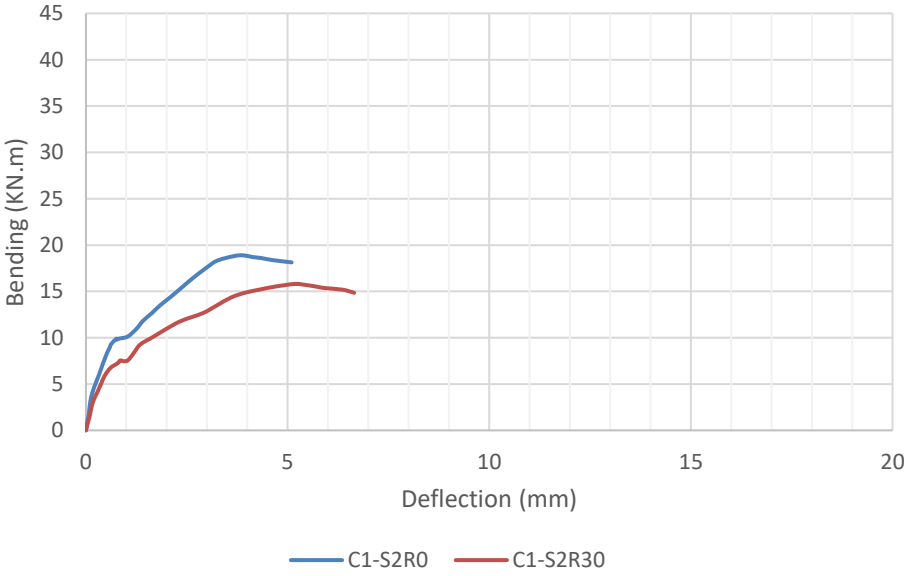

Figure (4-35): The curve of bending – deflection for specimens when **λ=1.**

4.4.2.4 Beams with λ= 2

- **Specimen C2-S2R0**

The specimen is built with reinforced concrete, but no rubber was utilized. Table (4-10) shows the initial cracking torque was 5.84 KN.m at a 45-degree angle, and when the applied loads increase, certain bending cracks occurred in the center of the beam in addition to spiral fractures, as illustrated in Plate (4-26). The maximum bending, ultimate torque, twist angle, and deflection values are shown in Tables (4-11) and (4-12).

- **Specimen C2-S2R30**

A rubber alternative makes up 30% of coarse aggregate in the reinforced concrete in this specimen. Table (4-10) shows a cracking torque of 4.96 kN.m between the loads on the left and right was the first crack. There were also some bending fractures in the test zone, in addition to spiral cracks. A specimen may be seen in Plate (4-27). Maximum torque, maximum bending, twist angles, and deflection are all shown in Tables (4-11) and (4-12). If you compare this beam to a control beam (**C2-S2R0**), the cracking torque was reduced by about 15.07%, the ultimate torque and the bending moment were also reduced by approximately 15.27%, but the twist angle was elevated by 44.37% and deflection by 33.17%.

Plate (4-26): Failure mode and crack pattern of beam specimen **C2-S2R0**.

Plate (4-27): Failure mode and crack pattern of beam specimen **C2-S2R30**.

When λ=2, torque-rotation and bending moment-deflection curves for comparing beams are shown in Figures (4-36) and (4-37), respectively.

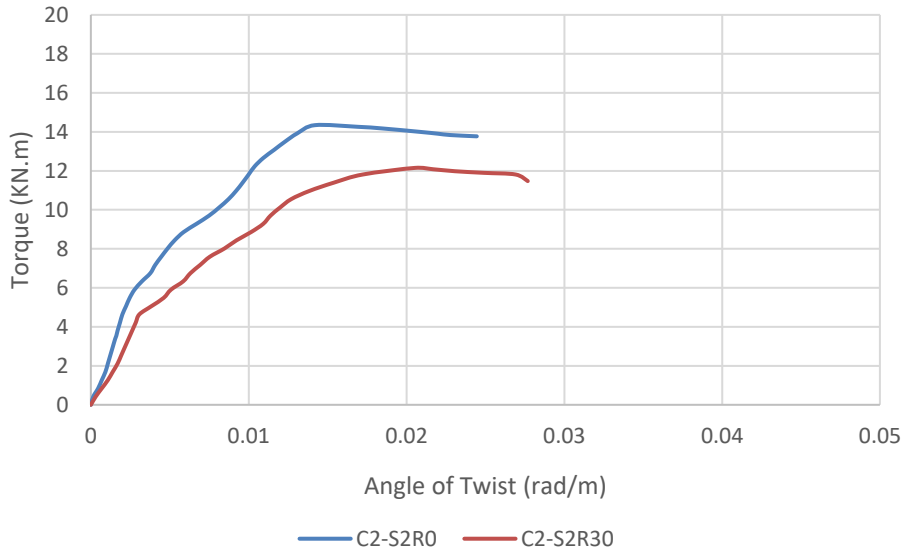

Figure (4-36): The curve of torque – angle of twist for specimens when **λ=2.**

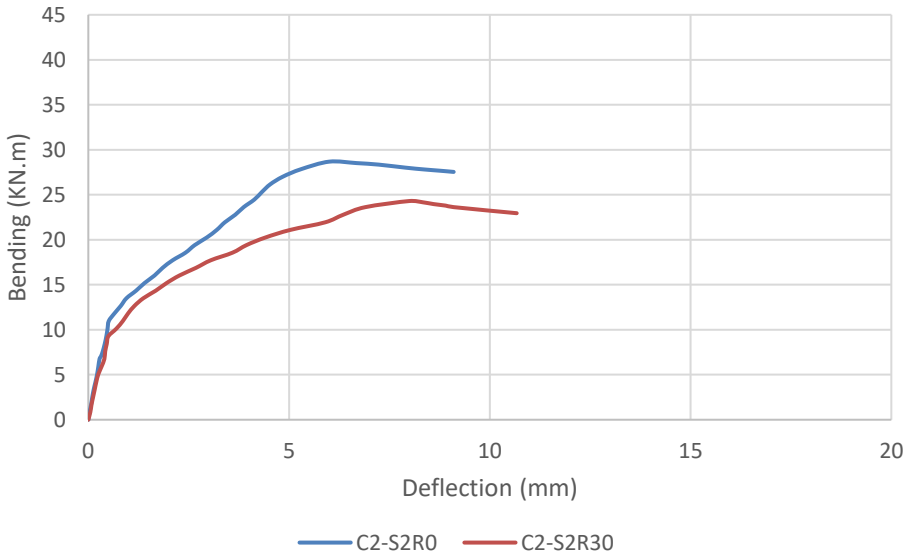

Figure (4-37): The curve of bending – deflection for specimens when **λ=2.**

4.4.2.5 Beams with λ= 3

- **Specimen C3-S2R0**

This sample is made completely of normal, reinforced concrete and does not include any rubber. Flexural fractures first emerged as vertical cracks in the middle of the beam, with a cracking moment of 11.72 KN.m, as shown in the Table (4-10). Bending cracks and spiral cracks appeared when loads were applied and propagated to the space between the load and its supporting structure, as shown in Plate (4-28). Tables (4-11) and (4-12) indicate the maximum bending, final torque, twist angles, and deflection values, respectively.

- **Specimen C3-S2R30**

This specimen is made from reinforced concrete with a rubber substitute of 30%. A flexural cracking of 10.03 KN.m between loads may be shown in Table (4-10) for the first visible fracture. After that, the test zone was seen to have spiral cracks and bending fractures. With increased load, the cracks propagated to the region between the load and support. A sample may be seen in Plate (4-29). Deflection, twist angles, ultimate bending, and ultimate torque are all shown in Tables (4-11) and (4-12). Overall, the cracking moment was decreased by 14.42 percent, the ultimate torque and ultimate bending are decreased by 15.73% when compared to the control beam (**C3-S2R0**). Although, there was a 38.22% increase in the twist angle.

Plate (4-28): Failure mode and crack pattern of beam specimen **C3-S2R0**.

Plate (4-29): Failure mode and crack pattern of beam specimen **C3-S2R30**.

Comparing beams when λ=3, torque-rotation and bending moment deflection curves are shown in Figures (4-38) and (4-39).

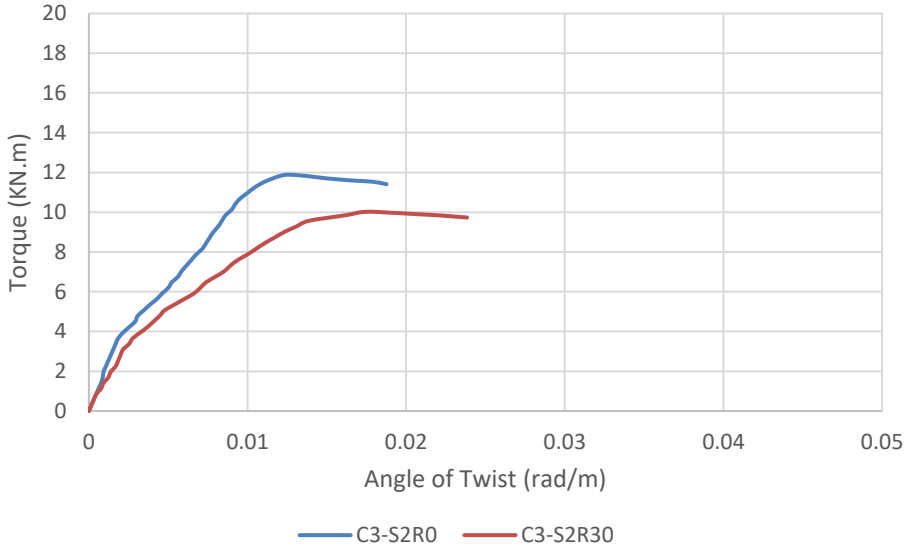

Figure (4-38): The curve of torque – angle of twist for specimens when **λ=3.**

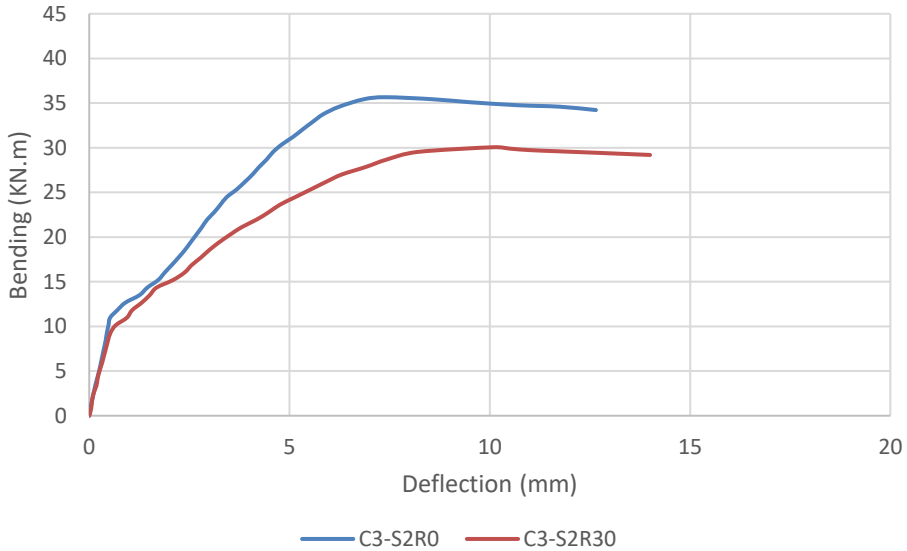

Figure (4-39): The curve of bending – deflection for specimens when **λ=3.**

4.4.2.6 Beams with λ= 4

- **Specimen C4-S2R0**

Normal reinforced concrete is used in this specimen, and no rubber alternatives are used. Table (4-10) shows the first visible crack is flexural cracks at a cracking moment of 12.52 kN.m in the center of the beam. When increases applied load, spiral fractures occurred in the test zone and bending cracks extending into an area between the load and support, as seen in Plate (4-30). Tables (4-11) and (4-12) provide bending and twisting statistics as well.

- **Specimen C4-S2R30**

Reinforced concrete is produced using this specimen, which contains a rubber replacement at a percentage of 30%. There is 9.51 kN.m flexural cracking in the first visible fracture in Table (4-10). In addition to spiral cracks and bending cracks between loads, the test zone was found to contain bending fractures that spread to the area between the load and support. This is shown on Plate (4-31). Tables (4-11) and (4-12) show the values of deflection, bending, torque, and twist angles. To account for decreased flexural cracking was 24.04%, the ultimate torque and ultimate bending were reduced by 14.56%, while the twist angle increase by 33.04% when compared to a control beam (**C4-S2R0**).

Plate (4-30): Failure mode and crack pattern of beam specimen **C4-S2R0**.

Plate (4-31): Failure mode and crack pattern of beam specimen **C4-S2R30**.

When comparing the torque-rotation and bending-deflection curves for beams when λ=4, the results are illustrated in Figures (4-40) and (4-41).

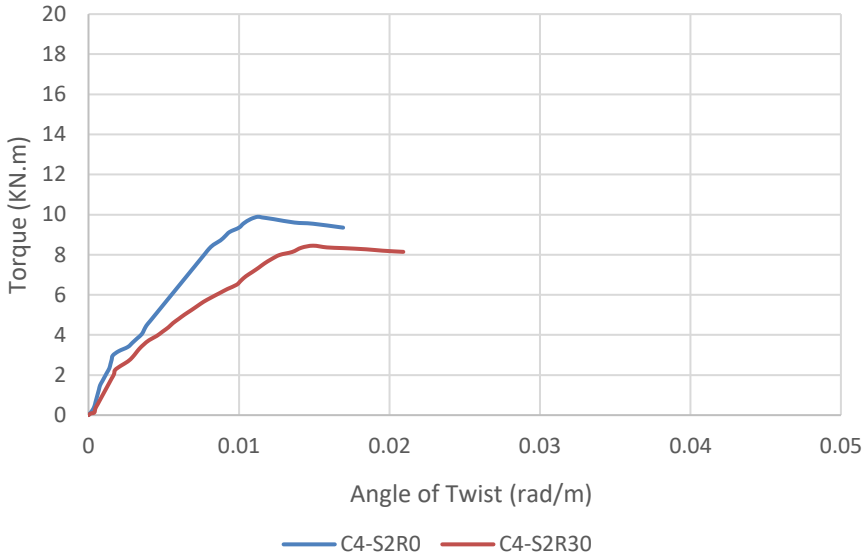

Figure (4-40): The curve of torque-angle of twist for specimens when **λ=4.**

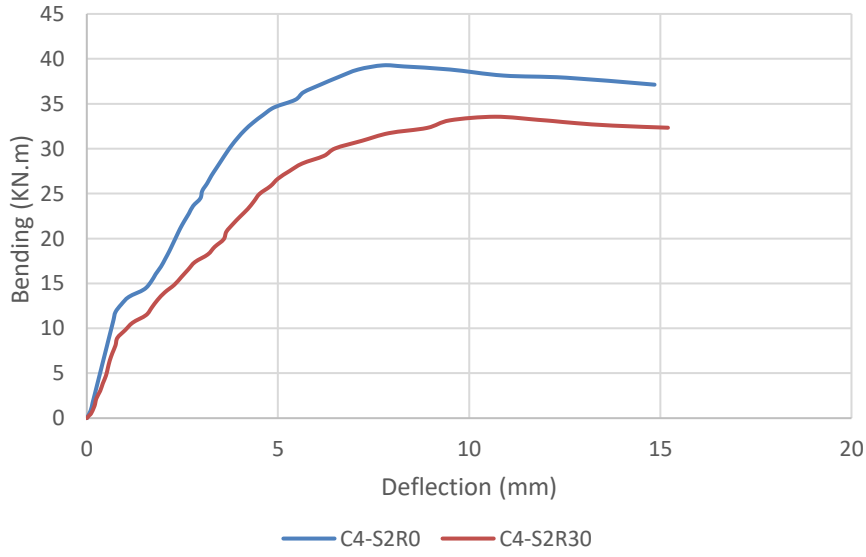

Figure (4-41): The curve of bending-deflection for specimens when **λ=4.**

Test results for beams in the second group show that the maximum torque and ultimate bending of beams decrease from 14.56% to 17.67% when 30% of coarse aggregate is replaced by chip rubber when λ is increased from 0.5 to 4, as compared to the control beam. This is not the only thing that changed. At last, the angle of twist at ultimate torque increase from 33.04% to 44.37%, and ultimate bending deflection increase from 33.14% to 36.24%.

4.4.3 Group three: (Results for beams under pure bending).

This section includes the results of samples with and without replacement rubber for the second section of beams subjected to bending, as well as samples with 30% replacement rubber. Experiments on the tested beam specimens, flexural cracking, ultimate bending, and deflection are summarized in the following Table (4-13).

Two-point loads on the middle third of the beam with a distance of 450 mm between them are placed. The specimens' longitudinal and transverse steel bars are 4 ϕ 12 mm and ϕ 8 mm at 86 mm spacing, respectively.

Table (4-13): Experimental results for specimens in group three.

Sample	Ultimate moment (KN.m)	* Diff. %	Ultimate deflection (mm)	* Diff. %
PB-S2R0	45.56	----	21.02	----
PB-S2R30	40.31	-11.52	28.61	36.11

- **Specimen PB-S2R0.**

This specimen was constructed mainly out of reinforced concrete. A cracking moment of 12.79 kN.m was found in the middle of this beam. With increasing loads, flexural cracks occurred between the loads and

expanded to the region between the load and support, as shown in Plate (4-32). Beam flexural cracks start at tension face and extend up to neutral axis at most, with the final arrival at near upper face. Bending and deflection values are shown in Table (4-13).

- **Specimen PB-S2R30.**

The middle region of the beam showed a flexural crack at 10.64 kN.m bending moment as a first evident fracture where the specimen having a 30% rubber replacement. As the load grew, bending fractures appeared in the test zone between the loads, which spread to the area between the load and the support. This may be seen in Plate (4-33). Table (4-13) shows the results of bending and deflection. When compare this to the control beam (**PB-S2R0**), there were less flexural cracks by 16.81%, less ultimate moment by 11.51%, and more deflection by 36.11% in this beam.

Plate (4-32): Failure mode and crack pattern of beam specimen **PB-S2R0**.

Plate (4-33): Failure mode and crack pattern of beam specimen **PB-S2R30**.

Bending moment-deflection curves for beams are shown in Figure (4-42) when pure bending is applied.

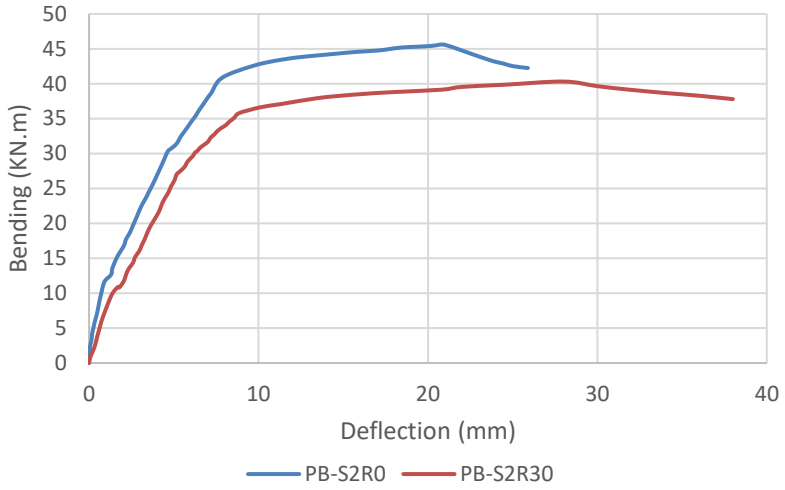

Figure (4-42): Bending–deflection curves for beams under pure bending**.**

4.5 Ductility

Ductility is the ability of a material to undergo large deformations without fracture. As a result, the ductility of rubberized concrete beam specimens was examined in this study. The test specimens' ductility could be determined using the formula (θ_{max}/θ_Y) or (Δ_u/Δ_Y), where θ_{max} is the rotation at ultimate torque, Δ_u is the ultimate deflection, θ_Y is the rotation in this area at yield, and Δ_Y is the deflection at yield, as shown in Figure (4-43) (**R. Park, 1989**). The twist–rotation curve and bending-deflection curve were used to calculate the ductility index of beams, as shown in Tables (4-14) and (4-15).

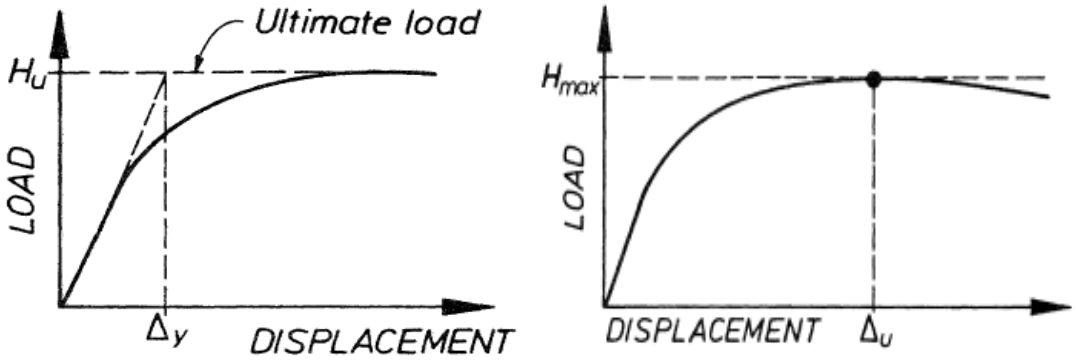

Figure (4-43): Definitions of ductility, (a) θ_Y: Based on Equivalent Elasto-Plastic Yield, (b) θ_{max}: Based on peak torque, **(R. Park, 1989).**

Table (4-14): Ductility index of test beams for first and second groups.

Sample			θ_{max} (rad/m)	θ_Y (rad/m)	μ	*Diff. %
Group One	Section One	PT-S1R0	0.0523	0.0210	2.49	----
		PT-S1R10	0.0581	0.0205	2.83	13.65
		PT-S1R20	0.0663	0.0213	3.11	24.90
		PT-S1R30	0.0730	0.0218	3.35	34.54
	Section Two	PT-S2R0	0.0435	0.0171	2.54	----
		PT-S2R10	0.0498	0.0174	2.86	12.60
		PT-S2R20	0.0558	0.0180	3.10	22.05
		PT-S2R30	0.0645	0.0191	3.38	33.07
	Section Three	PT-S3R0	0.0388	0.0154	2.52	----
		PT-S3R10	0.0442	0.0160	2.78	9.52
		PT-S3R20	0.0500	0.0170	2.94	16.67
		PT-S3R30	0.0559	0.0180	3.11	23.41
Group Two	λ= 0.5	C0.5-S2R0	0.0339	0.0120	2.83	----
		C0.5-S2R30	0.0476	0.0140	3.40	20.14
	λ= 0.75	C0.75-S2R0	0.0309	0.0100	3.09	----
		C0.75-S2R30	0.0431	0.0116	3.72	20.39
	λ= 1	C1-S2R0	0.0178	0.0064	2.78	----
		C1-S2R30	0.0249	0.0074	3.36	20.86
	λ= 2	C2-S2R0	0.0142	0.006	2.37	----
		C2-S2R30	0.0205	0.0071	2.89	21.94
	λ= 3	C3-S2R0	0.0126	0.0054	2.33	----
		C3-S2R30	0.0174	0.006	2.90	24.46
	λ= 4	C4-S2R0	0.0112	0.0047	2.38	----
		C4-S2R30	0.0149	0.0052	2.87	20.59
* Compare with control beam (for each case).						

Table (4-15): Ductility index of test beams for third group.

Sample		Δ_{max} (mm)	Δ_Y (mm)	μ	*Diff. %
Group Three	PB-S2R0	21.02	4.4	4.78	**----**
	PB-S2R30	28.61	5.0	5.72	19.67
* Compare with control beam (PB-S2R0).					

One can deduce that the ductility of the specimens in group one under pure torsion that have replacement rubber is superior to the reference specimen for each cross-section; this is due to rubber's influence on concrete and on the ductility of beams over that corresponding normal concrete (R0). The ductility index of test beams increased from 9.52% to 34.54% when the percentage of coarse aggregate substitution with chip rubber was increased from 10% to 30%.

It is also clear that the ductility of the specimens in group two under combined load (torsion + bending) with replacement rubber increased for each instance of λ. When λ was increased from 0.5 to 4, the ductility index of test beams varied from 20.14 % to 24.46 % if the coarse aggregate was replaced with chip rubber to the extent of 30%.

Specimen in the third group is more ductile than control beam when bent with replacement rubber, as shown in Table (4-14).

Figures (4-44) and (4-45) depict the relationship between the percentage of rubber and the ductility of beams.

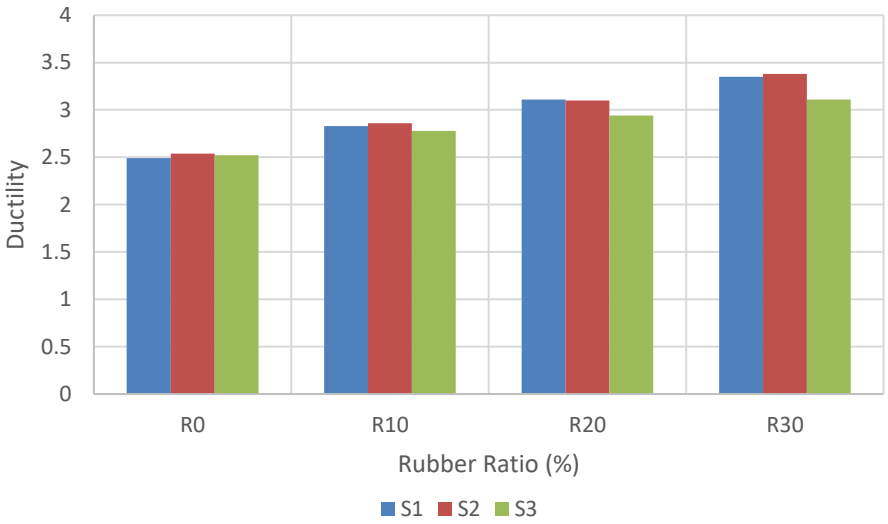

Figure (4-44): Effect of rubber substitution on beam ductility in the first group for various cross-sections.

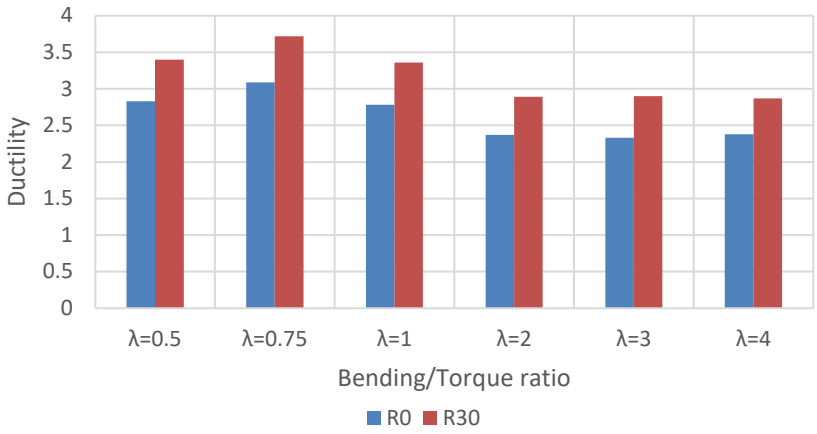

Figure (4-45): Effect of rubber substitution on beam ductility in the second group for various ratio of λ.

4.6 Stiffness of Beam Specimens

Stiffness is defined as the object's rigidity and the range of deformation it resists when subjected to an applied force. Experimentally measured ultimate torque-to-twisting-angle (or ultimate load-to-deflection) ratios were used to determine each specimen's stiffness as shown in Figure (4-46) (**Gunasekaran et al., 2014**). Concrete structural stiffness may be measured using a technique called cracking stiffness (K). Results of stiffness are shown in Tables (4-16) and (4-17).

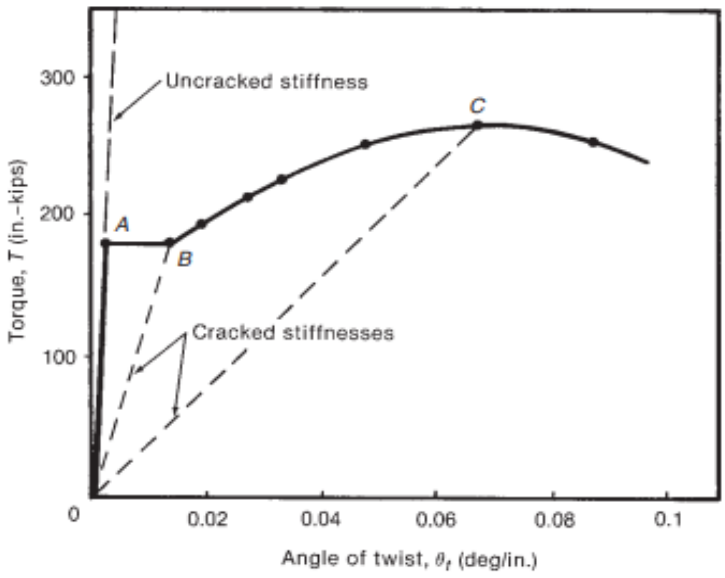

Figure (4-46): Calculation cracking stiffness, (**Gunasekaran et al., 2014**).

Table (4-16): Ultimate stiffness of test beams in first and second groups.

Sample			Tu (kN.m)	θu (rad./m)	K (kN.m)	Diff. %
Group One	Section One	PT. S1R0	13.59	0.05226	260.05	----
		PT. S1R10	12.98	0.05809	223.45	-14.07
		PT. S1R20	12.22	0.06626	184.42	-29.08
		PT. S1R30	11.69	0.07300	160.14	-38.42
	Section Two	PT. S2R0	13.14	0.0500	262.8	----
		PT. S2R10	12.42	0.0561	221.39	-15.76
		PT. S2R20	11.68	0.0639	182.79	-30.45
		PT. S2R30	10.96	0.0707	155.02	-41.01
	Section Three	PT. S3R0	12.13	0.0388	312.63	----
		PT. S3R10	11.58	0.0442	262.00	-19.32
		PT. S3R20	11.15	0.0500	223.00	-40.19
		PT. S3R30	10.47	0.0559	147.79	-52.73
Group Two	λ= 0.5	C0.5-S2R0	13.64	0.0339	402.36	----
		C0.5-S2R30	11.23	0.0476	235.92	-41.37
	λ=0.75	C0.75-S2R0	12.89	0.0309	417.15	----
		C0.75-S2R30	10.79	0.0431	250.35	-39.98
	λ=1	C1-S2R0	18.90	0.0178	1061.80	----
		C1-S2R30	15.80	0.0249	634.54	-40.24
	λ=2	C2-S2R0	14.34	0.0142	1009.86	----
		C2-S2R30	12.15	0.0205	592.68	-41.31
	λ=3	C3-S2R0	11.89	0.0126	943.65	----
		C3-S2R30	10.02	0.0174	575.86	-38.98
	λ=4	C4-S2R0	9.89	0.0112	883.04	----
		C4-S2R30	8.45	0.0149	567.11	-35.78
* Compare with control beam (for each case).						

Table (4-17): Cracking stiffness of test beams in third group.

Sample		Ultimate load (kN)	Ultimate deflection (mm)	K (kN/mm)	*Diff. %
Group Three	PB-S2R0	135	21.02	6.42	**----**
	PB-S2R30	119.46	28.61	4.18	-34.89

From studying the results of cracking stiffness, one can observe that the inclusion of a different percentage of rubber replacement with coarse aggregate in beam specimens decreased stiffness significantly compared with normal concrete beams due to the low stiffness of rubber compared with coarse aggregate. Figures (4-47) and (4-48) show the decrease in stiffness when comparing the stiffness of the specimens with the percentage of rubber.

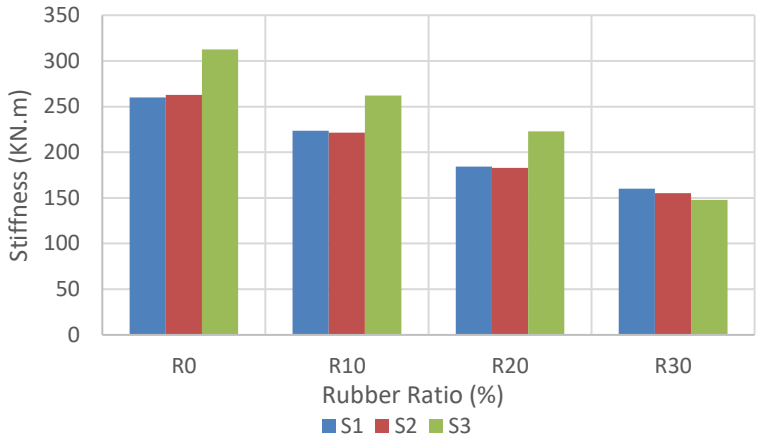

Figure (4-47): Effect of rubber substitution on stiffness of beams in the first group for various cross-sections.

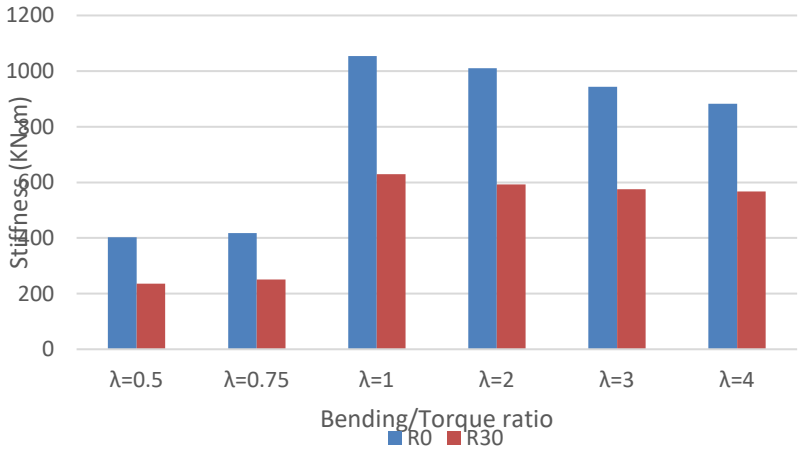

Figure (4-48): Effect of rubber substitution on stiffness of beams in the second group for various ratio of λ.

4.7 Crack Width and Failure Mode

Crack width and failure mechanism are shown in Table (4-18) for all specimen cracks in reinforced concrete beams. It has been shown that increasing the rubber replacement ratio resulted in a reduction in the

ultimate failure crack width but an increase in the number of cracks, compared to the reference beam built of normal concrete.

Table (4-18): Crack width for all tested beams.

Sample			Crack width at first crack (mm)	Crack width at ultimate load (mm)	Failure mode
Group One	Section One	PT. S1R0	----	----	Torsion
		PT. S1R10	----	----	Torsion
		PT. S1R20	----	----	Torsion
		PT. S1R30	0.06	0.90	Torsion
	Section Two	PT. S2R0	0.10	0.90	Torsion
		PT. S2R10	0.08	0.82	Torsion
		PT. S2R20	0.12	0.70	Torsion
		PT. S2R30	0.10	0.64	Torsion
	Section Three	PT. S3R0	0.08	0.70	Torsion
		PT. S3R10	0.10	0.58	Torsion
		PT. S3R20	0.08	0.46	Torsion
		PT. S3R30	0.06	0.40	Torsion
Group Two	λ= 0.5	C0.5-S2R0	0.18	0.54	Torsion + Bending
		C0.5-S2R30	0.16	0.42	Torsion + Bending
	λ= 0.75	C0.75-S2R0	0.12	0.90	Torsion + Bending
		C0.75-S2R30	0.10	0.74	Torsion + Bending
	λ=1	C1-S2R0	0.12	1.00	Torsion + Bending
		C1-S2R30	0.10	0.82	Torsion + Bending
	λ=2	C2-S2R0	0.08	0.96	Torsion + Bending
		C2-S2R30	0.08	0.74	Torsion + Bending
	λ=3	C3-S2R0	0.06	1.00	Torsion + Bending
		C3-S2R30	0.08	0.80	Torsion + Bending
	λ=4	C4-S2R0	0.10	0.94	Torsion + Bending
		C4-S2R30	0.06	0.70	Torsion + Bending
Group Three		PB-S2R0	0.08	2.9	Bending
		PB-S2R30	0.06	2.56	Bending

As shown in Figure (4-49), From zero to 30 percent, the proportion of chip rubber was changed, the width of the specimens' final failure cracks was decreased from 0.9-0.4 mm and 0.7-0.4 mm for sections two and three of group one, respectively. Figure (4-50) shows that the breadth of the ultimate failure cracks in the second group has shrunk when there is an increase from 0% to 30% in the use of chip rubber. Because the rubber's compression resistance and ultimate failure load were reduced in the specimens when the rubber concentration was increased, the final failure cracks of the rubberized reinforced concrete beams narrowed. Rubberized concrete specimens have a higher crack count because of the rubber's elastic properties, which has a lower elastic modulus and a higher Poisson's ratio than ordinary aggregate. This causes the differential stress rate between the cement paste and rubber partials to increase during the loading stage. A drop in the torque-rotation curve slope for rubberized reinforced concrete beams shows that high tensile stresses at the cement paste/rubber partial interfacial zone have led directly to a decrease in the overall stiffness values of the reinforced concrete beams that have been rubberized.

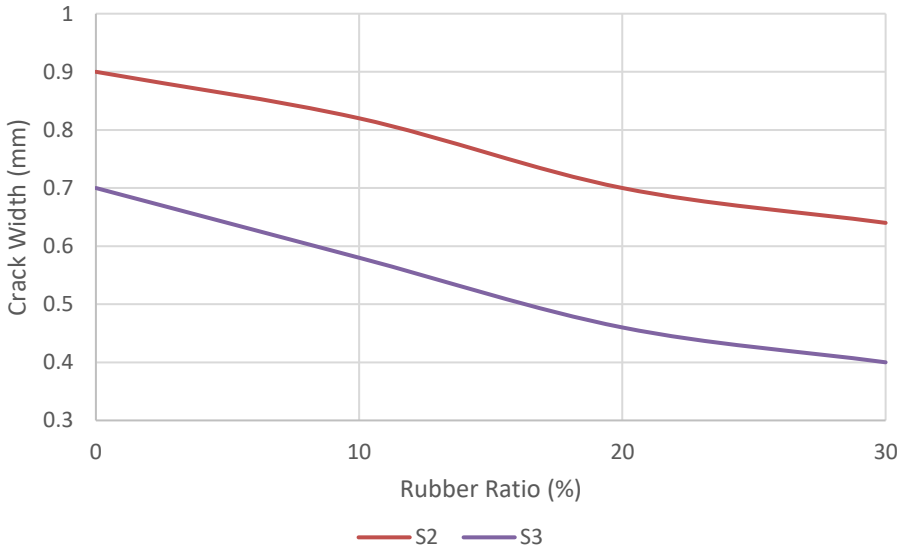

Figure (4-49): Crack width of beams for sections two and three in first group.

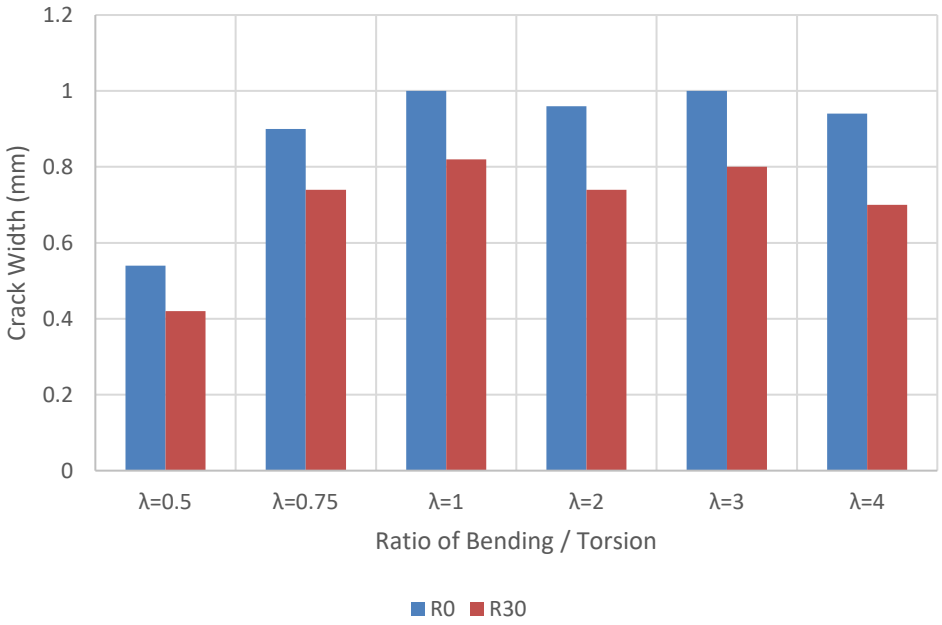

Figure (4-50): Crack width for beams in second group.

4.8 Torsional Toughness

Toughness is the ability of a material to absorb energy and plasticity deform without fracture. But the mix of strength and ductility has a role in the overall strength of the material. There are a number of reasons why energy absorption capacity is crucial for beams and other statically indeterminate structures, particularly for structures subjected to cyclic or recurrent stresses. A measure of toughness was obtained by dividing the total of the three area parts by the area of part I and computing the area under each curve (**Okay & Engin, 2012**), as illustrated in Figure (4-51). (Part I is the pre-cracking zone, Part II is the post-cracking zone, and Part III is the transition zone). The values reflect the energy in a length unit absorbed by an element during testing; the energy is acquired from a region beneath the rotational angle unit of the test torque curves; and the findings are organized as shown in Table (4-19).

Table (4-19): Energy absorption for all beams in three groups and the percentage increase with respect to control beams.

Sample			P_I	P_{II}	P_{III}	$P_I+P_{II}+P_{III}$	EAI	Diff. %
Group One	Section One	PT. S1R0	0.052	0.449	0.2	0.701	13.481	----
		PT. S1R10	0.051	0.5	0.216	0.767	15.039	11.56
		PT. S1R20	0.052	0.553	0.218	0.823	15.827	17.40
		PT. S1R30	0.05	0.584	0.238	0.872	17.440	29.37
	Section Two	PT. S2R0	0.044	0.365	0.207	0.616	14.000	----
		PT. S2R10	0.043	0.39	0.224	0.657	15.279	9.14
		PT. S2R20	0.0431	0.416	0.244	0.703	16.313	16.52
		PT. S2R30	0.041	0.462	0.248	0.751	18.317	30.84
	Section Three	PT. S3R0	0.03	0.297	0.157	0.484	16.133	----
		PT. S3R10	0.0293	0.323	0.17	0.522	17.826	10.49
		PT. S3R20	0.0287	0.34	0.178	0.547	19.049	18.07
		PT. S3R30	0.028	0.377	0.175	0.580	20.714	28.39
Group Two	λ= 0.5	C0.5-S2R0	0.034	0.296	0.267	0.597	17.559	----
		C0.5-S2R30	0.031	0.381	0.294	0.706	22.774	29.70
	λ=0.75	C0.75-S2R0	0.019	0.26	0.239	0.518	27.263	----
		C0.75-S2R30	0.0175	0.308	0.302	0.628	35.857	31.52
	λ=1	C1-S2R0	0.016	0.213	0.171	0.400	25.000	----
		C1-S2R30	0.015	0.322	0.149	0.486	32.400	29.60
	λ=2	C2-S2R0	0.008	0.119	0.147	0.274	34.250	----
		C2-S2R30	0.007	0.157	0.155	0.319	45.571	33.06
	λ=3	C3-S2R0	0.004	0.088	0.071	0.163	40.750	----
		C3-S2R30	0.0035	0.107	0.077	0.188	53.571	31.46
	λ=4	C4-S2R0	0.004	0.066	0.052	0.122	30.500	----
		C4-S2R30	0.0035	0.076	0.062	0.142	40.429	32.55
Group Three		PB-S2R0	6.05	849.19	248.01	1103.250	182.355	----
		PB-S2R30	5.7	1040.48	389.45	1435.630	251.865	38.12
* Compare with control beam (for each case).								

Due to the decreased stiffness of rubber particles, toughness indices (EAI) increase as rubber content rises (increasing flexibility and energy absorption). The difference in toughness indices for beams in group one ranged from 9.14% to 30.84% when the replacement of rubber increased from 10% to 30%, as shown in Figure (4-52).

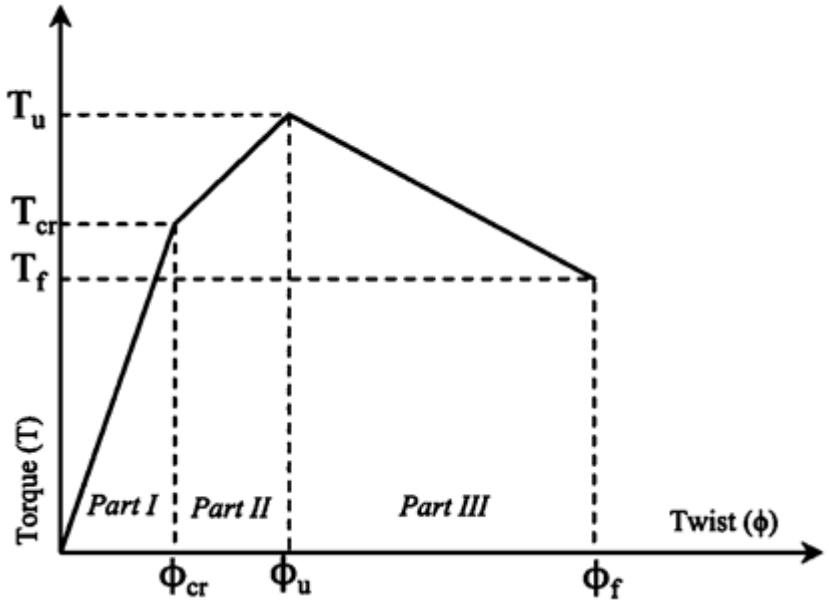

Figure (4-51): Torsion model **(Okay & Engin, 2012)**.

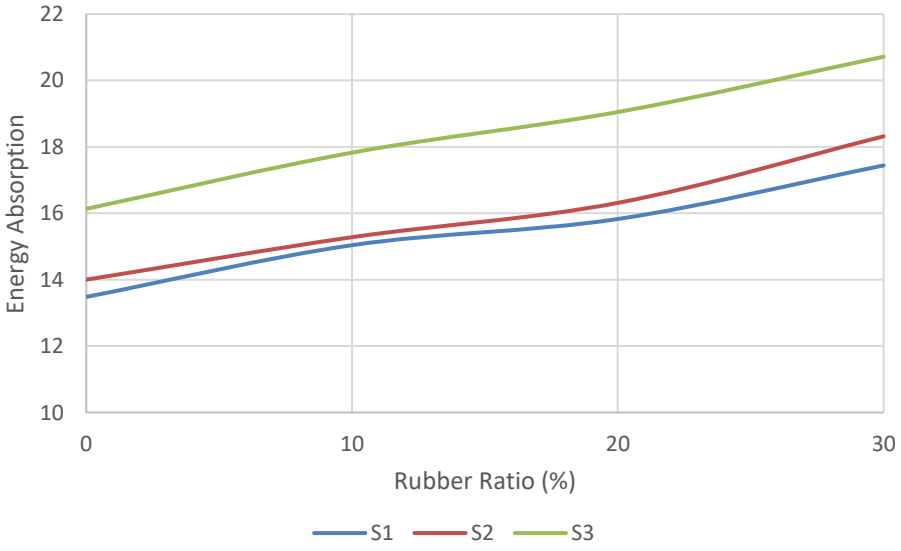

Figure (4-52): Energy absorption for beams in group one.

Beams in the second group with 30% coarse aggregate substitution with chip rubber had the difference in toughness indices that ranged from 29.60% to 33.06% when the ratio of λ increased from 0.5 to 4, as shown in Figure (4-53).

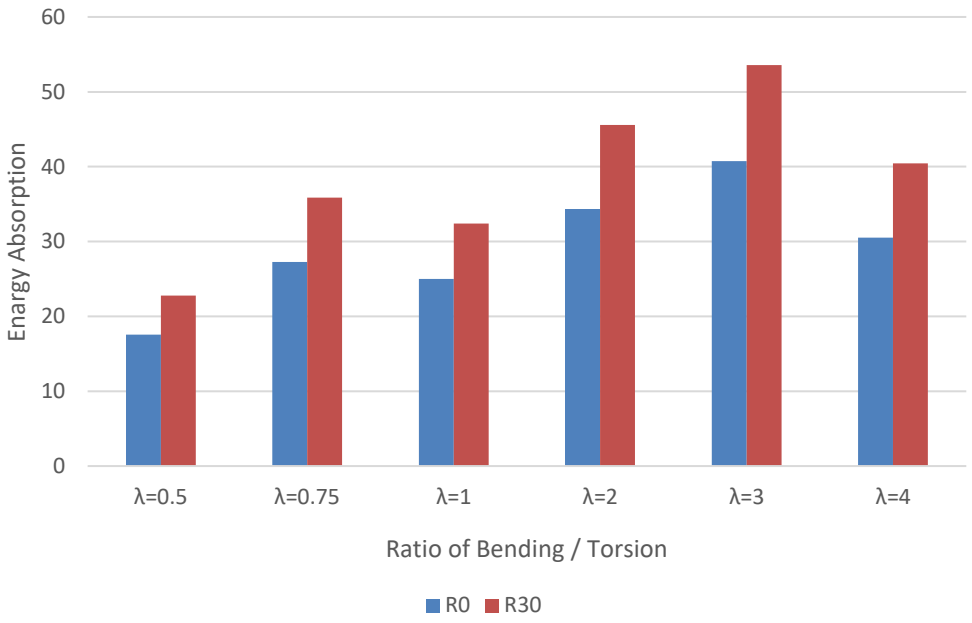

Figure (4-53): Energy absorption for beams in second group.

4.9 The Influence of Considered Variables

4.9.1 Rubber Content

Under pure torsion or combined loads (torsion and bending), the cracking load, ultimate load, and stiffness of all beam specimens are reduced, while the twist angle, crack width, ductility, and energy absorption are significantly increased with increasing the rubber, as shown in the Figures (4-54) to (4-59). This is due to the partial volumetric replacement of coarse aggregate with chip rubber. All of this is due to the difference in particle softness between waste tire rubber and aggregates, which causes this decrease. Weak adhesion between rubber and cement paste (the interfacial transition area between the rubber particles and the cement paste has low strength). In order to increase the flexibility of the

rubber cement, more rubber is added to the concrete mix in place of the gravel particles. This results in a lower rubber module elasticity.

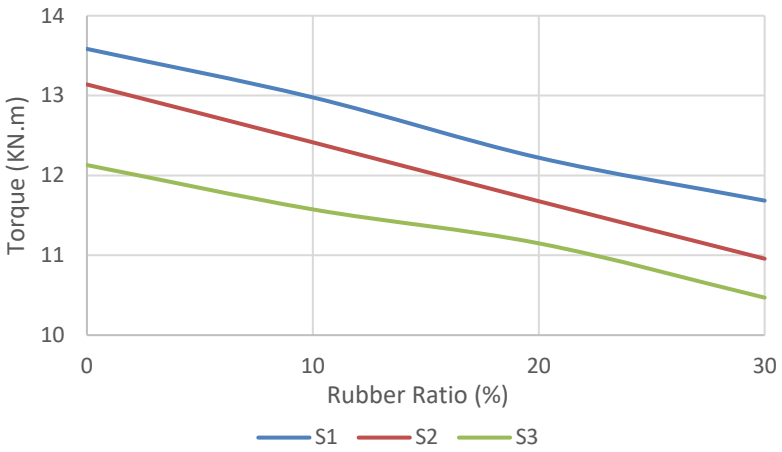

Figure (4-54): Torque-rubber relation for first group.

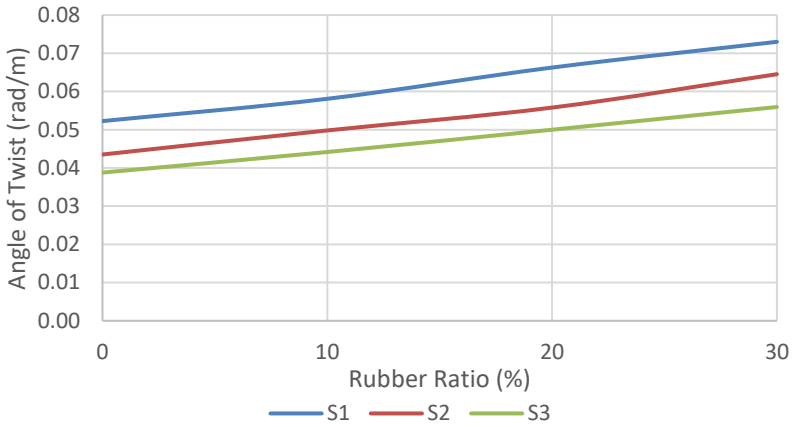

Figure (4-55): Angle of twist and rubber ratio relation for first group.

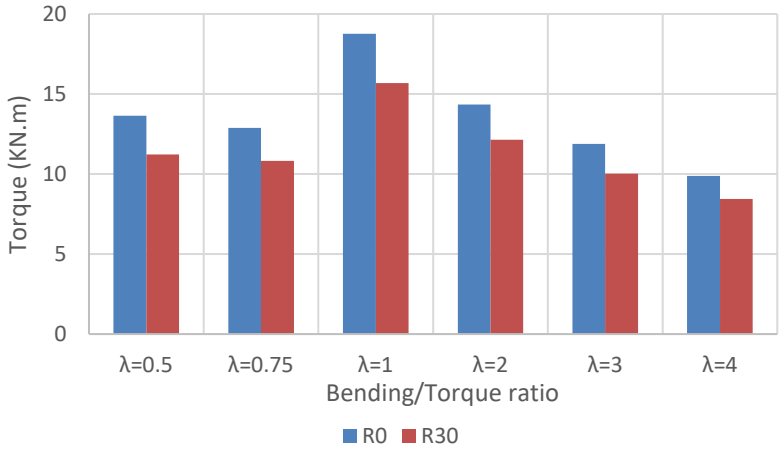

Figure (4-56): Torque and bending-to-torsion ratio relation for second group.

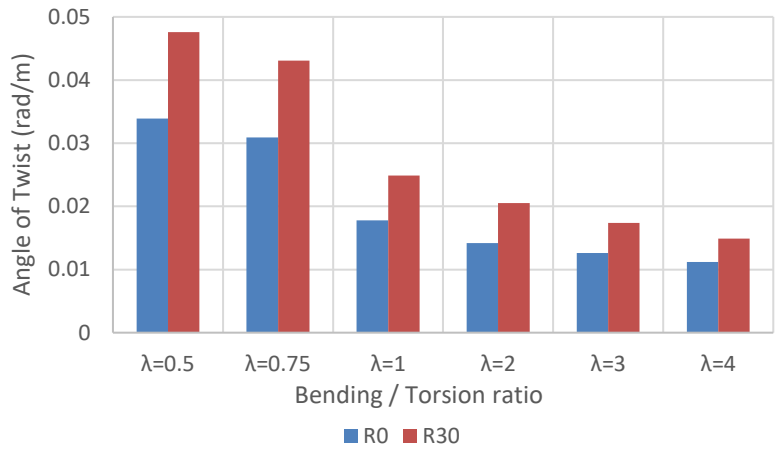

Figure (4-57): Angle of twist and bending-to-torsion ratio relation for second group.

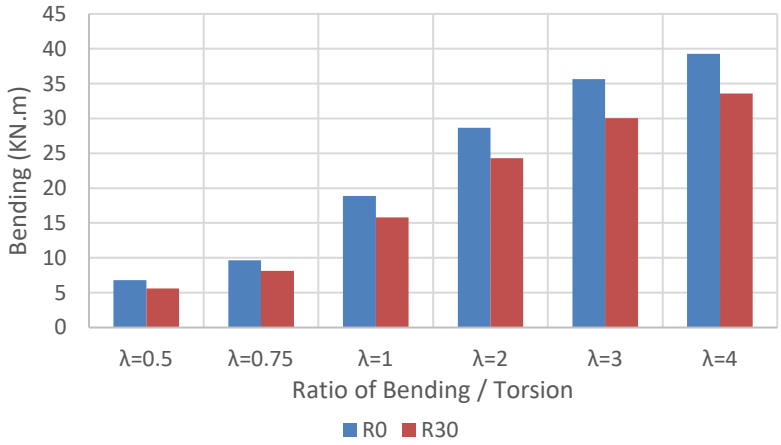

Figure (4-58): Bending and bending-to-torsion ratio relation for second group.

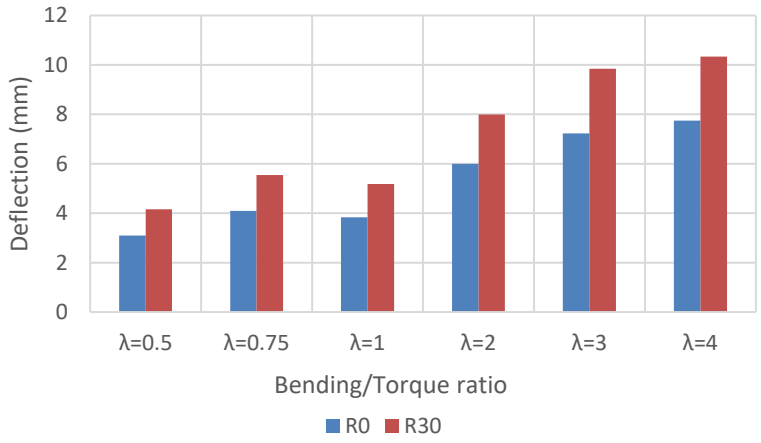

Figure (4-59): Deflection and bending-to-torsion ratio relation for second group.

4.9.2 Ratio of Height / Breadth

The first set of samples is separated into three divisions based on the height to breadth ratio (h/b). These numbers are 1, 2, and 3 for sections 1, 2, and 3 accordingly in terms of h/b. Increasing h/b percent from 1 to 3 reduced beam torsion and twist angle, but improved beam stiffness. h/b has a direct effect on the section's circumference and, consequently, on its torsion, as illustrated in the Figure (4-60). Because of the increased stiffness of the section, the twist angle reduces as (h/b) ratio increases, as seen in Figure (4-61).

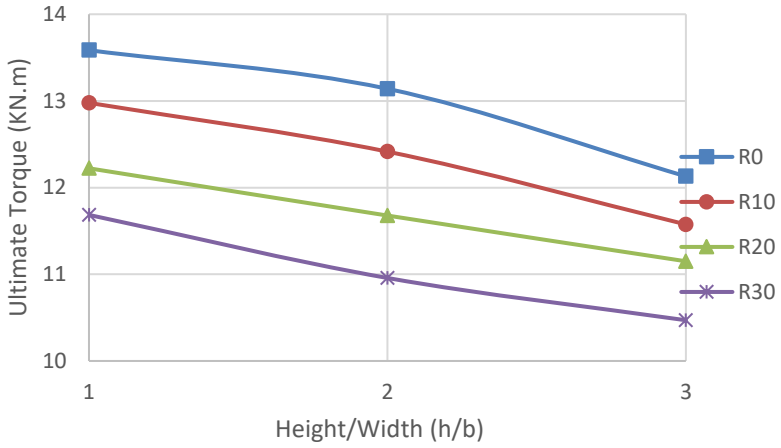

Figure (4-60): Relation of Torque and h/b for beams in first group.

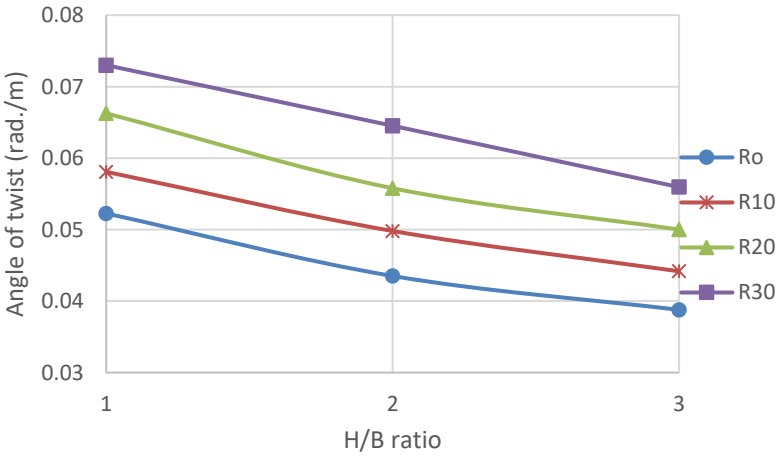

Figure (4-61): Relation of twist angle and h/b for beams in group one.

4.9.3 Types of Loading

For beams under pure torsion in the first group, there were many 45-degree and spiraling fractures, and the ultimate collapse was due to torsional stress. Torsion and bending loads in various proportions were applied to the beams in the second group, while they were also subjected to combination loads. Figure (4-62) shows that if the ratio of bending to torsion is increased, there is a reduction in torsion and an increasing in bending effect. In the third group, beams were checked while being bent, and the fractures were found to be vertical to the top, indicating that the failure was caused by bending cracks.

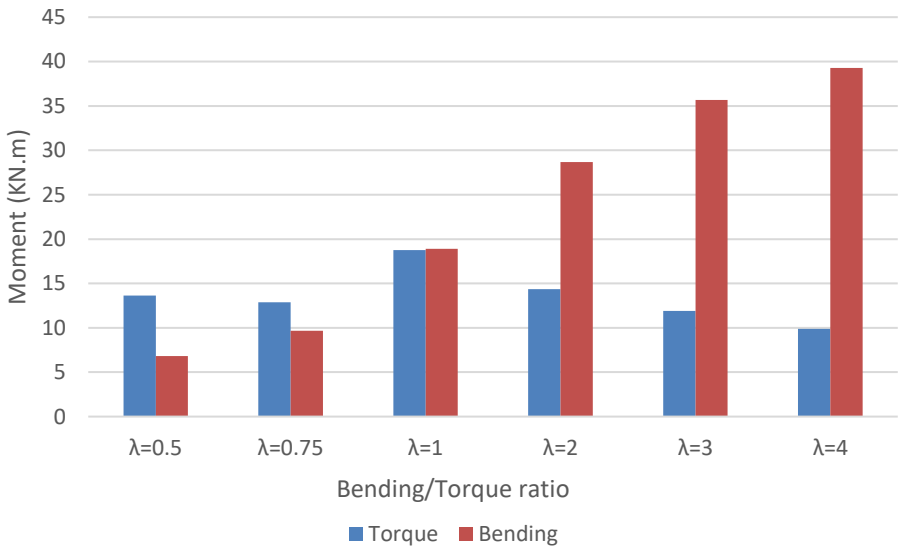

Figure (4-62): Relation between moment (Torque or bending) and λ for control beams in second group.

CHAPTER FIVE

PREDICTION OF THE TORSIONAL CAPACITY OF RUBBERIZED REINFORCED CONCRETE BEAMS

5.1 Introduction

In chapter four, the findings of thirty beams composed of normal reinforced concrete and rubberized reinforced concrete were given and discussed. When the rubber was used to partially replace coarse aggregate, the depth-to-width ratio was also evaluated, as was the sort of loading that was used. The beams in group one failed in torsion, the beams in group two failed in torsion and flexur, and the beams in group three failed in flexural. Therefore, the cracks in groups one, two, and three formed spiral cracks, spiral and flexural cracks, and flexural cracks, respectively. Reinforced concrete beams can only apply the elasticity theory before a major crack forms. A non-linear stress response in reinforced concrete beams proved difficult to adequately characterize using elastic analysis after cracks occurred. Many techniques were devised to analyze and design torsion.

Findings from experiments to determine a concrete beam's maximum carrying capacity will be compared with analytical predictions based on a thin-walled tube/space truss analogy in this chapter. Loading predictions for rubberized reinforced concrete utilizing American and European codes will be tested and compared to experimental data. These methods were shown to be ineffective in assessing the impact of rubber content in the concrete mix. As a result, this study suggests an additional useful component for achieving ACI-code experimental criteria.

5.2 Torsion for beams in ACI-code.

A thin-walled tube space truss analogy is used in **(ACI 318-19, 2019**) to torsional design. As illustrated in Figure (5-1a), the cross section of the core concrete in a solid beam is neglected when modeling a torsional stressed beam as an idealized thin-walled tube. After a reinforced concrete beam has cracked in torsion, the bulk of its torsional strength comes from closed stirrups and longitudinal bars located near the member's surface. It is considered that in the thin-walled tube analogy the outer skin of the cross section, approximately centered on the closed stirrups, is responsible for the tube's strength. Thin-walled tubes are idealized for both hollow and solid portions before and after cracking.

A closed thin-walled tube's shear flow, $q = \tau t$, may be defined as that which is obtained by multiplying the shear stress τ by the thickness of the wall t. In Figure (5-1a), the torsion-induced shear flow q operates as illustrated, and is constant along the tube's perimeter. There is a circular channel that goes around the tube at mid-thickness of the tube's walls. It is possible to determine shear stress due to torsion at any point along the tube's circumference using the formula:

$$\tau = \frac{T}{2A_{\circ}t} \tag{5-1}$$

From eq. (5-1), the shear flow q equals to:

$$q = \frac{T}{2A_{\circ}} \tag{5-2}$$

where A_o is the gross area contained by the shear flow channel, shaded in Figure (5-1b), and t is wall thickness. The area of a hole in a hollow part with continuous walls is included in A_o. Concrete's torsional

strength contribution is neglected, and the concrete's shear strength contribution is not diminished when shear and torsion are combined. The test results of (**MacGregor,J. G. and Ghoneim, 1995**) and (**Hsu, 1997**) is compared to the design approach of the ACI 318-19.

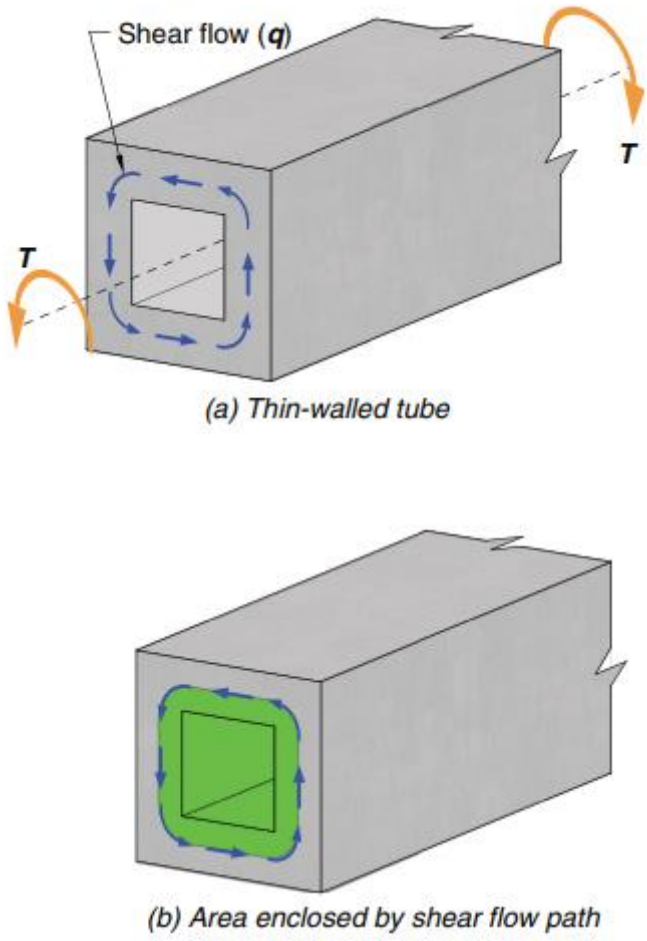

Figure (5-1): (a) Thin-walled tube; and (b) area enclosed by shear flow path, (**ACI 318-19, 2019**).

Using an identical thin-walled tube with a wall thickness t prior to cracking of $0.75A_{cp}/p_{cp}$ and an area contained by the centerline of the wall A_o equal to $2A_{cp}/3$, the cracking torsional moment T_{cr} may be computed. When the major tensile stress exceeds $0.33\sqrt{f_c^-}$, cracking is anticipated to occur. Using $0.33\sqrt{f_c^-}$ as a lower limit on tension at cracking was

intentional. Equation (5-1) may be solved by replacing the variables A_o, t, and τ by A_{cp}, p_{cp}, and f_c^- which gives the cracking torsional moment T_{cr} as defined in the following equation:

$$T_{cr} = 0.33\sqrt{f_c^-}\frac{A_{cp}^2}{P_{cp}} \quad (5\text{-}3)$$

Where:

p_{cp} = perimeter of the outer concrete cross-section.

A_{cp} = The area enclosed by the outside perimeter of a concrete cross-section.

For the purpose of determining the torsional strength of reinforced concrete beams, we will utilize the space truss analogy shown in Figure (5-2), which assumes that the concrete does not resist tension and that the reinforcement provides.

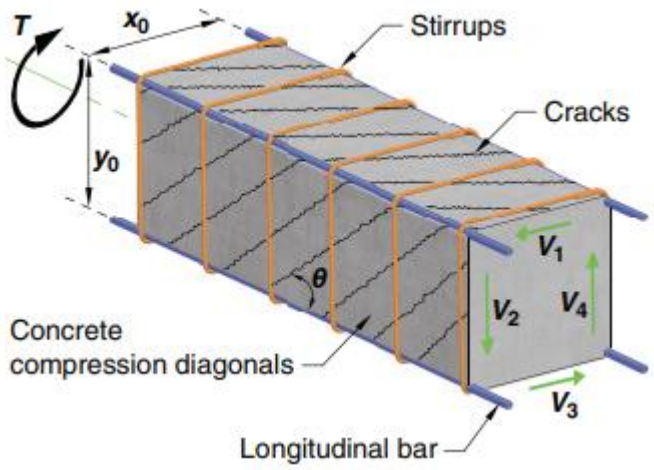

Figure (5-2): Space truss analogy, (**ACI 318-19, 2019**).

After torsional cracking begins, the bulk of the torsional strength is provided by closed stirrups, longitudinal reinforcing, and compression diagonals. The concrete that surrounds these stirrups does not do much. To account for this A_o, the gross area of the shear flow route around the tube's perimeter is described after cracking in terms of A_{oh}, the area

around the centerline of the outermost closed transverse torsional reinforcement. The shear flow q in the tube's walls may be broken down into the shear forces V1 to V4 operating on each of the tubes or space trusses separate sides.

A diagonal compression component, $D_i = V_i / \sin \theta$, in the concrete resists shear flow V_i, as illustrated in Figure (5-3). The longitudinal reinforcement must be subjected to an axial tension force, $N_i = V_i (\cot \theta)$, in order to fully resolve V_i. D_i and N_i act at side i mid-height because of the continual shear flow caused by torsion at every point on its circumference. Consequently, each top and bottom chord resists half of Ni, as seen. All of the N_i forces, N_i, operating on the tube's walls must be resisted by longitudinal reinforcement with a strength $A_l f_y$.

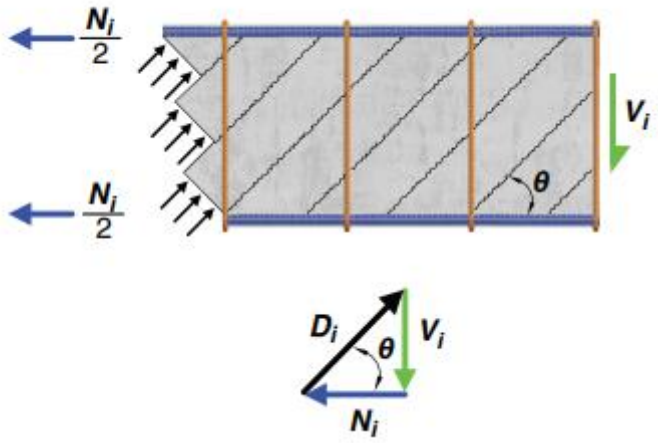

Figure (5-3): Resolution of shear force Vi into diagonal compression force Di and axial tension force Ni in one wall of tube, **(ACI 318-19, 2019**).

$$q = V_i \tag{5-4}$$

$$V_i = \frac{A_t f_{yt}}{s} \cot\theta \tag{5-5}$$

Substitute eq. (5-5) into eq. (5-2):

$$\frac{A_t f_{yt}}{s}\ cot\theta = \frac{T_n}{2A_\circ}$$

$$\text{Tn} = \frac{2A_\circ A_t f_{yt}}{S} cot\theta \quad (5\text{-}6)$$

There is an axial tension force around the perimeter of the A_o region. The length of these sides is about the same as the distance between the centers of the bars in the tube's corners. For the sake of calculation simplicity, the circumference of the closed stirrups, P_h, has been substituted for this.

$$N_i = V_i * \cot\theta \quad (5\text{-}7)$$

$$N_i = \frac{A_l f_y}{P_h} \quad (5\text{-}8)$$

Substitute eq. (5-8) in eq. (5-7), and $V_i = q = \frac{T_n}{2A_\circ}$ then:

$$\frac{A_l f_y}{P_h} = \frac{T_n}{2A_\circ} \cot\theta$$

$$\text{Tn} = \frac{2A_\circ A_l f_y}{P_h} \tan\theta \quad (5\text{-}9)$$

Where:

$A_o = 0.85A_{oh}$.

θ = more than or equal to 30 degrees but not more than 60

A_t = a closed stirrup with torsion resistance equal to the area of one leg.

A_ℓ = Torsional-reinforced longitudinal area.

P_h = the outermost closed stirrup's centerline perimeter.

f_y and f_{yt} = The longitudinal and transverse reinforcement torsional values.

S = spacing between closed stirrup.

To get nominal torsional (Tn) from ACI 318-19, use the equation that is the smallest of equations (5-6) and (5-9).

5.3 Torsion for beams in European codes.

A truss model with a thin-walled closed section theory and an inclined angle θ between the concrete compression strut and the beam axis is adopted to construct the torsional resistance moment in European codes. The angle θ should be restricted to $1 \leq \cot\theta \leq 2.5$ (45 degrees ≥ θ ≥ 22 degrees), which is the generally accepted recommendation. Equation (5-10) may be used to determine the torsional capacity of beams designed in accordance with (**BS EN 1992-1-1., 2004**).

$$Tn = \frac{A_t}{s}\ 2A_k f_{ywd} \cot\theta \qquad (5\text{-}10)$$

Where:

A_t = area of one leg of closed stirrups.

S = spacing between closed stirrup.

$f_{ywd} = \frac{f_{ty}}{\gamma_s}$ = design yield stress of transversal reinforcement.

A_k = The area enclosed by the centerlines of the connecting thin-walls.

$$A_k = (b_w - t_{ef}) * (h - t_{ef}) \qquad (5\text{-}11)$$

t_{ef} = effective wall thickness of the equivalent thin-walled section (mm).

5.4 Evaluation of torsional strength in design codes

In order to evaluate the torsional capacity of the reinforced beams, the thin-walled tube/space truss analogy stated above may be used in accordance with the ACI 318-19 and EC2-2004 codes. To determine the cracking torque (T_{cr}) in ACI 318-19, an equation (5-3) was used. Using equations (5-6) and (5-10) are utilized in order to estimate the torsional capacity in the ACI 318-19 and EC2-2004 codes, respectively.

Using the American and European codes and experimental data, the reinforced beams in Group 1 in Table (5-1) were tested for their torsional capabilities under pure torsion. Figure (5-4) shows how conservative the ACI prediction is in estimating the cracking torque

strength in comparison to experimental data. To be clear, the equation (5-3) used to calculate cracking torque does not take reinforcing features into account and is solely dependent on concrete strength and cross-sectional characteristics. Experiment findings for three cross sections with varied percentages of rubber are shown in Figure (5-5) compared to the predicted torsional from EC2-2004 and ACI 318-19 codes, as shown in the figure. Comparing experimental findings with the EC2-2004 and ACI 318-19 codes demonstrates a consistent torsional value for beams in each cross-section. Any adjustment in rubber ratios between 0% and 30% had no effect on the ACI 318-19 code-calculated torsion for beams containing rubber, which was greater than the experimental torsion measurements. Experimental findings showed that the torsion predicted by the EC2-2004 code was underestimated. Using high-range (Tn experimental/Tn calculated) ratios, it is able to accurately anticipate the torsional capabilities of the tested specimens, with m values of (0.939, 1.222 percent) and a COV value of (5.981, 7.374 percent) for ACI 318-19 and EC2-2004 codes, respectively.

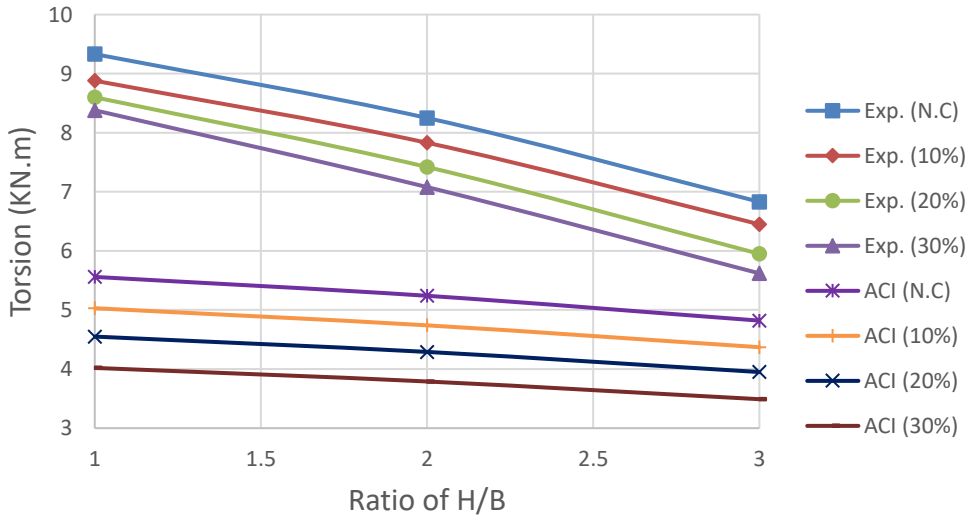

Figure (5-4): Experimentation and the ACI 318-19 code for cracking torque were compared for specimens subjected to pure torsion.

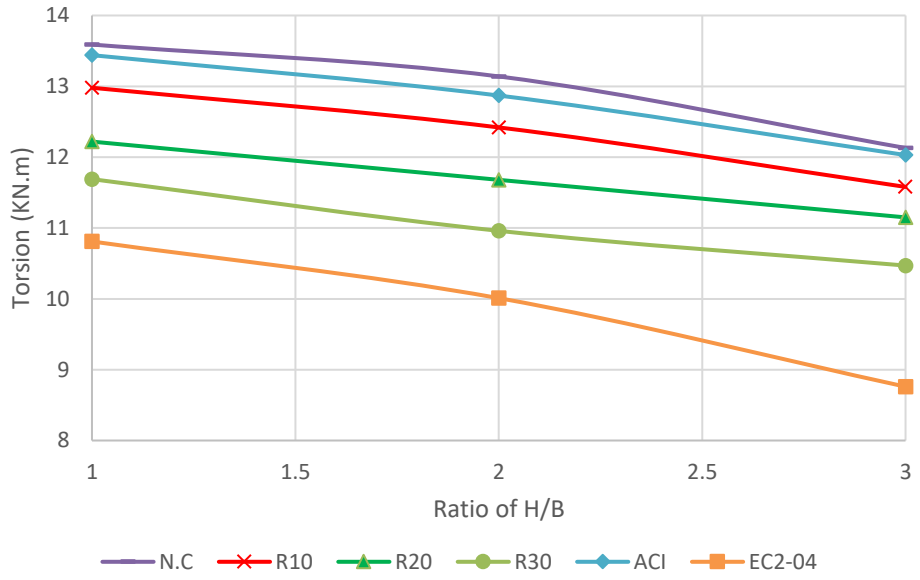

Figure (5-5): Evaluation of torsional capacity of experimental, EC2-2004 and ACI 318-19 codes for specimens under pure torsion.

Table (5-1): Difference between experimental and calculated results by using the code equations, under pure torsion.

Sample	T_{cr} Exp	T_{cr} ACI	$\frac{T_{cr}\ Exp}{T_{cr}\ ACI}$	T_n Exp	T_n ACI	T_n Euro	$\frac{T_n \text{ Exp}}{T_n \text{ ACI}}$	$\frac{T_n \text{ Exp}}{T_n \text{ Euro}}$
PT-S1R0	9.33	5.56	1.68	13.59	13.44	10.81	1.011	1.257
PT-S1R10	8.88	5.03	1.77	12.98	13.44	10.81	0.966	1.201
PT-S1R20	8.60	4.55	1.89	12.22	13.44	10.81	0.909	1.130
PT-S1R30	8.38	4.02	2.08	11.69	13.44	10.81	0.870	1.081
PT-S2R0	8.25	5.24	1.57	13.14	12.87	10.01	1.021	1.313
PT-S2R10	7.83	4.74	1.65	12.42	12.87	10.01	0.965	1.241
PT-S2R20	7.42	4.29	1.73	11.68	12.87	10.01	0.908	1.167
PT-S2R30	7.08	3.79	1.87	10.96	12.87	10.01	0.852	1.095
PT-S3R0	6.83	4.82	1.42	12.13	12.03	8.76	1.008	1.385
PT-S3R10	6.45	4.37	1.48	11.58	12.03	8.76	0.963	1.322
PT-S3R20	5.95	3.95	1.51	11.15	12.03	8.76	0.927	1.273
PT-S3R30	5.62	3.49	1.61	10.47	12.03	8.76	0.870	1.195
Mean							0.939	1.222
SD%							5.616	9.008
COV%							5.981	7.374

Table (5-1) shows that the ACI code's conservative estimation of cracking torque results in underestimates of experimental data ranging from 41% to 108% for the cracking torque calculated using the American code equation.

The American code equations for torsion strength do not accurately represent the impact of reinforced rubberized concrete beams, where the overestimation ranges from 3.42% to 14.84%. Therefore, the American code equations for torsion strength should be modified.

5.5 The Proposed Equation for Torsional Capacity in ACI

The overestimation of the torsional capacities calculated by the ACI 318-19 code for reinforced rubberized concrete beams, in contrast to conventional concrete, was not completely reflected by experimental results. (**Kadhim & Al-Mutairee, 2021**) proposed formulae for the effectiveness factor of ultimate shear load for rubberized reinforced concrete continuous deep beams to get further valid forecast convergence with the experimental results. Also, (**Sahib & Al-Mutairee, 2020**) recommended combining correction factors with theoretical ACI-code formulae to determine the punching shear capacity of reinforced rubberized concrete slabs.

From experimental data and comparisons with the ACI-code, the rubberized reinforced concrete beam factor was calculated to get even closer predictions to the experimental one as shown in Figure (5-6). As demonstrated in Eq. (5-12), the new formulae provided have been expressed as a percent of volumetric substitution with coarse aggregate for rubber in the concrete mix.

$$F = 1.023e^{-0.006x_r} \quad (5\text{-}12)$$

$R^2 = 0.9992$ (square root accuracy).

Where:

F = A factor of reduction for ACI calculated torsional strength.

X_r = percent of rubber.

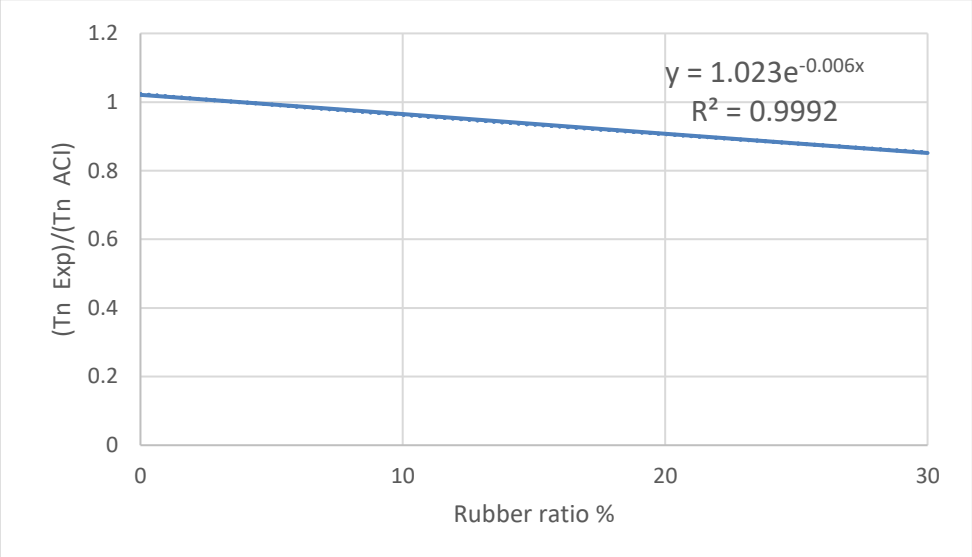

Figure (5-6): Show the equation for factor of reduction and square root accuracy

Torsional capacity (Tn) was calculated as previously described, multiplied by the suggested factor produced by equation (5-12) to obtain an estimation (Tn cal.) adapted to the specimens' specific needs. The suggested formula's accuracy in predicting torsional capacity is shown in Table (5-2) and Figure (5-7).

For the test samples, the suggested formula (5-12) was multiplied by equation (5-6) to provide credible forecasts rather than the code stipulations. In calculating the torsional prediction capacity for rubberized reinforced concrete beams as well as conventional reinforced concrete beams, the suggested factor is more accurate since the (m) and (COV) values are 1,009 and 0,874 percent, respectively, for (Tn experimental/Tn calculated).

Table (5-2): Values of torsional capacity predictions of ACI-code using proposed formula.

Sample	Tn Exp.	Tn Cal. *	$\frac{\text{Tn Exp.}}{\text{Tn Cal.}}$
PT-S1R0	13.59	13.44	1.01
PT-S1R10	12.98	12.94	1.00
PT-S1R20	12.22	12.19	1.00
PT-S1R30	11.69	11.48	1.02
PT-S2R0	13.14	12.87	1.02
PT-S2R10	12.42	12.39	1.00
PT-S2R20	11.68	11.67	1.00
PT-S2R30	10.96	10.99	1.00
PT-S3R0	12.13	12.03	1.01
PT-S3R10	11.58	11.58	1.00
PT-S3R20	11.15	10.91	1.02
Mean			1.009
SD%			0.882
COV%			0.874

Note: Tn Cal. *= Tn ACI * F

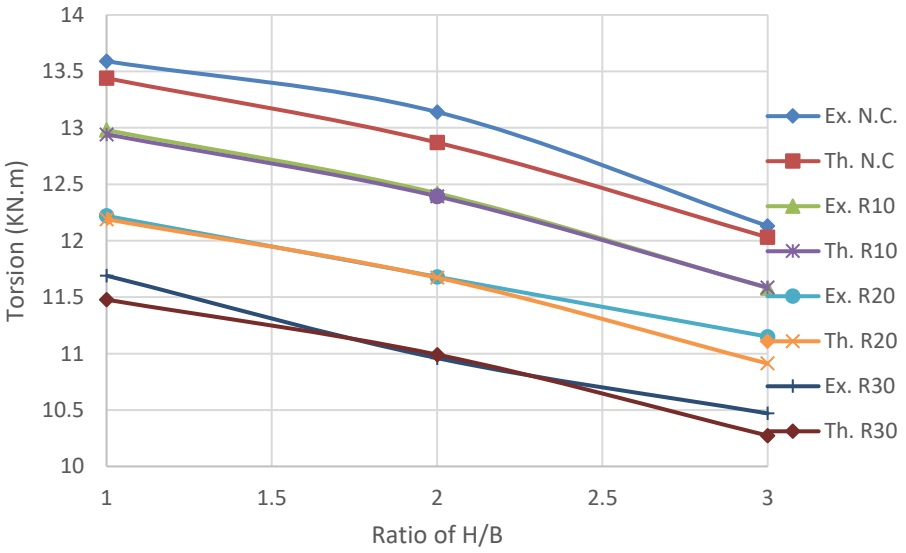

Figure (5-7): Evaluation of suggested formula's accuracy in predicting torsional capacity of all specimens under pure torsion.

5.6 Interaction Diagrams

It is important to consider the combination of torsion (T) and flexural (M) moments in the design process. The M/T ratio affects the

diagonal compression angle and the beam crack pattern. The presence of a flexural moment introduces tensile and compressive strains on the bottom and top faces of the section, respectively. Compression in the top face delays cracking, in some cases, until ultimate strength is reached (**Johnston & Zia, 1975**). In the case of pure torsion, the crack angle on the bottom face is diagonal, and in the case of pure flexure, the crack angle becomes orthogonal to the beam longitudinal axis. The angle on the sides is steep nearby the section in the bottom due to tensile strains and becomes flatter near the top from the compressive strains caused by flexural moments. Numerous theories ((**McMullen & Warwaruk, 1967**), (**Walsh et al., 1967**), (**Lampert & Collins, 1972**), **(Elfgren et al., 1974**)) recognize the phenomenon. Interaction curves recommended by Lampert and Collins (1972) have been simplified. They suggested that in under-reinforced sections, an increase in torsional strength is related to the ratio of the yield force of the compression reinforcement to tension reinforcement, r = (As′fy/Asfy). The flexural moment creates a tensile force M/dv in the bottom stringer and an equal compressive force in the top stringer. The torsion induces a total tensile force of $Tp_o/2A_o\cot\theta$ in the longitudinal reinforcement, where dv is the distance between the top and bottom longitudinal reinforcement, p_o and A_o are the shear flow perimeter and area, respectively, and θ is the diagonal crack angle. The longitudinal reinforcement forces are additive, as shown in Figure (5-8). Two simple equations (Eqs. (5-13) and (5-14)) are derived based on this theory. Equation (5-13) is for the case where the bottom longitudinal reinforcement yields along with the stirrups and occurs for symmetrically reinforced beam and unsymmetrically reinforced beam subjected to a small torsional moment and a large flexural moment **(ACI 445.1R-12, 2013**).

Equation (5-14) applies when the weaker top longitudinal reinforcement yields along with the stirrups, and occurs for unsymmetrically reinforced beam subjected to a large torsional moment and a small flexural moment.

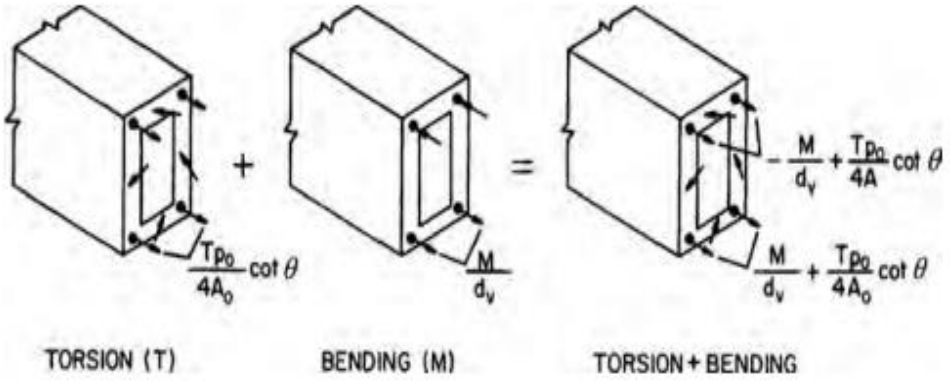

Figure (5-8): Superposition of forces due to torsion and bending, **(Hsu, 1993**).

$$r\left(\frac{T}{T_\circ}\right)^2 + \frac{M}{M_\circ} = 1 \qquad (5\text{-}13)$$

$$\left(\frac{T}{T_\circ}\right)^2 - \frac{1}{r}\frac{M}{M_\circ} = 1 \qquad (5\text{-}14)$$

Where:

$T_\circ$ = Pure ultimate torsion strength from ACI 318-19, Eq. (5-5).

$M_\circ$ = Pure ultimate flexural strength from ACI 318-19.

T, M = ultimate torsional and flexural strength under combined loading.

r = ratio of the area of top longitudinal reinforcement to the area of bottom longitudinal reinforcement.

$$M_\circ = A_s f_y \left(d - \frac{a}{2}\right) \qquad (5\text{-}15)$$

Where:

A_s = area of tension reinforcement.

f_y = yield strength of longitudinal reinforcement.

d = distance from external compression fiber to centroid of tension reinforcement.

$$a = \frac{A_s f_y}{0.85\, f_c^{/} b}$$

According to the expressed findings of beams in group two under combined load (torsion and bending) with varying bending to torsion percentages (λ), for each ratio of (λ), two beams were tested, one with standard concrete and the other with rubberized concrete when 30% of the rubber was replaced. In order to compare experimental and theoretical findings using an interaction diagram, equation (5-13) was utilized to calculate theoretical results since the longitudinal reinforcement in the beam is symmetrical at the top and bottom. The theoretical results for torsion from equation (5-13) do not account for the effect of rubber, so the torsion given from this equation is multiplied by a factor (F) from equation (5-12). The experimental and theoretical findings of beams under combined load are shown in the Tables (5-3) and (5-4) for normal and rubberized concrete, respectively. Figures (5-9) and (5-10) illustrate the interaction diagrams for normal and rubberized concrete, respectively. Figures (5-11) and (5-12) show the comparison between normal and rubberized concrete for experimental and theoretical results, respectively.

From Figures (5-9) and (5-10), notice that the interaction diagram for the experimental results is approximately the same trend as the theoretical results curve. From the practical interaction diagram, it is noted that the point (λ = 1) is far from the theoretical interaction diagram, while the points that precede this point, that is, when (λ<1), the theoretical and practical curves in the interaction diagram are very close, while when (λ>1), the theoretical and practical curves in the interaction diagram gradually approach as the value of (λ) increases.

Table (5-3): Experimental and theoretical results for normal concrete beams under combined load.

Sample	λ= (M/T)	Experimental		Theoretical		Experimental		Theoretical	
		T KN.m	M KN.m	T KN.m	M KN.m	$\frac{T}{T_o}$	$\frac{M}{M_o}$	$\frac{T}{T_o}$	$\frac{M}{M_o}$
PT-S2R0	0	13.14	0	12.87	0	1.00	0.00	1.00	0.00
C0.5-S2R0	0.5	13.64	6.82	11.78	5.89	1.04	0.15	0.92	0.16
C0.75-S2R0	0.75	12.89	9.67	11.28	8.46	0.98	0.21	0.88	0.23
C1-S2R0	1	18.9	18.9	10.8	10.8	1.44	0.41	0.84	0.30
C2-S2R0	2	14.34	28.68	9.11	18.22	1.09	0.63	0.71	0.50
C3-S2R0	3	11.89	35.67	7.76	23.28	0.90	0.78	0.60	0.64
C4-S2R0	4	9.89	39.27	6.68	26.72	0.75	0.86	0.52	0.73
PB-S2R0	∞	0	45.56	0	36.59	0.00	1.00	0.00	1.00

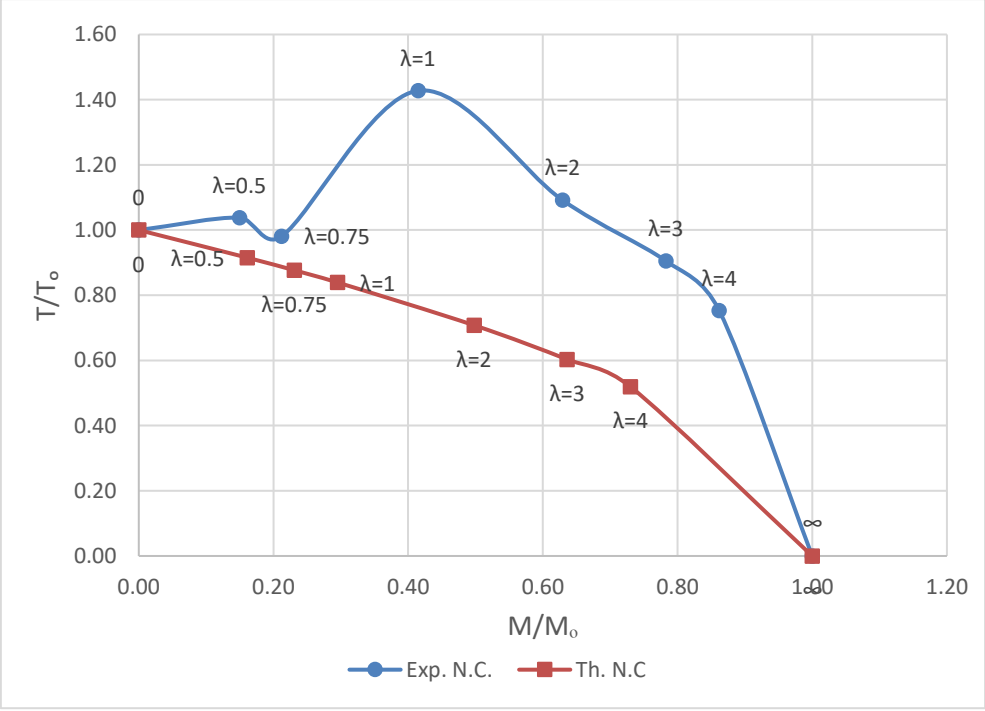

Figure (5-9): Interaction diagram for experimental and theoretical results of reinforced normal concrete beams subjected to combined load.

Table (5-4): Experimental and theoretical results for rubberized concrete beams under combined load.

Sample	λ= (M/T)	Experimental		Theoretical		Experimental		Theoretical	
		T KN.m	M KN.m	*T KN.m	M KN.m	$\frac{T}{T_o}$	$\frac{M}{M_o}$	$\frac{T}{T_o}$	$\frac{M}{M_o}$
PT-S2R30	0	10.96	0	11.00	0	1.00	0.00	1.00	0.00
C0.5-S2R30	0.5	11.23	5.62	10.02	5.87	1.02	0.14	0.91	0.17
C0.75-S2R30	0.75	10.82	8.12	9.57	8.4	0.99	0.20	0.87	0.24
C1-S2R30	1	15.8	15.8	9.15	10.71	1.44	0.39	0.83	0.31
C2-S2R30	2	12.15	24.3	7.66	17.92	1.11	0.60	0.70	0.51
C3-S2R30	3	10.02	30.06	6.48	22.74	0.91	0.75	0.59	0.65
C4-S2R30	4	8.45	33.56	5.55	25.96	0.77	0.83	0.50	0.75
PB-S2R30	∞	0	40.31	0.00	34.8	0.00	1.00	0.00	1.00
*T = T equation (5-13) * F									

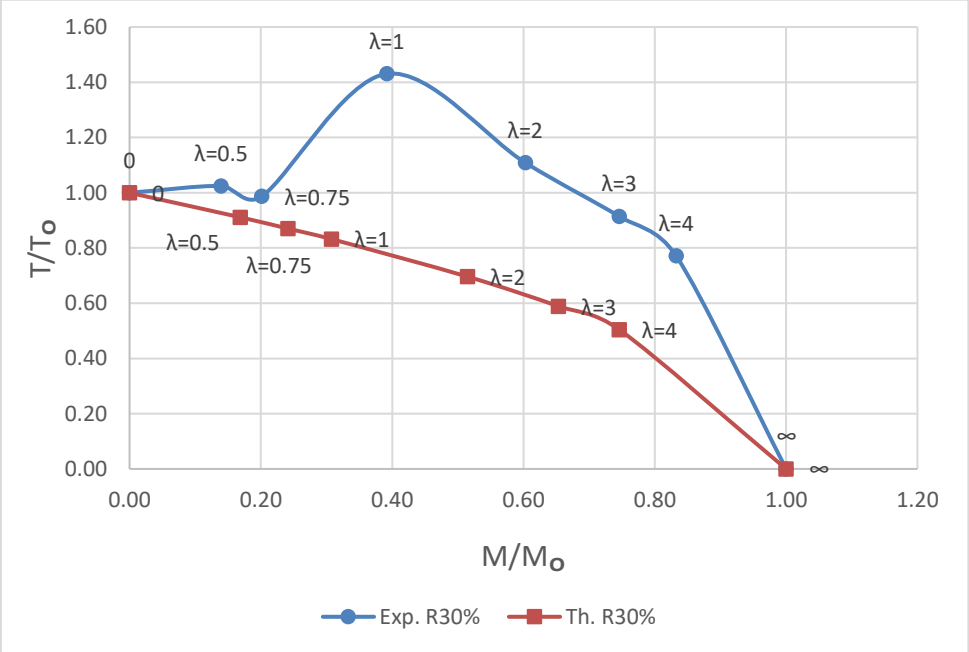

Figure (5-10): The interaction diagram depicts the experimental and theoretical results of reinforced rubberized concrete beams subjected to combined load with 30% replacement rubber.

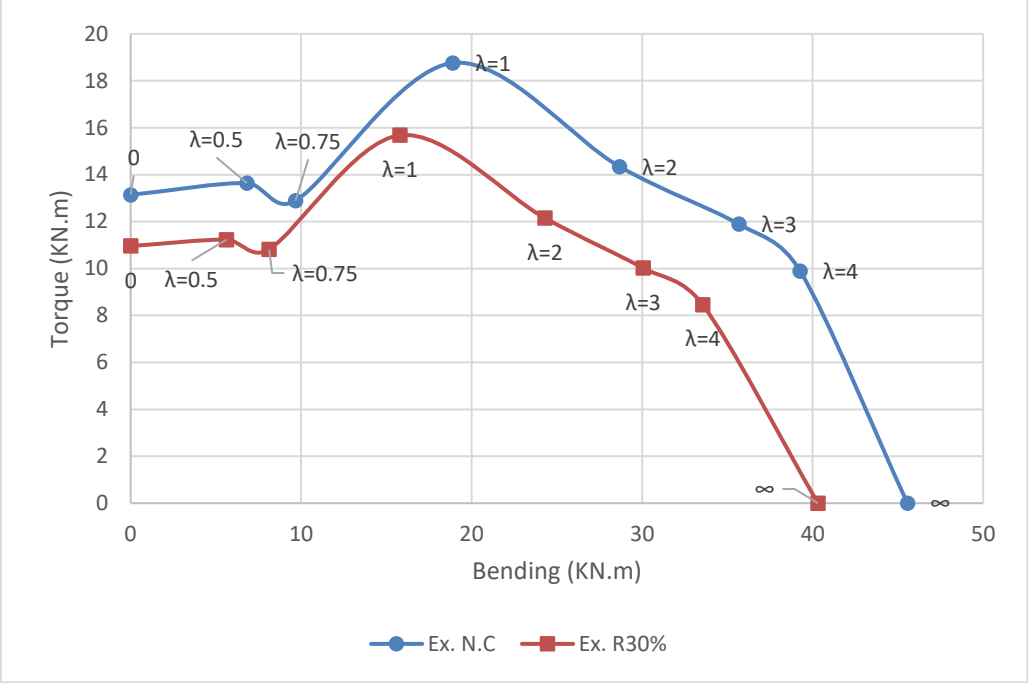

Figure (5-11): The comparison of experimental results is between normal concrete and rubberized concrete specimens.

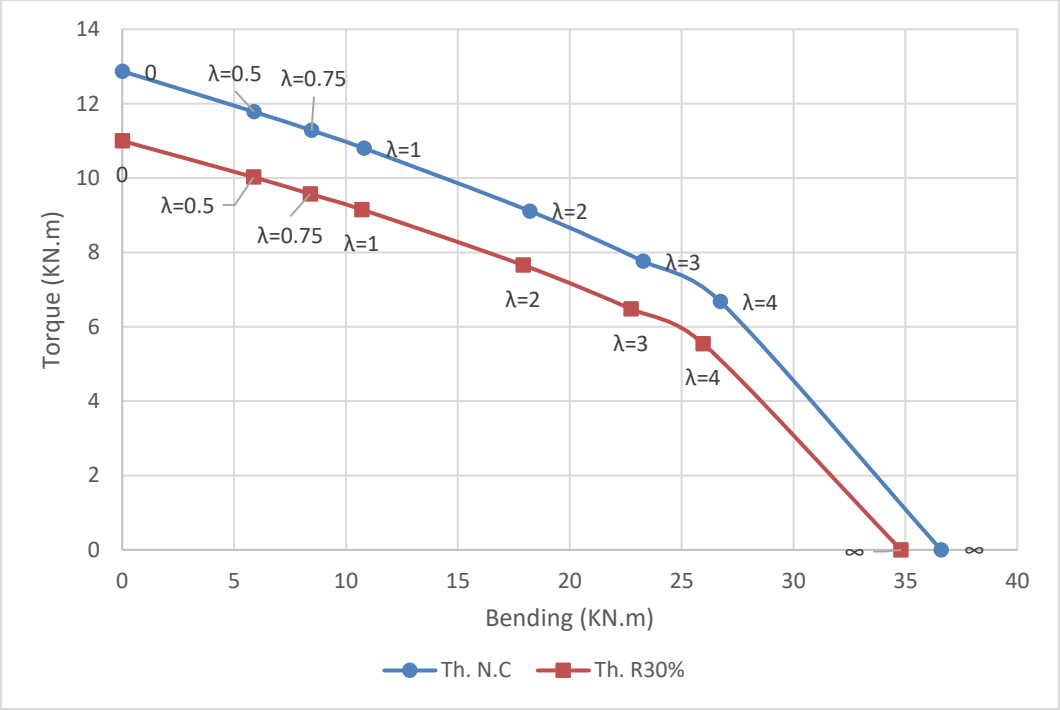

Figure (5-12): Rubberized concrete specimens are compared to normal concrete specimens in the theoretical analysis.

CHAPTER SIX

CONCLUSIONS AND RECOMMENDATIONS

6.1 Introduction

In the preceding chapter, experimental and theoretical findings for reinforced concrete beams rely on a wide range of parameters, including the depth-to-width ratio, the kind of stress, and the substitution of coarse aggregate with rubber.

A summary of the study's major findings and recommendations for further research can be found in this chapter.

6.2 Conclusions from Properties of Rubberized Concrete Mixes.

As a result of the replacement of 30% of the coarse aggregate with rubber chips the following conclusion can be written:

1. Rubber chips boost the impact resistance of concrete by 356%, which means it will become more flexible.
2. The thermal conductivity of concrete reduced by 20.6%. Rubberized concrete might be used as an insulating material and contribute to environmental conservation. Rubberized concrete recommended to be used instead of normal concrete for structures.
3. The workability of concrete is reduced by 37%. The difference between higher specific gravity values with smoother surfaces for coarse aggregate than rubber and the thin layer of defilements, such as fine rubber fuzz or dust, on the rubber particles' surface reduces the fresh rubber concrete free water, which also reduces the flow capacity.
4. The density of rubberized concrete mixes is 9% lower than that of standard mixtures.

5. The compressive strength, splitting tensile strength, and modulus of rupture are all reduced by 47.64%, 35.34%, and 44.75%, respectively.
6. The modulus of elasticity is lowered by 50.49%.
7. The American Standard's compression strength to the British Standard's compression strength ratio for concrete (normal and rubberized) is (0.8-0.81) as same of normal concrete.

6.3 Conclusions From the Experimental Program for Reinforced Concrete Beams.

6.3.1 Beams Under Pure Torsion.

1. The ultimate torque of normal concrete beams decreases by 3.31% and 10.74% when the depth/width ratio is increased from 1 to 3. The twist angle also decreases by 16.76% and 25.79%.
2. Compared to the reference beam for each one, the ultimate torque of concrete beams decreases by 13.98%, 16.59%, and 13.69% when the depth/width ratio is increased from 1, 2, 3, respectively, while the twist angle increases by 39.69%, 48.28%, and 44.25%, for a 30% replacement of rubber.
3. At 30% replacement of rubber, the torque decrement at first crack is 10.18%, 14.18%, and 17.72% when the depth/width ratio is raised from 1 to 3, respectively, while the twist angle increases by 24.02%, 34.10%, and 33.49% when compared with the reference beam for each one.
4. For non-reinforcement beams, the maximum torque dropped by an average of 31% and 45% for beams. Also, the angle of twist decreased by an average of 74% and 67% when the depth/width ratio was equal to 1 and 3, respectively, when compared to the reinforced beam for each one.

5. When the rubber ratio was increased by 30%, the non-reinforcement beams with depth/width ratios of 1 and 3 showed an increase of 25.43% and a 61.67% in twist angle compared to the control beam.
6. Rubber substituted for 30% of the coarse aggregate raised the ductility index of specimens by 34.54%, 33.07%, and 23.41%, respectively, whether the depth/width ratio was 1, 2, or 3.
7. For 30% rubber replacement, the ultimate stiffness is reduced by 38.42%, 41.01%, and 52.73% when the depth/width ratio is equal to 1, 2, and 3, respectively, as compared to the control beam for each one.
8. When 30% rubber replacement, the crack width is reduced by 28.89% and 42.86% when the depth/width ratio is equal to 2 and 3, respectively, as compared to the control beam for each one.
9. The energy absorption is increased by 29.37%, 30.84%, and 28.39% when the depth/width ratio is equal to 1, 2, and 3, respectively, as compared to the control beam for each one, when 30% rubber replacement.
10. For three sections, S1, S2, and S3, when h/b increases from 1 to 3, the ultimate torque decreases by about 10% for N.C and rubberized concrete (R30%) under pure torsion.

6.3.2 Beams under combined load (torsion + bending).

1. The ultimate torque decreases by about 47.28% for normal concrete beams and the twist angle decreases by about 37.08% when the ratio of bending/torsion (λ) increases from 1 to 4, while the ultimate bending moment increases by 107.78% and the deflection increases by 102.35% as compared to beam with λ= 1.
2. The ultimate torque decreases by about 5.50% for normal concrete beams and the twist angle decreases by about 8.85% when increased λ from 1/2 to 3/4, while the ultimate bending moment increases by

41.79% and the deflection increases by 32.36% as compared to beam with a λ= 1/2.

3. When 30% of the gravel is substituted by chip rubber, the ultimate torque and the ultimate bending moment decreases by a mean of 15.95%, while the twist angle increases by a mean of 39.24% and the deflection increases by a mean of 34.36%, as compared to the control beams of them, for range of λ of 1/2 to 4.
4. The ductility index of test beams increases by an average of 21.40% for all values of λ, when 30% of the gravel is substituted by chip rubber, as compared to the control beams of them.
5. The ultimate stiffness of test beams decreases by an average of 39.61% for all values of λ, when 30% of the gravel is substituted by chip rubber, as compared to the control beam of each ratio λ.
6. The crack width of test beams at ultimate load decreases by an average of 21.08% for all values of λ, when rubber replaces 30% of the coarse aggregate, as compared to the control beam of each ratio λ.
7. When rubber replaces 30% of the coarse aggregate, the energy absorption of test beams rises by an average of 31.32% for all values of λ, relative to the control beam for each ratio λ.

6.3.3 Beams under bending.

When rubber is used to make up 30% of the coarse aggregate, the following conclusion can be drawn:

1. According to the control beam, the ultimate bending moment of the test beam decreases by 11.52%. The deflection at this point increases by 36.11%.
2. The ductility index of the test beam increases by 19.67% compared to the control beam.

3. The ultimate stiffness decreases by 34.99% compared to the control beam.
4. The fracture width of the test beam at ultimate load decreased by 11.72 percent, as compared to the control beam.
5. Increment 38.12% in energy absorption may be seen.

6.4 Conclusions From the Theoretical Analysis.

1. From the American (ACI 318-19) and European (EC2-2004) codes calculated, the results seem to suggest that the American code offers findings that are closer to reality when compared to the practical outcomes.
2. Under pure torsion, the American (ACI 318-19) code provides an underestimated and more conservative torsion capacity of beams from experimental control beams; nevertheless, it becomes an overestimate when compared to reinforced rubberized concrete beams.
3. The suggested formula has benefits over the American (ACI 318-19) code when it comes to taking the rubber material ratio effect in concrete and offers more accurate predictions when substituting coarse aggregate with rubber, where the (m) and (COV) for the ratio (Tu experimental/Tu calculated) are 1.009 and 0.874%, respectively.
4. Under combined (torsion and bending), the interaction diagram for the experimental results shows approximately the same trend as the theoretical result curve.
5. When 30% of the coarse aggregate is replaced with rubber, the torsional capacity is reduced by approximately (14.9%-17.0%) for a range λ of 1/2 to 4.

6.5 Recommendations for Further Research.

1. Investigating the torsional behavior of continuous reinforced rubberized concrete beams.

2. Effect of steel fiber on the structural behavior of reinforced rubberized concrete beams under torsion.
3. The structural behavior of a reinforced rubberized concrete beam when subject to torsion with the same concrete strength for each ratio of rubber.
4. Studying torsional behavior of reinforced rubberized concrete beams under repeated and dynamic loading.
5. Using other materials to produce rubberized concrete such as crumb or fiber waste tire rubber and effect on torsional capacity for beams.

References:

1) Abduljalil, B. S., Aziz, A. H., & Muhsen, I. K. (2012). **Strengthening of Reinforced Concrete Beams Under Combined Torsion and Bending Using Carbon Fiber Reinforced**. *The Iraqi Journal For Mechanical And Material Engineering*, *12*(4).
2) ACI 318-19. (2019). **Building Code Requirements for Structural Concrete and Commentary**. In *American Concrete Institute* (p. 628). https://doi.org/10.14359/51716937
3) ACI 445.1R-12. (2013). **Report on Torsion in Structural Concrete**.
4) ACI 544.2R-89. (1999). **Measurement of Properties of Fiber Reinforced Concrete**. *Publication SP - American Concrete Institute*, *89*(Reapproved), 1–12.
5) ACI Committee 211.1-91. (2002). **Standard Practice for Selecting Proportions for Normal , Heavyweight , and Mass Concrete** (ACI 211 . 1-91). *ACI committee report, Reapproved*, 1–38.
6) Ajeel, A. E. (2016). **Torsion Plus Bending and Shear on Reinforced on Reinforced Concrete Beams**. *Journal of Engineering and Sustainable Development*, *20*(04), 277–288.
7) Alfayez, S. A., Suleiman, A. R., & Nehdi, M. L. (2020). **Recycling Tire Rubber in Asphalt Pavements: State of The Art**. *Sustainability (Switzerland)*, *12*(21), 1–15. https://doi.org/10.3390/su12219076
8) Aniruddh, Kumar, A., & Khan, M. A. (2016). **Effect On Compressive Strength of Concrete by Using Waste Rubber as Partial Replacement of Fine Aggregate: A Review**. *International Research Journal of Engineering and Technology (IRJET)*, *3*(3), 86–89.

9) ASTM A615 / A615M-16. (2016). **Standard Specification for Deformed and Plain Carbon-Steel Bars for Concrete Reinforcement**. ASTM International. https://doi.org/10.1520/A0615_A0615M-16

10) ASTM C1113/C1113M-09. (2013). **Standard Test Method for Thermal Conductivity of Refractories by Hot Wire (Platinum Resistance Thermometer Technique)**. *ASTM International*, *Reapproved*, 1–6. https://doi.org/10.1520/C1113_C1113M-09R13.

11) ASTM C143M. (2012). **Standard Test Method for Slump of Hydraulic-Cement Concrete.** *ASTM International*, *i*(Reapproved), 1–4. https://doi.org/10.1520/C0143_C0143M-12

12) ASTM C192/C192M-00. (2000). **Standard Practice for Making and Curing Concrete Test Specimens in the Laboratory**. *ASTM International*, *04*, 1–8.

13) ASTM C39/C 39M-01. (2001). **Standard Test Method for Compressive Strength of Cylindrical Concrete Specimens**. *American Society for Testing and Materials*, *04.02*, 1–5. https://doi.org/10.1520/C0039

14) ASTM C469/469M-14. (2014). **Standard Test Method for Static Modulus of Elasticity and Poisson ' s Ratio of Concrete**. *ASTM International*, 2–6. https://doi.org/10.1520/C0469-C0469M-14

15) ASTM C494/C494M. (2017). **Standard Specification for Chemical Admixtures for Concrete**. https://doi.org/10.1520/C0494_C0494M-17

16) ASTM C496/Ca96M-11. (2011). **Standard Test Method for Splitting Tensile Strength of Cylindrical Concrete Specimens**. *ASTM International*, 1–5.

https://doi.org/10.1520/C0496_C0496M-11

17) ASTM C78/C78M-18. (2018). **Standard Test Method for Flexural Strength of Concrete (Using Simple Beam with Third-Point Loading)**. *ASTM International*, *C78-18*(C), 1–4. https://doi.org/DOI: 10.1520/C0078_C0078M-18. 2

18) Benazzouk, A., Douzane, O., Langlet, T., Mezreb, K., Roucoult, J. M., & Quéneudec, M. (2007). **Physico-Mechanical Properties and Water Absorption of Cement Composite Containing Shredded Rubber Wastes**. *Cement and Concrete Composites*, *29*(10), 732–740. https://doi.org/10.1016/j.cemconcomp.2007.07.001

19) Bignozzi, M. C., & Sandrolini, F. (2006). **Tyre Rubber Waste Recycling In Self-Compacting Concrete**. *Cement and Concrete Research*, *36*(4), 735–739. https://doi.org/10.1016/j.cemconres.2005.12.011

20) BS 1881-116. (1983). **Testing concrete — compressive strength of concrete cubes**. *British Standard Institution*, *1*.

21) Chalioris, C. E. (2003). **Cracking and Ultimate Torque Capacity of Reinforced Concrete Beams. *Role of Concrete Bridges in Sustainable Development*** - *Proceedings of the International Symposium - Celebrating Concrete: People and Practice*, 109–117. https://doi.org/10.1680/rocbisd.32484.0010

22) Collins, M. P. (1973). **Torque-Twist Characteristics of Reinforced Concrete Beams**. In *Inelasticity and Non-Linearity in Structural Concrete* (pp. 211–231). University of Waterloo Press.

23) Deifalla, A., Awad, A., Seleem, H., & Abdelrahman, A. (2020). **Investigating The Behavior of Lightweight Foamed Concrete T-Beams under Torsion, Shear, and Flexure. *Engineering Structures***, *219*(March), 110741.

https://doi.org/10.1016/j.engstruct.2020.110741

24) Dumne, S. M. (2013). **An Experimental Study on Performance of Recycled Tyre Rubber-Filled Concrete**. *International Journal of Engineering Research & Technology (IJERT)*, *2*(12), 766–772. https://doi.org/IJERTV2IS120377

25) Elfgren, L., Karlsson, I., & Losberg, A. (1974). **Torsion-Bending-Shear Interaction for Concrete Beams**. *Journal of the Structural Division*, *100*(8), 1657–1676.

26) Fanella, D. A., & Rabbat, B. G. (1997). **Design of Concrete Beams for Torsion (2nd ed.)**. Portland cement association.

27) Fattuhi, N. I., & Clark, L. A. (1996). **Cement-Based Materials Containing Shredded Scrap Truck Tyre Rubber**. *Construction and Building Materials*, *10*(4), 229–236. https://doi.org/10.1016/0950-0618(96)00004-9

28) Ganjian, E., Khorami, M., & Maghsoudi, A. A. (2009). **Scrap-Tyre-Rubber Replacement for Aggregate and Filler in Concrete**. *Construction and Building Materials*, *23*(5), 1828–1836. https://doi.org/10.1016/j.conbuildmat.2008.09.020

29) Gunasekaran, K., Ramasubramani, R., Annadurai, R., & Prakash Chandar, S. (2014). **Study on Reinforced Lightweight Coconut Shell Concrete Beam Behavior under Torsion**. *Materials and Design*, *57*, 374–382. https://doi.org/10.1016/j.matdes.2013.12.058

30) Hasan, T. M. (2018). **Behavior of Fiber Reinforced Self Compacting Rubberized Members Under Loading**. M.Sc. thesis, College of Engineering, University of Al-Nahrain.

31) Hassanli, R., Youssf, O., & Mills, J. E. (2017). **Experimental Investigations of Reinforced Rubberized Concrete Structural Members**. *Journal of Building Engineering*.

https://doi.org/10.1016/j.jobe.2017.03.006

32) Hsu, T. T. C. (1968). **Torsion of Structural Concrete-Behavior of Reinforced Concrete Rectangular Members**. *Torsion of Structural Concrete, American Concrete Institute*, *18*, 261–306.

33) Hsu, T. T. C. (1984). **Torsion of Reinforced Concrete**. Van Nostrand Reinhold.

34) Hsu, Thomas T. C. (1968). **Torsion of Structural Concrete—Plain Concrete Rectangular Sections**. In *Torsion of Structural Concrete* (pp. 203–238). SP-18, American Concrete Institute.

35) Hsu, Thomas T. C. (1993). ***Unified Theory of Reinforced Concrete*.** CRC Press, Boca Raton.

36) Hsu, Thomas T. C. (1997). **ACI Shear and Torsion Provisions for Prestressed Hollow Girders**. *ACI STRUCTURAL JOURNAL*, *94*(6), 787–799.

37) Ibrahim, M. S., Gebreyouhannes, E., Muhdin, A., & Gebre, A. (2020). **Effect of Concrete Cover on The Pure Torsional Behavior of Reinforced Concrete Beams**. *Engineering Structures*, *216*(May), 110790. https://doi.org/10.1016/j.engstruct.2020.110790

38) Iraq Specification No.45/1984, second modify 2010. (2010). **Natural Sources for Gravel that is used in concrete and construction**.

39) Iraqi Specification No.5 -1984, second modify 2010. (2010). **Portland cement**.

40) Johnston, D. W., & Zia, P. (1975). **Prestressed Box Beams Under Combined Loading**. *Journal of the Structural Division*, *101*(7), 1313–1331.

41) Johnston, David W., & Zia, P. (1975). **Prestressed Box Beams under Combined Loading**. *Journal of the Structural Division*, *101*(7), 1313–1331. https://doi.org/https://doi.org/10.1061/JSDEAG.0004089

42) Kadhim, A. A. (2020). **Experimental Behavior of Rubberized Reinforced Concrete Continuous Deep Beam**. *M.Sc. Thesis, Civil Engineering Department, University of Babylon. 2020*.

43) Kadhim, A. A., & Al-Mutairee, H. M. K. (2021). **Experimental Investigation of Rubberized Reinforced Concrete Continuous Deep Beams**. *Journal of King Saud University - Engineering Sciences*, *33*(4), 1–11. https://doi.org/10.1016/j.jksues.2021.03.001

44) Kamara, M. E., & Rabbat, B. G. (2007). **Torsion Design of Structural Concrete Based on ACI 318-05** (Issue September, p. 8). Special Advertising Section — Portland Cement Association.

45) Kandekar, S. B., & Talikoti, R. S. (2018). **Study of Torsional Behavior of Reinforced Concrete Beams Strengthened with Aramid Fiber Strips**. *International Journal of Advanced Structural Engineering*, *10*(4), 465–474. https://doi.org/10.1007/s40091-018-0208-y

46) Karthikeyan, R., Raghunath, P. N., & Suguna, K. (2019). **Strength and Ductility of Rubberized Concrete Beams with Micro-Reinforcement**. *Asian Journal of Civil Engineering*, *21*(1). https://doi.org/10.1007/s42107-019-00178-2

47) Lampert, P., & Collins, M. P. (1972). **Torsion, Bending, and Confusion—An Attempt to Establish the Facts**. *ACI Journal*, *69*(8), 500–504.

48) Leonard, M. (1967). **Torsion Creep of Circular and**

Noncircular Tubes. *JOURNAL OF RESEARCH of the National Bureau of Standards - C. Engineering and Instrumentatian*, *71C*(3), 209–225.

49) Leu, L. J., & Lee, Y. S. (2000). **Torsion Design Charts for Reinforced Concrete Rectangular Members.** *JOURNAL OF STRUCTURAL ENGINEERING*, *126*(2), 210–218. https://doi.org/https://doi.org/10.1061/(ASCE)0733-9445(2000)126:2(210)

50) MacGregor,J. G. and Ghoneim, M. G. (1995). **Design for Torsion**. *ACI STRUCTURAL JOURNAL*, *92*(2), 211–218.

51) Marie, I. (2017). **Thermal Conductivity of Hybrid Recycled Aggregate Rubberized Concrete**. *Construction and Building Materials*, *133*, 516–524. https://doi.org/10.1016/j.conbuildmat.2016.12.113

52) McMullen, A. E., & Warwaruk, J. (1967). **The Torsional Strength of Rectangular Reinforced Concrete Beams Subjected to Combined Loading** (Issue 2).

53) Miller, N. M., & Tehrani, F. M. (2017). **Mechanical Properties of Rubberized Lightweight Aggregate Concrete.** *Construction and Building Materials*, *147*, 264–271. https://doi.org/10.1016/j.conbuildmat.2017.04.155

54) Mitchell, D., & Collins, M. P. (1974). **Diagonal Compression Field theory-A Rational Model For Structural Concrete in Pure Torsion**. *ACI Journal*, *71*(8), 396–408.

55) Mohaisen, S. K., Abdulhameed, A. A., & Kharnoob, M. M. (2016). **Behavior of Reinforced Concrete Continuous Beams under Pure Torsion**. *Journal of Engineering*, *22*(12), 1–15.

56) Nethercot, D. A., Salter, P. R., & Malik, A. S. (1989). ***Design of Members Subject to Combined Bending and Torslon***

(Reprinted,). The Steel Construction Institute.

57) Nitesh, K. J. N. S., Rao, S. V., & Kumar, P. R. (2019). **An Experimental Investigation on Torsional Behaviour of Recycled Aggregate Based Steel Fiber Reinforced Self Compacting Concrete**. *Journal of Building Engineering*, *22*, 242–251. https://doi.org/10.1016/j.jobe.2018.12.011

58) Okay, F., & Engin, S. (2012). **Torsional behavior of steel fiber reinforced concrete beams**. *Construction and Building Materials*, *28*(1), 269–275. https://doi.org/10.1016/j.conbuildmat.2011.08.062

59) R. Park. (1989). **Structural Assemblages From Laboratory Testing.** *Bulletin of the New Zealand National Society for Earthquake Engineering*, *22*(3), 155–166.

60) Rahal, K. N., & Collins, M. P. (1995). **Effect of Thickness of Concrete Cover on Shear-Torsion Interation- An Experimental Investigation**. *ACI STRUCTURAL JOURNAL*, *92*(3), 334–342.

61) Rahal, K. N., & Collins, M. P. (1996). Simple Model for Predicting Torsional Strength of Reinforced and Prestressed Concrete Sections. *ACI STRUCTURAL JOURNAL*, *93*(6), 658–666.

62) Sahib, F. N. (2020). **Punching Shear Strength of Rubberized Reinforced Concrete Flat Plates**. M.Sc. thesis, College of Engineering, University of Babylon. 2020.

63) Sahib, F. N., & Al-mutairee, H. M. K. (2020). **Punching strength behavior of reinforced concrete slabs with chips waste tire rubber**. *Periodicals of Engineering and Natural Sciences*, *8*(4), 2389–2404. https://doi.org/DOI: http://dx.doi.org/10.21533/pen.v8i4.1735

64) Siddiqui, M. M. A. (2016). **Study of Rubber Aggregates in Concrete An Experimental Investigation.** *International Journal of Latest Research in Engineering and Technology (IJLRET)*, *02*(12), 36–57. http://www.iaeme.com/MasterAdmin/UploadFolder/STUDY OF RUBBER AGGREGATES.pdf

65) Thomas, B. S., Gupta, R. C., & Panicker, V. J. (2016). **Recycling of Waste Tire Rubber As Aggregate in Concrete: Durability-Related Performance**. *Journal of Cleaner Production*, *112*, 504–513. https://doi.org/10.1016/j.jclepro.2015.08.046

66) Tudu, C. (2012). **Study of Torsional Behaviour of Rectangular Reinforced Concrete BeamS Wrapped with GFRP**. *Department of Civil Engineering National Institute of Technology Rourkela Odisha -769008, India*.

67) Walsh, P. F., Collins, M. P., & Archer, F. E. (1967). **The Flexure-Torsion and Shear-Torsion Interaction Behaviour of Reinforced Concrete Beams**. *Civil Engineering Transactions*, *CE9*(2), 313–320.

68) Xu, J., Chen, S., Guo, Q., Ye, Y., Diao, B., & Mo, Y. L. (2018). **Experimental and Analytical Studies of U-Shaped Thin-Walled RC Beams Under Combined Actions of Torsion, Flexure and Shear**. *International Journal of Concrete Structures and Materials*, *12*(1). https://doi.org/10.1186/s40069-018-0245-8

APPENDIX A

DESIGN OF BEAM UNDERGO PURE TORSION BY ACI CODE 318-19

A.1 Group one: under pure torsion

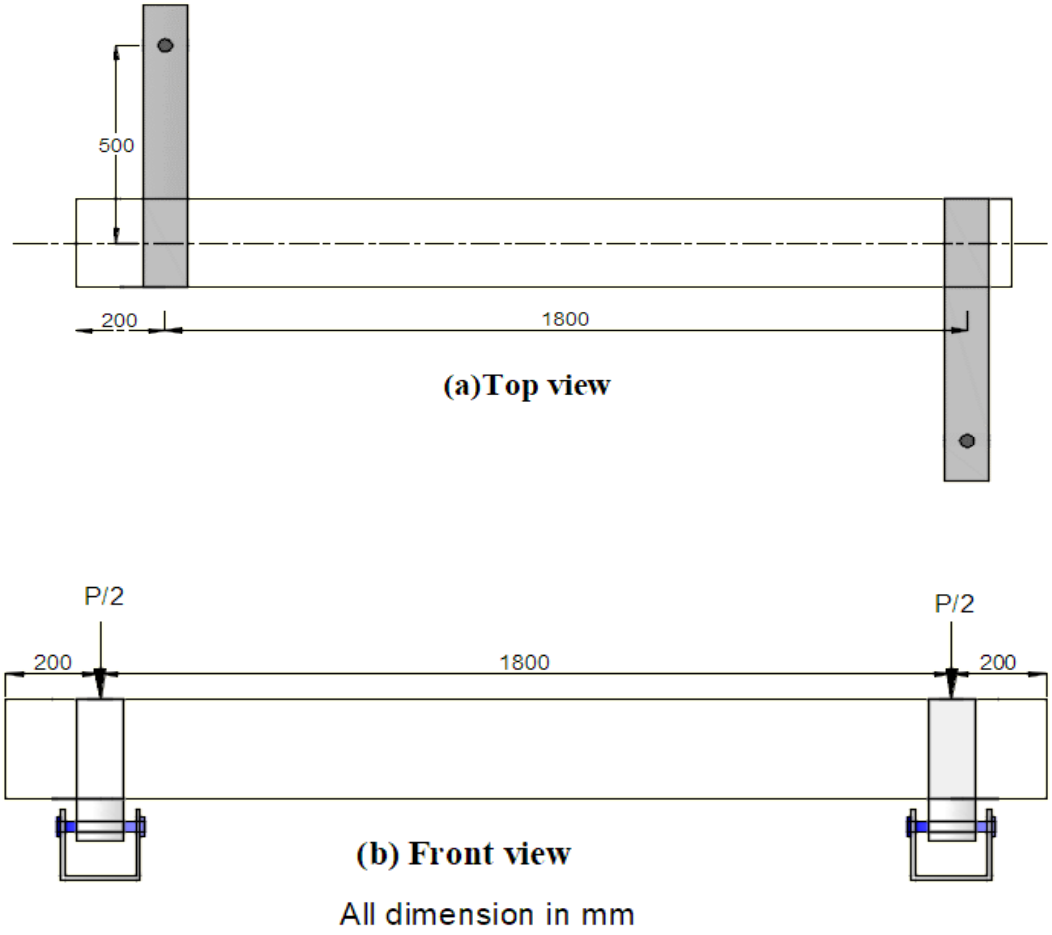

Figure (A-1): shown the details for beam under pure torsion

A.2 Section one (225*225) mm

b = 225, h = 225, $f_c^- = 35\ MPa$, A_{cp} = 50625 mm^2 , P_{cp} = 900 mm , $\emptyset$ = 0.75 .

1- Torsional effect may be neglected when:

$T_{u(ext)} < \emptyset\ 0.083\ \sqrt{f_c^-}\ \frac{A_{cp}^2}{P_{cp}}$ ACI-Code 318-19; 22.7.4.1

$T_{u(ext)}$ = 8.35 kN.m > 1.05 kN.m

∴ Torsional effect must be considered

Check cross section dimension for torsion:

For solid section under pure torsion:

$\frac{T_u P_h}{1.7 A_{oh}^2} \leq \emptyset\ [\frac{V_c}{b_w d} + 0.66\sqrt{f_c^-}\ ]$ ACI-Code 318-19; 22.7.7.1

- The size of a cross section is limited for two reasons: first, to reduce excessive cracking, and second, to minimize the potential for crushing of the surface concrete due to inclined compressive stresses due to shear and torsion.

For cover = 20mm & diameter of stirrups = 8 mm.

X_o = 225-2*20-2*($\frac{8}{2}$)= 177 mm

Y_o = 225-2*20-2*($\frac{8}{2}$)= 177 mm

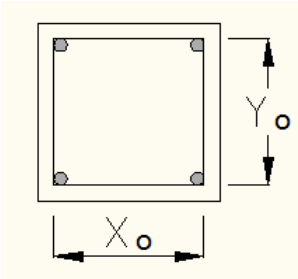

P_h = X_o * 2 + Y_o * 2 = 708 mm

A_{oh} = X_o * Y_o = 31329 mm^2

$\frac{T_u P_h}{1.7 A_{oh}^2} = 3.54\ MPa \leq \emptyset\ [\frac{V_c}{b_w d} + 0.66\sqrt{f_c^-}\ ]$ = 3.68 MPa , Ok

2- Transverse reinforcement for torsion:

$\frac{A_t}{s} = \frac{T_u}{\emptyset 2 A_o\ f_{yt} \cot(\theta)}$ ACI-Code 318-19; 22.7.6.1a

$where: \theta = 45°\ , f_{yt} = 420\ MPa\ , A_o = 0.85\ A_{oh}$

$\frac{A_t}{s}$ = 0.4977 mm^2/mm

S_{max} = min ($\frac{P_h}{8}$, 300 mm) ACI-Code 318-19; 9.7.6.3.3

$S_{max} = 88.5\ mm$

- For torsional reinforcement, minimum transverse reinforcement $(A_v+2A_t)_{min}/s$ shall be the greater of (a) and (b):

  (a) $\frac{0.062\sqrt{f_c'}\ b_w}{f_{yt}}$ ACI-Code 318-19; 9.6.4.2.a

  (b) $\frac{0.35\ b_w}{f_{yt}}$ ACI-Code 318-19; 9.6.4.2.b

For beam under pure torsion A_v=0, then the equation become:

(a) $\frac{A_t}{s}$ min.= $\frac{0.062\sqrt{f_c'}\ b_w}{2\ f_{yt}}$ = 0.098 mm^2/mm

(b) $\frac{A_t}{s}$ min.= $\frac{0.35\ b_w}{2\ f_{yt}}$ = 0.094 mm^2/mm

∴ $\frac{A_t}{s} > \frac{A_t}{s}$ min. Ok.

For stirrups Ø 8 mm , A_t = 50.27 mm^2.

$\frac{A_t}{s}$ = 0.4977, S= 101mm > S_{max}, then used S= 86 mm

3- Longitudinal reinforcement:

$A_l = \frac{A_t}{s}\ P_h \frac{f_{yt}}{f_{yl}}\ cot^2(\theta)$ ACI-Code 318-19; 22.7.6.1b

$where: f_{yl} = 420\ MPa$

A_l = 352.38 mm^2

- For longitudinal reinforcement in torsional, minimum area of longitudinal reinforcement ($A_{l\ min.}$) shall be the lesser of (a) and (b):

(a) $\frac{0.42\sqrt{f_c^-}\ A_{cp}}{f_{yl}} - \frac{A_t}{s}\ P_h \frac{f_{yt}}{f_{yl}}$ ACI-Code 318-19; 9.6.4.3.a

(b) $\frac{0.42\sqrt{f_c^-}\ A_{cp}}{f_{yl}} - \frac{0.175 b_w}{f_{yt}}\ P_h \frac{f_{yt}}{f_{yl}}$ ACI-Code 318-19; 9.6.4.3.b

$A_{l\ min.} = \frac{0.42\sqrt{f_c^-}\ A_{cp}}{f_{yl}} - \frac{A_t}{s}\ P_h \frac{f_{yt}}{f_{yl}}$ = -52.88 mm^2

$A_{l\ min.} = \frac{0.42\sqrt{f_c^-}\ A_{cp}}{f_{yl}} - \frac{0.175 b_w}{f_{yt}}\ P_h \frac{f_{yt}}{f_{yl}} = 233.13$ mm^2

$A_{l\ min.}$ =233.13 mm^2 < A_l = 352.38 mm^2 , Ok.

Used $d_b \geq$ max [$0.042\ S$, $10\ mm$] ACI-Code 318-19; 9.7.5.2

max [$0.042\ S = 0.042 * 86 = 3.61\ mm$, $10\ mm$]

∴ Used 4 ∅ $12\ mm = 452$ mm^2 > 352.38 mm^2

Vertical distance between longitudinal reinforcement = 225-(2*20) -(2*8)-12 = 157 mm < S_{max}=300 mm ACI-Code 318-19; 9.7.5.1

∴ Middle layer of longitudinal reinforcement is not needed.

Clear horizontal distance between longitudinal reinforcement =

$\frac{225-(2*20)-(2*8)-(2*12)}{1} = 145\ mm.$

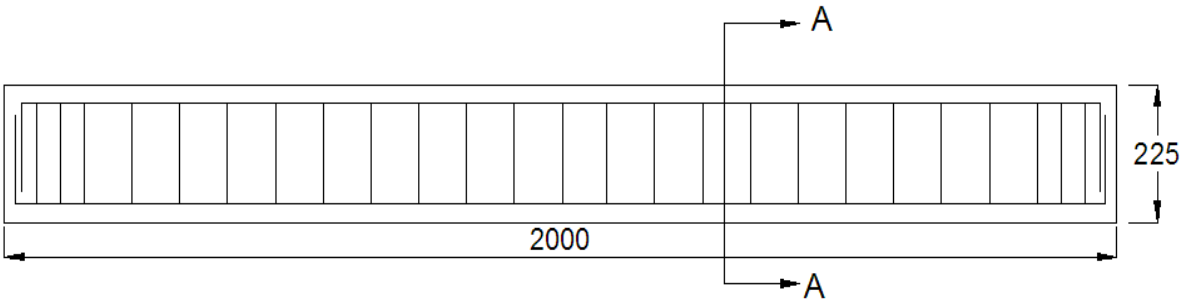

Figure (A-2): Details of reinforcement beams for group one section 1.

(All dimension in mm)

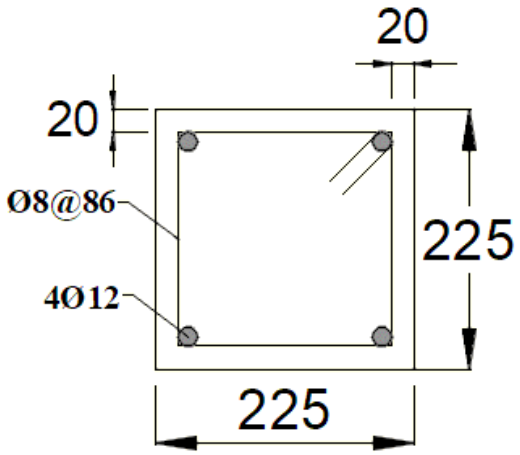

Figure (A-3): Cross section (A-A) for beams in group one section 1.
(All dimension in mm)

Standard hooks for the development of deformed bars in tension (90-degree hook).

ℓ_{ext}, longitudinal = $12d_b$ = 12*12 = 144 mm ACI-Code 318-19; 25.3.1

Standard hooks for bars used to anchor stirrups (135-degree hook)

ℓ_{ext}, stirrups = Greater of ($6d_b$ and 75 mm) ACI-Code 318-19; 25.3.2

$6d_b$ = 60 <75 mm then used 75 mm.

A.3 Section (160*316) mm

b = 160, h = 316, $f_c^- = 35\ MPa$, A_{cp} = 50560 mm^2, P_{cp} = 952 mm, $\emptyset$ = 0.75 .

1- Torsional effect may be neglect when:

$T_{u(ext)} < \emptyset\ 0.083 \sqrt{f_c^-}\ \frac{A_{cp}^2}{P_{cp}}$ ACI-Code 318-19; 22.7.4.1

$T_{u(ext)}$ = 7.1 kN.m > 0.99 kN.m

∴ Torsional effect must be considered

2- Check cross section dimension for torsion:

For solid section under pure torsion:

$\frac{T_u P_h}{1.7 A_{oh}^2} \leq \emptyset \left[\frac{V_c}{b_w d} + 0.66\sqrt{f_c^-} \right]$ ACI-Code 318-19; 22.7.7.1

For cover = 20mm & diameter of stirrups = 8 mm

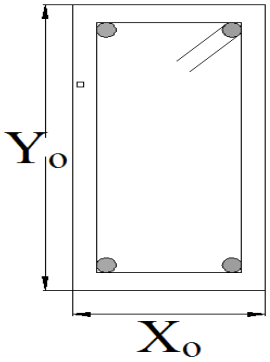

X_o = 160-2*20-2*($\frac{8}{2}$)= 112 mm

Y_o = 316-2*20-2*($\frac{8}{2}$)= 268 mm

$P_h = X_o * 2 + Y_o * 2 = 760$ mm

$A_{oh} = X_o * Y_o = 30016$ mm^2

$\frac{T_u P_h}{1.7 A_{oh}^2} = 3.523\ MPa \leq \emptyset \left[\frac{V_c}{b_w d} + 0.66\sqrt{f_c^-} \right] = 3.68$ MPa , Ok

3- Transverse reinforcement for torsion:

$\frac{A_t}{s} = \frac{T_u}{\emptyset 2 A_o\, f_{yt} \cot(\theta)}$ ACI-Code 318-19; 22.7.6.1a

$where: \theta = 45°\ , f_{yt} = 420\ Mpa\ , A_o = 0.85\ A_{oh}$

$\frac{A_t}{s}$ = 0.4417 mm^2/mm

S_{max} = min ($\frac{P_h}{8}$, 300 mm) ACI-Code 318-19; 9.7.6.3.3

$S_{max} = 95\ mm$

- For torsional reinforcement, minimum transverse reinforcement $(A_v+2A_t)_{min}/s$ shall be the greater of (a) and (b):

(a) $\frac{0.062\sqrt{f_c^-}\, b_w}{f_{yt}}$ ACI-Code 318-19; 9.6.4.2.a

(b) $\frac{0.35\, b_w}{f_{yt}}$ ACI-Code 318-19; 9.6.4.2.b

For beam under pure torsion A_v=0, then the equation become:

(a) $\frac{A_t}{s}$ min.= $\frac{0.062\sqrt{f_c^-}\, b_w}{2\, f_{yt}}$ = 0.0699 mm^2/mm

(b) $\frac{A_t}{s}$ min.= $\frac{0.35\, b_w}{2\, f_{yt}}$ = 0.0667 mm^2/mm

$\therefore$ $\frac{A_t}{s} > \frac{A_t}{s}$ min. Ok.

For stirrups $\emptyset$ 8 mm , A_t = 50.27 mm^2.

$\frac{A_t}{s}$ = 0.4417, S= 113.81 mm > S_{max}, then used S= 86 mm

4- Longitudinal reinforcement:

$A_l = \frac{A_t}{s}\, P_h \frac{f_{yt}}{f_{yl}}\, cot^2(\theta)$ ACI-Code 318-19; 22.7.6.1b

$where: f_{yl} = 420\ MPa$

A_l = 335.7mm^2

- For longitudinal reinforcement in torsional, minimum area of longitudinal reinforcement ($A_{l\ min.}$) shall be the lesser of (a) and (b):

(a) $\frac{0.42\sqrt{f_c^-}\, A_{cp}}{f_{yl}} - \frac{A_t}{s}\, P_h \frac{f_{yt}}{f_{yl}}$ ACI-Code 318-19; 9.6.4.3.a

(b) $\frac{0.42\sqrt{f_c^-}\, A_{cp}}{f_{yl}} - \frac{0.175 b_w}{f_{yt}}\, P_h \frac{f_{yt}}{f_{yl}}$ ACI-Code 318-19; 9.6.4.3.b

$A_{l\ min.} = \frac{0.42\sqrt{f_c^-}\, A_{cp}}{f_{yl}} - \frac{A_t}{s}\, P_h \frac{f_{yt}}{f_{yl}}$ = -36.58 mm^2

$A_{l\ min.} = \frac{0.42\sqrt{f_c^-}\, A_{cp}}{f_{yl}} - \frac{0.175 b_w}{f_{yt}}\, P_h \frac{f_{yt}}{f_{yl}} = 248.45$ mm^2

$A_{l\ min.}$ =248.45 mm^2 < A_l = 335.7 mm^2 , Ok.

Used $d_b \geq$ max [$0.042\, S$, $10\ mm$] ACI-Code 318-19; 9.7.5.2

max [$0.042\ S = 0.042 * 86 = 3.61\ mm$, $10\ mm$]

∴ Used 4 ∅ $12\ mm = 452$ mm^2 > 335.7 mm^2

Vertical distance between longitudinal reinforcement = 316-(2*20)-(2*8)-12= 248 mm < S_{max}=300 mm ACI-Code 318-19; 9.7.5.1

∴ Middle layer of longitudinal reinforcement is not needed.

Clear horizontal distance between longitudinal reinforcement =

$\frac{160-(2*20)-(2*8)-(2*12)}{1}$ = 80 mm.

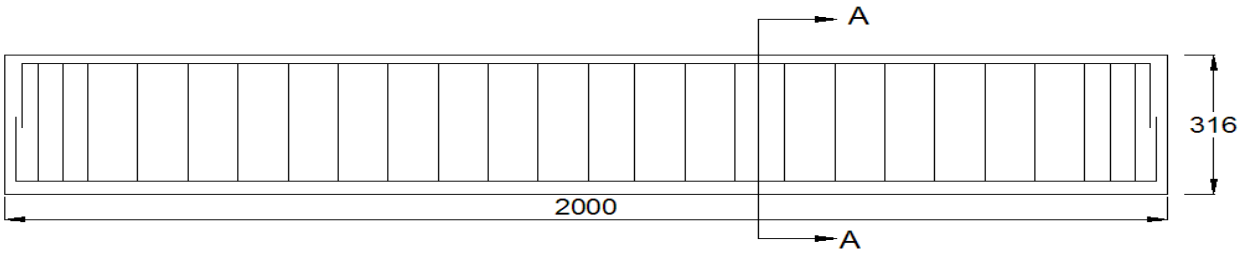

Figure (A-4): details of reinforcement beams for group one section 2.
(All dimension in mm)

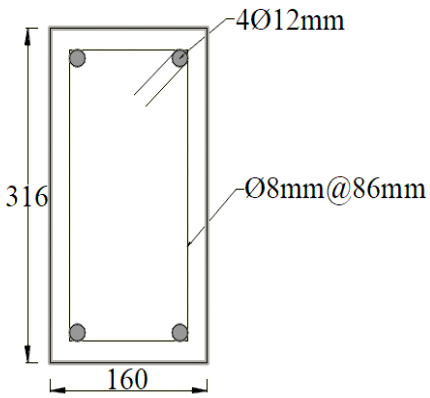

Figure (A-5): cross section (A-A) for beams in group one section 2.
(All dimension in mm)

Standard hooks for the development of deformed bars in tension (90-degree hook).

ℓ_{ext}, longitudinal = $12d_b$ = 12*12 = 144 mm ACI-Code 318-19; 25.3.1

Standard hooks for bars used to anchor stirrups (135-degree hook)

ℓ_{ext}, stirrups = Greater of ($6d_b$ and 75 mm) ACI-Code 318-19; 25.3.2

$6d_b$ = 60 <75 mm then used 75 mm.

A.4 Section (130*390) mm

b = 130, h = 390, $f_c^- = 35\ MPa$, A_{cp} = 50700 mm^2, P_{cp} = 1040 mm, $\emptyset = 0.75$.

1- Torsional effect may be neglect when:

$T_{u(ext)} < \emptyset\ 0.083 \sqrt{f_c^-}\ \frac{A_{cp}^2}{P_{cp}}$ ACI-Code 318-19; 22.7.4.1

$T_{u(ext)}$ = 5.75 kN.m > 0.94 kN.m

∴ Torsional effect must be considered

2- Check cross section dimension for torsion:

For solid section under pure torsion:

$\frac{T_u P_h}{1.7 A_{oh}^2} \leq \emptyset\ [\frac{V_c}{b_w d} + 0.66\sqrt{f_c^-}\ ]$ ACI-Code 318-19; 22.7.7.1

For cover = 20mm & diameter of stirrups = 8 mm

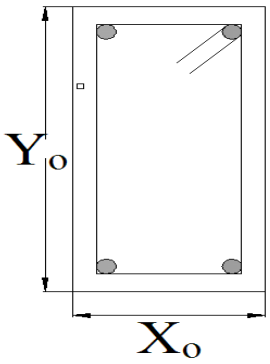

X_o = 130-2*20-2*($\frac{8}{2}$)= 82 mm

Y_o = 390-2*20-2*($\frac{8}{2}$)= 342 mm

$P_h = X_o * 2 + Y_o * 2$ = 848 mm

$A_{oh} = X_o * Y_o$ = 28044 mm^2

$\frac{T_u P_h}{1.7 A_{oh}^2} = 3.65\ MPa \leq \emptyset\ [\frac{V_c}{b_w d} + 0.66\sqrt{f_c^-}\ ]$ = 3.68 MPa, Ok

3- Transverse reinforcement for torsion:

$$\frac{A_t}{s} = \frac{T_u}{\emptyset 2A_o\, f_{yt} \cot(\theta)}$$ ACI-Code 318-19; 22.7.6.1a

$$where: \theta = 45° \ , f_{yt} = 420\ Mpa\ , A_o = 0.85\ A_{oh}$$

$\frac{A_t}{s}$ = 0.3829 mm^2/mm

S_{max} = min ($\frac{P_h}{8}$, 300 mm) ACI-Code 318-19; 9.7.6.3.3

$S_{max} = 106\ mm$

- For torsional reinforcement, minimum transverse reinforcement $(A_v+2A_t)_{min}/s$ shall be the greater of (a) and (b):

(a) $\frac{0.062\sqrt{f_c'}\ b_w}{f_{yt}}$ ACI-Code 318-19; 9.6.4.2.a

(b) $\frac{0.35\ b_w}{f_{yt}}$ ACI-Code 318-19; 9.6.4.2.b

For beam under pure torsion A_v=0, then the equation become:

(a) $\frac{A_t}{s}$ min.= $\frac{0.062\sqrt{f_c'}\ b_w}{2\ f_{yt}}$ = 0.0568 mm^2/mm

(b) $\frac{A_t}{s}$ min.= $\frac{0.35\ b_w}{2\ f_{yt}}$ = 0.0542 mm^2/mm

∴ $\frac{A_t}{s} > \frac{A_t}{s}$ min. Ok.

For stirrups ∅ 8 mm , A_t = 50.27 mm^2.

$\frac{A_t}{s}$ = 0.3829, S= 131.3 mm > S_{max}, then used S= 86 mm

4- Longitudinal reinforcement :

$A_l = \frac{A_t}{s}\ P_h \frac{f_{yt}}{f_{yl}}\ cot^2(\theta)$ ACI-Code 318-19; 22.7.6.1b

$where: f_{yl} = 420\ MPa$

$A_l = 324.7 mm^2$

- For longitudinal reinforcement in torsional, minimum area of longitudinal reinforcement ($A_{l\ min.}$) shall be the lesser of (a) and (b):

  (a) $\frac{0.42\sqrt{f_c'}\ A_{cp}}{f_{yl}} - \frac{A_t}{s}\ P_h \frac{f_{yt}}{f_{yl}}$ ACI-Code 318-19; 9.6.4.3.a

  (b) $\frac{0.42\sqrt{f_c'}\ A_{cp}}{f_{yl}} - \frac{0.175 b_w}{f_{yt}}\ P_h \frac{f_{yt}}{f_{yl}}$ ACI-Code 318-19; 9.6.4.3.b

$A_{l\ min.} = \frac{0.42\sqrt{f_c'}\ A_{cp}}{f_{yl}} - \frac{A_t}{s}\ P_h \frac{f_{yt}}{f_{yl}} = -82.44\ mm^2$

$A_{l\ min.} = \frac{0.42\sqrt{f_c'}\ A_{cp}}{f_{yl}} - \frac{0.175 b_w}{f_{yt}}\ P_h \frac{f_{yt}}{f_{yl}} = 254\ mm^2$

$A_{l\ min.} = 254\ mm^2 < A_l = 324.7\ mm^2$, Ok.

Used $d_b \geq$ max [$0.042\ S$, $10\ mm$] ACI-Code 318-19; 9.7.5.2

max [$0.042\ S = 0.042 * 86 = 3.61\ mm$, $10\ mm$]

∴ Used 4 ∅ $12\ mm = 452\ mm^2 > 324.7\ mm^2$

Vertical distance between longitudinal reinforcement = 390-(2*20) -(2*8)-12= 322 mm > S_{max}=300 mm ACI-Code 318-19; 9.7.5.1

∴ The middle layer of longitudinal reinforcement is needed but not used to be the same reinforcement for all sections.

Clear horizontal distance between longitudinal reinforcement =

$\frac{130-(2*20)-(2*8)-(2*12)}{1} = 50$ mm.

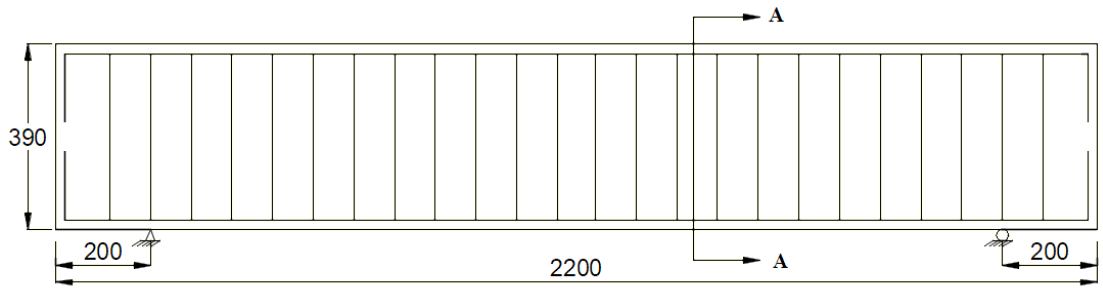

Figure (A-6): Details of reinforcement beams for group one section 3. (All dimension in mm)

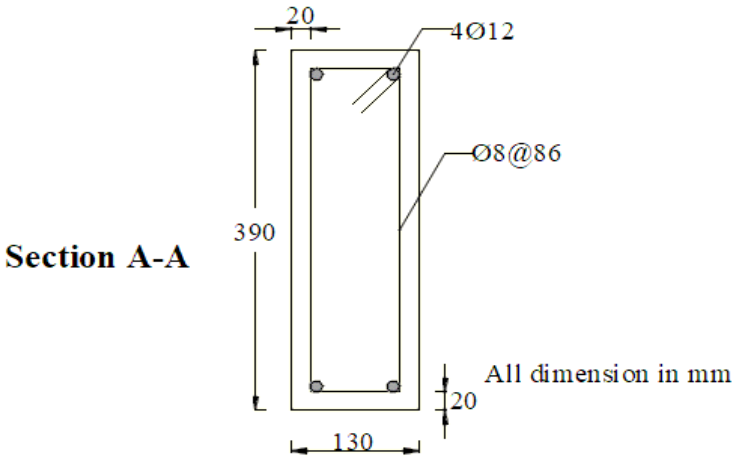

Figure (A-7): Cross section (A-A) for beams in group one section 3.

Standard hooks for the development of deformed bars in tension (90-degree hook).

ℓ_{ext}, longitudinal = $12d_b$ = 12*12 = 144 mm ACI-Code 318-19; 25.3.1

Standard hooks for bars used to anchor stirrups (135-degree hook)

ℓ_{ext}, stirrups = Greater of ($6d_b$ and 75 mm) ACI-Code 318-19; 25.3.2

$6d_b$ = 60 <75 mm then used 75 mm.

APPENDIX B

Arm for Loading the Second Group

A.1 When λ = 0.5

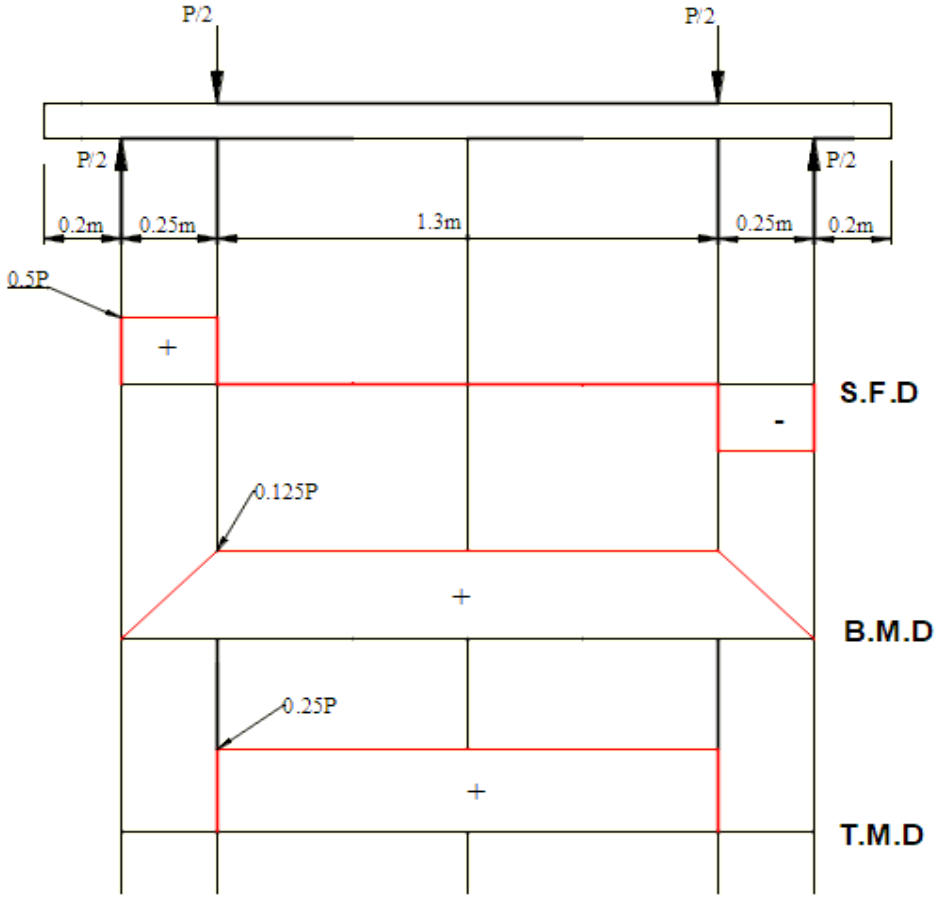

λ = Bending / Torsion = $\frac{M}{T}$

λ= 0.5 = $\frac{M}{T}$

Then T= $\frac{M}{0.5}$

∵ M= 0.125P

∴ T= 0.25P

Torque (T)= Load (P/2) * arm

Arm = $\frac{2T}{P}$ = 0.5m

A.2 When λ = 0.75

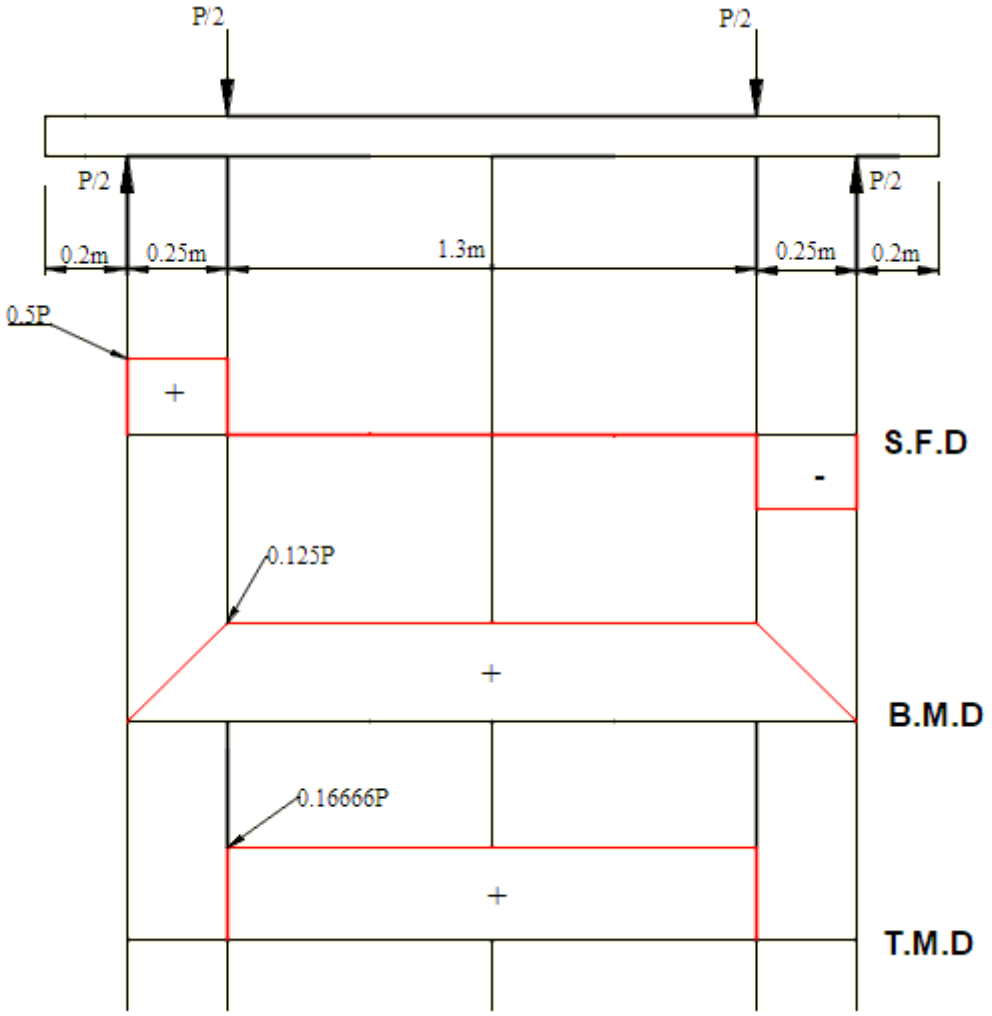

λ = Bending / Torsion = $\frac{M}{T}$

λ= 0.75 = $\frac{M}{T}$

Then T= $\frac{M}{0.75}$

∵ M= 0.125P

∴ T= 0.16666P

Torque (T)= Load (P/2) * arm

Arm = $\frac{2T}{P}$ = 0.3333m

A.3 When λ = 1

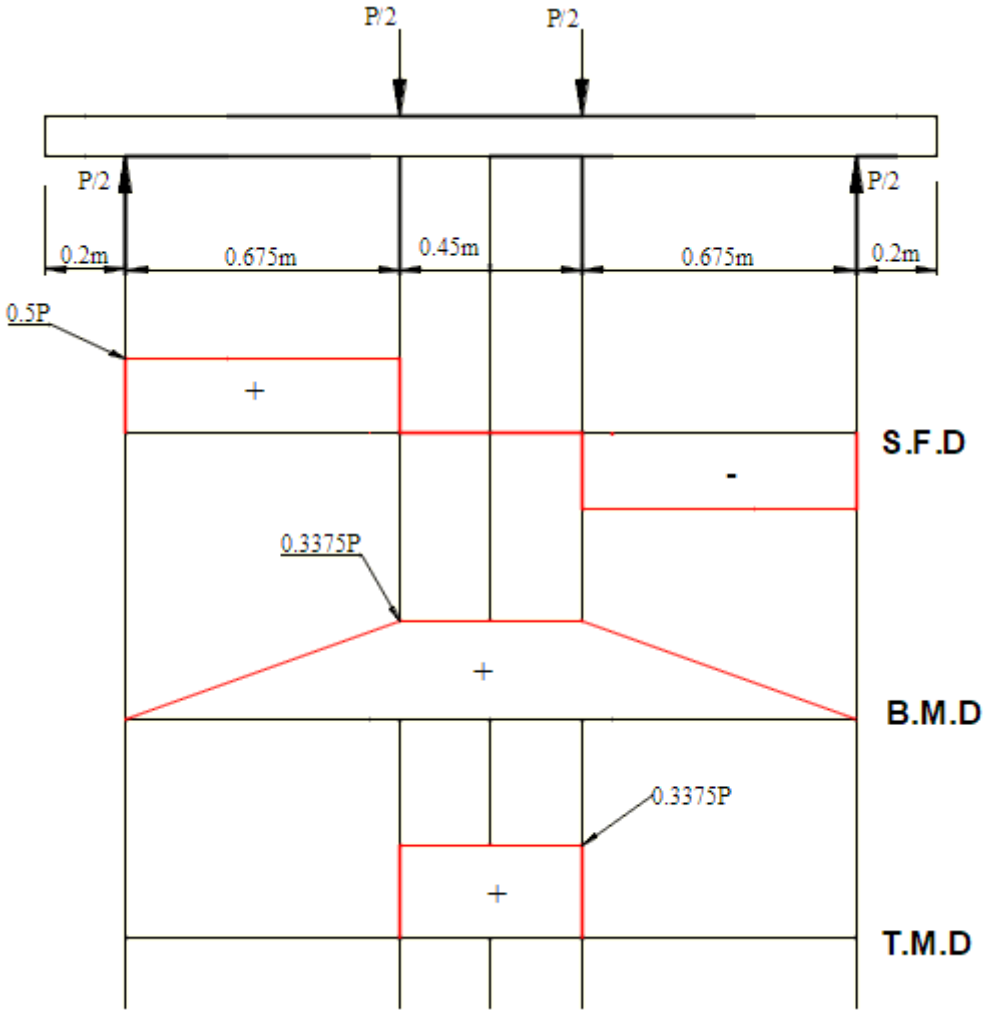

λ = Bending / Torsion = $\frac{M}{T}$

λ= 1 = $\frac{M}{T}$

Then T= M

∵ M= 0.3375P

∴ T= 0.3375P

Torque (T)= Load (P/2) * arm

Arm = $\frac{2T}{P}$ = 0.675m

A.4 When λ = 2

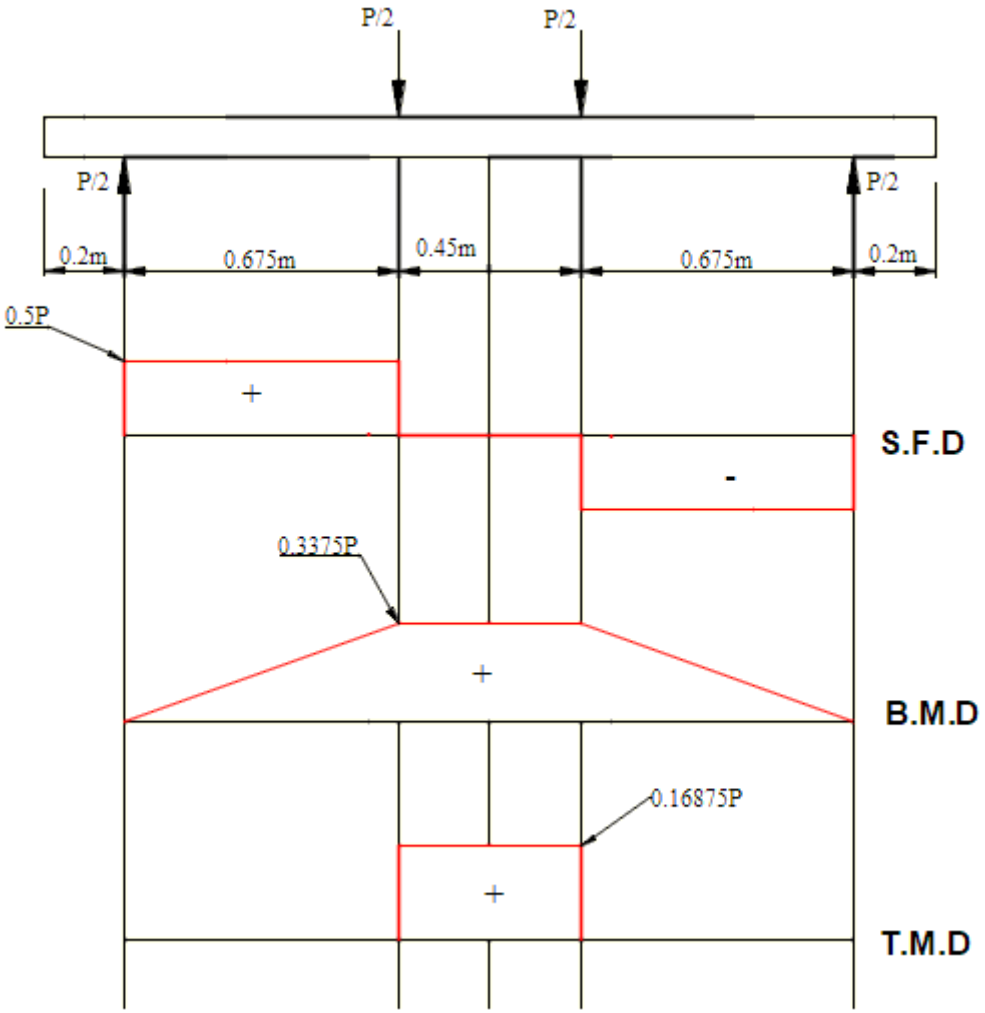

λ = Bending / Torsion = $\frac{M}{T}$

λ= 2 = $\frac{M}{T}$

Then T= $\frac{M}{2}$

∵ M= 0.3375P

∴ T= 0.16875P

Torque (T)= Load (P/2) * arm

Arm = $\frac{2T}{P}$ = 0.3375m

A.5 When λ = 3

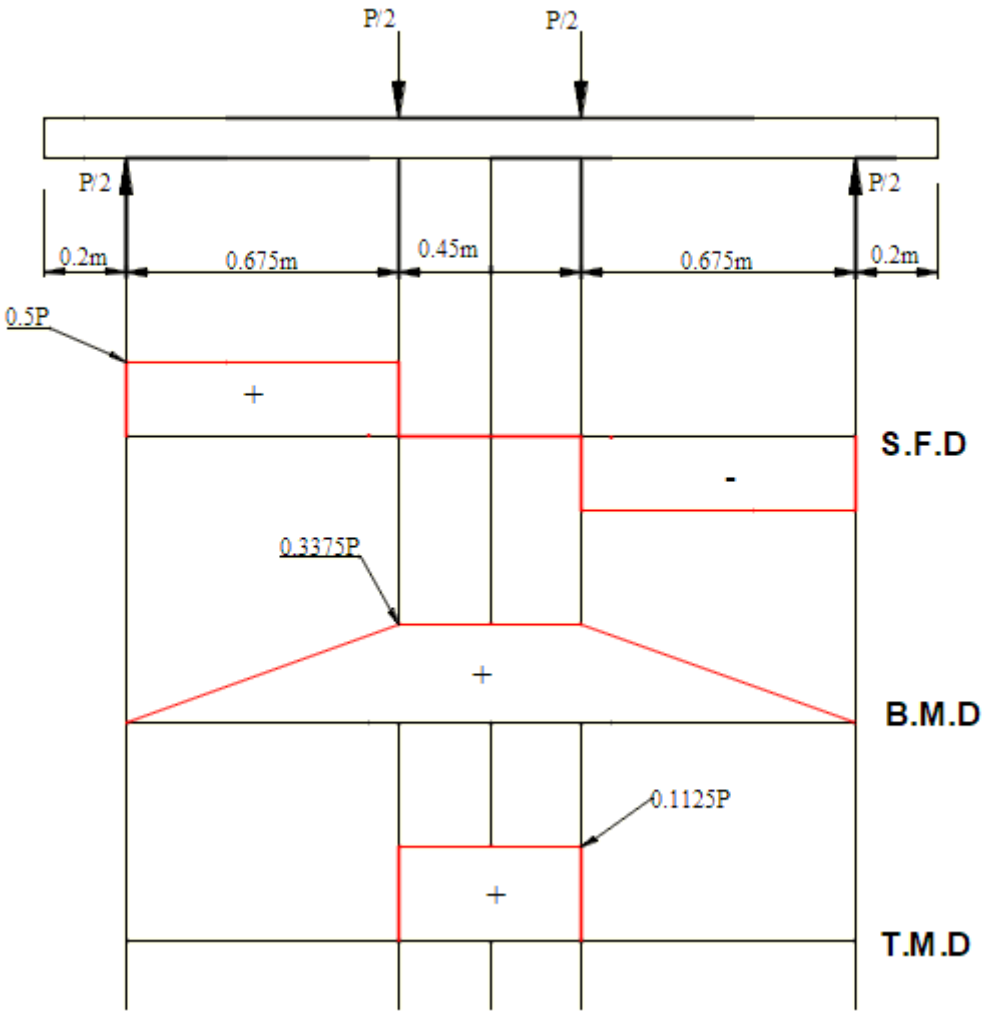

λ = Bending / Torsion = $\frac{M}{T}$

λ= 3 = $\frac{M}{T}$

Then T= $\frac{M}{3}$

∵ M= 0.3375P

∴ T= 0.1125P

Torque (T)= Load (P/2) * arm

Arm = $\frac{2T}{P}$ = 0.225m

A.6 When λ = 4

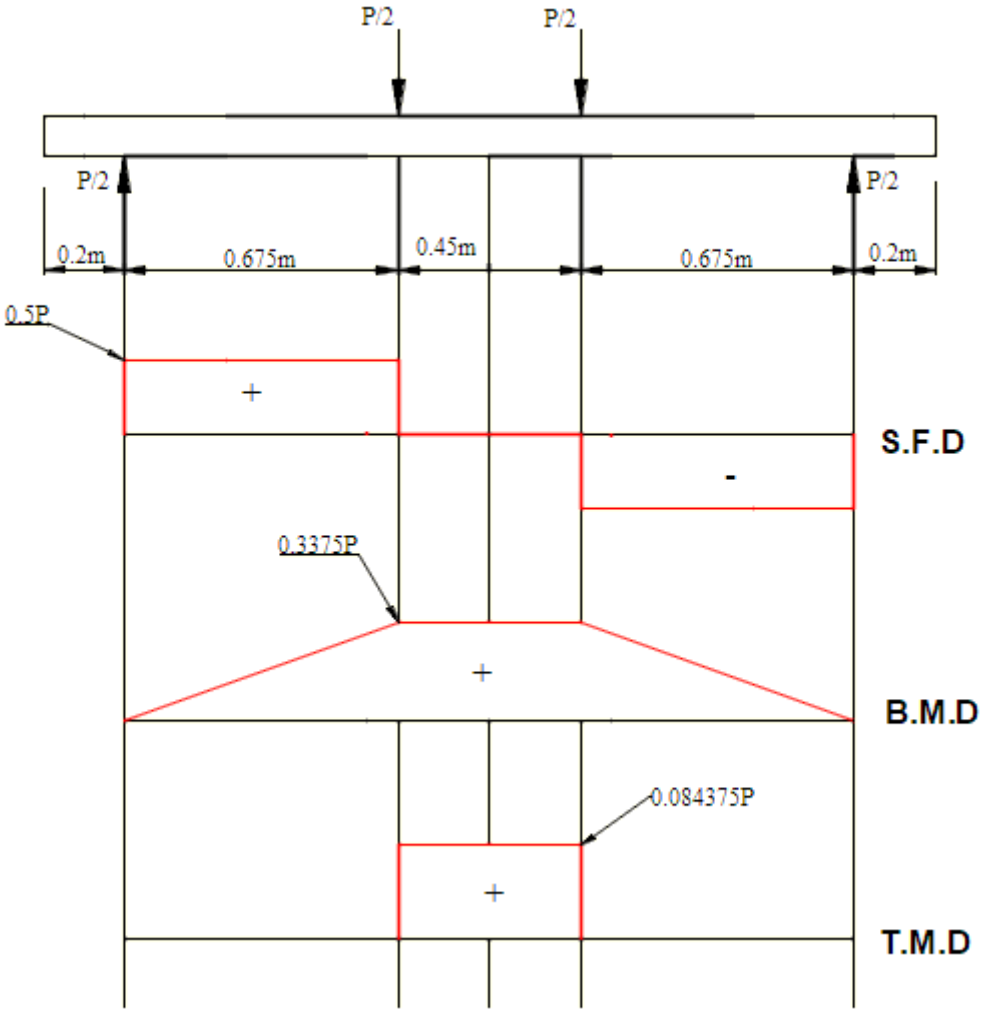

λ = Bending / Torsion = $\frac{M}{T}$

λ= 4 = $\frac{M}{T}$

Then T= $\frac{M}{4}$

∵ M= 0.3375P

∴ T= 0.084375P

Torque (T)= Load (P/2) * arm

Arm = $\frac{2T}{P}$ = 0.17m

الخلاصة

خصص هذا العمل لدراسة سلوك الاعتاب الخرسانة المطاطية عند حمل الالتواء. تشمل العوامل في هذا البحث النسبة المئوية للركام الخشن الذي تم استبداله برقائق المطاط (10٪، 20٪، 30٪)، ونسبة العمق إلى العرض، ونوع الأحمال. تم استخدام ثلاثين أنموذجاً في الدراسة، مع اختبار ستة عشر عتباً تحت تأثير الالتواء في المجموعة الأولى، واختبار اثني عشر عتباً تحت تأثير الالتواء والانحناء مجتمعة في المجموعة الثانية، وتم اختبار أنموذجين تحت تأثير الانحناء في المجموعة الثالثة. تم إخضاع ستة وعشرين عينة لتسليح حديد طولي وعرضي متطابق، وكانت أربع عينات بدون حديد التسليح.

مقارنةً بالخرسانة التقليدية، فإن الخلطات الخرسانية المطاطية أقل كثافة وأقل قابلية للتشغيل بحوالي 9.08٪ و37.04٪ على التوالي. من حيث قوة الانضغاط وقوة الشد للانقسام ومعامل التمزق ومعامل المرونة، عند استبدال 30٪ من الركام الخشن برقائق المطاط، أظهرت الخرسانة المطاطية خسارة أكبر في الخواص الميكانيكية بحوالي 47.64٪، 35.34٪، 44.75٪، و50.49٪ على التوالي. من خلال استبدال 30٪ من الحصى برقائق مطاطية، زادت مقاومة الصدمات والتوصيل الحراري للخرسانة المطاطية بنسبة 356٪ و 20.6٪ على التوالي، مما يعني أن الخرسانة المطاطية يمكنها امتصاص المزيد من الطاقة وتكون أكثر مرونة وتكون أفضل في العزل الحراري.

ووجد أن عزم الالتواء الاقصى انخفض بنسبة 14.75٪، بينما زادت زاوية الالتواء بنسبة 44.07٪ عند عزم الالتواء الاقصى وانخفضت صلابة التكسير القصوى بنسبة 44.05٪ وزاد مؤشر الليونة بنسبة 30.34٪، عندما تم استبدال المطاط بنسبة 30٪ تحت تأثير الالتواء النقي. وفقاً للنتائج التجريبية للعينات تحت حمل مركب من (الالتواء والانحناء)، عندما تزداد نسبة العزم / الالتواء (λ) من 1 الى 4، ينخفض عزم الالتواء الاقصى بنسبة 47.28٪ ولكن عزم الانثناء الاقصى يرتفع بنسبة 107.78٪. ينخفض الحد الاقصى لعزم الالتواء بنسبة 14.56٪ الى 17.67٪ عندما يتم استبدال 30٪ من الركام الخشن برقائق المطاط، لقيم λ (0.5 إلى 4) بينما تزداد زاوية الالتواء عند عزم الالتواء الاقصى بنسبة 33.04٪ الى 44.37٪.

يوصي الكود الأمريكي باستخدام تشبيه الجمالون الفضائي الأنبوبي ذي الجدران الرقيقة لمقارنة النتائج التجريبية لعزم الالتواء الاقصى مع النتائج التحليلية. تعطي نتائج الكود الأمريكي قابلية التواء أقل من تقدير الكمرات الخرسانية العادية المسلحة وقابلية الالتواء مبالغ فيها لعوارض الخرسانة المسلحة المطاطية وبنسبة فرق 15٪ عند نسبة استبدال 30٪. ثبت أن هذه الطريقة غير فعالة في تقييم تأثير محتوى المطاط في الخلطة الخرسانية. لذلك يُنصح بضرب النتائج النظرية من الكود الأمريكي بعامل من الصيغة المقترحة لتلبية الاحتياجات التجريبية، وذلك باستخدام قيم المتوسط (m) ومعامل التباين (COV) البالغة 1.009٪ و0.874٪ على التوالي، تبين النتائج المتوقعة والتجريبية متوافقة جيداً. وفقاً لمخطط التفاعل، تتبع النتائج التجريبية نمطاً مشابهاً للنتائج النظرية للأعتاب المعرضة لأحمال مركبة (الالتواء والانحناء). هناك علاقة وثيقة للغاية بين المنحنيات النظرية والعملية لنسبة λ (عزم الانحناء \ عزم الالتواء) أقل من 1، في حين أن المنحنيات النظرية والعملية تقترب تدريجياً من بعضها البعض مع تزايد λ.

جمهورية العراق
وزارة التعليم العالي والبحث العلمي
جامعة بابل- كلية الهندسة
قسم الهندسة المدنية

السلوك المختبري لأعتاب الخرسانة المطاطية المسلحة تحت تأثير الالتواء

اطروحة مقدمة الى

كلية الهندسة/ جامعة بابل

كجزء من متطلبات الحصول على درجة الدكتوراه فلسفة في الهندسة / الهندسة المدنية/ انشاءات

من قبل

عمار عبد الامير حسين عبود

اشراف

أ.د حيدر محمد كاظم المطيري

2022